Investigation of Geopolymer as a Sustainable Alternative Binder for Fiber-Reinforced Strain-Hardening Composites

A Thesis Submitted in Fulfillment of the Requirements for the Degree of

Doctor of Philosophy

by

Behzad Nematollahi

Faculty of Science, Engineering and Technology

Swinburne University of Technology

Hawthorn, VIC, 3122

Australia

January 2017

ABSTRACT

Strain hardening cementitious composite (SHCC) is a special class of fiber-reinforced cementitious composites which exhibits pseudo strain-hardening (PSH) behavior with very high tensile strain capacity of up to 6%. Typically high cement content is used in this composite resulting in high autogenous shrinkage, heat of hydration, and cost. In addition, the associated increase in the CO_2 emissions and embodied energy arising from the production of ordinary Portland cement (OPC) can compromise sustainability credentials of SHCCs. In this thesis, a sustainable alternative to typical SHCCs is studied.

Geopolymer is studied as a sustainable alternative to OPC to develop strain-hardening composites. Geopolymer is an emerging OPC-less binder purported to provide a sustainable alternative to OPC. Geopolymer may be manufactured from industrial by-products such as fly ash and slag that are rich in silica and alumina with high alkaline activators. This doctoral research is aimed on multiscale development and investigation of properties of strain-hardening geopolymer composite (SHGC). The research works presented in this thesis are divided into two main parts. Part I focuses on heat cured two-part fly ash-based SHGCs, while the focus of Part II is on ambient temperature cured one-part SHGCs.

In Part I, the effects of matrix-related parameters such as type of activator, water content, sand size and sand content on the properties of fly ash-based SHGCs were evaluated. The results indicated that the type of activator had significant effects on the matrix, fiber-matrix interface, and thereby composite properties of fly ash-based SHGCs. Among the activators investigated, the composite made from a sodium-based activator solution exhibited the highest compressive and tensile strengths with very high tensile strain capacity of 63.7 MPa, 4.7 MPa and 4.3%, respectively. The excessive use of fine sand and the use of coarse sand in the geopolymer matrix resulted in a matrix with considerably high fracture toughness, which in turn increased the first-crack strength of the composite compared to the maximum bridging stress of the fibers and violated the conditions for saturated PSH behavior. These findings are consistent with micromechanics design theory.

The mechanical and thermal properties of lightweight fly ash-based SHGCs incorporating three types of lightweight aggregates as complete replacement of micro-silica sand were

also evaluated. The results indicated that the density and compressive strength of all developed SHGCs were less than 1833 kg/m^3 and more than 43.4 MPa, respectively, meeting the density and compressive strength requirements for structural lightweight concrete. In addition, the thermal conductivity of SHGCs containing lightweight aggregates were significantly lower than that of the composite containing micro-silica sand, resulting in composites that are lighter and provide better thermal insulation than typical SHCCs.

The microscale investigation of fly ash-based SHGCs involving determination of the fiber-matrix interface properties using single-fiber pullout tests was also conducted, which explains the experimentally observed macroscopic tensile ductility of SHGCs. The applicability of the existing micromechanics-based model for the design of SHGCs was also verified. It was demonstrated, via a parametric study, how the model guides towards composite optimization and component tailoring to achieve saturated PSH behavior with the lowest amount of fiber in fly ash-based SHGCs.

In Part II, an ambient temperature cured one-part SHGC developed to enhance the commercial viability of SHGCs is presented. The developed composite as a "dry mix" uses a small amount of solid activator and eliminates the necessity for heat curing and handling hazardous liquids. The quantitative influences of curing condition, type of slag and type of fiber on the composite tensile performance were evaluated. The developed composite demonstrated strong PSH behavior comparable to typical SHCCs with high tensile strength of 4.6 MPa and very high tensile strain capacity of 4.2%. The crack-bridging relation of the developed composite, computed via the micromechanics-based model, satisfied the necessary strength and energy-based conditions of PSH behavior. The material sustainability evaluation results indicated that the developed composite provides 76% less carbon emissions and 36% less energy consumption as compared to typical SHCCs. Finally, a sustainable lightweight precast composite floor composed of a 40 mm thick one-part SHGC slab and C-section purlins was designed, constructed and tested. The composite floor has a similar strength to that of "conventional" precast composite floor, but is 70% lighter.

In summary, the performances of the developed SHGCs are either comparable or superior to typical SHCCs in all mechanical aspects considered in this doctoral research. At the

same time, they have significantly lower environmental footprints as compared to typical SHCCs.

ACKNOWLEDGEMENTS

First and foremost, I wish to express my greatest gratitude to God Almighty, for all his blessings on me during the course of life and for bestowing me with enough courage and strength to pursue my studies.

I would like to express my sincere appreciation and gratitude to my Principal Coordinating Supervisor, Professor Jay Sanjayan for his continuous support and invaluable guidance during my study. This thesis would not have been possible without his support. I am forever indebted for his great mentorship.

I would like to extend my appreciation to Assistant Professor En-Hua Yang from Nanyang Technological University, Singapore for helping to conduct the single-fiber pullout tests and his constructive comments for fiber-bridging constitutive modelling in this research. I would also like to thank Assistant Professor Ravi Ranade from State University of New York, Buffalo, USA for his valuable comments and advice on analysis of the results of lightweight strain-hardening geopolymer composites.

I also acknowledge Swinburne University of Technology for supporting and funding this research project through a Swinburne University Postgraduate Research Award (SUPRA). I would also like to thank the technical staff of the Smart Structures Laboratory for their assistance during the experimental work conducted in this research. My special thanks is extended to the Test Engineer Mr. Kia Rasekhi for his invaluable technical assistance and guidance during the experimental work. I wish to thank all my colleagues and friends who made my Ph.D. study at Swinburne University of Technology an enjoyable experience.

Finally, from the bottom of my heart, I wish to express my sincere gratitude to my family whose love, patience and encouragement has given me power, enthusiasm, and motivation not only during my Ph.D. study, but throughout my life.

DECLARATION

I declare that the thesis is my original work except for quotations and citations which have been duly acknowledged. I also declare that it has not been previously, and is not concurrently, submitted for any other degree at any other institutions. I hereby declare that I am the sole author of this thesis. This is a true copy of the thesis, including any required final revisions, as accepted by my examiners.

Behzad Nematollahi

January 2017

DEDICATION

I would like to dedicate this thesis to my parents whom I love and owe my life to.

LIST OF PUBLICATIONS

- **Patent:**

"Geopolymer Composite and Geopolymer Matrix Composition", Australian Provisional Patent No. 2015904424.

- **Peer-Reviewed Journal Papers:**

(1) **Nematollahi, B.**, Qui, J., Yang, E.H., and Sanjayan, J. (2017). "Micromechanics Constitutive Modelling and Optimization of Strain Hardening Geopolymer Composite". *Ceramics International*, Article in Press.

(2) **Nematollahi, B.**, Sanjayan, J., Qui, J., and Yang, E.H. (2017). "Micromechanics-based investigation of a sustainable ambient temperature cured one-part strain hardening geopolymer composite". *Construction and Building Materials*, 131, 552-563. *No. of citations in Scopus: 2, No. of citations in Google Scholar: 2.*

(3) **Nematollahi, B.**, Sanjayan, J., Qui, J., and Yang, E.H. (2017). "High Ductile Behavior of a Polyethylene Fiber-Reinforced One-Part Geopolymer Composite: A Micromechanics-based Investigation". *Archives of Civil and Mechanical Engineering*, 17, 555-563. *No. of citations in Scopus: 1, No. of citations in Google Scholar: 1.*

(4) **Nematollahi, B.**, Ranade, R., Sanjayan, J., and Ramakrishnan, S. (2017). "Thermal and Mechanical Properties of Sustainable Lightweight Strain Hardening Geopolymer Composites". *Achieves of Civil and Mechanical Engineering*, 17, 55-64. *No. of citations in Scopus: 1, No. of citations in Google Scholar: 2.*

(5) **Nematollahi B.**, Sanjayan J., and Shaikh F.U.A. (2016). "Matrix Design of Strain Hardening Engineered Geopolymer Composites". *Composites Part B: Engineering*, 89, 253-265. *No. of citations in Scopus: 5, No. of citations in Google Scholar: 4.*

(6) **Nematollahi, B.**, Sanjayan, J., and Shaikh, F.U.A. (2015). "Tensile Strain Hardening Behavior of PVA Fiber-Reinforced Engineered Geopolymer Composite." *ASCE Journal of Materials in Civil Engineering*, 27(10), 04015001. *No. of citations in Scopus: 10, No. of citations in Google Scholar: 10.*

(7) **Nematollahi, B.**, Sanjayan, J., and Shaikh, F.U.A. (2015). "Synthesis of Heat and Ambient Cured One-Part Geopolymer Mixes With Different Grades of Sodium Silicate". *Ceramics International*, 41(4), 5696-5704. *No. of citations in Scopus: 15, No. of citations in Google Scholar: 21.*

(8) **Nematollahi B.**, Sanjayan J. and Shaikh F.U.A. (2015). "Strain Hardening Behavior of Engineered Geopolymer Composites: Effects of the Activator Combination". *Journal of The Australian Ceramic Society*, 51(1), 54 – 60. *No. of citations in Scopus: 5, No. of citations in Google Scholar: 5.*

(9) **Nematollahi, B.**, Sanjayan, J., and Shaikh, F.U.A. (2014). "Comparative Deflection Hardening Behavior of Short Fiber Reinforced Geopolymer Composites". *Construction and Building Materials*, 70, 54-64. *No. of citations in Scopus: 12, No. of citations in Google Scholar: 13.*

(10) **Nematollahi, B.** and Sanjayan, J. (2014). "Effect of Different Superplasticizers and Activator Combinations on Workability and Strength of Fly Ash Based Geopolymer". *Materials & Design*, 57, 667-672. *No. of citations in Scopus: 43, No. of citations in Google Scholar: 59.*

(11) **Nematollahi, B.** and Sanjayan, J. (2014). "Efficacy of Available Superplasticizers on Geopolymers". *Research Journal of Applied Sciences, Engineering and Technology*. 7(7), 1278-1282. *No. of citations in Scopus: 7, No. of citations in Google Scholar: 8.*

(12) **Nematollahi B.**, Sanjayan J., Chai J.X.H. and Lu T.M. (2014). "Properties of Fresh and Hardened Glass Fiber Reinforced Fly Ash Based Geopolymer Concrete". *Key Engineering Materials*, 594, 629-633. *No. of citations in Scopus: 5, No. of citations in Google Scholar: 6.*

- **Under Review Journal Papers:**

(1) **Nematollahi, B.**, Qui, J., Yang, E.H., and Sanjayan, J. (2016). "Microscale Investigation of Fiber-Matrix Interface Properties of Strain Hardening Geopolymer Composite". *Journal of Composites Part B: Engineering*, Submitted for publication.

- **Peer-Reviewed Conference Papers:**

(1) **Nematollahi, B.** and Sanjayan, J. (2016). "Strain Hardening Geopolymer Composites". Proceedings of *ACF 2016−The 7th International Conference of Asian Concrete Federation. 30 October-2 November, Hanoi, Vietnam.*

(2) **Nematollahi, B.** and Sanjayan, J. (2016). "Ambient Temperature Cured One-Part Engineered Geopolymer Composite: A Sustainable Alternative to Engineered Cementitious Composite". Proceedings of *BEFIB 2016−The 9th RILEM International Symposium on Fiber Reinforced Concrete.* September 19-21, Vancouver, Canada, 1117-1126.

(3) **Nematollahi, B.** and Sanjayan, J. (2016). "Influence of type of fiber on tensile performance of one-part "dry-mix" strain hardening geopolymer composite (SHGC)". Proceedings of *the 11th fib International PhD Symposium in Civil Engineering*. 29−31 August, The University of Tokyo, Tokyo, Japan, 831-838.

(4) **Nematollahi, B.**, Sanjayan, J., and Shaikh, F.U.A. (2015). "Influence of Matrix Related Parameters on Strain Hardening Behavior of Engineered Geopolymer Composite (EGC)". Proceedings of *Concrete 2015−The 27th Biennial National Conference of the Concrete Institute of Australia in conjunction with the 69th RILEM Week conference*. 30 August−02 September, Melbourne, Australia, 1041−1050.

(5) **Nematollahi, B.**, Sanjayan, J., and Shaikh, F.U.A. (2014). "Influence of the Type of Activator Combinations on the Deflection Hardening Behavior of Geopolymer Composites". Proceedings of *SHCC3−3rd International RILEM Conference on Strain Hardening Cementitious Composites*, RILEM Publications S.A.R.L., 03−05 November, Dordrecht, The Netherlands, 105-112.

(6) **Nematollahi, B.**, Sanjayan, J., and Shaikh, F.U.A. (2014). "Effect of Different Activator Combinations on the Properties of Fly Ash Based Geopolymer". Proceedings of *ACF 2014−The 6th International Conference of Asian Concrete Federation*. 21−24 September, Seoul, Korea, 1417-1423.

(7) **Nematollahi, B.**, Sanjayan, J., and Shaikh, F.U.A. (2014). "Comparative Deflection Hardening Behavior of Fly Ash-Based Geopolymer Composite with the Conventional

Cement-Based Composite". Proceedings of *ACEDS 2014−International Conference on Advances in Civil Engineering for Sustainable Development*. 27−29 August, Thailand, 543-548.

(8) **Nematollahi, B.** and Sanjayan, J. (2013). "Effect of Superplasticizers on Workability of Fly Ash Based Geopolymer". Proceedings of *InCIEC 2013−International Civil and Infrastructure Engineering Conference*. 22−24 September, Kuching, Malaysia. Published by Springer Science+Business Media, Singapore, 2014, R. Hassan et al. (eds.), DOI: 10.1007/978-981-4585-02-6_61, 713-719.

TABLE OF CONTENTS

LIST OF FIGURES

LIST OF TABLES

LIST OF ABBREVIATIONS

ASR	Alkali Silica Reaction
DFRCC	Ductile Fiber Reinforced Cementitious Composite
ECC	Engineered Cementitious Composite
FRCC	Fiber Reinforced Cementitious Composite
FRC	Fiber Reinforced Concrete
HPMC	Hydroxypropyl Methyl Cellulous
HPFRCC	High Performance Fiber Reinforced Cementitious Composite
IOT	Iron Ore Tailing
JSCE	Japan Society of Civil Engineers
LVDT	Linear Variable Differential Transducer
LOP	Limit of Proportionality
MTPS	Modified Transient Plane Source
MSI	Material Sustainability Indicators
OPC	Ordinary Portland Cement
POFA	Palm Oil Fuel Ash
PSH	Pseudo Strain-Hardening
PVA	Poly Vinyl Alcohol
PE	Polyethylene
PCE	Poly Carboxylate Ether
RC	Reinforced Concrete
SSD	Saturated Surface Dry
SCM	Supplementary Cementitious Material
SHCC	Strain-Hardening Cementitious Composite
SHGC	Strain-Hardening Geopolymer Composite
R/SHGC	Steel reinforced Strain-Hardening Geopolymer Composite
SP	Superplasticizer
UHPFRC	Ultra-High Performance Fiber-Reinforced Concrete
UHMWPE	Ultra-High-Molecular-Weight Polyethylene
XRF	X-Ray Fluorescence

CHAPTER 1

INTRODUCTION

1.1 Background

Concrete is the most used construction material in the world. According to Cement Sustainability Initiative: Recycling Concrete (2009), currently about 25 billion tons of concrete is manufactured annually worldwide. On the other hand, plain (unreinforced) concrete is brittle in nature with low tensile strength and tensile strain capacity. Thus, reinforcements in the forms of continuous reinforcing bars and/or fibers are required when concrete is used as the construction material. Over the last decades, there has been an increasing trend in the use of fibers, either in the form of continuous aligned fibers (Aveston and Kelly, 1973) or randomly oriented short fibers (Li and Wu, 1992), to control the cracking behavior of the material through crack bridging, which thereby offer post-cracking ductility (Bentur and Mindess, 2007).

In the recent years, significant advances have been made in the area of fiber reinforced cementitious composites (FRCCs). A special class of FRCCs that demonstrates pseudo strain-hardening (PSH) behavior under uniaxial tension accompanied by multiple fine cracks up to relatively high strain levels has been referred to as high performance fiber reinforced cementitious composites (HPFRCCs) (Naaman, 2008). Multiple cracking is desirable rather than single cracking, as it results in enhanced ductility, toughness, fracture energy, strain hardening, strain capacity, and deformation capacity under tension, compression and bending (Matsumoto and Mihashi, 2003). Among various classes of HPFRCCs, this doctoral research is focused on a particular class of HPFRCC that generally exhibits moderate tensile strength (3–8 MPa), along with strong PSH behavior and ultra-high ductility, which has been referred to as fiber-reinforced strain-hardening cementitious composite (SHCC) (van Zijl and Wittmann, 2011). Most HPFRCCs use large quantities of fibers (i.e. 4% to 20% by volume) to exhibit the PSH behavior with a tensile strain capacity of about 1% (Naaman and Reinhardt, 1995). However, based on micromechanics principles, SHCC is designed to exhibit extreme tensile ductility of up to 6% with the incorporation of small amount of discontinues fibers, typically 2% or less by volume (Kong et al., 2003). Over the years, the material characteristics of SHCC have

been studied in depth and its practical applications have been established (Li and Leung, 1992; Li, 1993; Maalej and Li, 1995; Mishra, 1995; Li and Kanda, 1998; Maalej et al., 2012; Yucel et al., 2012).

Nowadays, sustainability and concern for environmental impacts are becoming major considerations in construction industry, in particular the CO_2 emissions and embodied energy of cement and concrete. CO_2 emissions is said to be the main cause of global warming as it has contributed to about 65% of global warming (McCaffery, 2002). The cement industry is known to be responsible for some of the CO_2 emissions globally. As a rule of thumb, every one ton of cement produced would emit approximately one ton of CO_2 (Davidovits, 1991; McCaffery, 2002). In addition, cement production also requires huge amount of energy. For instance, the total energy consumption and carbon emissions associated with production of one ton of cement in USA were reported to be on average 4.8 GJ and 0.927 ton, respectively (Marceau et al., 2006). In addition to CO_2 emissions, manufacture of cement is also said to have contributed to considerable amounts of SOx, NOx, particulate matter and other pollutants (Price et al., 2001). On the other hand, according to the European Cement Association (CEMBUREAU) (2015), the world cement production has increased drastically over the recent years to 4.3 billion tons in 2014, compared to only about 10 million tons in 1900. In addition, China alone produced and used 56.5% of the world cement production in 2014. These statistics support the fact that cement is the second most utilized material by human being after water and put a clear perspective on the 5−7% of total CO_2 emissions worldwide associated with the cement production (Huntzinger and Eatmon, 2009). Therefore, the investigation on high-performance and/or environmentally sustainable alternatives to ordinary Portland cement (OPC) is a rapidly advancing field of research area.

Geopolymer is an emerging cement-less binder purported to provide an environmentally friendly and sustainable alternative to OPC. The term geopolymer was initially introduced by Davidovits (1991). Geopolymer is a class of largely X-ray amorphous aluminosilicate binder materials (Provis, 2006), which may be manufactured from materials of geological origin (e.g. metakaolin) or industrial by-products such as fly ash and slag that are rich in silica and alumina with high alkaline activators. Previous studies reported that manufacture of fly ash-based geopolymer has at least 80% less CO_2 emission and requires approximately 60% less energy compared to manufacture of OPC (Li et al., 2004; Duxson

et al., 2007). Commercial and industrial use of geopolymer concrete has become progressively widespread over the past decades as an environmentally sustainable alternative to conventional OPC concrete (Davidovits, 1991). Previous studies reported that geopolymer concrete exhibits superior properties such as higher compressive strength, chemical, fire and frost resistance to conventional OPC concrete (Provis and Van Deventer, 2009).

1.2 Statement of Problem

Material sustainability has not often been a concern in the development of HPFRCCs as high cement content is commonly found in the mixture design of several types of HPFRCCs such as slurry infiltrated fiber concrete (Lankard and Newell, 1984), ultra-high performance fiber-reinforced concrete (UHPFRC) (Nematollahi et al., 2014a; Nematollahi et al., 2014b; Nematollahi et al., 2014c; Nematollahi et al., 2016; Voo and Foster, 2010) and typical SHCC (Wang and Li, 2007) compared to conventional concrete. The cement content of typical SHCCs (with 100% cement and no fly ash) is about 830 to 1200 kg/m^3, which is typically two to three times higher than that of conventional concrete that typically uses about 390 kg of cement per cubic meter of concrete (Wang and Li, 2007). This high cement content results in high autogenous shrinkage, heat of hydration, and cost. In addition as mentioned earlier, cement manufacturing is a highly energy and emissions intensive industry. The associated increase in the CO_2 emissions and embodied energy due to the high cement content apparently compromise material sustainability performance of SHCC (Wang and Li, 2007; Yang et al., 2007). It is thereby necessary to develop green SHCCs with lower global warming potential associated with CO_2 emissions of the cement production, which maintain the desirable tensile ductility property, but also include sustainability considerations.

One of the solutions to achieve this goal is partial replacement of OPC in the SHCC mix design by supplementary cementitious materials (SCMs) such as fly ash, slag, iron ore tailings (IOTs) and palm oil fuel ash (POFA) to reduce the use of OPC, and thereby reducing the global warming potential associated with the CO_2 emission of the cement production. Within the last decade, several efforts have been made to consider the environmental sustainability aspects in the development of SHCCs through replacing a large amount of OPC by SCMs such as fly ash (Wang and Li, 2007; Yang et al., 2007),

slag (Kim et al., 2007) and IOTs (Huang et al., 2012). For instance, Wang and Li (2007) partially replaced cement in SHCC mix design by fly ash. Among the mix proportions investigated in their study, a large quantity of fly ash (with fly ash to cement ratio of 1.2) was used in PVA-SHCC mix 45 (M45), which significantly enhanced the material sustainability of the composite, yet the desirable PSH behavior of the composite was maintained. According to available literature, SHCC M45 is the most widely used SHCC mixture in the field which has been considered as the typical SHCC mixture in several studies (Yang et al., 2008).

Although SHCC M45 is more environmentally friendly than the first generation of SHCCs which use 100% cement with no fly ash, its cement content is still 1.5 times that of normal concrete (Yang et al., 2007). Among the ingredients of SHCC M45, cement is still responsible for 45.3% and 78.8% of total embodied energy and CO_2 emissions of the composite, respectively (Huang et al., 2012). This is in spite of replacing large amount of cement by fly ash in SHCC M45 (fly ash/cement =1.2). Therefore, further research is needed to improve material sustainability of SHCC, without sacrificing the desirable tensile ductility of the composite. This is the main motivation behind this doctoral research. A more sustainable approach to achieve this goal is to completely replace the OPC binder in SHCC mixture by an alternative cement-less binder such as geopolymer.

At the commencement of this doctoral research in September 2012, there was only one feasibility study available conducted by Lee et al. (2012) in South Korea, which investigated the viability of developing cement-less fiber-reinforced strain-hardening geopolymer composite (SHGC) through complete replacement of cement by 100% slag-based geopolymer as the sole binder. The slag-based SHGCs developed by Lee et al. (2012) exhibited density of 1970−2020 kg/m^3, compressive strength of 19.4−30.6 MPa, first-crack strength of 2.55−3.87 MPa, ultimate tensile strength of 2.83−4.69 MPa, and tensile strain capacity of 1.53−4.48% at 28 days, depending on the type of activator and water to binder ratio. Although the viability of developing slag-based SHGCs was demonstrated in Lee et al. (2012) study, the authors did not conduct any detail studies on micromechanical parameters such as matrix toughness and fiber-matrix interfacial properties to understand the underlying reasons for different tensile performance of the developed slag-based SHGCs.

According to Uranium Information Centre Ltd. Australia (2005), 78% of the national electricity in Australia is supplied through coal-burning power stations. In 2002, about 12.5 million tons of fly ash was produced in Australia and New Zealand, of which only 4.1 million tons was used in different applications especially in blended cement concrete (Heidrich, 2002). These statistics support the fact that fly ash is available in large quantities in Australia, which can be used as a good aluminosilicate source material for production of geopolymer. As mentioned earlier, the CO_2 emission associated with production of fly ash-based geopolymer is at least 80% less than that of the OPC production (Duxson et al., 2007). In addition, approximately 60% less energy is required for the manufacture of fly ash-based geopolymer compared to the energy required for OPC production (Li et al., 2004). Furthermore, using fly ash as an existing waste (by-product) material in production of geopolymer reduces the need for its disposal, along with better use of natural resources. Therefore, development of fly ash-based SHGCs, where the OPC binder is completely replaced by the fly ash-based geopolymer binder, results in outstanding environmental benefits which support the concept of sustainable development. However, at the start of this doctoral research there has been no study available on fly ash-based SHGCs. This doctoral research is aimed to fill this knowledge gap.

1.3 Research Objectives

According to the problem statement, the main aim of this doctoral research is to develop sustainable strain hardening composites incorporating geopolymer (in particular fly ash-based geopolymer) as the sole binder. Material sustainability of the composite is expected to be significantly enhanced compared to typical SHCCs due to greenness potential of geopolymer, yet the mechanical properties of these geopolymer composites should still be comparable to typical SHCCs. In other words, such cement-less SHGCs are purported to provide a promising sustainable alternative to typical SHCCs. They are expected to promote sustainability of the infrastructures via concurrent improvements of material greenness and infrastructure durability through ultra-high ductility and tight crack width control.

This doctoral research is aimed to provide an in-depth knowledge on properties and performance of such SHGCs and to fully understand the mechanisms governing strain

hardening behavior in these cement-less composites by conducting a series of systematic and detailed studies at different length scales using a micromechanics-based approach. The following specific objectives are set out to achieve the aforementioned aim:

(a) To evaluate the effects of matrix-related parameters including type of activator, water to geopolymer solids ratio (W/GP solids), sand size and sand content on the matrix and composite properties of fly ash-based SHGCs.

(b) To evaluate the mechanical and thermal properties of green lightweight fly ash-based SHGCs incorporating three types of lightweight aggregates as complete replacement of micro-silica sand, to achieve the following two objectives: (1) to reduce the density of the composite, and (2) to reduce the thermal conductivity of the composite.

(c) To evaluate the effects of type of activator, W/GP solids and fiber surface oil coating on the fiber-matrix interface properties of fly ash-based SHGCs. And to investigate the quantitative influence of the measured interface properties on the crack bridging $\sigma(\delta)$ relation and tensile performance of fly ash-based SHGCs using a micromechanics-based model.

(d) To verify the applicability of the available micromechanics-based model for evaluating the tensile performance of the fly ash-based SHGCs. And to demonstrate how the micromechanics-based model guides towards composite optimization and component tailoring to achieve saturated strain hardening behavior with the lowest amount of PVA fiber in fly ash-based SHGCS.

(e) To develop an ambient temperature cured one-part SHGC to enhance commercial viability of these cement-less composites.

(f) To evaluate the quantitative influences of type of fiber and curing condition on the tensile performance of one-part SHGCs using a micromechanics-based approach.

(g) To develop a sustainable lightweight composite floor incorporating one-part SHGCs.

1.4 Scope of Work and Organization of Thesis

This thesis consists of 13 chapters as follows:

Chapter 1 presents the background and the problem statement of the study. It is then followed by the objectives of the study. Chapter 2 presents the literature review of the study, which is divided into two parts. The first part provides a brief review regarding the evolution of FRCCs with special focus on SHCC materials. Constituent materials, micromechanics-based design criteria, applications and material sustainability of typical SHCCs are reviewed. The second part focuses on geopolymer technology. A brief review of terminology, chemistry and constituent materials of geopolymers are provided. A comprehensive review of previously published studies on the efficacy of superplasticizers on geopolymers is then provided. The properties of geopolymer and conventional concrete are broadly compared. A brief review of published thesis on fly ash-based geopolymer is also presented. The studies on developing sustainable cement-less SHGCs which have been available before the submission of this thesis are also reviewed. Chapter 3 investigates the effect of six different commercial SPs on the workability and compressive strength of a low calcium fly ash-based geopolymer paste activated by two different activator combinations. The activators investigated include 8.0 M NaOH solution and a multi-compound activator composed of 8.0 M NaOH and Na_2SiO_3 solutions with Na_2SiO_3/NaOH mass ratio of 2.5.

The rest of this doctoral thesis is organized into two main parts, namely Part I and Part II. Part I is comprised of five chapters (i.e. Chapters 4 to 8). This part is focused on the development of heat cured two-part fly ash-based SHGCs. Objective (a) motivates Chapters 4 and 5. In Chapter 4, four different activator combinations were selected to evaluate the effects type of activator on the matrix and composite properties of fly ash-based SHGCs. They include two sodium-based (Na-based) and one potassium-based (K-based) activator combinations in the form of solution and one lime-based activator combination in the form of powder. Only fly ash (with no sand) was used in the matrix of the fly ash-based SHGC developed in this chapter. This was similar to the first generation of SHCCs where only OPC and silica fume (with no sand) were used in the matrix (Li et al., 1995; Kanda and Li, 1999). The best performing activator in terms of tensile performance of the composite was therefore identified in this chapter. In Chapter

5, two values of W/GP solids and two different sand sizes with two values of sand to fly ash ratio by mass were selected to evaluate the effects of W/GP solids (i.e. water content) as well as sand size and sand content (i.e. sand to fly ash ratio) on the matrix and composite properties of fly ash-based SHGCs made by using the best performing activator identified in Chapter 4. The best performing mixture with the appropriate W/GP solids, sand size and sand content was identified in this chapter.

Objective (b) motivates Chapter 6. Three types of lightweight aggregates including expanded perlite, microscopic hollow ceramic spheres and expanded recycled glass were selected to be used as complete replacement of micro-silica sand in the best performing mixture identified in Chapter 5. The aims were to reduce the density and thermal conductivity of the composite. The mechanical and thermal properties of lightweight fly ash-based SHGCs were determined. Objective (c) motivates Chapter 7, where the focus is placed on the microscale investigation of fly ash-based SHGCs. The investigation involved experimental determination of the fiber-matrix interaction properties using single-fiber pullout tests. Subsequently, the effects of the measured interface properties on the crack bridging $\sigma(\delta)$ relation and tensile performance of fly ash-based SHGCs were quantitatively investigated via a micromechanics-based model. Objective (d) motivates Chapter 8. The applicability of the available micromechanics-based model for design of fly ash-based SHGCs was investigated. This model was originally developed by Yang et al. (2008) for design of SHCCs. Subsequently, different scenarios were discussed to illustrate how that micromechanical model can be used for systematic optimization of the fly ash-based PVA-SHGCs to achieve optimal composite tensile performance with the lowest volume fraction of PVA fibers.

Part II of this thesis is comprised of four chapters, (i.e. Chapters 9 to 12). This part is focused on the development of ambient temperature cured one-part SHGCs. Objective (e) motivates Chapters 9 and 10. In Chapter 9, the focus is placed to manufacture a suitable ambient temperature cured one-part geopolymer matrix with desirable mechanical properties, moderate setting time and adequate rheology for uniform fiber dispersion. In Chapter 10, the best performing ambient temperature cured one-part geopolymer matrix is used to develop the ambient temperature cured one-part SHGC based on the micromechanics-based design principles of SHCC. Objective (f) motivates Chapters 11. A one-part SHGC reinforced by ultra-high-molecular-weight polyethylene (UHMWPE, henceforth referred to as PE) fibers was manufactured. The quantitative

influences of curing condition, namely heat and ambient temperature curing, on the macroscale properties of the matrix and composite were evaluated. The results of the ambient temperature cured one-part PVA-SHGC developed in Chapter 10 are used as the benchmark, enabling us to also investigate the quantitative influences of type of fiber, viz. hydrophilic PVA fiber and hydrophobic PE fiber, on the macroscale properties of the matrix and composite. Objective (g) motivates Chapters 12. A precast lightweight composite floor manufactured from one-part SHGC and lightweight purlin sections is developed.

Finally, Chapter 13 reviews the major conclusions and contributions of this doctoral research. Further, recommendations for the future works are also presented.

1.5 References

AVESTON, J. & KELLY, A. 1973. Theory of multiple fracture of fibrous composites. *Journal of Materials Science,* 8, 352-362.

BENTUR, A. & MINDESS, S. 2007. *Fibre reinforced cementitious composites*, Taylor & Francis.

CEMENT SUSTAINABILITY INITIATIVE: RECYCLING CONCRETE. 2009. The World Business Council for Sustainable Development (WBCSD). DOI: 978-3-940388-49-0.

DUXSON, P., PROVIS, J. L., LUKEY, G. C. & VAN DEVENTER, J. S. 2007. The role of inorganic polymer technology in the development of 'green concrete'. *Cement and Concrete Research,* 37, 1590-1597.

EUROPEAN CEMENT ASSOCIATION (CEMBUREAU). 2015. Figures of World Cement Production 2014 by region and main countries. Retrieved 12 June 2015, from http://www.cembureau.be/sites/default/files/Worldcementproduction2014byregionandmaincountries.pdf.

HEIDRICH, C. Ash Utilisation-An Australian Perspective. Geopolymers 2002 International Conference 2002 Melbourne, Australia.

HUANG, X., RANADE, R. & LI, V. C. 2012. Feasibility study of developing green ECC using iron ore tailings powder as cement replacement. *Journal of Materials in Civil Engineering,* 25, 923-931.

HUNTZINGER, D. N. & EATMON, T. D. 2009. A life-cycle assessment of Portland cement manufacturing: comparing the traditional process with alternative technologies. *Journal of Cleaner Production,* 17, 668-675.

KIM, J.-K., KIM, J.-S., HA, G. J. & KIM, Y. Y. 2007. Tensile and fiber dispersion performance of ECC (engineered cementitious composites) produced with ground granulated blast furnace slag. *Cement and Concrete Research,* 37, 1096-1105.

KONG, H.-J., BIKE, S. G. & LI, V. C. 2003. Development of a self-consolidating engineered cementitious composite employing electrosteric dispersion/stabilization. *Cement and Concrete Composites,* 25, 301-309.

LANKARD, D. R. & NEWELL, J. K. 1984. Preparation of highly reinforced steel fiber reinforced concrete composites. *Special Publication,* 81, 287-306.

LEE, B. Y., CHO, C.-G., LIM, H.-J., SONG, J.-K., YANG, K.-H. & LI, V. C. 2012. Strain hardening fiber reinforced alkali-activated mortar–a feasibility study. *Construction and Building Materials,* 37, 15-20.

LI, V. C. 1993. From micromechanics to structural engineering—The design of cementitious composites for civil engineering applications. *Journal of Structural Mechanics and Earthquake Engineering,* 10, 37-48.

LI, V. C. & KANDA, T. 1998. Innovations Forum: Engineered cementitious composites for structural applications. *Journal of Materials in Civil Engineering,* 10, 66-69.

LI, V. C. & LEUNG, C. K. 1992. Steady-state and multiple cracking of short random fiber composites. *Journal of Engineering Mechanics,* 118, 2246-2264.

LI, V. C. & WU, H.-C. 1992. Conditions for pseudo strain-hardening in fiber reinforced brittle matrix composites. *Applied Mechanics Reviews,* 45, 390-398.

LI, Z., DING, Z. & ZHANG, Y. 2004. Development of sustainable cementitious materials. *International workshop on sustainable development and concrete technology, Beijing, China.*

MAALEJ, M. & LI, V. C. 1995. Introduction of strain-hardening engineered cementitious composites in design of reinforced concrete flexural members for improved durability. *Structural Journal,* 92, 167-176.

MAALEJ, M., QUEK, S., AHMED, S., ZHANG, J., LIN, V. & LEONG, K. 2012. Review of potential structural applications of hybrid fiber Engineered Cementitious Composites. *Construction and Building Materials,* 36, 216-227.

MARCEAU, M., NISBET, M. A. & VAN GEEM, M. G. 2006. Life cycle inventory of portland cement manufacture. Portland Cement Association Skokie, IL, US.

MATSUMOTO, T. & MIHASHI, H. 2003. DFRCC terminology and application concepts. *Journal of Advanced Concrete Technology,* 1, 335-340.

MCCAFFREY, R. 2002. Climate change and the cement industry. *Global cement and lime magazine (environmental special issue),* 15-19.

MISHRA, D. 1995. *Design of pseudo strain-hardening cementitious composites for a ductile plastic hinge.* Ph.D. Thesis, University of Michigan.

NAAMAN, A. E. 2008. High Performance Fiber Reinforced Cement Composites. *Engineering Materials for Technological Needs High-Performance Construction Materials Science and Applications.* World Scientific Publishing Co. Pte. Ltd.

NAAMAN, A. E. & REINHARDT, H. W. 1995. Characterization of high performance fiber reinforced cement composites. *International RILEM Workshop on High Performance Fiber Reinforced Cement Composites (HPFRCC2).* Bagneux, France.

NEMATOLLAHI, B., SAIFULNAZ, M. R. & VOO, Y. L. 2014a. Sustainability assessment of precast ultra-high performance fiber reinforced concrete (UHPFRC) cantilever retaining walls. *Research Journal of Applied Sciences, Engineering and Technology,* 7, 3971-3977.

NEMATOLLAHI, B., VOO, Y. L. & SAIFULNAZ, M. R. R. 2014b. Structural Behavior of Precast Ultra-High Performance Fiber Reinforced Concrete (UHPFRC) Cantilever Retaining Walls: Part I-Analysis and Design Procedures and Environmental Impact Calculations (EIC). *KSCE Journal of civil engineering,* 18, 1470-80.

NEMATOLLAHI, B., VOO, Y. L. & SAIFULNAZ, M. R. R. 2014c. Structural behavior of precast Ultra-High Performance Fiber Reinforced Concrete (UHPFRC) cantilever retaining walls: Part II—Full scale experimental testing. *KSCE Journal of civil engineering,* 18, 1481-1495.

NEMATOLLAHI, B., VOO, Y. L. & SANJAYAN, J. 2016. Design and Construction of a Precast Ultra-High Performance Concrete Cantilever Retaining Wall. *First International Interactive Symposium on UHPC – 2016.* Des Moines, Iowa.

PRICE, L., WORRELL, E., GALITSKY, C. & PRICE, L. 2008. Energy Efficiency Improvement Opportunities for the Cement Industry. Ernest Orlando Lawrence Berkeley National Laboratory, Berkeley, CA (US).

PROVIS, J. L. 2006. *Modelling the formation of geopolymers.* Ph.D. Thesis, University of Melbourne.

PROVIS, J. L. & VAN DEVENTER, J. S. J. 2009. *Geopolymers: structures, processing, properties and industrial applications,* Cambridge (UK), Woodhead Publishing.

URANIUM INFORMATION CENTER LTD. AUSTRALIA. 2005. Nuclear Energy Prospects in Australia. Retrieved 12 June 2006, from http://www.uic.com.au/nip44.htm.

VAN ZIJL, G. P. A. G. & WITTMANN, F. H. (eds.) 2011. *Durability of Strain-Hardening Fibre-reinforced Cement-based Composites (SHCC): RILEM State of the Art Report* Springer.

VOO, Y. L. & FOSTER, S. J. 2010. Characteristics of ultra-high performance 'ductile'concrete and its impact on sustainable construction. *The IES Journal Part A: Civil & Structural Engineering,* 3, 168-187.

WANG, S. & LI, V. C. 2007. Engineered cementitious composites with high-volume fly ash. *ACI Materials Journal-American Concrete Institute,* 104, 233-241.

YANG, E.-H., WANG, S., YANG, Y. & LI, V. C. 2008. Fiber-bridging constitutive law of engineered cementitious composites. *Journal of advanced concrete technology,* 6, 181-193.

YANG, E.-H., YANG, Y. & LI, V. C. 2007. Use of high volumes of fly ash to improve ECC mechanical properties and material greenness. *ACI materials journal,* 104, 620-628.

YUCEL, H. E., JASHAMI, H., SAHMARAN, M., GULER, M. & YAMAN, I. O. 2013. Thin ECC overlay systems for rehabilitation of rigid concrete pavements. *Magazine of Concrete Research,* 65, 108-120.

CHAPTER 2

LITERATURE REVIEW

2.1 Introduction

The first part of this chapter briefly provides a literature review on FRCCs. In particular, emphasis is placed on SHCC which is the main focus of this doctoral research. Constituent materials, micromechanics-based design criteria, application and material sustainability performance of SHCC materials are briefly reviewed. As mentioned in Chapter 1, a more sustainable approach to develop green SHCCs is to completely replace the OPC binder in SHCC mix proportion with a geopolymer binder. Therefore, the second part of this chapter focuses on geopolymer technology. Terminology, chemistry, constituent materials of geopolymers are briefly presented. Subsequently, a state-of-the-art review on efficacy of available superplasticizers on geopolymers, along with a general comparison between geopolymer and conventional OPC concrete are presented. This is then followed by a brief review of published thesis on low calcium fly ash-based geopolymer concrete. Finally, the available studies on developing green SHCCs incorporating a geopolymer binder are reviewed.

2.2 Fiber Reinforced Cementitious Composite

Concrete is the most widely used construction material in the world, with approximately 25 billion tons of concrete manufactured annually worldwide (Cement Sustainability Initiative: Recycling Concrete, 2009). However, plain, unreinforced cementitious materials such as cement paste, mortar and concrete are brittle in nature with low tensile strengths and tensile strain capacities. Therefore, reinforcement is needed when plain cementitious materials are used as construction material. Continuous reinforcing bars have been traditionally used as the reinforcement in the structure at the proper locations to resist the imposed tensile and shear stresses (Bentur and Mindess, 2007). On the other hand, there has been a steady increase over the last 40 years in the use of FRCCs. In FRCCs fibers, either in the form of continuous aligned fibers (Aveston et al., 1973) or randomly oriented short fibers (Li and Wu, 1992), are used to modify the brittle behavior of plain cementitious materials. It is essential to note that the use of fibers as reinforcement is not generally considered as an alternative to “conventional” steel bars.

Continuous reinforcing bars and fibers are used for different purposes. Indeed, there are many applications, where both fibers and continuous steel bars are to be used simultaneously. It should be pointed out that the use of fibers are not intended to enhance the strength, although strength of the material could also moderately increased. In fact, fibers are mainly used to control the cracking of the material and modify the brittle behavior of plain cementitious materials after cracking of the matrix via bridging across these cracks, and thereby offer post-cracking ductility (Bentur and Mindess, 2007).

As illustrated in Figure 2-1, for practical purposes and mechanical modeling, FRCCs are usually defined as composites with two primary constituents, namely the matrix and the reinforcing fiber (Naaman, 2008). Although the matrix may itself be a composite material with some constituents, it is presumed to represent the first main constituent of the FRCCs. The matrix is presumed to comprise all the additives and aggregates specified, depending whether it is a paste, mortar, or concrete. In addition, entrapped air voids in the matrix are considered to be part of the matrix. In the context of this doctoral research, the fiber as the second main component of the FRCCs, is considered to be discontinuous and randomly distributed within the composite volume. Thanks to fiber-matrix interface bond, the fiber and the cementitious matrix both work together to make the FRCCs (Naaman, 2008).

In the literature, FRCCs are categorized based on different parameters. For instance, as illustrated in Figure 2-2, Japan Society of Civil Engineers (JSCE) presents a classification for FRCCs, in which different classes of FRCCs are categorized based on their strength and ductility level (Recommendations for Design and Construction of High Performance Fiber Reinforced Cement Composites with Multiple Fine Cracks (HPFRCC), 2008). Among different classes of FRCCs, terminology and scope of ductile fiber reinforced cementitious composites (DFRCCs) and HPFRCCs which are of particular interests are outlined in the following sub-sections.

2.2.1 Ductile fiber reinforced cementitious composite

Conventional fiber reinforced concrete (FRC), similar to plain cementitious materials (cement, mortar and concrete) exhibits an immediate stress drop after first cracking. In DFRCC, on the other hand, multiple cracking with increasing load occurs and an immediate stress drop after first cracking is prevented. Therefore, DFRCC has higher

deflection capacity at peak load in comparison to conventional FRCs, which characterized by deflection hardening in bending after first cracking, accompanied by multiple cracks.

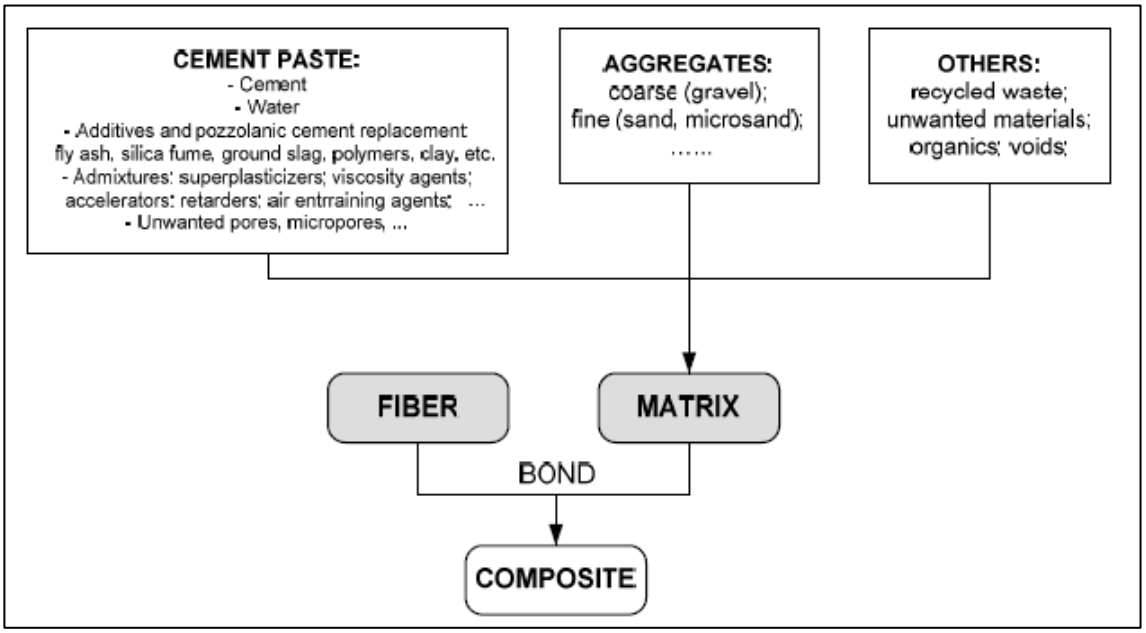

Figure 2-1: FRCC is defined as a composite with two main components, namely the matrix and the fiber (Source: Namaan, 2008)

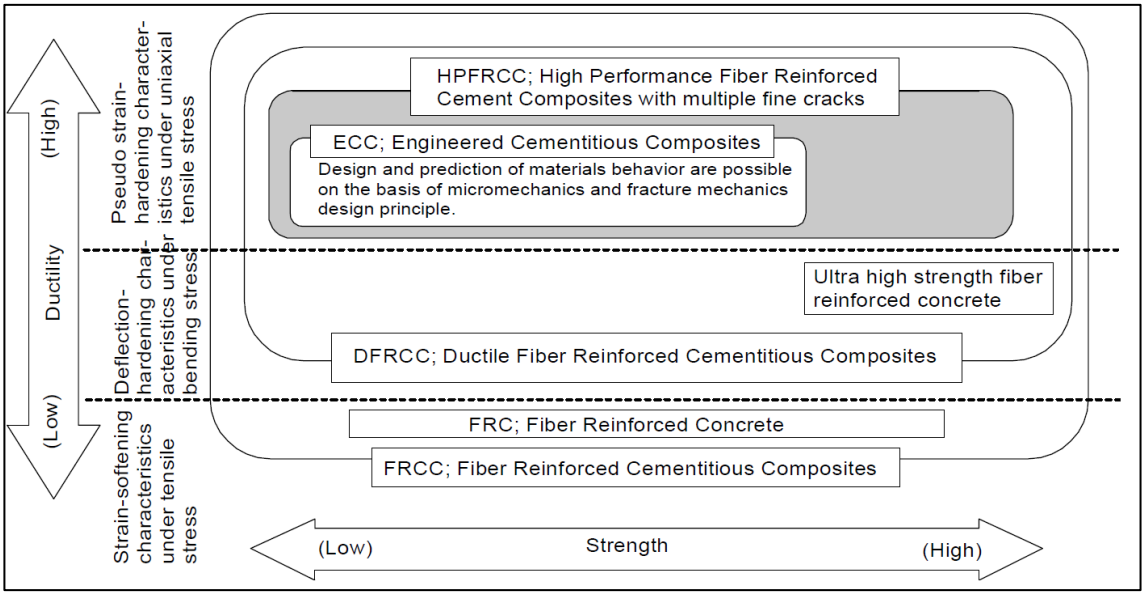

Figure 2-2: Classification of FRCCs According to Recommendations for Design and Construction of High Performance Fiber Reinforced Cement Composites with Multiple Fine Cracks (HPFRCC) (2008)

According to Japan Concrete Institute on DFRCCs (JCI-DFRCC) Committee's terminology, DFRCC is a class of FRCCs which exhibits multiple cracking (Matsumoto and Mihashi, 2003), unlike conventional FRCs which exhibit one single crack. Multiple cracking is a desirable feature leading to development in properties such as ductility, toughness, fracture energy, strain hardening, strain capacity, and deformation capacity under tension, compression and bending (Matsumoto and Mihashi, 2003).

2.2.2 High performance fiber reinforced cementitious composite

A special class of FRCCs designed to exhibit strain hardening behavior under uniaxial tension accompanied by multiple fine cracks up to relatively high strain levels has been referred to as HPFRCCs (Naaman, 2008). As shown in Figure 2-2, HPFRCC is a narrower class of materials than DFRCC. HPFRCC is a FRCC that shows multiple cracking and strain hardening behavior in direct tension, and thereby in bending (Naaman, 2008). However, DFRCC comprises a group of FRCCs that exhibits multiple cracking in bending only.

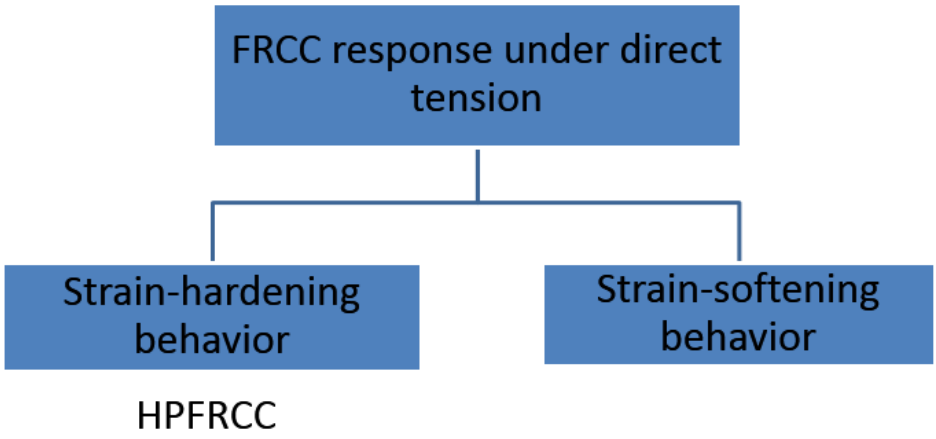

Figure 2-3: Simple classification of FRCC based on their tensile stress-strain response

One approach proposed by Naaman (2008) to determine whether a FRCC can be classified as HPFRCC is based on the shape of its stress-strain response under direct tension. As illustrated in Figures 2-3 and 2-4(b), if the tensile stress-strain curve of the composite under direct tension exhibits strain hardening or pseudo-strain hardening

behavior after first cracking, the FRCC is classified as HPFRCC. Otherwise, a conventional FRCC exhibits immediate drop in tensile stress after first cracking characterized by strain-softening response, as illustrated in Figures 2-3 and 2-4(a). In other words, it can be said that the shape of the stress-strain curve of HPFRCCs in direct tension is comparable or superior to elastic-perfectly plastic behavior (Naaman, 2008). The term "pseudo strain-hardening behavior" is introduced to highlight the difference in mechanism with strain hardening behavior generally observed in metallic materials after yielding (Recommendations for Design and Construction of High Performance Fiber Reinforced Cement Composites with Multiple Fine Cracks (HPFRCC), 2008).

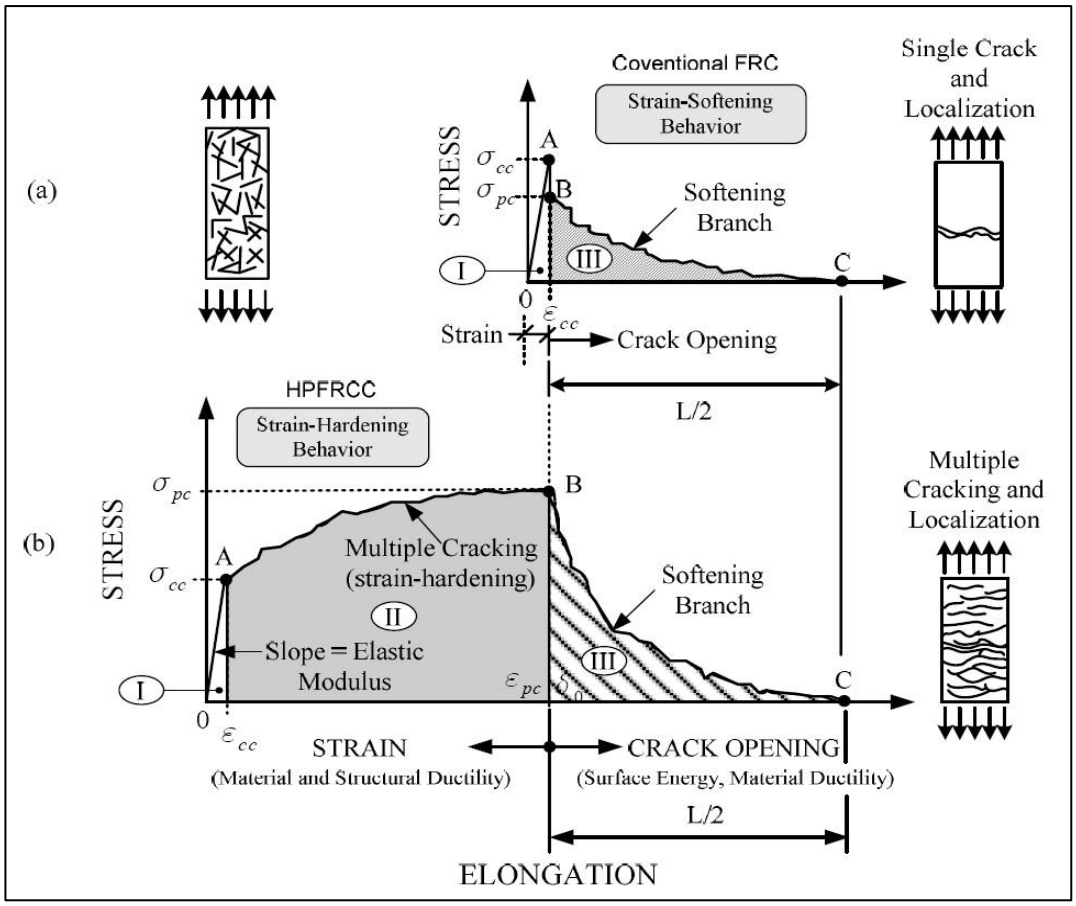

Figure 2-4: Typical stress-strain or stress-elongation curve in tension up to complete separation in (a) Conventional strain softening FRCC, and (b) Strain hardening FRCC or HPFRCC (Source: Naaman, 2008)

Figure 2-5 presents the classification of FRCCs based on their stress-strain response under direct tension and their implication for flexural response of structural elements. As can be seen, it can be said that (1) all strain hardening FRCCs (i.e. HPFRCCs) result in deflection hardening structural elements, (2) a tensile strain softening FRCCs can exhibit either deflection hardening or deflection softening behaviors in bending (Naaman, 2008).

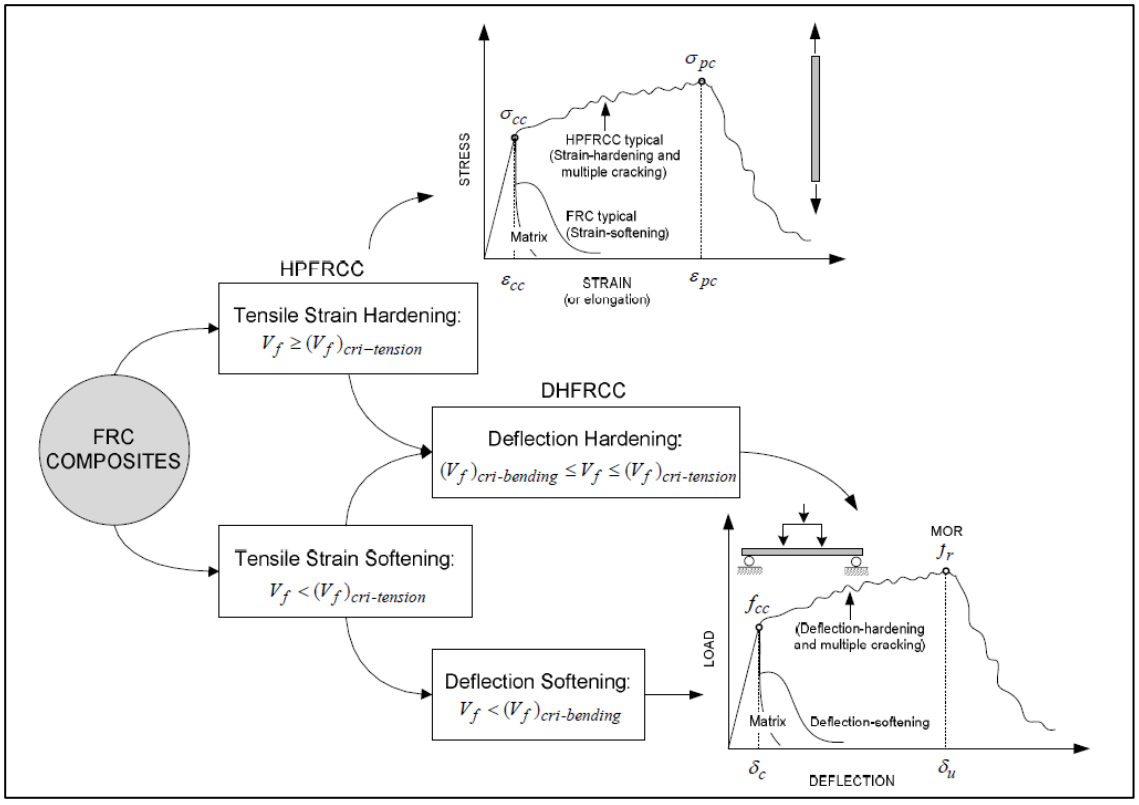

Figure 2-5: Classification of FRCCs based on their tensile response and implication for bending response of structural elements (Source: Naaman, 2008)

Over the years significant interests have been demonstrated by several researchers around the world in the area of HPFRCC, leading to development of various classes of HPFRCC. The focus of this doctoral research is on a particular class of HPFRCC with generally moderate tensile strength (3–8 MPa), but with strong PSH behavior and ultra-high ductility, which has been referred to as fiber-reinforced SHCC (van Zijl and Wittman, 2011). The focus of the following section is on such SHCC materials.

2.3 Strain Hardening Cementitious Composite

While most HPFRCCs employ large amounts of fiber (i.e. 4% to 20% by volume) to exhibit PSH behavior with a tensile ductility of about 1% (Naaman and Reinhardt, 1995), SHCC is a special class of HPFRCCs which utilizes a small amount of discontinues fibers (typically 2% or less by volume) and exhibits very high tensile strain capacity up to 6% (Li and Kanda, 1998; Kong et al., 2003). As can be seen in Figure 2-6, SHCC demonstrates multiple finely spaced cracks with tight crack width (typically below 100 μm) in the strain hardening stage (van Zijl and Wittman, 2011). SHCCs with such superior uniaxial tensile performance, yet low volume fraction of fibers can be engineered based on micromechanics and fracture mechanics principles (Li, 1998). This has resulted in introduction of the term "Engineered Cementitious Composites; ECC" by Professor Victor Li and co-workers (Li and Leung, 1992) at the University of Michigan for such SHCC materials. In the following sub-sections, the constituent materials, micromechanics-based design criteria, applications and material sustainability of SHCC materials are reviewed.

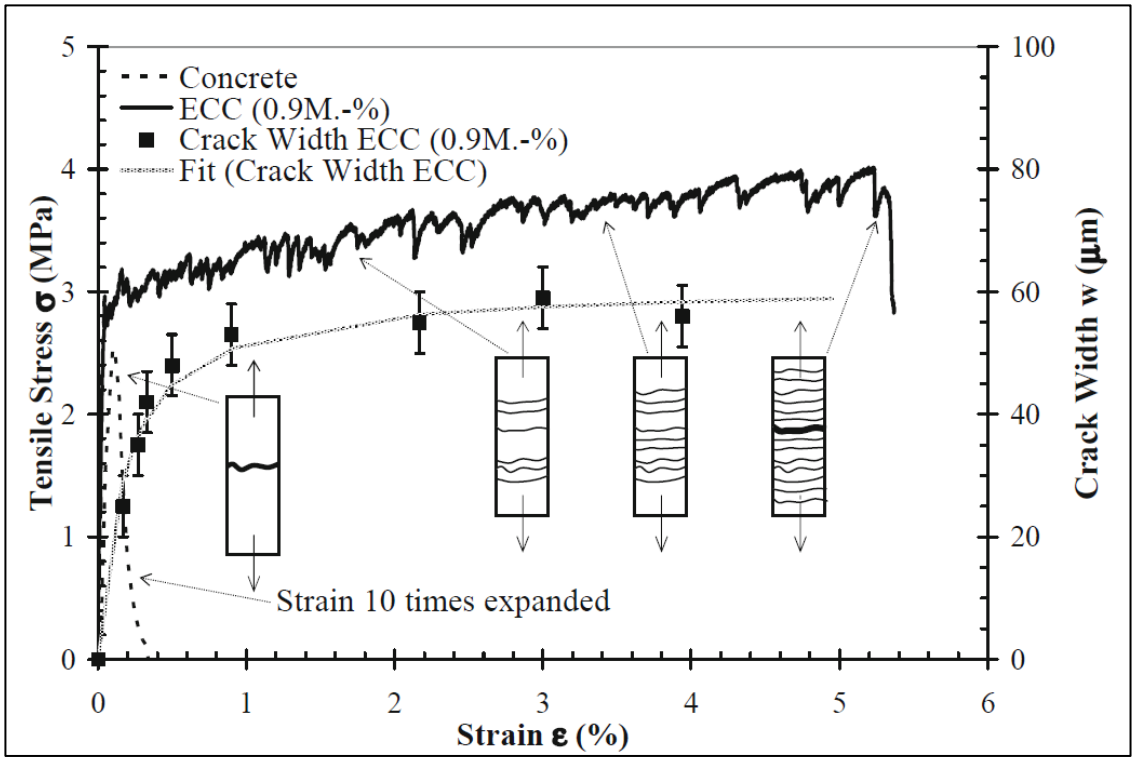

Figure 2-6: Direct tensile stress-strain response of SHCC with tight crack width control (Source: Weimann and Li, 2003; van Zijl and Wittman, 2011)

2.3.1 Constituent materials of SHCC

SHCC similar to the most FRCCs uses the same ingredients such as OPC, fine sand, water, a small amount of admixtures (superplasticizer and viscosity modifying agent), except coarse aggregates. Inclusion of coarse aggregates increases the matrix fracture toughness, which in turn adversely affects the desirable PSH behavior of the composite. The water to cement ratio (W/C) and sand to cement ratio (S/C) used in typical SHCC mixtures are usually equal to 0.5 or lower (Li and Kanda, 1998). Although the composite is designed for structural applications, as mentioned earlier a relatively small amount (2% or less by volume) of short fibers are generally used in the mix design and the composite exhibits very high ductility with a tensile strain capacity of up to 6% (Li and Kanda, 1998; Kong et al., 2003). This is one of the advantages of SHCC over some HPFRCCs which utilize large quantities of fibers (i.e. 4% to 20% by volume) to exhibit PSH behavior with a tensile ductility of about 1% (Naaman and Reinhardt, 1995). The mixing procedure of SHCC is similar to that of normal concrete, thanks to the use of relatively small amount of chopped fibers. The commercial viability and economic advantages of SHCC in particular structural applications have been demonstrated in some proprietary studies (Li and Kanda, 1998). While several types of fibers can be used in SHCC, poly vinyl alcohol (PVA) and high modulus polyethylene (PE) fibers are the most common types of fibers used in SHCC mix proportions. It should be noted that the correct mix proportion of the composite is governed by micromechanics-based principles. In other words, in order to achieve the desirable tensile ductility in the composite, the combination of the matrix, fiber and interface properties must meet the micromechanics-based design criteria for PSH behavior (Li, 1998; Kanda and Li, 1998).

2.3.2 Micromechanics-based design criteria of SHCC

The strategy to design strain hardening behavior in short fiber reinforced brittle matrix composites is based on realizing and tailoring the interaction between matrix, fiber and fiber-matrix interface. Micromechanics is an effective tool to establish the links between material microstructures and composite properties (Yang et al., 2010). In fiber reinforced brittle matrix composite the PSH behavior is due to sequential development of matrix multiple cracking. An essential requirement for the multiple cracking behavior is that steady-state cracking prevails under tension (Yang et al., 2008). In other words, the crack

initiated from a defect site, such as air bubbles and other micro-scale heterogeneities, must propagate in a flat crack mode instead of modified Griffith crack mode. In steady-state flat crack extension, the ambient loading and the crack opening remain constant and bridging fibers sustain and transfer the load without rupturing and diminishing. Additional loading results in another micro-crack initiation from another defect site and subsequent flat crack extension. Repeated formation of such steady-state cracks lead to multiple cracking and PSH behavior of the composite (Yang et al., 2008). Predominance of modified Griffith crack mode over flat crack mode results in infinite increase of crack opening behind the crack tip and eventually exhausting the fiber bridging capacity due to either fiber pullout or rupture. Since the bridging stress reduces, no further crack can be initiated afterward resulting in tension-softening behavior with large opening of a single crack (Wang, 2005).

The condition for steady-state cracking was analyzed by Marshall and Cox (1998) using J-integral method. When fiber bridging behavior is characterized by bridging stress-crack opening σ(δ) relation, the condition for steady-state cracking, often referred as energy-based condition for PSH behavior, can be expressed in the following simple form:

$$J_{tip} \leq \sigma_0 \delta_0 - \int_0^{\delta_0} \sigma(\delta)\, d\delta \equiv J_b' \tag{2.1}$$

where J_b' is the complementary energy calculated from the σ(δ) curve of the composite, σ_0 is the maximum bridging stress corresponding to the crack opening δ_0 and J_{tip} is the crack tip toughness which for small fiber volume fraction can be approximated from the following equation:

$$J_{tip} = \frac{K_m^2}{E_m} \tag{2.2}$$

where K_m and E_m are the fracture toughness and elastic modulus of the matrix, respectively (Li et al., 1995). The energy-based condition for PSH behavior represented by Equation (2.1) is obtained by considering the energy changes during steady-state flat crack propagation (Li et al., 2001). The area under the σ(δ) curve shows the energy consumed by fiber bridging action per unit crack advance. On the other hand, the J_b' represents the net energy available for crack propagation. In other words, J_b' is the difference between energy supplied by external work and energy consumed by fiber

bridging action. However, J_{tip} is understood as the matrix crack toughness resisting the crack propagation. Equation (2.1), thereby, expresses that the maximum energy available for steady-state flat crack propagation must exceed the energy required for matrix break down (Kanda and Li, 2006). Such energy balance concept is schematically illustrated in Figure 2-7. The energy-based condition for PSH behavior determines the crack propagation mode (steady-state flat crack mode or modified Griffith crack mode) (Yang et al., 2010).

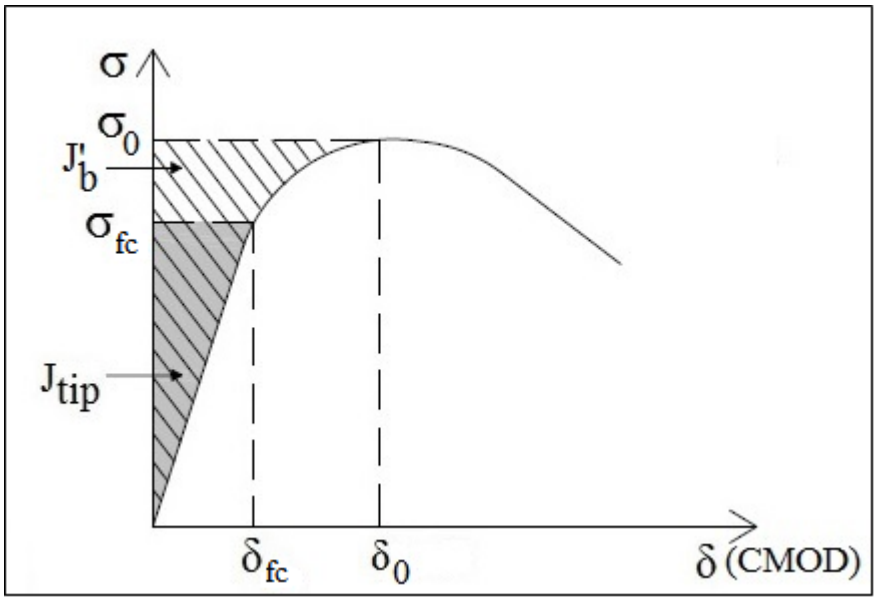

Figure 2-7: Typical σ(δ) curve of strain hardening composites. Hatched area represents complementary energy and shaded area represents crack tip toughness

Another condition for PSH behavior is that the tensile first cracking strength (σ_{fc}) must not exceed the maximum fiber bridging strength (σ_0). This condition, often referred as the strength-based condition, can be expressed in the following form:

$$\sigma_{fc} \leq \sigma_0 \tag{2.3}$$

where σ_{fc} is determined by the pre-existing flaw size and K_m (Li et al., 2001). When a brittle matrix shows PSH behavior, the ultimate tensile strength of the composite (σ_{cu}) coincides with the σ_0. Satisfaction of Equation (2.3) ensures initiation of a micro-crack from a defect site at a load level below the fiber bridging capacity. In other words, the

strength-based condition governs the initiation of cracks. Both criteria namely strength-based and energy-based conditions must be satisfied in order to achieve strain hardening composite; otherwise, conventional fiber reinforced concrete exhibiting tension softening behavior results (Yang et al., 2008). It should be noted that from a standard point of view, usually a fiber reinforced material can be regarded as strain hardening in tension, not only if it is able to satisfy the two conditions synthesized in the Equations (2.1) and (2.3), but also if the average ultimate tensile strain of the composite material is larger than at least 0.5% (Recommendations for Design and Construction of High Performance Fiber Reinforced Cement Composites with Multiple Fine Cracks (HPFRCC), 2008).

Due to the random nature of fiber distribution and the pre-existing flaw size in fiber reinforced composite, sufficient margin between σ_0 and σ_{fc} as well as J_b' and J_{tip} ensures the possibility of PSH behavior (Yang et al., 2010). Thus, to quantitatively evaluate the margin, two PSH performance indices namely stress-performance index (σ_0/σ_{fc}) and energy-performance index (J_b'/J_{tip}) were proposed (Kanda and Li, 2006). To achieve PSH behavior in a fiber reinforced composite both PSH performance indices have to theoretically exceed unity. The higher the values of the performance indices, the greater the possibility of saturated multiple cracking and PSH behavior leading to higher tensile strain capacity of the composite. Unsaturated PSH behavior often results in small tensile strain capacity and large variation in tensile ductility of the composite (Yang et al., 2010). Higher energy-performance index (J_b'/J_{tip}) can be achieved by either reducing J_{tip} which is correlated to K_m as shown in Equation (2.2), or increasing J_b'. Reducing J_{tip} is more desirable because low J_{tip} (i.e. K_m) indicates low first crack strength (Li et al., 2001). Kanda and Li (2006) demonstrated experimentally that PSH performance indices $\sigma_0/\sigma_{fc} > 1.3$ and $J_b'/J_{tip} > 2.7$ ensures saturated PSH behavior in PVA-SHCC.

2.3.3 Applications of SHCC

2.3.3.1 Structural applications

So far several studies have been conducted on the application of SHCCs in structural members such as in shear wall retrofitting of reinforced concrete (RC) buildings, in shear members subjected to cyclic loading, in mechanical fuse elements in beam-column connections, in RC beams as durable cover for reinforcement corrosion control, and in

general structural concrete repair (Li and Kanda, 1998). Some of these investigations are highlighted in the following to demonstrate the potential applicability of SHCC in structural members.

Kanda et al. (1998) investigated the flexural strength and ductility of PVA-SHCC beams reinforced with conventional reinforcements (R/SHCC) under cyclic loading. A four-point bending test setup was used in their study where the mid-span was subjected to fully reversed uniform shear load. The parameters under investigation were the span to depth ratio and the amount of shear reinforcement. The R/SHCC specimens demonstrated significantly (about four times) higher crack density than that of the control specimens made with conventional RC of comparable compressive strength. While the crack opening in control RC specimens were in the range of mm, almost all cracks in R/SHCC specimens had a crack width of 0.1 mm. The results indicated that replacing conventional RC by R/SHCC resulted in 50% increase in load capacity of shear beam specimens under both shear tension and shear compression failure modes. In addition, the ultimate deformation of shear beams increased by 200% under shear tension failure mode, while it remained constant under shear compression failure mode. Kanda et al. (1998) concluded that R/SHCC specimens have superior shear performance (in terms of load capacity, ductility and crack control) to conventional RC specimens. The R/SHCC specimens demonstrated ductile behavior even with no transverse reinforcements and short shear span, whereas RC specimens with short shear span are known to have brittle failure. In summary, it can be said that Kanda et al. (1998) study established the application of SHCC in structural shear members.

Mishra (1995) studied the application of SHCC in the hinging zone of a beam-column connection. He concluded that in a PE-SHCC connection with normal detailing the hysteretic loops were fuller with many more load cycles sustained. The total energy absorption of PE-SHCC connection was thereby significant (2.8 times) higher than that of the control RC specimen. He reported that the cracking pattern of PE-SHCC connection was similar to those explained above in the Kanda et al. (1998) study. As designed, the damage was initiated inside the hinge zone, thanks to the lower first crack strength of SHCC used in that study. In summary, it can be said that Mishra (1995) study established the feasibility of using SHCC as a mechanical fuse in critical structural members subjected to extreme dynamic loads such as earthquake (Li and Kanda, 1998).

Kabele et al. (1997) used a finite element model simulating rigidly jointed shear panels to numerically investigate the application of a PVA-SHCC in precast shear panels for building wall retrofits. Later on Kanda et al. (1998) conducted an experimental study to investigate the same using a material constitutive model that captures the PSH behavior of SHCC. They reported that the PVA-SHCC shear panels exhibited superior performance (in terms of load and deformation capacity) to control specimens made with plain concrete, resulting in enhanced structural strength and ductility of SHCC panels. This is attributed to the ability of SHCC to relax and redistribute the damage at the joints to the interior of the shear panel (Li and Kanda, 1998). Kanda et al. (1998) also demonstrated that localized fracture in a shear test of a dry joint using steel bolt can be prevented by replacing plain concrete by SHCC.

Qudah and Maalej (2014) investigated the feasibility of using a PE-SHCC to improve the performance of beam–column connections under reverse cyclic loading. Nine one-third scale specimens were tested by simulating seismic excitation at a zone of high seismicity. The parameters under investigation were the amount and arrangement of transverse reinforcements, and the materials within the plastic zone of the connection. They concluded that using PE-SHCC in the plastic zone of beam-column connection as alternative to plain concrete and partial replacement of transverse reinforcement significantly improved the shear resistance, energy absorption capacity and cracking behavior of the beam-column connection. The significantly enhanced joint seismic resistance results in reducing reinforcement congestion and construction complexity in this type of connection.

2.3.3.2 Non-structural applications of SHCC

Some studies have also been conducted so far on the application of SHCC in non-structural members. For instance, Maalej and Li (1995) investigated the application of a PE-SHCC as a protective layer to improve the corrosion durability of RC structures. They reported that the presence of multiple fine cracks and the anti-spalling properties of PE-SHCC makes it a suitable material for enhancing the corrosion resistance of RC structures. Lim and Li (1997) reported that the deterioration mechanism of delamination and spalling of the repair material can be eliminated when SHCC is used a repair material in RC structures, thanks to its novel kink-crack trapping behavior.

According to Li and Kanda (1998), SHCC can also be used in high energy absorption structures or devices such as short columns, dampers, joints for steel elements and connections for hybrid steel/RC structures. In addition, thanks to the isotropic energy absorption behavior of SHCC, it could also be used in those structures that are subjected to impact or 3D loading such as such as highway pavements, bridge decks and blast-resistant building core elements (Li and Kanda, 1998). Another potential application of SHCC could be in those structures that are subjected to large deformations including underground structures that should be compatible with soil deformation and also prevent leakage (Li and Kanda, 1998). SHCC could also be considered for use in permanent formwork, extruded structural members, and FRP reinforced concrete structures. In addition, Wu et al. (1996) reported the application of SHCC as a binder for radioactive waste treatment to control leaching.

2.3.3.3 Field applications of SHCC

SHCC so far has been used in a number of large scale applications in USA, Korea, Switzerland and Japan. In most of these applications, SHCC has been used for repair of infrastructures including repair of a dame and the under-deck of a bridge in Japan, a sewage line in Korea, a concrete bridge deck in USA and a tunnel linings in Switzerland (Li, 2003). Some of these large scale projects are highlighted in the following.

Kojima et al. (2004) reported the repair of a dam in Japan in 2003 by spraying a 20 mm thick layer of SHCC. The 600 m^2 surface of Mitaka Dam built 60 years ago near Hiroshima, Japan was severely damaged, where several cracks, spalling and some water leakage were observed. Li et al. (2009) reported the repair of an earth retaining wall in Gifu, Japan in 2003 using SHCC. It was reported that due to severe cracking condition of the retaining wall, OPC was not a suitable repair material as it would have caused reflective cracking. However, SHCC was an ideal repair material to minimize this problem. It was reported that after one year only micro cracks with tight crack width were observed on the surface of the retaining wall.

SHCC has also been successfully used as coupling beams in high-rise buildings in Japan to reduce the earthquake damage. For instance, 54 SHCC coupling beams (2 per story) were used in the 95 m Glorio Roppongi high-rise apartment building in Tokyo and 4 coupling beams per floor were used in the 41-story Nabeaure Yokohama Tower, Japan

(Li, 2006). In seismic resistance applications, SHCC has superior performance to OPC which is attributed to its high damage tolerance, high energy absorption, and deformation capacity under shear (Li, 2006).

According to Li (2003), a thin composite SHCC/steel deck was used in the 1 km long Mihara Bridge in Hokkaido, Japan in 2005, where the thickness of SHCC layer was only 5 mm (2 inches). Thanks to the tensile ductility and tight crack width control of SHCC, 40% reduction in weight and a significant reduction in cost along with an expected service life of 100 years were reported. In a similar project, a 225-mm thick SHCC bridge deck was made on interstate 94 in Michigan, USA (Kim et al., 2004). Thanks to the outstanding properties of SHCC, less material was used in the SHCC bridge deck compared to the conventional concrete bridge deck. The bridge was opened to traffic in 2005 and it has been monitored since then by both the University of Michigan and the Michigan Department of Transportation to ascertain the superior durability of the bridge deck made from SHCC compared to conventional concrete. Lepech and Li (2009) reported that the performance of the bridge deck after 4 years was still satisfactory.

2.3.4 Material sustainability performance of SHCC

High cement content is commonly found in the mixture design of several types of HPFRCCs, such as slurry infiltrated fiber concrete (Lankard and Newell, 1984), UHPFRC (Nematollahi et al., 2014a; Nematollahi et al., 2014b; Nematollahi et al., 2014c; Nematollahi et al., 2016; Voo and Foster, 2010) and SHCC (Wang and Li, 2007). The mixture proportions of typical high modulus PE-SHCC and PVA-SHCC (with 100% cement and no fly ash), along with conventional structural concrete are presented in Table 2-1. As can be seen, the cement content of typical SHCC mix proportion is typically two to three times higher than that of the conventional concrete. Matrix toughness control for strain hardening behavior as well as rheology control for easy fiber dispersion are responsible for the high cement content in typical SHCCs. This high cement content results in undesirable high autogenous shrinkage and heat of hydration along with high material cost (Wang and Li, 2007; Yang et al., 2007).

In addition, manufacture of OPC involves substantial CO_2 emissions and energy consumption. Several authors in different countries have computed the emissions caused by manufacture of cement and concrete. For instance, Marceau et al. (2006) reported

detailed analysis of energy consumption and CO_2 emissions associated with production of OPC in USA. The authors considered transportation of raw materials to cement plants in their analysis. The total energy consumption (embodied energy) and carbon emissions were on average computed to be 4.8 GJ and 0.927 ton per ton of cement, respectively. Wet processing resulted in the highest embodied energy and carbon emissions of 6.4 GJ and 1.1 tone per ton of cement, respectively. Masanet et al. (2005) reported that the cement production in California emits 0.932 tone CO_2-e/tone of cement. The carbon emission and embodied energy input values in CO_2 estimator tool for roads developed by the Centre for Sustainability (2006) were 0.801 ton CO_2-e and 4.78 MJ per ton of cement. The reported figures were according to consideration of European and UK data.

Table 2-1: Mix proportions of conventional concrete and SHCC materials

Materials	Cement (kg/m^3)	Aggregates (kg/m^3)	Water (kg/m^3)	HPMC[a] (kg/m^3)	HRWRA[b] (kg/m^3)	Fiber (kg/m^3)
Conventional concrete	390	1717	166	---	---	---
PE-SHCC	1205	603	314	0.60	12	17
PVA-SHCC R0	838	838	366	1.26	17	26

Note: The mix proportions were adopted from Wang and Li (2007).

[a] Hydroxypropyl methyl cellulous (Viscosity modifying agent).

[b] Melamine formaldehyde sulfonate-based high-range water-reducing admixture (Superplasticizer).

Carbon emission and embodied energy associated with both fuels and materials in European cement industry are reported by Damtoft et al. (2008). They reported that in a modern, efficient rotary kiln fuel-derived carbon emissions and energy consumption ranged from 0.31 kg CO_2-e per kg of clinker and 3.1 GJ per ton of clinker, respectively. These figures for an inefficient wet kiln were ranged from 0.6 kg CO_2-e per kg of clinker and 6 GJ per ton of clinker. The carbon emissions associated with materials was reported to be 0.53 kg per kg of clinker.

Flower and Sanjayan (2007) conducted a detail analysis of carbon emissions associated with cement production in Melbourne, Australia. They considered carbon emissions associated with transportation in their analysis and reported that each of ton of cement

being produced in Melbourne emits 0.82 ton of CO_2. According to their study, for a 32 MPa concrete incorporating 100% OPC, the total emissions was 0.322 ton of CO_2-e per cubic meter of concrete. They reported that the higher the strength of concrete, the higher the carbon emissions. For instance, the total emissions of a 40 MPa concrete with 390 kg/m^3 of OPC would be 0.691 ton of CO_2-e per m^3 of concrete, while this figure would be 0.720 ton of CO_2-e per m^3 of a 50 MPa concrete with 450 kg/m^3 of OPC (Berndt et al., 2013).

According to the above studies and the volume of cement used in typical SHCC mixtures (Table 2-1), CO_2 emissions from manufacture of OPC have a significant effect on emissions associated with the built environment. According to Huntzinger and Eatmon (2009) and Chen et al. (2010), production of OPC is generally responsible for almost 5-7% of total CO_2 emissions worldwide, which is considered as the main cause of global warming. The associated increase in the CO_2 emission as well as embodied energy apparently compromise sustainability performance of typical SHCCs (Wang and Li, 2007; Yang et al., 2007). Hence, it is necessary to develop green SHCCs with lower global warming associated with CO_2 emission of the cement production, which maintain the tensile ductility properties, but also include sustainability considerations.

Different approaches can be adopted to reduce the energy consumption and carbon emissions of cement production (Gartner, 2004; Damtoft et al., 2008, Hasanbeigi et al., 2012; Cement Sustainability Initiative, 2009; Worrell et al., 2008). For instance, the efficiency of the cement production process can be significantly enhanced by reducing the quantity of clinker burnt via using blast furnace slag. Josa et al. (2004) quantified the improved efficiency for European cement industry. According to Damtoft et al. (2008), one strategy to reduce carbon emissions of cement production is using alternative fuels and waste materials such as slag as replacement of limestone.

Nowadays, substantial quantities of pozzolanic or SCMs such as fly ash, blast furnace slag, silica fume, rice husk ash and metakaolin are commonly used as partial replacements of OPC. Apart from the well-established advantages of the SCMs such as durability, the use of these materials as partial cement replacement also results in some reductions in carbon emissions of concrete production due to reducing the cement content (Berndt et al., 2013). Therefore, one obvious approach to manufacture green SHCCs is to partially

replace OPC in typical SHCC mix proportions with SCMs. Within the last decade several efforts have been made to incorporate high volumes of ground granulated blast-furnace slag, fly ash and IOTs as partial replacement of OPC in the SHCC mixture design to reduce the use of OPC; thereby, reducing the global warming potential associated with the CO_2 emission of the cement industry (Ahmed et al., 2006; Wang and Li, 2007; Kim et al., 2007; Yang et al., 2007; Şahmaran and Li, 2009; Şahmaran et al., 2009; Zhu et al., 2012; Altwair et al., 2012; Huang et al., 2012; Özbay et al., 2013).

For instance, Wang and Li (2007) investigated the mechanical properties of SHCCs incorporating high volume of Class F fly ash as partial replacement of OPC. The fly ash to cement ratio (FA/C) ranged from 0.1 to 1.5. The quantitative influences of fly ash content on the fiber-matrix interface properties, matrix fracture toughness and tensile performance of resulting composites were evaluated. The results indicated that both frictional and chemical bonds between the PVA fiber and the SHCC matrix generally decreased with increase of fly ash content, except for FA/C = 0.1. It should be noted that the reduction in chemical bond at high fly ash content was more considerable compared to that of frictional bond. However, the fly ash content had marginal effect on slip hardening coefficient. With increase of fly ash content, significant reduction in matrix fracture toughness and crack tip toughness were observed. The trends observed in terms of fiber-matrix interface properties and matrix fracture toughness are both beneficial for achieving PSH behavior in the composite. According to the uniaxial tension test results, composites with FA/C $\geq$ 0.8 exhibited clear PSH behavior with tensile strain capacities ranging from 1.11% to 2.69%. Among the composites containing fly ash, the tensile first-crack strength and ultimate tensile strength of the composite marginally decreased with increase of fly ash content, except for FA/C = 0.8. However, steady improvement was improved in the tensile strain capacity of the composite with increase of fly ash content, where tensile strain capacity stabilized at about 2.5% for FA/C = 1.2 and 1.5.

Among the composites containing fly ash investigated in Wang and Li (2007) study, PVA-SHCC mix 45 (M45) exhibited optimal mechanical properties, and thereby SHCC M45 was selected as the typical SHCC mixture in several studies. For instance, Yang et al. (2008) reported that SHCC M45 is the most widely used SHCC mixture in the field. Mix proportions and uniaxial tensile properties of SHCC R0 (that does not contain fly ash) and typical SHCC M45 are presented in Tables 2-2 and 2-3, respectively. As can be

seen, while a large amount of cement was replaced by fly ash (FA/C = 1.2) in typical SHCC M45, which significantly enhances the material sustainability, the desirable PSH behavior of the composite is still maintained. The material sustainability of SHCC R0 and typical SHCC M45 could be quantitatively compared by material sustainability indicators (MSI) proposed by Li et al. (2004). The life cycle inventory data of the ingredients used for calculating the MSI are also presented in Table 2-2. The inventory data was obtained from Yang et al. (2007) and Huang et al. (2012). It should be noted that two assumptions were made in deriving the life cycle inventory data presented in Table 2-2. First, the embodied energy and CO_2 emissions associated with fly ash are zero as it is a by-product of coal power station, most of which is disposed in landfills. Second, the embodied energy and CO_2 emissions associated with water are negligible relative to other ingredients.

Table 2-2: Mix proportions of SHCC R0 and typical SHCC M45 and life cycle inventory data of the ingredients used for calculating the MSI

Ingredients	SHCC M45[1] (kg/m^3)	SHCC R0[1] (kg/m^3)	Embodied energy (MJ/kg)	CO_2 emissions (kg/kg)
OPC	583	838	5.06[3]	0.898[3]
Fly ash	700	---	---	---
Micro-silica sand	467	838	0.175[3]	0.026[3]
Water	298	366	---	---
Superplasticizer	19	17	36.76[3]	1.48[3]
PVA fiber	26	26	106.54[3]	3.6[3]

[1] The mix proportions were adopted from Wang and Li (2007).

[3] Derived from Huang et al. (2012) and Yang et al. (2007).

Table 2-3: Uniaxial tensile properties of SHCC R0 and typical SHCC M45

Mixture ID	First-cracking strength, (MPa)	Ultimate tensile strength, (MPa)	Tensile strain capacity, (%)
SHCC R0	2.92 ± 0.06	4.41 ± 0.15	4.88 ± 0.59
SHCC M45	4.11 ± 0.66	4.86 ± 0.47	2.49 ± 0.57

Note: Test results were adopted from Wang and Li (2007).

Figure 2-8 presents the embodied energy and CO_2 emissions associated with production of a unit volume of SHCC R0 and typical SHCC M45. As can be seen, the CO_2 emissions

of typical SHCC M45 is 26% lower than that of SHCC R0. This is mainly attributed to the partial replacement of OPC by fly ash. In addition, the embodied energy of typical SHCC M45 is also 16% lower than that of SHCC R0. It can be concluded that typical SHCC M45 is a sustainable alternative to SHCC R0 in terms of carbon emission and energy consumption.

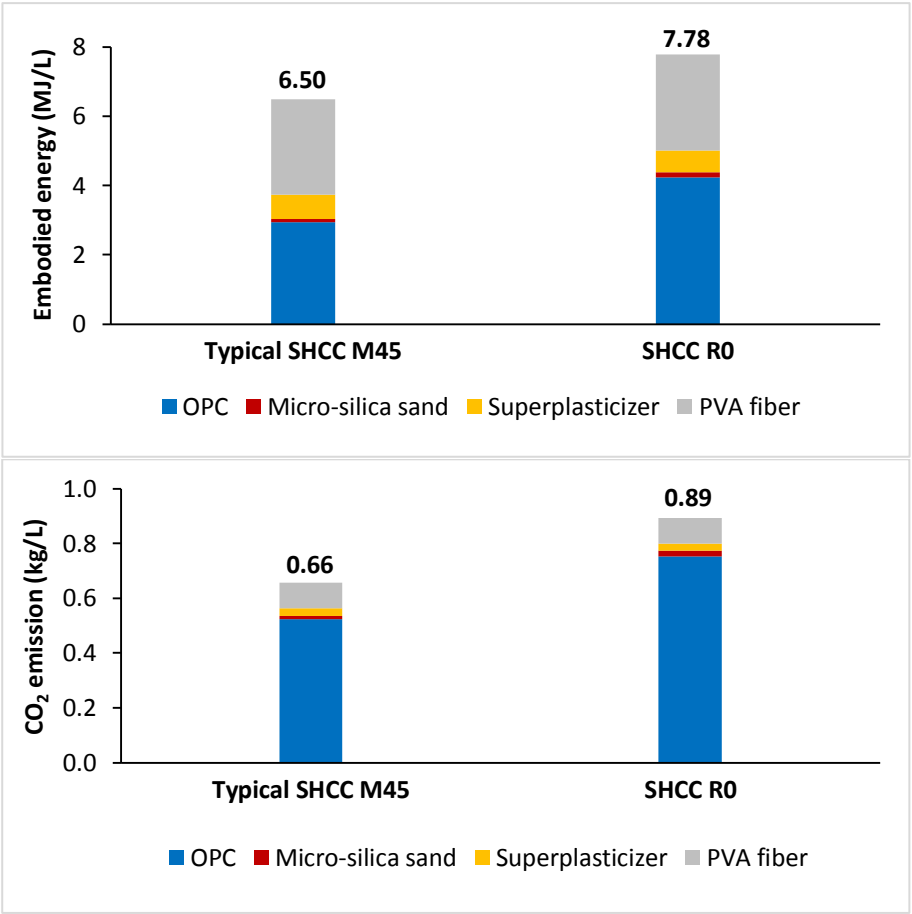

Figure 2-8: Material sustainability indicators of SHCC R0 and typical SHCC M45

As can be seen in Figure 2-8, although typical SHCC M45 is more environmentally friendly than SHCC R0, among its ingredients, cement is still a major contributor to the environmental impact accounting for 45.3% and 78.8% of total embodied energy and CO_2 emissions, respectively. This is despite the use of relatively large quantity of fly ash as partial replacement of cement (FA/C =1.2). Therefore, further research is required to enhance the material greenness of typical SHCC M45. This is the main motivation behind this doctoral research. A more sustainable approach to develop green SHCCs is to

completely replace the OPC binder in SHCC M45 mixture by an alternative cement-less binder such as geopolymer.

As mentioned in Section 2.3.1 and can be seen in Tables 2-1 and 2-2, a small amount of admixtures such as Superplasticizers (SPs) and viscosity modifying agents are commonly used in SHCC mix proportions to ensure adequate workability and rheology for uniform fiber dispersion. It should be noted that SPs are intended for use with OPC paste, mortar and concrete. The suppliers of SP do not intend them to be used in geopolymer mixes since SPs are attacked by alkaline solutions and degrade rapidly. However, some SPs may be used with geopolymer with limited effectiveness. Therefore, a prerequisite for using SPs in geopolymer mixes is to investigate the effects of different SPs on various geopolymer mixes, to understand their effectiveness and possible detrimental effects on properties of geopolymers. Therefore, the available literature on the effect of different SPs on geopolymers was critically reviewed in this doctoral research.

The focus of the following section is on geopolymer technology. At first, terminology, chemistry and constituent materials of geopolymer are briefly presented. Subsequently, a state-of-the-art review on the efficacy of the superplasticizers on geopolymers, along with a comparison between geopolymer and conventional concrete properties are presented. This is then followed by a brief review of published thesis on fly ash-based geopolymer. The available studies on developing sustainable cement-less strain hardening composites incorporating geopolymer as the sole binder are also presented.

2.4 Geopolymer Technology

2.4.1 Terminology

Geopolymer is a generic term commonly used for a broad range of aluminosilicate products manufactured with different formulations under heat or ambient curing regimes. Geopolymer technology is an emerging technology in various applications comprising cosmetics, pharmacology, agriculture, ceramics, insulation and concrete infrastructure (Shayan, 2013). In the context of concrete technology, geopolymer is considered as an emerging cement-less and sustainable alternative binder to OPC purported to provide significant environmental advantages. Geopolymer refers to a class of largely X-ray amorphous aluminosilicate binder materials (Provis, 2006), synthesized from a wide

range of source materials (precursors) that are rich in silica and alumina at different curing conditions. Industrial by-products such as fly ash and slag, or geological materials such as calcined clays are examples of aluminosilicate source materials. Geopolymer concrete has gained great interest in the recent years since sustainability and concern for environmental impacts are nowadays becoming major considerations in construction industry and geopolymer concrete is believed to have considerably less environmental impacts and potentially beneficial engineering properties and commercial features compared to conventional OPC concrete (Shayan, 2013).

The term geopolymer was initially introduced by Davidovits (1991) representing a wide range of inorganic materials. According to Davidovits (2005), among nine different classes of geopolymers, geopolymer cement and concrete are of particular interest comprised of aluminosilicate materials that could potentially be used to completely replace OPC and conventional concrete in transportation infrastructure applications. According to the U.S. Federal Highway Administration's Pavement Office TechBrief (Van Dam, 2010), this class of geopolymers are referred to as alkali-activated cements or inorganic polymer cements which are produced by dissolving thermally activated natural materials such as kaolinite clay or industrial by-products such as fly ash or slag in an alkaline activating solution to provide a source of silicon (Si) and aluminum (Al) which then polymerizes into inorganic molecular chains and networks which create the hardened binder.

Large amount of energy is needed for manufacture of OPC. That energy is consumed to reach the very high temperatures necessary for burning of clay and lime ($CaCO_3$) mixtures. This leads to the release of large amount of CO_2 from the limestone into the air. As a rule of thumb, almost one ton of CO_2 is emitted due to manufacture of one ton of OPC, half of which is attributed to the energy needed to burn the limestone at 1800^{o} C and the rest of the emissions is attributed to chemical release of CO_2 from $CaCO_3$ to make CaO (Davidovits, 1994). In contrast, production of fly ash-based geopolymer is reported to consume almost 60% less energy than that needed for production of OPC, which results in less carbon emission into the atmosphere (Li et al., 2004). In addition according to Duxson et al. (2007), at least 80% less CO_2 emission is resulted from the production of fly ash-based geopolymer compared to the manufacture of OPC. The environmental advantages of geopolymer cement and concrete are mainly due to the fact that burning of

limestone is not involved in the manufacturing process, and therefore much less energy is needed for production of geopolymers. In addition, the fact that geopolymer materials are often synthesized from already existing waste products (by-products) such as fly ash and slag, results in better use of natural resources, along with added environmental benefits due to the reduced need for disposal of these waste materials (Shayan, 2013).

2.4.2 Chemistry of geopolymers

Geopolymers are a special class of inorganic polymers. While the chemical composition of geopolymer is comparable to natural zeolitic materials, their microstructure is amorphous rather than crystalline (Palomo et al., 1999; Xu and van Deventer, 2000). According to Davidovits (1999), unlike hydration reaction in cement-based materials, polymerization reaction occurs in geopolymers, which is a significantly fast chemical reaction in an alkaline environment on Si-Al minerals. Davidovits (1999) reported that polymerization reaction leads to formation of a three dimensional polymeric chain and ring structure comprising of Si-O-Al-O bonds, in which it can be presented in the following form:

$$M_n [-(SiO2)_z–AlO_2]_n . wH_2O \quad (2.4)$$

Where M is the alkaline element or cation (e.g. potassium, sodium or calcium), the sign – indicates the existence of a bond, n is the degree of polycondensation or polymerization, and z is 1, 2, 3, or higher, up to 32 (Hardjito and Rangan, 2005).

The formation of geopolymer is schematically presented in Figure 2-9 (van Jaarsveld et al., 1997; Davidovits, 1999). According to Davidovits, (1999) and Xu and van Deventer, (2000), the following stages may occur in the geopolymerisation reaction:

i. Dissolution of Si and Al atoms from the source material by the action of hydroxide ions.

ii. Transportation, orientation or condensation of precursor ions into monomers.

iii. Setting or polycondensation/polymerization of monomers into polymeric structures.

It is important to note that Palomo et al. (1999) reported that the above stages can overlap with each other and happen almost simultaneously, which makes it hard to isolate each step separately (Hardjito and Rangan, 2005).

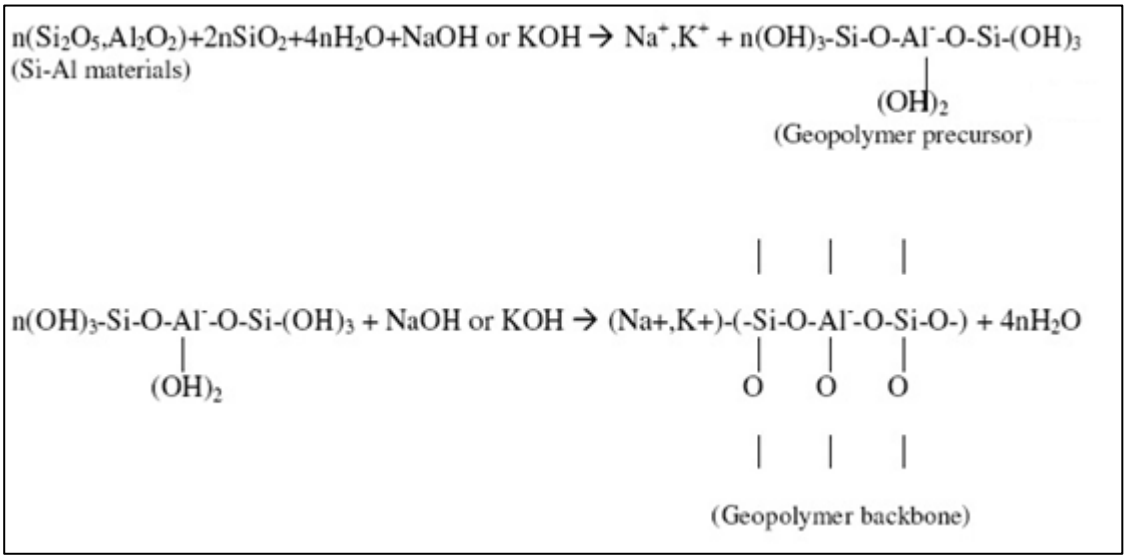

Figure 2-9: Schematic reactions of geopolymer formation (Source: Hardjito and Rangan, 2005)

Previous studies reported that the Si to Al ratio (Si/Al) has considerable effects on the geopolymer structure (Hardjito et al., 2004; Davidovits, 2008). The Si/Al typically ranges from 2 to 3.5 for geopolymer materials which are suitable for transportation infrastructure applications (Hardjito et al., 2004; Davidovits, 2008). Davidovits (1999) reported that a geopolymer material can be in one of the following basic forms, in which "sialate" is an abbreviation for silicon-oxo-aluminate:

i. Poly (sialate) Si/Al = 1, which has [-Si-O-Al-O-] as the repeating unit.

ii. Poly (sialate-siloxo) Si/Al = 2, which has [-Si-O-Al-O-Si-O-] as the repeating unit.

iii. Poly (sialate-disiloxo) Si/Al = 3, which has [-Si-O-Al-O-Si-O-Si-O-] as the repeating unit.

According to the U.S. Federal Highway Administration's Pavement Office TechBrief (Van Dam, 2010), water is not involved in the polymerization reaction and does not

become part of the final geopolymer structure, instead as shown in Figure 2-9, it is expelled during curing and subsequent drying process. Therefore, it can be said that the presence of water is not for participating in the chemical reactions but to aid the workability of the geopolymer mixture. This is opposite to hydration reaction in cement-based materials, where water becomes part of the primary hydration products (calcium silicate hydrate and calcium hydroxide). Davidovits (1999) reported that this critical difference has considerable influences on both chemical and mechanical properties of final geopolymer materials, which make them more resistant to water ingress, heat, alkali–aggregate reactivity, and other forms of chemical attacks.

2.4.3 Constituent materials of geopolymer

The two main constituent materials used for preparing geopolymer materials include the source materials, and the alkaline activators. The source materials are also known as feedstock or precursors or raw materials, and the alkaline activators could be in the form of solution or powder, which need to be dissolved in water.

2.4.3.1 Source materials

According to Xu and Van Deventer (2002), the source materials should contain high amount of silicon (Si) and aluminum (Al) in amorphous form. The source materials can have geological origins (natural minerals) such as kaolinite and calcined kaolinite (metakaolin) or could be industrial by-products such as fly ash and slag (Davidovits, 1984). There are several factors such as availability, cost, type of application, and specific demand of the end users which affect the selection of the source materials for manufacture of geopolymer (Hardjito and Rangan, 2005). There are several studies available in the literature which investigated the properties and application of geopolymer materials made by using either kaolinite or metakaolin as the source materials (Davidovits, 1984; Xu and Van Deventer, 2002; Barbosa and Mackenzie, 2003a; Barbosa and Mackenzie, 2003b; Cioffi et al., 2003). Similarly, there are extensive research studies on the application and properties of geopolymer material made by using fly ash (Palomo et al., 1999; van Jaarsveld et al., 1999; van Jaarsveld et al., 2002; Fernández-Jiménez et al., 2003; Fernández-Jiménez et al., 2006; Rangan, 2008; Pan et al., 2011) and slag (Cheng and Chiu, 2003; Ismail et al., 2013).

Fly ash is the main source material used in this doctoral research. The properties and characteristics of fly ash to be used as the source material for making geopolymer is highlighted in the following paragraphs.

Fly ash (or pulverized fuel ash) is fine solid residue (i.e. an industrial by-product) of coal fired power stations (ASTM C 618, 2003). Before releasing the gases produced due to combustion of coal to the atmosphere, fly ash particles are collected using electrostatic precipitators or bag houses (Ng, 2011). Nowadays, most of the electricity in the world is produced from coal fired power plants, and hence fly ash is abundantly available around the world (Ng, 2011). Mehta (1999) reported that more than 300 million tone of fly ash are collected annually from the power stations in India and China, whereas Malhotra (1999) reported that in 1998 only less than 20 million tons of fly ash was utilized. According to Ng (2011), in 2004 around 64 million tons of fly ash was produced from coal fired power stations in USA, while only 25 million tons of which was utilized.

According to Uranium Information Centre Ltd. Australia (2005), about 78% of the electricity in Australia is generated using coal fired power stations. Beretka (1978) reported that about 2.76 million tons of fly ash was annually produced in Australia. According to Beretka and Whitfield (1993), the annual production of fly ash in Australia had increased to almost 8.1 million tons, of which only about 0.75 million tons per year was utilized in production of blended cement. Heidrich (2002) reported that in 2002 the production of fly ash in Australia and New Zealand was about 12.5 million tons, but only about 4.1 million tons of fly ash was utilized in various applications. The cement and concrete industry is the main consumer of utilized fly ash. The utilized fly ash can also be used in geotechnical engineering applications, mining applications and the agriculture industry (Heidrich, 2003). Malhotra (1999) reported that the remaining unused fly ash is usually dumped into landfills or flushed out directly into the ocean, which not only results in the environment hazard, but also wasting fly ash as a valuable material which can be potentially used in other applications (Ng, 2011). Based on above statistics, it can be said that fly ash is abundantly available in Australia, which can be used as a good source material for manufacture of geopolymer.

Fly ash normally has spherical particles with particles sizes typically ranging from less than 1 μm to 150 μm, smaller than Portland cement (Ng, 2011). The main chemical

components of fly ash are silica (SiO_2), alumina (Al_2O_3), iron oxide (Fe_2O_3) and calcium oxide (CaO). There may be a wide variation in the color, particle size and shape, and proportions of the chemical components of fly ash generated from different power plants or even one power plant but different coal sources (Ng, 2011). Previous studies reported that the source and uniformity of the coal, the degree of pulverization prior to burning and the type of collection system used affect the chemical composition of fly ash (Ng 2011; Hemmings and Berry, 1988). It is also reported that the physical properties of fly ash depend on the combustion temperature of the coal as well as the rate of combustion (Ng, 2011). The wide variation of chemical compositions and physical properties of fly ash from one power station to another is clearly a challenge for researchers and industries to use fly ash (Ng, 2011).

To overcome this challenge, ASTM C 618 (2003) categorizes fly ash into two classes, namely Class C and Class F, based on the type of burning coal. Fly ash generated from burning lignite or sub-bituminous coal is referred to as Class C or high calcium fly ash, which has more than 20% of CaO in its composition. On the other hand, fly ash produced from burning anthracite or bituminous coals is known as Class F or low calcium fly ash, which has hematite (Fe_2O_3), magnetite (Fe_3O_4), mullite ($3Al_2O_3.2SiO_2$), quartz (SiO_2), and sillimanite ($Al_2O_3.SiO_2$), along with traces of CaO (Ng, 2011). Table 2-4 presents the classification criteria of fly ash based on ASTM C 618 (2003). It should be pointed out that Class F fly ash requires activation by an alkaline solution (e.g. sodium hydroxide) to possess cementing properties, as it is a latent type of cementing material which has no cementing properties when mixed with water (Neville, 1995).

Table 2-4: Properties of Class C and Class F fly ash based on ASTM C 618 (2003) (Source: Ng, 2011)

Properties	Class of fly ash	
	Class F	Class C
SiO_2, Al_2O_3, Fe_2O_3; minimum weight in %	70.0	50.0
SO_3; maximum weight in %	5.0	5.0
Moisture content; maximum weight in %	3.0	3.0
Loss on Ignition (LOI); maximum weight in %	6.0	6.0

The Loss on Ignition (LOI) which is an indication of the amount of unburned carbon in fly ash is an important feature when fly ash is utilized in manufacture of concrete (Ng, 2011). High LOI (i.e. high carbon content) of fly ash has detrimental effect on the workability of concrete (Neville, 1995). Ng (2011) reported that the presence of carbon in fly ash causes air entrainment in the concrete.

Heidrich (2003) reported that most of fly ashes generated from Australian power stations have the appearance of cement powder with light to mid-grey color, which contain high amounts of silica and alumina (80 - 85%); thereby can be considered as Class F fly ash based on ASTM C 618 (2003) classification. Table 2-5 presents the typical chemical compositions of fly ashes generated in Australian power stations.

Table 2-5: Typical chemical compositions of Australian fly ash (Source: Heidrich, 2003)

Composition	% by mass
SiO_2	48.1-71.0
Al_2O_3	21.8-30.3
Fe_2O_3	0.7-12.2
CaO	0.2-5.9
MgO	0.2-1.8
SO_3	0.0-0.7
Na_2O	0.1-3.7
K_2O	0.4-2.2
LOI*	0.2-10.0

*Loss on Ignition

Fernández-Jimenez and Palomo (2003) investigated the suitability of different types of fly ash to be used for production of geopolymer. They reported that in order to manufacture fly ash-based geopolymer with optimal binding properties, the carbon and Fe_2O_3 contents of a class F fly ash should not exceed 5% and 10%, respectively. In addition, the reactive silica content should be between 40-50%. Moreover, 80-90% of fly ash particles should be smaller than 45 μm (Hardjito and Rangan, 2005). van Jaarsveld et al. (2003) also reported that the higher carbon content of fly ash resulted in the lower compressive strength, but higher porosity of the resulting geopolymer. In addition, van Jaarsveld et al. (2003) found out that the higher CaO content of fly ash resulted in the

higher compressive strength of the resulting geopolymer. This is attributed to the formation of calcium-aluminate-hydrate and other calcium compounds, particularly in the early ages (Ng, 2011). According to van Jaarsveld et al. (2003), different material properties of fly ash such as the water content, thermal history, particle size, and degree of crystallinity or amorphicity affect the final structure and physical properties of the resulting geopolymer.

2.4.3.2 Alkaline activators

According to Rowles (2004), in terms of alkaline activators any strong alkaline solution may be used for manufacture of geopolymers. Davidovits (1987) reported that for building the pyramids in ancient days lime solution $Ca(OH)_2$ and volcanic ash were used as the alkaline activator and the source material, respectively. Alonso and Palomo (2001) also studied the use of $Ca(OH)_2$ as alkaline activator for production of geopolymers. Nowadays, a combination of sodium hydroxide (NaOH) and sodium silicate (Na_2SiO_3) or potassium hydroxide (KOH) and potassium silicate (K_2SiO_3) solutions are commonly used as the alkaline activators for production of geopolymers (Barbosa et al., 2000; Xu and Van Deventer, 2002; Phair et al., 2003; Hardjito et al., 2004; Kong and Sanjayan, 2010; Ng, 2011).

Fernández-Jiménez and Palomo (2005) investigated the effect of type of alkaline activator on the properties of geopolymer. NaOH, sodium carbonate (Na_2CO_3) and Na_2SiO_3 solutions were used in their study to produce fly ash-based geopolymer mortars. They found out that the type of alkaline activator has significant effect on the geopolymerisation process. They reported that the geopolymer made by NaOH solution exhibited the highest compressive strength, followed by the mix using Na_2SiO_3 solution. In contrast, the compressive strength was decreased when Na_2CO_3 solution was used as the activator, due to presence of CO_3^{2-}. They concluded that the amount of sodium oxide (Na_2O) in a mixture plays an important role in the compressive strength of geopolymer. The higher the amount of Na_2O in a mix, the higher the compressive strength of the resulting geopolymer. In their study, the highest compressive strength was achieved when the molar ratio "SiO_2/Na_2O" was equal to 0.118. They also concluded that the use of soluble silica as the alkaline activator influences the compressive strength development of the resulting geopolymer.

Palomo et al. (1999) reported that the addition of soluble silicate (such as Na_2SiO_3 or K_2SiO_3 solution) to alkali hydroxide (such as NaOH or KOH solution) increases the rate of geopolymerisation reaction. Xu and van Deventer (2000) also demonstrated that the presence of soluble silicate in the alkaline solution improves the formation of geopolymer precursors upon contact between a mineral and the solution. Likewise, Fernández-Jimenez et al. (2006) demonstrated that significant improvement in mechanical strength was achieved when the alkaline solution contained soluble silicate compared to using only alkali hydroxide as the activator. This is attributed to increase of paste density due to presence of soluble silica in the alkaline solution (Fernández-Jiménez et al., 2006).

Xie and Xi (2001) investigated the effect of amount of activator in a mix on the strength of geopolymer and concluded that the higher amount of activator to fly ash ratio resulted in the higher strength of the fly ash-based geopolymer. Sun (2005) also demonstrated that the higher amount of NaOH solution increased both the compressive strength and workability of the geopolymer, due to the higher dissolution of source materials and presence of more Na+ cations for geopolymerisation.

Apart from the content of the alkaline activator in the mix, the concentration (i.e. the molarity) of the alkaline solution also affect the strength development of geopolymer. Previous studies reported that the higher molarity of alkaline solution results in a greater dissolution of source materials, which in return increases the compressive strength of the resulting geopolymer (Xu and Van Deventer, 2000; Xu and Van Deventer, 2001; Van Jaarsveld and Van Deventer, 1999; Phair and Van Deventer, 2001). According to Fernández-Jimenez et al. (2006), the geopolymer mix made by 12.5 M NaOH solution exhibited higher compressive strength compared to the mix made by 8 M NaOH solution. It is important to note that excessive concentration of alkaline solution results in reduction of strength of geopolymer. Nonetheless, the reason for this behavior is unknown. Palomo et al. (1999) reported that compressive strength of geopolymer paste made by 18 M KOH solution was lower than that of paste made by 12 M KOH.

According to Provis et al. (2008), the type of activator and liquid to solid ratios usually have influence on the chemical structure of geopolymer. They studied the interrelationship between the strength of fly ash-based geopolymers and the type of activator and liquid to solid ratios. They concluded that the best performing geopolymers

in terms of strength showed a small expansion when exposed to elevated temperature (i.e. 700 to 800^{o} C) which is attributed to the swelling of a high-silica phase pockets within the gel structure of the geopolymer. The fly ash-based geopolymer exhibited low extent of binder formation, and hence low strength, when the high-silica phase was not present in the gel structure. Nevertheless, they also reported that excessive amount of silica in the gel structure resulted in strength reduction of the resulting geopolymer.

2.4.4 A state-of-the-art review on efficacy of available superplasticizers on geopolymers

This section is based on the paper "Efficacy of Available Superplasticizers on Geopolymers", by Nematollahi, B. and Sanjayan, J., published in Research Journal of Applied Sciences, Engineering and Technology, 2014, 7(7), 1278-1282.

As mentioned in Section 2.3.4, it is necessary to understand the effects of different SPs on various geopolymer mixes, since the SPs are not intended to be used in geopolymer mixes with high alkaline solutions. Therefore, this section presents a state-of-the-art-review of the effect of different SPs on slag and fly ash-based geopolymers.

SPs are added to OPC concrete to reduce its water content while maintaining a constant workability resulting in higher strength and durability of concrete. Alternatively, SPs can be used to "plasticize" or fluidize the concrete by maintaining a constant water content resulting the concrete to flow better with no change in the compressive strength. There are several types of SPs available, such as lignosulphonates (Lig), naphthalene (N) and melamine-based (M), and modified Polycarboxylate (PC). According to Rixom and Mailvaganam (1999), lignosulphonates based SP is considered as the first generation of SPs while melamine-based and naphthalene based SPs are classified as the second generation of SPs where their fluidization mechanism is based on electrostatic inter-particle repulsion. However, modified Polycarboxylate SPs are considered as the third generation (the latest generation) of SPs which in addition to electrostatic repulsion benefits from steric repulsion produced by lateral ether chains on the SP's molecule.

The effect and mechanism of SPs in OPC paste, mortar and concrete has been studied in depth by several authors such as Hanehara and Yamada (1999), Brooks et al. (2000), Puertas and Vazquez (2001), Chandra and Bjornstrom (2002) and many others. SPs are

not designed to work on geopolymers, however, researchers have attempted to use them in geopolymers to improve the rheology of the geopolymer mixes. SPs have been found to degrade in the alkaline environment provided by the activators and hence found to be not very effective in geopolymers. However, some SPs have found to work to a limited extent in geopolymer mixes probably related to their ability to resist the alkaline activators attack. In this regard, this paper presents a state of the art review of the effect of different SPs on workability, strength and rheological parameters (i.e. yield stress and plastic viscosity) of the slag and fly ash based geopolymers.

2.4.4.1 Effect of SPs on slag-based geopolymer

To date, several studies have been conducted on the effect of the SPs on the slag-based geopolymers. Douglas and Barndstetr (1990), for instance, studied the effect of Lig and N based SPs on workability and strength of Na_2SiO_3 activated slag based mortars with two different additives including 2% Lime + 1% Na_2SO_4 and 2% Lime + 5% fly ash + 1% Na_2SO_4. In the case of using Lig based SP with the dosages of 0.2, 0.5 and 1% of the binder mass, it was concluded that Lig based SP did not improve the workability of the mixes but also reduced the 1-day compressive strength of the specimens with reference to mixes without using SP. In addition, N based SP in the amounts of 0.5, 1, 5 and 9% by mass of binder (i.e. slag + 2% Lime + 1% Na_2SO_4) was added and it was observed that this type of SP did not also cause any increase in workability except for mortars with 9% of SP. However, addition of N based SP also decreased the 1-day compressive strength of the mortar specimens with reference to the mixes without using SP. It should be pointed out that these researchers did not investigate the effect of other type of SPs such as M and PC based SPs. They also did not study the effect of using different kind of activators. Moreover, the investigated binder was not pure slag (i.e. additives such as lime, fly ash and Na_2SO_4 were added to the slag).

Bakharev et al. (2000) investigated the effect of Lig and N based SPs on the workability and strength of slag based geopolymer concrete activated by three different activators. The investigated activators were mixture of NaOH + Na_2SiO_3 with a SiO_2/Na_2O ratio of 0.75 (for 4% Na by mass of slag) and 1.25 (for 7% Na by mass of slag). A multi-compound activator composed of NaOH (6.3% Na) + Na_2CO_3 (1.7% Na) with a total of 8% Na by mass of slag was also used in their study. Based on the experimental results, they concluded that Lig based SP increased the workability of the slag based concrete

activated with all the activators. However, this kind of SP was found to reduce the flexural strength of the concrete and may cause retarding effect in the strength development. On the contrary when N based SP was used, workability of the slag concrete was only increased at the initial stage and then a quick set occurred. With regards to shrinkage, Lig based SP slightly decreased the shrinkage, whereas N based SP considerably increased the shrinkage resulting in reduction in strength of slag based geopolymer concrete. These researchers also did not investigate the effect of M and PC based SPs in their study.

Puertas et al. (2003) investigated the effect of latest generation of SPs based upon vinyl copolymer and polyacrylate copolymer on the workability and strength of slag based geopolymer pastes and mortars activated by NaOH + Na_2SiO_3 solution (4% in mass of Na_2O). Their specimens were tested for compression and flexural strengths measurement after 2 and 28 days of casting. They also conducted a calorimetric study on different slag pastes with and without SPs. With regards to strength, they concluded that effect of SP on strength of slag based geopolymer mortars directly depends on the type of SP used. Vinyl copolymer SP reduced the compressive and flexural strengths of the mortars specimens. The reduction in strength was 70%-85% and 27%-40% for 2 and 28 days strength, respectively with reference to the specimens without using the SP. However, polyacrylate copolymers SP had no considerable effect on the strength of slag mortar specimens regardless of the age of the specimens. With regards to workability, it was concluded that both vinyl copolymer and polyacrylate copolymers SPs did not improve the workability of the activated slag pastes. Based on the results of the calorimetric study, vinyl copolymer SP delayed the activation process of activated slag pastes causing lower compressive and flexural strengths of the mortar specimens after 2 days; however, polyacrylate copolymers SP did not change the activation process of the activated slag pastes. This explains that this type of SP does not cause any considerable degradation in the strength of activated slag based mortar. These researchers did not evaluate the effect of different activators in their study. Following this study, a comprehensive research has been undertaken by Palacios and Puertas (2005).

Palacios and Puertas (2005) studied the effects of five different SPs (2 PC based, one M based, one N based and one vinyl copolymer based SPs) on the workability and setting time of fresh activated slag based pastes. They also investigated the effect of these SPs on compressive and flexural strengths of the activated slag based mortars. Their

specimens were cured at 20 ± 2°C and 99% relative humidity and tested after 2, 7 and 28 days. Two different activators were used in their study including NaOH + Na_2SiO_3 with a SiO_2/Na_2O ratio of 3.4 and only NaOH. Two different concentrations of 4% and 5% Na_2O by mass of slag were used for each kind of these activators. All these tests were also conducted on OPC paste and mortars to be compared with the results of the activated slag paste and mortar specimens. Admixtures stability tests were also conducted to investigate the stability of these SPs in high alkaline solutions. These authors concluded that the effect of SPs on alkali-activated slag is considerably different from the effects of these SPs on OPC. This is due to instability of these SPs in high alkaline solutions such as NaOH. According to Palacios and Puertas (2004, 2005), the only type of SP which is chemically stable in NaOH solution as the activator is N based SP causing increase in compressive and flexural strengths of activated slag specimens. N based SP also improved the workability of the paste and delayed the initial and final setting times with reference to slag paste and mortar specimens without using SP. It should be noted that in the case of using OPC the highest reduction in liquid to solid ratio was observed for PC based SPs. With regards to strength, it is found that both the compressive and flexural strengths of OPC mortars were much higher than slag based mortars activated by only NaOH.

Palacios et al. (2008) studied the effects of four different SPs (N, M, vinyl copolymer and PC based SPs) on the rheological behavior of activated slag pastes and mortars. Two different activators including NaOH + Na_2SiO_3 with a SiO_2/Na_2O ratio of 1.0 and NaOH solution, in both cases with 4% Na_2O by mass of slag, were used. These researchers concluded that the rheology of alkali-activated slag pastes and mortars is considerably depends on the type of the activators used. In the case of using only NaOH solution as the activator, these pastes and mortars follow Bingham model, whereas they match to Hershel-Bulkley model when NaOH + Na_2SiO_3 used as the activator. With regards to effect of SPs, it was concluded that none of the SPs used considerably influenced the rheological behavior of these pastes activated by NaOH + Na_2SiO_3. By contrast, N based SP significantly reduced the yield stress of NaOH activated slag pastes by 80%.

Wang et al. (2009) investigated the effect of N and M based SPs on workability, tensile and compressive strength of the slag-metakaolin based geopolymer pastes and mortars activated by NaOH + Na_2SiO_3 with 3 different SiO_2/Na_2O ratios of 1.0, 1.2 and 1.4. The proportion of metakaolin to slag was 3:7. With regards to workability, they concluded

that both N and M based SPs increased the fluidity of the paste and the saturation point for N and M based SPs were 2.0% and 2.3% respectively. With respect to strength, it was concluded that the tensile and compressive strengths of the mortar specimens with the addition of both N and M based SPs were increased initially and then decreased. The optimum content for N and M based SPs were 0.6% and 1.6% respectively. It should be noted that the investigated binder in this study was not pure slag (i.e. slag-metakaolin by the proportion of 3:7 was used as the binder).

Palacios et al. (2009) studied the adsorption of three different SPs (M, N and vinyl copolymer based SPs) on the slag particles in activated slag pastes activated by two different NaOH solution with 0.005 M (pH=11.7) and 2.57 M (pH=13.6) concentrations compared with that of the OPC paste. They also investigated the effect of these SPs on the rheological parameters (i.e. yield stress and plastic viscosity) of OPC and slag pastes. It was concluded that adsorption of these SPs on NaOH activated slag pastes is not dependent on the pH of the activator and is 3 to 10 times lower than on OPC pastes. However, the effect of these SPs on rheological properties (yield stress and plastic viscosity) of OPC and slag pastes directly depends on the type of binder in addition to the type and content of the SP. Moreover, in the case of activated slag paste, it also depends on the pH of the alkaline solution. N based SP was the only type of SP that affected the rheological parameters of the slag pastes when the activator was 2.57 M NaOH (pH=13.6) due to its chemical stability in such a high alkaline solution. However, in the case of slag pastes activated by 0.005 M (pH=11.7), it was observed that vinyl copolymer SP resulted the highest reduction in the yield stress. They also concluded that the amounts of SP needed to achieve similar decrease in the yield stress of the OPC pastes are 10 times higher with reference to 0.005 M NaOH activated slag pastes.

As demonstrated in the review above, the inconsistency in the research results reported is due to diversities in the conditions in which slag-based geopolymer pastes, mortars and concrete were made such as composition of the slag, type and amount of additives to slag as the binder (such as fly ash and metakaolin), nature and concentration of the activators used, type and dosage of the SPs, time and temperature of curing, etc.

2.4.4.2 Effect of SPs on fly ash-based geopolymer

In contrast to the several studies conducted on the effects of SPs on slag-based geopolymer, few studies have been conducted so far to investigate the effect of these SPs in fly ash-based geopolymer system. Puertas et al. (2003), for instance, studied the effect of latest generation of SPs based upon vinyl copolymer and polyacrylate copolymer on the workability and strength of fly ash based geopolymer pastes and mortars activated by only 8 M NaOH solution. Their specimens were heat cured for 24 hours at 85°C and then tested for compression after 2 and 28 days of casting. They concluded that addition of these SPs does not cause any significant changes in strength of the activated fly ash mortars. Moreover, these SPs did not increase the workability of the activated fly ash pastes.

Hardjito et al. (2004) studied the effect of a N based SPs on workability and compressive strength of the fly ash based geopolymer concrete activated by 8 M NaOH solution (28.6%) + Na_2SiO_3 (71.4%) with a SiO_2/Na_2O ratio of 2.0. Their specimens were heat cured for 24 hours at 60°C and then tested for compression after 7 days of casting. It was concluded that addition of N based SP improved the workability of fresh concrete. With respect to the compressive strength, they observed that when the dosage of SP is up to approximately 2% by mass of fly ash, the compressive strength was almost unchanged; however, dosages beyond 2% caused degradation in compressive strength (addition of 3.5% by mass of fly ash resulted in 33.3% decrease in compressive strength with reference to the original concrete).

Criado et al. (2009) evaluated the effect of Lig, M and PC based SPs on paste rheology (i.e. yield stress and plastic viscosity) of alkali activated fly ash. They concluded that when 12.5 M NaOH solution (85%) + Na_2SiO_3 (15%) with a SiO_2/Na_2O ratio of 3.3 used as the activator the PC based SPs (with a dosage of 0.8%) seems to be the most effective type, however, these researchers have not evaluated the effect of these SP on strength of fly ash paste. Moreover, they have not studied the effect of N based SP in their study. They have not also investigated the effect of the SPs when different activators such as only NaOH are used in fly ash based geopolymer.

Kong and Sanjayan (2010) studied the effect of two different SPs (N based and PC based) in the workability and compressive strength of the fly ash-based geopolymer concrete.

They concluded that N and PC based SPs did not greatly improve the workability of fly ash based geopolymer concrete activated by 7.0 M KOH solution (28.6%) + Na_2SiO_3 (71.4%) with a SiO_2/Na_2O ratio of 2.0. Their specimens were cured 24 hours at room temperature and then heat cured for 24 hours at 80°C and then tested for compression after 3 days of casting. They observed that using these SPs had significant negative effect on the compressive strength of the original concrete. Based on their results, PC based SP with the dosage of 3.3% by mass of fly ash caused significant reduction (54%), while N based SP with the dosage of 1.19% by mass of fly ash caused 21.8% reduction in strength with reference to the original concrete.

Memon et al. (2012) studied the effect of a PC based SPs on workability and strength of self-compacting geopolymer concrete. Their specimens were heat cured for 48 hours at 70°C and then tested for compression after 3 days of casting. They concluded that addition of PC based SP with the dosages of 3% to 7% by mass of fly ash resulted in increase in the workability and the compressive strength of the fly ash based geopolymer concrete activated by 12 M NaOH solution (28.6%) + Na_2SiO_3 (71.4%) with a SiO_2/Na_2O ratio of 2.06 with respect to the concrete containing 3% SPs. However, these researchers did not report the effect of the SP (i.e. increase/decrease in the workability and the strength of the concrete) with respect to the original concrete without any SP.

As illustrated in the review above, the variation in the research results is due to varieties in the conditions in which fly ash-based geopolymer mixes were prepared such as composition of the fly ash, nature and concentration of the activators used, type and dosage of the SPs, time and temperature of heat curing, etc. As the results are not yet conclusive, further research in this area is still required, which is the motivation behind the research study conducted in this doctoral research on the effect of different activators and SPs on workability and strength of fly ash-based geopolymer prepared with the local materials. The results of the study are presented in Chapter 3.

2.4.5 Comparison between geopolymer and conventional concrete properties

Recent studies on fly ash-based geopolymer concrete revealed the potential benefits of using this material as an alternative constriction material over conventional OPC concrete for many civil and infrastructure engineering projects. The advantages of using fly ash-

based geopolymer concrete versus the conventional OPC concrete are briefly presented below.

The main benefit of using fly ash-based geopolymer concrete over conventional OPC concrete is in terms of environmental issues. As mentioned earlier, the production of OPC consumes intensive energy and one ton OPC produced emits approximately one ton of CO_2 into the atmosphere, which causes the global warming (Davidovits, 1994). On the other hand, fly ash as a by-product of coal power station is abundantly available in the world which nowadays a small portion of it is employed in the production of blended cement and its remaining volume is dumped in the landfills, which causes several environmental issues to human being. Having said these, using fly ash-based geopolymer concrete can provide significant environmental benefits. First of all, as reported by Li et al. (2004), the production of fly ash-based geopolymer requires almost 40% of energy required for OPC production leading to low carbon emission. Secondly, Duxson et al. (2007) stated that the manufacture of fly ash-based geopolymer concrete emits at least 80% less CO_2 in comparison to manufacture of OPC. In addition, using fly ash which is a waste material as the feedstock for the production of geopolymer concrete could reduce its disposal and provide environmental benefits.

Fly ash-based geopolymer concrete has high acid and sulfate attack resistance. In terms of acid resistance, many researchers such as Bakharev (2005) and Wallah and Rangan (2006) demonstrated that geopolymer concrete has superior performance with regards to resistance to sulfuric acid exposure compared to OPC concrete. With regards to sulfate attack, Hardjito et al. (2004) and Wallah and Rangan (2006) reported that after 12 weeks of exposure to 5% sodium sulfate solution no considerable changes in the compressive strength, the mass and the length of the fly ash based geopolymer concrete specimens were recorded. This simply translates to excellent resistance of heat cured fly ash-based geopolymer concrete to sulfate attack.

In terms of alkali-silica reaction (ASR), Wesche (1991) reported that there is lower possibilities of ASR in fly ash-based geopolymer concrete due to insufficient availability of alkalis to react with silica. García-Lodeiro et al. (2007) and Kupwade-Patil and Allouche (2011) also reported that fly ash-based geopolymer concrete is considerably less susceptible to ASR compared to OPC concrete. This is due to the chemical reaction

between alkalis and the amorphous component in the fly ash producing cementitious binders that increase the concrete density, reduce its permeability and decrease the mobility of its aggressive agent.

The other advantage of fly ash-based geopolymer concrete over OPC concrete is its high early strength gain. Hardjito et al. (2004) reported that with regards to age of concrete, there is no significant change in the compressive strength of heat cured fly ash-based geopolymer concrete. This is due to the fact that the geopolymerisation process is a substantially fast chemical reaction under alkaline condition on Si and Al contents of fly ash resulting high early strength gain, if cured at elevated temperature (Davidovits, 1999). This behavior of geopolymer concrete is in contrast with the well-known behavior of OPC concrete that gains strength over time due to hydration reaction.

Hardjito et al. (2004) and Wallah and Rangan (2006) investigated the creep and shrinkage of heat cured fly ash-based geopolymer concrete and concluded that the heat cured fly ash-based geopolymer concrete specimens experienced low creep and negligible shrinkage. These authors reported that the creep coefficient, defined as the ratio of creep strain-to-instantaneous strain, after one year for heat-cured fly ash based geopolymer concrete with the compressive strength of 40 to 67 MPa is ranging from 0.4 to 0.7 which are about 50% of those values for OPC concrete predicted by Gilbert method given in the draft Australian Standard for Concrete Structures AS3600 (2009). The shrinkage of heat cured fly ash-based geopolymer concrete was in the order of about 100 micro strains after one year which is considerably smaller than that of the OPC concrete (i.e. 500 to 800 micro strains) as predicted by Gilbert method given in the draft Australian Standard for Concrete Structures AS3600 (2009).

Hardjito et al. (2004) stated that according to their laboratory information, the cost of one cubic meter of fly ash based geopolymer concrete is almost equal to that of OPC concrete. However, if the impact of possible CO_2 tax on the cement price and the environmental benefits of using fly ash have been taken into account, the economic advantages of fly ash-based geopolymer concrete could be established. It should be pointed out that the above mentioned superior characteristics of fly ash-based geopolymer concrete (negligible drying shrinkage, the low creep, the excellent sulfate attack resistance, and

the good acid resistance) grants extra economic advantages when this material is employed in infrastructure applications.

A comprehensive study was recently conducted by Centre for Sustainable Infrastructure at Swinburne University of Technology and Centre for Infrastructure Engineering and Safety at the University of New South Wales on pathways for tackling obstacles for employment of low CO_2 concrete. The study was undertaken on behalf of the CRC for Low Carbon Living whose activities are funded by the Australian Government's Cooperative Research Centre Program (Berndt et al., 2013). As can be seen in Table 2-6, that study provides a general comparison between geopolymer and conventional OPC concrete properties, since properties of any concrete are greatly rely on its ingredients and mixture proportions.

According to Table 2-6, it can be said that there is not always a clear differences between properties and performance of conventional OPC concrete versus geopolymer concrete, which is mainly attributed to dissimilarity in materials, specifically activator concentrations and chemistry. In fact, it is not always possible to provide a definitive comparison, as the studies conducted by different researchers have not been always coordinated. Nevertheless, as can be seen in Table 2-6, it can be concluded that compared to conventional OPC concrete, geopolymer concrete generally has higher compressive, flexural and tensile strength with higher rates of strength gain. Limited research studies also indicated that geopolymer concrete has similar to superior bond to reinforcement compared to conventional OPC concrete. Geopolymer concrete has generally lower shrinkage than that of conventional OPC concrete. However, elastic modulus of geopolymer concrete is lower than that of conventional OPC concrete. Durability comparisons reported in Table 2-6 are typically based on concretes with comparable compressive strength. As can be seen, there are sometimes variable comparisons with regards to durability properties, which indicate the requirement of further research in real exposure environment. It is also essential to investigate whether test methods and procedures made for conventional OPC concrete are applicable to geopolymer concrete.

Table 2-6: General comparison between properties of geopolymer and conventional concrete (Source: Berndt et al., 2013)

Property	Geopolymer versus conventional concrete
Compressive Strength	Similar, higher rate of early strength gain
Tensile Strength	Indirect tensile strength typically higher for similar compressive strength
Flexural Strength	Similar to higher depending on alkali activator, higher rate of early strength gain
Modulus of Elasticity	Typically lower
Density	Similar to lower
Poisson's Ratio	Typically lower or similar
Shrinkage	Lower to similar
Creep Coefficient	Lower
Bond Strength to Reinforcement	Similar for similar compressive strengths; higher for higher compressive strengths
Carbonation Coefficient	Higher
Chloride Diffusion Coefficient	Lower (migration test); lower (core test)
Rapid Chloride Permeability	Lower to similar depending on mix proportions
Corrosion Rate of Embedded Steel	Limited research, particularly field exposure, prevents conclusive comparison.
Sorptivity	Higher
Sulphate Resistance	Somewhat higher, depends on cation
Acid Resistance	More resistant to organic and inorganic acid attack
Alkali-Silica Reaction Susceptibility	Variable based on limited research
Fire Resistance	More resistant
Freeze-Thaw Durability	More durable
Volume of Permeable Voids	Varies depending on mix proportions; higher
Water Absorption	Similar

2.4.6 Brief review of published thesis on low calcium fly ash-based geopolymer concrete

To date, several research studies have been undertaken on fly ash-based geopolymers in Australia and overseas especially in USA. In Australia, several studies were conducted by geopolymer research team at Curtin University to investigate the characteristics of the low calcium fly ash-based geopolymer concrete. For instance, Hardjito and Rangan (2005) studied the development, the mixture proportions, and the short-term properties of low-calcium fly ash-based geopolymer concrete. Subsequently, Wallah and Rangan (2006) investigated the long-term properties of low-calcium fly ash-based geopolymer

concrete including creep, drying shrinkage, sulfate resistance, and sulfuric acid resistance. The outcomes of these investigations have shown the potential use of the low calcium fly ash-based geopolymer concrete as a new construction material. According to these studies, fly ash-based geopolymer concrete has high compressive strength, negligible drying shrinkage, low creep, good bond with reinforcing steel, and good resistance to acid, sulfate and fire (Sarker, 2009). Concurrently, Sumajouw and Rangan (2006) studied the behavior and strength of reinforced low-calcium fly ash-based geopolymer concrete structural beams and columns. Their study revealed that the performance of fly ash-based geopolymer concrete structural members such as beams and columns is similar to that of OPC concrete members.

Soltaninaveh (2008) investigated the salient parameters affecting the properties of fly ash-based geopolymer concrete incorporating red sand. Red sand is a by-product of alumina manufacturing from bauxite using Bayer process. A series of experimental tests were conducted to measure mechanical properties including workability, compressive, tensile and flexural strengths, elastic modulus of fly ash based geopolymer concrete when natural fine aggregates were replaced by different percentages of red sand. According to the results, it was found that the using red sand as the fine aggregate significantly reduced the workability and compressive strength of the mix. This is due to the high surface area and water absorption of red sand compared with natural fine aggregate. The flexural strength of the mix using red sand was also lower than the corresponding mix using natural sand. However, the indirect tensile strength of the mix using red sand was comparable to that of the mix using natural sand.

Later on, Chang (2009) investigated the shear and bond behavior of reinforced low calcium fly ash-based geopolymer concrete beams. In his study, for the study of shear behavior of geopolymer concrete beams, a total of nine beams with the dimensions of 200 mm by 300 mm in cross section and effective length of 1680 mm were cast. The longitudinal tensile reinforcement ratios were 1.74%, 2.32% and 3.14%. The experimental results proved that shear behavior of reinforced geopolymer concrete beams including the failure modes and crack patterns is similar to those of the reinforced OPC concrete beams. A good correlation (an average test-to-prediction ratio of 1.08 and a coefficient of variation of 8.3%) between the test and prediction values was achieved using VecTor2 Program incorporating the Disturbed Stress Field Model proposed by

Vecchio (2000). It was also demonstrated that the shear strength of reinforced geopolymer concrete beams can be predicted using the same methods of calculations including code provisions used in the case of reinforced OPC concrete beams.

For the study of bond behavior of geopolymer concrete beams, Chang (2009) tested twelve tensile lap-spliced beams with no transverse reinforcement in the splice region and with the dimensions of 200 mm by 300 mm in cross section and 2500 mm in length. The investigated parameters were concrete cover, bar diameter, splice length and concrete compressive strength. The experimental results showed that the failure mode and crack patterns for reinforced geopolymer concrete beams were similar to those of reinforced OPC concrete beams as reported in the literature. It was found that the bond strength of geopolymer concrete is strongly proportional to the tensile strength of geopolymer concrete. When the actual tensile strength of geopolymer concrete was used in the analytical model proposed by Canbay and Frosch (2005), the average ratio of experimental bond strength to predicted bond strength was 1.0 with a coefficient of variation of 15.21%. It was also demonstrated that the bond strength of lap splices in reinforced geopolymer concrete beams can be predicted using the design provisions and analytical models available for reinforced OPC concrete beams.

Olivia (2011) at Curtin University investigated the durability of fly ash based in a seawater environment such as seawater resistance and corrosion of steel reinforcement bars. Regarding the seawater resistance, a series of experimental tests were conducted to measure the chloride ion penetration, change in strength, change in mass, change in Young's modulus of elasticity, change in effective porosity and change in length. The corrosion performance of steel reinforcement in fly ash based geopolymer concrete was studied by measuring the corrosion potential by half-cell potential, accelerated corrosion test by impressed voltage method and microbiologically influenced corrosion incorporating algae. Moreover, the microstructure of the mixes was also studied via SEM. According to the sweater resistance tests, it was found that a high chloride ion penetrated into the fly ash based geopolymer concrete which is due to lack of a chloride binding ability and continuous hydration under aqueous medium. It was also found that the fly ash based geopolymer concrete had a higher strength and small expansion following exposure to wet and drying cycles. The corrosion rate of the steel bars in the fly ash based geopolymer concrete was smaller than that of the OPC concrete; however, there was a

rapid depassivation of reinforcement which could postpone the pressure of generating cracks in the concrete cover. In the long term, this would be unfavorable due to a due to a sudden loss of load carrying capacity. The results of the corrosion performance study in algae medium revealed that due to the low alkalinity of the fly ash based geopolymer concrete, there is a risk of steel bar corrosion in this type of concrete.

Adam (2009) at RMIT University, Australia investigated the strength development and the durability performance in terms of chloride and carbonation resistance of alkali activated slag and fly ash based geopolymer concrete. A series of experiments were conducted to measure the workability, compressive strength, sorptivity, depth of carbonation, rapid chloride permeability, and chloride ponding of the mixes. Microstructure of the fly ash based geopolymer concrete was studied via scanning electron microscopy (SEM) and energy dispersive X-ray spectroscopy (EDAX). Based on the results, it was found that the performance of fly ash based geopolymer concrete is better than OPC concrete in terms of water sorptivity and chloride penetration. It was also found that fly ash based geopolymer concrete demonstrated high charge and high conductivity in the accelerated chloride diffusion tests. This is due to the concentration and composition of the free ions present rather than the ability to resist the chloride ions diffusion.

Recently some studies have been conducted on fiber reinforced fly ash based geopolymer concrete at University of New South Wales (UNSW) in Sydney. For instance, Amin (2010) cast and tested a total of ten large scale fiber reinforced geopolymer concrete beams with different fiber types (end-hooked or straight) and volume fractions of fiber (ranging from 0-1.5% by volume). Based on the experimental results, an increase in fiber content resulted in a linear increase in the ultimate shear capacity and also an increase in the deformability behavior of the fiber reinforced geopolymer concrete beams. It was also found that cracking load of the fiber reinforced geopolymer concrete did not considerably influenced by type and quantity of fiber used; however, they have a significant effect on the crack propagation rate and crack width reductions. He also conducted an experimental study to investigate some common short term mechanical properties including the fracture energy, modulus of rupture, indirect tensile strength, and stress-strain response of fiber reinforced geopolymer concrete. The results of this study demonstrated that an increase in fiber content enhanced each of these properties.

Following the above mentioned experimental studies, Amin (2010) also conducted a numerical study using a commercially available finite element package, ATENA 2D, to focus on modeling and verifying the experimental results. A very good correlation between the experimental results and prediction values was obtained using material parameters derived from the Unified Variable Engagement Model developed by Htut and Foster (2010) to describe the shear versus deflection response, principal strain distributions and crack patterns. In addition, the accuracy of available design models to predict the shear capacity of fiber reinforced geopolymer concrete beams was examined. A predictive design model developed by Foster (2010) was used to predict the fiber contribution to the shear resistance of fiber reinforced geopolymer concrete beams. An excellent correlation with a mean value of 0.99 and a coefficient of variation of 12% between the ratio of experimental results and the model was obtained. It was also found that replacing 0.75% by volume of 35 mm long end-hooked fibers satisfies the minimum conventional stirrups requirements for shear as described in AS3600 (2009).

Subsequently, Ng (2011) at UNSW, Australia comprehensively studied the fabrication and characteristics of some high performance geopolymer concrete including design of high strength geopolymer concrete mix, structural performance of steel fiber reinforced geopolymer concrete and properties and application of lightweight geopolymer mortar. In the first part of this study, high performance geopolymer mortars and concrete with the compressive strengths above 80 MPa were developed. In the second part, the behavior of steel fiber reinforced geopolymer composite was investigated and a constitutive tensile model for steel fiber reinforced geopolymer composite was developed. According to the experimental results for the shear carrying capacity of the steel fiber reinforced geopolymer concrete beams without stirrups, an increase in fiber content resulted in increased shear capacity of the beam. Finally, some high performance lightweight geopolymer mortar beams with similar strength to that of a conventional OPC concrete but with half of its density were manufactured and reinforced with steel fibers and aramid fiber reinforced polymer reinforcement. Based on the results, it was found that steel fibers and aramid fiber reinforced polymer core increased the flexural stiffness and shear capacity of the beam.

Later on, Ferdous (2012) at UNSW in Canberra proposed and investigated a sleeper system composed of fly ash-based geopolymer concrete and pultruded FRP profile

composites. He proposed a mix design methodology for determining the mix proportions of geopolymer concrete containing low calcium fly ash. A series of four point bending tests were conducted on the proposed sleeper to measure it bending modulus and modules of rupture. A good correlation was found between the experimental results and predicted values derived from structural analysis. According to the experimental results, the proposed sleeper satisfied the minimum requirements stated in the relevant codes and guidelines and can be used as an alternative to the conventional timber/steel or concrete sleepers leading to several environmental benefits.

An example of overseas studies on fly ash based geopolymers is that of Sun (2005) at Wayne State University, USA, who investigated the ways to recycle the fly ash into high performance construction materials using the geopolymer technology. He studied the mechanism of geopolymerisation in a fly ash based system especially the role of metakaolin and optimized the mix proportion of raw materials for the best cost-property ratio. He also conducted the performance evaluation per relevant codes and specifications.

Montes (2010) at Louisiana Tech University in the US evaluated the suitability of geopolymer as a candidate material for the rehabilitation of aging buried concrete infrastructure. In other words, his research project was focused on the incorporation of geopolymers as a new material for Trenchless projects which provides considerable assistance to municipalities to meet their rehabilitation requirements. Trenchless technologies are considered as methods, materials and equipment which can be used for the installation of new or replacement or rehabilitation of existing underground infrastructure with minimum disturbance to surface traffic, business, and other actions. In this study, the main parameters involved in geopolymerisation were studied and a geopolymer-based rehabilitation method was developed with enhanced workability by means of a surface-active agent. As spray coatings are a very common and convenient method for the application of cementitious materials, a sprayable geopolymer admixture was developed. Studies was also conducted to evaluate the final properties of the resulting material and a comparison with products currently used by the industry.

Tempest (2010) in the US investigated the engineering characterization of fly ash based geopolymer concrete for structural applications. In this study, the mechanical properties of fly ash based geopolymer concrete including the compressive, tensile and elastic

behaviors were determined. A series of durability tests were performed to evaluate the long term behavior such as creep and shrinkage of fly ash based geopolymer concrete. Flexural tests of prestressed and mild steel reinforced fly ash based geopolymer concrete beams were conducted and it was found that the conventional concrete design criteria and techniques used for OPC concrete are applicable for fly ash based geopolymer concrete with small changes to some design values. The sustainability of the developed fly ash based geopolymer concrete was also verified via life cycle analysis.

Later on, Edouard (2011) in the US evaluated the durability characteristics of low calcium fly ash-based geopolymer concrete subjected to the marine environment to be compared with OPC concrete with similar exposure. He studied the corrosion resistance performance of steel reinforced fly ash based geopolymer concrete beams with submergence in salt water using an accelerated electrochemical method. Based on the experimental results, it was found that the fly ash based geopolymer concrete has excellent resistance to chloride attack, with longer time to corrosion cracking, in comparison to OPC concrete.

Recently, Ravikumar (2012) in the US provided extensive information on the properties, microstructure and performance of alkali activated fly ash based geopolymer systems. The effects of the activator's concentration and the activator to binder ratio on the on the compressive strengths, pore structure features, and microstructure of fly ash based geopolymer concrete with optimized curing time and temperatures were investigated. According to the results, it was found that the activator's concentration has considerable influence on the compressive strength of the fly ash based geopolymer concrete. It was also concluded that alkali activated fly ash pastes and concretes were more porous and contains a larger fraction of pores greater than 10 μm in size in comparison with alkali activated slag-based geopolymers.

2.4.7 Available literature on developing sustainable cement-less strain hardening composites incorporating a geopolymer binder

As mentioned earlier, a more sustainable approach to develop green SHCCs is to completely replace the OPC binder in SHCC mix proportion with a geopolymer binder. In this section, the available studies conducted on this research topic are presented. It should be noted that when this doctoral research was started in September 2012, there

was only one research article available authored by Lee et al. (2012) from South Korea, which demonstrated the feasibility of developing a cement-less fiber-reinforced strain hardening composite, where the OPC binder is completely replaced by a 100% slag-based geopolymer binder. During the conduct of this doctoral research, few studies on similar research topics have also been undertaken simultaneously by other researchers, which are also presented in this section.

100% slag-based geopolymer was used in Lee et al. (2012) study. Three different mix proportions by using two different activator combinations and water to binder ratios were prepared. Fine silica sand with sand to binder ratio of 0.4 by mass was also used in the mixtures. Oil-coated PVA fibers (2% by volume) with a surface oil coating of 1.2% by weight, length of 12 mm and diameter of 39 μm were used to reinforce the slag-based geopolymer matrix. Standard water curing was adopted in their study. In other words, fresh specimens were covered in plastic sheets and cured in the laboratory at ambient temperature (23 °C ± 3 °C) for 24 hours. The hardened specimens were then removed from the molds and cured in a water tank for 28 days at ambient temperature. A series of experiments were conducted to characterize the properties of slag-based geopolymer composites including density, compressive strength and uniaxial tensile performance. The density, compressive strength, first-crack strength, ultimate tensile strength, and tensile strain capacity of strain hardening slag-based geopolymer composites developed by Lee et al. (2012) were in the range of 1970−2020 kg/m^3, 19.4−30.6 MPa, 2.55−3.87 MPa, 2.83−4.69 MPa, and 1.53−4.48% at 28 days, depending on the type of activator and water to binder ratio. Although the feasibility of developing slag-based geopolymer composite was established in Lee et al. (2012) study, no detail studies on micromechanical parameters including matrix toughness and fiber-matrix interfacial properties were undertaken in their study to gain an in-depth knowledge on underlying mechanisms governing strain hardening behavior in this cement-less composite.

As mentioned in Section 2.4.3, 78% of the national electricity in Australia is provided through coal-burning power stations (Uranium Information Centre Ltd. Australia, 2005). In addition, 12 million tons of fly ash has been annually produced in Australia, of which 5.5 million tons were utilized in different applications, in particular in blended cement concrete (Heidrich, 2013). On the basis of these statistics, it can be said that in Australia fly ash that is available in large amounts is a good precursor for manufacture of

geopolymer. As mentioned earlier at the time of start of this doctoral research, there has been no study to investigate the properties and behavior of strain hardening fly ash-based geopolymer composites where the OPC binder is completely replaced by the fly ash-based geopolymer binder. This is the main motivation behind this doctoral research.

Concurrent to this doctoral research, Ohno and Li (2014) in University of Michigan, USA conducted a research study to investigate the feasibility of developing strain hardening fly ash-based geopolymer composite. A mixture proportion incorporating two different types of Class F fly ash and a sodium-based (Na-based) activator combination was determined through experiments in their study. They reported that the reason for using two types of fly ash was to prepare a mix with adequate setting time so there is enough time for casting the specimens without any problem and also the mix can be hardened in ambient temperature after 24 hours. The Na-based activator was composed of NaOH and Na_2SiO_3 solutions. The NaOH solution was prepared using NaOH pellet (59% w/w) and tab water (41% w/w) resulting a very high concentration of more than 14.0 M. The Na_2SiO_3 solution had a modulus ratio (Ms) equal to 3.22 (where $Ms=SiO_2/Na_2O$, $Na_2O=8.9\%$ and $SiO_2=28.7\%$). Fine silica sand with sand to binder ratio of 0.3 by mass was also used in the mixture. Extra water with water to fly ash ratio of 0.12 by mass was also used to provide adequate rheology for uninform fiber dispersion. Oil-coated PVA fibers (2% by volume) with a surface oil coating of 1.2% by weight, length of 12 mm and diameter of 39 μm were used to reinforce the fly ash-based geopolymer matrix. All specimens were demolded after 24 hours, and divided into three groups and subjected to three different curing conditions. The first group after demolding was air cured at a room temperature (23 °C ± 3 °C) until the age of 28 days prior to testing. The second and third groups after demolding were placed in an oven at 60 °C for 4 and 8 hours, respectively. Subsequently, they were air cured at a room temperature (23 °C ± 3 °C) until the age of 28 days prior to testing.

A series of experiments were conducted to characterize the properties of fly ash-based geopolymer composite including compressive strength and uniaxial tensile performance and crack pattern analysis using digital image correlation (DIC) technique. The strain hardening fly ash-based geopolymer composites developed by Ohno and Li (2014) exhibited low to moderate compressive strength of 17.4−27.6 MPa, low to moderate ultimate tensile strength of 2.9−3.4 MPa, and very high tensile strain capacity of

2.7−4.3% at 28 days, depending on the curing condition. Test results indicated that heat curing can improve both compressive and tensile strengths and tensile ductility of the composite. It was reported that DIC technique is a good approach to clearly visualize the multiple cracking pattern of the composite. Maximum and average crack widths of 117μm and 45 μm, respectively were reported for a dogbone specimen with a tensile strain capacity of 4.6%, which confirmed that the composite had a tightly controlled crack width control even under a high imposed strain level of 4.6%. Although the feasibility of developing fly ash-based geopolymer composite was established in Ohno and Li (2014) study, the low to moderate compressive and tensile strengths of the developed composite can limit the application of the composite in the construction industry. Therefore, the author of this doctoral research set out to further build on Ohno and Li (2014) formulation and improve the formulation in a number of ways. The identified areas for improvements were compressive and uniaxial tensile strengths. In addition, as mentioned earlier, Ohno and Li (2014) used a very high concentration of more than 14.0 M NaOH solution for their composite mixture design. This is another potential area where improvement can be made by using low concentration activator solution. One advantage of reducing the concentration of NaOH solution is that it increases the safety in handling large quantities. Furthermore, similar to Lee et al. (2012) study, no detail studies on micromechanical parameters including matrix toughness and fiber-matrix interfacial properties were undertaken in Ohno and Li (2014) study to explain the underlying mechanisms governing strain hardening behavior in fly ash-based geopolymer composite.

Choi et al. (2015) in South Korea conducted a study to manufacture strain hardening slag-based geopolymer composite with low viscosity for grout or oil well applications. Previous studies reported that the plastic viscosity of SHCC mixture should be in the range of 5−14 Pa.S to warrant uniform fiber dispersion under the shear force provided by a force-based or gravity-based concrete mixer (Li, 2009). However, in grout or oil well applications the material should be able to be pumped into holes. Thus, the plastic viscosity of the material in grout or oil well applications should be below 1 Pa.S (Sonebi, 2006), which is one order of magnitude lower than the recommended plastic viscosity range in SHCC mixture. Choi et al. (2015) set the target plastic viscosity and yield stress of the composite to be below 1 Pa.S and 25 Pa, respectively. They also set the target ductility and compressive strength to be above 1.5% and 15 MPa, respectively.

Four mix proportions were determined through preliminary tests. A combination of calcium hydroxide and sodium sulfate in powder form was used as the activator. Oil-coated PVA fibers with a surface oil coating of 0.6% by weight, length of 8 mm and diameter of 39 μm were used to reinforce the slag-based geopolymer matrix. The effect of fiber amount and water content on the rheological properties (plastic viscosity and yield stress) of the composite were investigated. The V-funnel flow time test and the mini-slump test were used in their study to measure the plastic viscosity and yield stress of the fresh composites. A series of experiments were conducted to characterize the mechanical properties and micromechanical parameters of slag-based geopolymer composite including compressive strength, uniaxial tensile performance, matrix fracture toughness and single-fiber pullout tests. Test results indicated that for a water to binder ratio of more than 0.4 and fiber volume of below 1.3%, the target plastic viscosity (below 1 Pa.S) was achieved by using appropriate amount of superplasticizer. The compressive strength of all mixtures investigated was more than the target strength (15 MPa). The strain hardening slag-based geopolymer composites developed by Choi et al. (2015) exhibited first-crack strength of 1.08−1.53 MPa, ultimate tensile strength of 1.41−2.26 MPa, and tensile strain capacity of 1.02−2.38% at 28 days, depending on the fiber content and water to binder ratio. Single-fiber pullout test results indicated that the increase in water content reduced both the frictional and chemical bonds between the fiber and the geopolymer matrix, while the slip hardening coefficient was constant. It should be noted that the reduction in chemical bond strength due to increase in water content was more pronounced than frictional bond strength. Among the mixtures, M40-1.3 mixture with water to binder ratio of 0.4 and fiber volume of 1.3% demonstrated the highest compressive and tensile strengths and tensile strain capacity of 18.3 MPa, 2.26 MPa and 2.38%, respectively. The micromechanical analysis indicated that this mixture had the highest PSH performance indices, which support the uniaxial tension test results. This mixture also exhibited the plastic viscosity and yield stress of 0.86 Pa.S, and 18 Pa, respectively, which were one order of magnitude lower than those of normal concrete in the fresh state. Hence, it can be said that the target compressive strength, tensile ductility, plastic viscosity and yield stress was reached for this composite.

Choi et al. (2016a) in South Korea also conducted a study to investigate the mechanical properties of strain hardening slag-based geopolymer composite reinforced by high

strength PE fibers. PE fibers (1.75% by volume) with a length of 12 mm, diameter of 16 μm, elastic modulus of 112 GPa, and tensile strength of 3030 MPa were used in their study. Two mixtures with different water to binder ratio were prepared to investigate the effect of water content on the properties of the slag-based geopolymer composite. Counterpart PE-SHCC mixtures with water to binder ratio corresponding to the slag-based geopolymer composites were also prepared for comparison purposes. Density, compressive strength and uniaxial tensile performance of the composites were measured experimentally. The strain hardening slag-based geopolymer composites exhibited compressive strength of 31.3−43.0 MPa, first-crack strength of 1.80−2.64 MPa, ultimate tensile strength of 5.96−7.89 MPa, and tensile strain capacity of 5.32−5.92% at 28 days, depending on the water to binder ratio. In contrast, the counterpart cement-based composites exhibited compressive strength of 60.8−75.9 MPa, first-crack strength of 3.43−3.97 MPa, ultimate tensile strength of 9.53−9.80 MPa, and tensile strain capacity of 3.91−4.88% at 28 days, depending on the water to binder ratio. The experimental results revealed that the compressive and tensile strengths of the slag-based geopolymer composites were lower than those of corresponding cement-based composites. However, slag-based geopolymer composites exhibited superior tensile strain capacity with smaller crack width and crack spacing to corresponding cement-based composites. In addition, the tensile strength to the compressive strength ratio of slag-based geopolymer composites were higher than that of corresponding cement-based composites. Although the results of Choi et al. (2016a) study indicated that slag-based geopolymer composite has higher tensile ductility but lower tensile strength compared to the corresponding cement-based composites, no detail studies on micromechanical parameters including matrix toughness and fiber-matrix interfacial properties were undertaken in their study to explain the underlying reasons for different tensile performance of the composites. Therefore, the author of this doctoral research set out to conduct a detailed micromechanical investigation to gain an in-depth knowledge on the tensile performance a fly ash-based geopolymer composite reinforced by PE fibers. Quantitative influences of curing condition and type of fiber, namely PE versus PVA fiber, on the composite properties were also investigated. The results of the study are presented in Chapter 10.

Choi et al. (2016b), as a follow up investigation, carried out a study to enhance the composite properties of their previously developed PE fiber reinforced slag-based

geopolymer composites (Choi et al., 2016a) and to demonstrate the feasibility of developing an ultra-high ductile PE fiber reinforced slag-based geopolymer composite. Four different mix proportions were prepared by changing the water to binder ratio from 0.26 to 0.38. The type of slag and type of activator used in this study were the same used in their previous study (Choi et al., 2016a). Appropriate amount of superplasticizer, viscosity modifying admixture and antifoaming were also used to ensure proper rheology to guarantee uniform fiber dispersion. PE fibers with the same 1.75% volume fraction were used in this study, but the properties of the fibers were different to those of used in their previous study (Choi et al., 2016a). In this study, PE fibers had a length of 18 mm, diameter of 12 μm, elastic modulus of 88 GPa, and tensile strength of 2700 MPa were used. Density, compressive strength and uniaxial tensile performance of the composites were measured experimentally. The ultra-high ductile slag-based geopolymer composites exhibited compressive strength of 36.3−54.8 MPa, first-crack strength of 3.37−4.87 MPa, ultimate tensile strength of 5.06−13.06 MPa, and tensile strain capacity of 4.58−7.50% at 28 days, depending on the water to binder ratio. It should be noted that the average ultimate tensile strength to compressive strength ratio was about 20%, which is almost double that of normal concrete. Average crack spacing and crack width in all mixtures were less than 2.25 mm and 101 μm, respectively. The results of Choi et al. (2016b) study established the feasibility of developing ultra-high ductile slag-based geopolymer composite with tensile strength and tensile strain capacity as high as 13.06 MPa and 7.5%, respectively with a moderate compressive strength of 55 MPa. However, no detail studies on micromechanical parameters including matrix toughness and fiber-matrix interfacial properties were undertaken in their study to fully understand the underlying mechanisms supporting ultra-high ductility in these cement-less composites. Further research is thus required to evaluate the microscale and other physical and mechanical properties of the developed composite to be able to use it as a construction material.

2.5 Summary

SHCCs represent a unique class of cement-based material exhibiting strain hardening subject to direct tension (Li and Wu, 1992; Li and Kanda, 1998). Based on micromechanics-based design principles, SHCC possesses extreme tensile ductility, several hundred times that of normal concrete, with the incorporation of small amount of

discontinues fibers, typically 2% or less by volume (Kong et al., 2003). High cement content, however, is commonly found in the mixture design of SHCC, which results in high autogenous shrinkage, heat of hydration, and cost. In addition, cement manufacturing is considered an energy intensive industry. The associated increase in the CO_2 emission as well as embodied energy apparently compromise sustainability performance of SHCC (Wang and Li, 2007; Yang et al., 2007).

To resolve this issue, researchers have partially replaced cement in the typical SHCC mix design by supplementary cementitious materials (SCMs). Within the last decade several efforts have been made to incorporate high volumes of ground granulated blast-furnace slag and/or fly ash as partial replacement of OPC in the SHCC mixture design to reduce the use of OPC; thereby, reducing the global warming potential associated with the CO_2 emission of the cement industry (Wang and Li, 2007; Yang et al., 2007). However, a more sustainable approach to develop green SHCCs is to completely replace the OPC binder in the SHCC mixture design by an alternative cement-less binder such as geopolymer.

Geopolymer is an emerging cement-less binder purported to provide a promising sustainable and environmentally friendly alternative to OPC binder. The term geopolymer was initially introduced by Davidovits (1991). Geopolymers can be manufactured at ambient or elevated temperature by alkali activation of materials of geological origin such as metakaolin, or industrial by-products such as fly ash and slag, which are rich in silica and alumina. Synthesis of fly ash-based geopolymer emits at least 80% less CO_2 and requires approximately 60% less energy compared to the production of OPC (Li et al., 2004; Duxson et al., 2007).

As mentioned in Section 2.4.6, at the time of commencement of this doctoral research in September 2012, there was only one research study available, authored by Lee et al. (2012) from South Korea, on the feasibility of developing a strain hardening slag-based geopolymer composite. In Australia fly ash is available in large quantities which can be used as a good source material for manufacture of geopolymer. However, at the time of start of this doctoral research, there has been no study on strain hardening fly ash-based geopolymer composites. This doctoral research is aimed to fill this knowledge gap by conducting a series of systematic and detailed studies on both micro and macro scales, which provide an in-depth knowledge on properties and behavior of strain hardening fly ash-based geopolymer composites.

2.6 References

AS 3600. 2009 Concrete structures. Australia: Standards Australia.

ASTM C618. 2003. Standard Specification for Coal Fly Ash and Raw or Calcined Natural Pozzolan for Use in Concrete. United States: ASTM Standards.

Cement Sustainability Initiative and European Cement Research Academy (ECRA). 2009. Development of State-of-the-Art Techniques in Cement Manufacturing: Trying to Look Ahead. Düsseldorf, Geneva.

ADAM, A. A. 2009. *Strength and Durability Properties of Alkali Activated Slag and Fly Ash-Based Geopolymer Concrete.* Ph.D., RMIT University.

AHMED, S. F. U., MAALEJ, M. & PARAMASIVAM, P. 2007. Flexural responses of hybrid steel–polyethylene fiber reinforced cement composites containing high volume fly ash. *Construction and Building Materials,* 21, 1088-1097.

ALONSO, S. & PALOMO, A. 2001. Alkaline activation of metakaolin and calcium hydroxide mixtures: influence of temperature, activator concentration and solids ratio. *Materials Letters,* 47, 55-62.

ALTWAIR, N. M., JOHARI, M. M. & HASHIM, S. S. 2012. Flexural performance of green engineered cementitious composites containing high volume of palm oil fuel ash. *Construction and Building Materials,* 37, 518-525.

AMIN, A. 2010. *GEOPOLYMER CONCRETE TO REDUCE THE ANTHROPOGENIC GREENHOUSE GAS EMISSIONS ASSOCIATED WITH THE CONCRETE AND CONSTRUCTION INDUSTRY.* M.Sc., University of New South Wales.

AVESTON, J. & KELLY, A. 1973. Theory of multiple fracture of fibrous composites. *Journal of Materials Science,* 8, 352-362.

BAKHAREV, T. 2005. Geopolymeric materials prepared using Class F fly ash and elevated temperature curing. *Cement and Concrete Research,* 35, 1224-1232.

BAKHAREV, T., SANJAYAN, J. & CHENG, Y.-B. 2000. Effect of admixtures on properties of alkali-activated slag concrete. *Cement and Concrete Research,* 30, 1367-1374.

BARBOSA, V. F. & MACKENZIE, K. J. 2003a. Synthesis and thermal behaviour of potassium sialate geopolymers. *Materials Letters,* 57, 1477-1482.

BARBOSA, V. F. & MACKENZIE, K. J. 2003b. Thermal behaviour of inorganic geopolymers and composites derived from sodium polysialate. *Materials Research Bulletin,* 38, 319-331.

BARBOSA, V. F., MACKENZIE, K. J. & THAUMATURGO, C. 2000. Synthesis and characterisation of materials based on inorganic polymers of alumina and silica: sodium polysialate polymers. *International Journal of Inorganic Materials,* 2, 309-317.

BENTUR, A. & MINDESS, S. 2007. *Fibre reinforced cementitious composites,* Taylor & Francis.

BERETKA, J. 1978. Survey of major industrial wastes and by products in Australia.

BERETKA, J. & WHITFIELD, D. G. 1993. *Survey of Industrial Process Wastes and By-Products Generated in Australia,* CSIRO.

BERNDT, M. L., SANJAYAN, J., FOSTER, S. & CASTEL, A. 2013. Pathways for overcoming barriers to implementation of low CO_2 concrete. *Research Project: RP1004.* CRC FOR LOW CARBON LIVING LTD.

BROOKS, J., JOHARI, M. M. & MAZLOOM, M. 2000. Effect of admixtures on the setting times of high-strength concrete. *Cement and Concrete Composites,* 22, 293-301.

CANBAY, E. & FROSCH, R. J. 2005. Bond strength of lap-spliced bars. *ACI Structural Journal,* 102, 605.

CEMENT SUSTAINABILITY INITIATIVE: RECYCLING CONCRETE. 2009. The World Business Council for Sustainable Development (WBCSD). DOI: 978-3-940388-49-0.

CENTER FOR SUSTAINABILITY AT TRL. 2006. The CO_2 Emissions Estimator Tool for the use of Aggregates in Construction -User Guide V 1.0. Waste Resources and Action Program (WRAP). Report AGG079-007.

CHANDRA, S. & BERNTSSON, L. 2002. Lightweight aggregate concrete: science, technology and applications. 2002, Norwich. New York, USA: William Andrew Publishing.

CHANG, E. H. 2009. *Shear and bond behaviour of reinforced fly ash-based geopolymer concrete beams.* Ph.D., Curtin University of Technology.

CHEN, C., HABERT, G., BOUZIDI, Y. & JULLIEN, A. 2010. Environmental impact of cement production: detail of the different processes and cement plant variability evaluation. *Journal of Cleaner Production,* 18, 478-485.

CHENG, T. & CHIU, J. 2003. Fire-resistant geopolymer produced by granulated blast furnace slag. *Minerals Engineering,* 16, 205-210.

CHOI, J.-I., LEE, B. Y., RANADE, R., LI, V. C. & LEE, Y. 2016a. Ultra-high-ductile behavior of a polyethylene fiber-reinforced alkali-activated slag-based composite. *Cement and Concrete Composites,* 70, 153-158.

CHOI, J.-I., SONG, K.-I., SONG, J.-K. & LEE, B. Y. 2016b. Composite properties of high-strength polyethylene fiber-reinforced cement and cementless composites. *Composite Structures,* 138, 116-121.

CHOI, S.-J., CHOI, J.-I., SONG, J.-K. & LEE, B. Y. 2015. Rheological and mechanical properties of fiber-reinforced alkali-activated composite. *Construction and Building Materials,* 96, 112-118.

CIOFFI, R., MAFFUCCI, L. & SANTORO, L. 2003. Optimization of geopolymer synthesis by calcination and polycondensation of a kaolinitic residue. *Resources, Conservation and Recycling,* 40, 27-38.

CRIADO, M., PALOMO, A., FERNÁNDEZ-JIMÉNEZ, A. & BANFILL, P. 2009. Alkali activated fly ash: effect of admixtures on paste rheology. *Rheologica Acta,* 48, 447-455.

DAMTOFT, J., LUKASIK, J., HERFORT, D., SORRENTINO, D. & GARTNER, E. 2008. Sustainable development and climate change initiatives. *Cement and concrete research,* 38, 115-127.

DAVIDOVITS, J. 1984. Synthetic mineral polymer compound of the silicoaluminates family and preparation process. Google Patents.

DAVIDOVITS, J. 1987. Ancient and modern concretes: What is the real difference? *Concrete International,* 9, 23-28.

DAVIDOVITS, J. 1991. Geopolymers. *Journal of thermal analysis,* 37, 1633-1656.

DAVIDOVITS, J. 1994. Geopolymers: inorganic polymeric new materials. *Journal of Materials Education,* 16, 91–139.

DAVIDOVITS, J. Chemistry of geopolymeric systems, terminology. Geopolymer, 1999. 9-40.

DAVIDOVITS, J. Geopolymer, Green Chemistry and Sustainable Development Solutions: Proceedings of the World Congress Geopolymer 2005. 2005. Geopolymer Institute.

DOUGLAS, E. & BRANDSTETR, J. 1990. A preliminary study on the alkali activation of ground granulated blast-furnace slag. *Cement and concrete research,* 20, 746-756.

DUXSON, P., PROVIS, J. L., LUKEY, G. C. & VAN DEVENTER, J. S. 2007. The role of inorganic polymer technology in the development of 'green concrete'. *Cement and Concrete Research,* 37, 1590-1597.

EDOUARD, J.-B. 2011. *EXPERIMENTAL EVALUATION OF THE DURABILITY OF FLY ASH-BASED GPC IN THE MARINE ENVIRONMENT.* M.Sc., Florida Atlantic University.

FERDOUS, M. W. 2012. *Static Flexural Behaviour of Fly Ash-Based Geopolymer Composite Beam: An alternative railway sleeper.* M.Sc., University of New South Wales.

FERNÁNDEZ-JIMÉNEZ, A. & PALOMO, A. 2003. Characterisation of fly ashes. Potential reactivity as alkaline cements. *Fuel,* 82, 2259-2265.

FERNÁNDEZ-JIMÉNEZ, A. & PALOMO, A. 2005. Composition and microstructure of alkali activated fly ash binder: effect of the activator. *Cement and concrete research,* 35, 1984-1992.

FERNANDEZ-JIMENEZ, A. M., PALOMO, A. & LOPEZ-HOMBRADOS, C. 2006. Engineering properties of alkali-activated fly ash concrete. *ACI Materials Journal,* 103, 106-112.

FLOWER, D. J. & SANJAYAN, J. G. 2007. Green house gas emissions due to concrete manufacture. *The international Journal of life cycle assessment,* 12, 282-288.

FOSTER, S. 2010. Design of FRC beams for shear using the VEM and the draft Model Code approach. *Proceedings of a Workshop on Shear and Punching Shear in RC and FRC Elements.* Salò, Lake Garda, Italy.

GARCÍA-LODEIRO, I., PALOMO, A. & FERNÁNDEZ-JIMÉNEZ, A. 2007. Alkali–aggregate reaction in activated fly ash systems. *Cement and Concrete Research,* 37, 175-183.

GARTNER, E. 2004. Industrially interesting approaches to "low-CO 2" cements. *Cement and Concrete research,* 34, 1489-1498.

HANEHARA, S. & YAMADA, K. 1999. Interaction between cement and chemical admixture from the point of cement hydration, absorption behaviour of admixture, and paste rheology. *Cement and Concrete Research,* 29, 1159-1165.

HARDJITO, D. & RANGAN, B. 2005. Development and properties of low-calcium fly ash-based geopolymer concrete. *Research Report GC 1,Faculty of Engineering, Curtin University of Technology, Perth, Australia.*

HARDJITO, D., WALLAH, S. E., SUMAJOUW, D. M. & RANGAN, B. V. 2004. On the development of fly ash-based geopolymer concrete. *ACI Materials Journal-American Concrete Institute,* 101, 467-472.

HASANBEIGI, A., PRICE, L. & LIN, E. 2012. Emerging energy-efficiency and CO 2 emission-reduction technologies for cement and concrete production: A technical review. *Renewable and Sustainable Energy Reviews,* 16, 6220-6238.

HEIDRICH, C. Ash Utilisation-An Australian Perspective. Geopolymers 2002 International Conference, Melbourne, Australia, Siloxo, 2002.

HEIDRICH, C., FEUERBORN, H.-J. & WEIR, A. Coal combustion products: a global perspective. World coal ash WOCA conference, Lexington, KY, 2013.

HEMMINGS, R. & BERRY, E. On the glass in coal fly ashes: recent advances. MRS Proceedings, 1987. Cambridge Univ Press, 3.

HTUT, T. & FOSTER, S. 2010. Unified model for mixed mode fracture of steel fiber reinforced concrete. *Proc., Fracture Mechanics of Concrete and Concrete Structures—High Performance, Fiber Reinforced Concrete, Special Loadings and Structural Applications (FraMCoS-7)*, 1469-1477.

HUANG, X., RANADE, R. & LI, V. C. 2012. Feasibility study of developing green ECC using iron ore tailings powder as cement replacement. *Journal of Materials in Civil Engineering,* 25, 923-931.

HUNTZINGER, D. N. & EATMON, T. D. 2009. A life-cycle assessment of Portland cement manufacturing: comparing the traditional process with alternative technologies. *Journal of Cleaner Production,* 17, 668-675.

ISMAIL, I., BERNAL, S. A., PROVIS, J. L., SAN NICOLAS, R., BRICE, D. G., KILCULLEN, A. R., HAMDAN, S. & VAN DEVENTER, J. S. 2013. Influence of fly ash on the water and chloride permeability of alkali-activated slag mortars and concretes. *Construction and Building Materials,* 48, 1187-1201.

JOSA, A., AGUADO, A., HEINO, A., BYARS, E. & CARDIM, A. 2004. Comparative analysis of available life cycle inventories of cement in the EU. *Cement and Concrete Research,* 34, 1313-1320.

KABELE, P., LI, V. C., HORII, H., KANDA, T. & TAKEUCHI, S. 1997. Use of BMC for ductile structural members. *5th International Symposium on Brittle Matrix Composites (BMC-5)*. Warsaw, Poland.

KANDA, T. & LI, V. C. 1998. Interface property and apparent strength of high-strength hydrophilic fiber in cement matrix. *Journal of materials in civil engineering,* 10, 5-13.

KANDA, T. & LI, V. C. 2006. Practical design criteria for saturated pseudo strain hardening behavior in ECC. *Journal of advanced concrete technology,* 4, 59-72.

KANDA, T., WATANABE, S. & LI, V. 1998. Application of pseudo strain hardening cementitious composites to shear resistant structural elements. *AEDIFICATIO Publishers, Fracture Mechanics of Concrete Structures,* 3, 1477-1490.

KIM, J.-K., KIM, J.-S., HA, G. J. & KIM, Y. Y. 2007. Tensile and fiber dispersion performance of ECC (engineered cementitious composites) produced with ground granulated blast furnace slag. *Cement and Concrete Research,* 37, 1096-1105.

KIM, Y. Y., FISCHER, G. & LI, V. C. 2004. Performance of bridge deck link slabs designed with ductile engineered cementitious composite. *ACI structural Journal,* 101, 792-801.

KOJIMA, S., SAKATA, N., KANDA, T. & HIRAISHI, T. 2004. Application of direct sprayed ECC for retrofitting dam structure surface-application for Mitaka-Dam. *Concrete Journal,* 42, 135-139.

KONG, D. L. & SANJAYAN, J. G. 2010. Effect of elevated temperatures on geopolymer paste, mortar and concrete. *Cement and concrete research,* 40, 334-339.

KONG, H.-J., BIKE, S. G. & LI, V. C. 2003. Development of a self-consolidating engineered cementitious composite employing electrosteric dispersion/stabilization. *Cement and Concrete Composites,* 25, 301-309.

KUPWADE-PATIL, K. & ALLOUCHE, E. Effect of alkali silica reaction (ASR) in geopolymer concrete. World of Coal Ash (WOCA) conference, 2011. 9-12.

LANKARD, D. R. & NEWELL, J. K. 1984. Preparation of highly reinforced steel fiber reinforced concrete composites. *Special Publication,* 81, 287-306.

LEE, B. Y., CHO, C.-G., LIM, H.-J., SONG, J.-K., YANG, K.-H. & LI, V. C. 2012. Strain hardening fiber reinforced alkali-activated mortar–a feasibility study. *Construction and Building Materials,* 37, 15-20.

LEPECH, M. D. & LI, V. C. 2009. Application of ECC for bridge deck link slabs. *Materials and Structures,* 42, 1185-1195.

LI, M. 2009. *Multi-scale design for durable repair of concrete structures.* Ph.D., University of Michigan.

LI, V. 2006. Technology Advances: Bendable Concrete Minimizes Cracking and Fracture Problems. *MRS Bulletin,* 31, 862.

LI, V., FISCHER, G. & LEPECH, M. 2009. Shotcreting with ECC. *Spritzbeton-tagung Alpbach*.

LI, V. C. 1998. Engineered cementitious composites-tailored composites through micromechanical modeling. *In:* N. BANTHIA, A. BENTUR, A. & MUFTI, A. (eds.) *Fiber Reinforced Concrete: Present and the Future.* Montreal: Canadian Society for Civil Engineering.

LI, V. C. 2003. On engineered cementitious composites (ECC). *Journal of advanced concrete technology,* 1, 215-230.

LI, V. C. & KANDA, T. 1998. Innovations Forum: Engineered cementitious composites for structural applications. *Journal of Materials in Civil Engineering,* 10, 66-69.

LI, V. C., LEPECH, M., WANG, S., WEIMANN, M. & KEOLEIAN, G. Development of green engineered cementitious composites for sustainable infrastructure systems. Proceedings of the International Workshop on Sustainable Development and Concrete Technology, 2004a. 181-191.

LI, V. C. & LEUNG, C. K. 1992. Steady-state and multiple cracking of short random fiber composites. *Journal of Engineering Mechanics,* 118, 2246-2264.

LI, V. C., MISHRA, D. K. & WU, H.-C. 1995. Matrix design for pseudo-strain-hardening fibre reinforced cementitious composites. *Materials and Structures,* 28, 586-595.

LI, V. C., WANG, S. & WU, C. 2001. Tensile strain-hardening behavior of polyvinyl alcohol engineered cementitious composite (PVA-ECC). *ACI materials Journal,* 98.

LI, V. C. & WU, H.-C. 1992. Conditions for pseudo strain-hardening in fiber reinforced brittle matrix composites. *Applied Mechanics Reviews,* 45, 390-398.

LI, Z., DING, Z. & ZHANG, Y. Development of sustainable cementitious materials. Proceedings of international workshop on sustainable development and concrete technology, Beijing, China, 2004b. 55-76.

LIM, Y. M. & LI, V. C. 1997. Durable repair of aged infrastructures using trapping mechanism of engineered cementitious composites. *Cement and Concrete Composites,* 19, 373-385.

MAALEJ, M. & LI, V. C. 1995. Introduction of strain-hardening engineered cementitious composites in design of reinforced concrete flexural members for improved durability. *Structural Journal,* 92, 167-176.

MALHOTRA, V. 1999. Making concrete" greener" with fly ash. *Concrete International*, 21, 61-66.

MARCEAU, M., NISBET, M. A. & VAN GEEM, M. G. 2006. Life cycle inventory of portland cement manufacture. Portland Cement Association Skokie, IL, US.

MARSHALL, D. & COX, B. 1988. A J-integral method for calculating steady-state matrix cracking stresses in composites. *Mechanics of materials,* 7, 127-133.

MASANET, E., PRICE, L., DE LA RUE DU CAN, S., BROWN, R. & WORRELL, E. 2005. Optimization of Product Life Cycles to Reduce Greenhouse Gas Emissions in California. California Energy Commission, PIER Energy-Related Environmental Research.

MATSUMOTO, T. & MIHASHI, H. 2003. DFRCC terminology and application concepts. *Journal of Advanced Concrete Technology*, 1, 335-340.

MEHTA, P. K. 1999. Concrete technology for sustainable development. *Concrete International,* 21, 47-53.

MEMON, F. A., NURUDDIN, M. F., DEMIE, S. & SHAFIQ, N. 2012. Effect of superplasticizer and extra water on workability and compressive strength of self-compacting geopolymer concrete. *Research Journal of Applied Sciences, Engineering and Technology,* 4, 407-414.

MISHRA, D. 1995. *Design of pseudo strain-hardening cementitious composites for a ductile plastic hinge.* PhD, University of Michigan.

MONTES, C. 2010. *DEVELOPMENT OF A GEOPOLYMER-BASED CEMENTITIOUS COATING FOR THE REHABILITATION OF BURIED CONCRETE INFRASTRUCTURE.* Ph.D., LOUISIANA TECH UNIVERSITY.

NAAMAN, A. & REINHARDT, H. W. 1995. Characterization of high performance fiber reinforced cement composites-HPFRCC. *The second international RILEM workshop on high performance fiber reinforced cement composites.* USA.

NAAMAN, A. E. 2008. High Performance Fiber Reinforced Cement Composites. *Engineering Materials for Technological Needs HIGH-PERFORMANCE CONSTRUCTION MATERIALS Science and Applications.* World Scientific Publishing Co. Pte. Ltd.

NEMATOLLAHI, B., SAIFULNAZ, M. R. & VOO, Y. L. 2014a. Sustainability assessment of precast ultra-high performance fiber reinforced concrete (UHPFRC)

cantilever retaining walls. *Research Journal of Applied Sciences, Engineering and Technology,* 7, 3971-3977.

NEMATOLLAHI, B. & SANJAYAN, J. 2014. Efficacy of available superplasticizers on geopolymers. *Research Journal of Applied Sciences, Engineering and Technology,* 7, 1278-1282.

NEMATOLLAHI, B., VOO, Y. L. & SAIFULNAZ, M. R. R. 2014b. Structural Behavior of Precast Ultra-High Performance Fiber Reinforced Concrete (UHPFRC) Cantilever Retaining Walls: Part I-Analysis and Design Procedures and Environmental Impact Calculations (EIC). *KSCE Journal of civil engineering,* 18, 1470-80.

NEMATOLLAHI, B., VOO, Y. L. & SAIFULNAZ, M. R. R. 2014c. Structural behavior of precast Ultra-High Performance Fiber Reinforced Concrete (UHPFRC) cantilever retaining walls: Part II—Full scale experimental testing. *KSCE Journal of civil engineering,* 18, 1481-1495.

NEMATOLLAHI, B., VOO, Y. L. & SANJAYAN, J. 2016. Design and Construction of a Precast Ultra-High Performance Concrete Cantilever Retaining Wall. *First International Interactive Symposium on UHPC – 2016.* Des Moines, Iowa.

NEVILLE, A. M. 1995. *Properties of concrete,* Harlow : Longman Group.

NG, T. S. 2011. *An investigation into the development of high performance geopolymer concrete.* Ph.D., University of New South Wales.

OHNO, M. & LI, V. C. 2014. A feasibility study of strain hardening fiber reinforced fly ash-based geopolymer composites. *Construction and Building Materials,* 57, 163-168.

OLIVIA, M. 2011. *Durability related properties of low calcium fly ash based geopolymer concrete.* Ph.D., Curtin University of Technology.

ÖZBAY, E., ŠAHMARAN, M., LACHEMI, M. & YÜCEL, H. E. 2013. Self-Healing of Microcracks in High-Volume Fly-Ash-Incorporated Engineered Cementitious Composites. *ACI Materials Journal,* 110.

PALACIOS, M., BANFILL, P. F. & PUERTAS, F. 2008. Rheology and setting of alkali-activated slag pastes and mortars: effect of organic admixture. *ACI Materials Journal,* 105, 140.

PALACIOS, M., HOUST, Y. F., BOWEN, P. & PUERTAS, F. 2009. Adsorption of superplasticizer admixtures on alkali-activated slag pastes. *Cement and Concrete Research,* 39, 670-677.

PALACIOS, M. & PUERTAS, F. 2004. Stability of superplasticizer and shrinkage-reducing admixtures in high basic media. *Materiales de Construcción,* 54, 65-86.

PALACIOS, M. & PUERTAS, F. 2005. Effect of superplasticizer and shrinkage-reducing admixtures on alkali-activated slag pastes and mortars. *Cement and concrete research,* 35, 1358-1367.

PALOMO, A., GRUTZECK, M. & BLANCO, M. 1999. Alkali-activated fly ashes: a cement for the future. *Cement and concrete research,* 29, 1323-1329.

PEIJIANG, S. 2005. *Fly ash based inorganic polymeric building material.* Ph.D., Wayne State University.

PHAIR, J., SMITH, J. & VAN DEVENTER, J. 2003. Characteristics of aluminosilicate hydrogels related to commercial "Geopolymers". *Materials Letters,* 57, 4356-4367.

PHAIR, J. & VAN DEVENTER, J. 2001. Effect of silicate activator pH on the leaching and material characteristics of waste-based inorganic polymers. *Minerals Engineering,* 14, 289-304.

PROVIS, J. L. 2006. *Modelling the formation of geopolymers.* PhD, University of Melbourne.

PROVIS, J. L., YONG, C. Z., DUXSON, P. & VAN DEVENTER, J. S. 2009. Correlating mechanical and thermal properties of sodium silicate-fly ash geopolymers. *Colloids and Surfaces A: Physicochemical and Engineering Aspects,* 336, 57-63.

PUERTAS, F., PALOMO, A., FERNÁNDEZ-JIMÉNEZ, A., IZQUIERDO, J. & GRANIZO, M. 2003. Effect of superplasticisers on the behaviour and properties of alkaline cements. *Advances in cement research,* 15, 23-28.

PUERTAS, F. & VÁZQUEZ, T. 2001. Early hydration cement Effect of admixtures superplasticizers. *Materiales de construcción,* 51, 53-61.

QUDAH, S. & MAALEJ, M. 2014. Application of Engineered Cementitious Composites (ECC) in interior beam–column connections for enhanced seismic resistance. *Engineering Structures,* 69, 235-245.

RANGAN, B. V. 2008. Fly ash-based geopolymer concrete. *Research Report GC4. Curtin University of Technology, Perth, Australia.*

Recommendations for Design and Construction of High Performance Fiber Reinforced Cement Composites with Multiple Fine Cracks (HPFRCC). *Concrete Engineering Series 82.* Japan Society of Civil Engineers.

RIXOM, M. & MAILVAGANAM, N. P. 1999. *Chemical admixtures for concrete,* ACI Education Bulletin E4-03, Taylor & Francis.

ROWLES, M. R. 2004. *The structural nature of aluminosilicate inorganic polymers: a macro to nanoscale study.* Ph.D., Curtin University of Technology.

ŞAHMARAN, M., LACHEMI, M., HOSSAIN, K. M., RANADE, R. & LI, V. C. 2009. Influence of aggregate type and size on ductility and mechanical properties of engineered cementitious composites. *ACI Materials Journal,* 106, 308-316.

SARKER, P. K. 2009. Analysis of geopolymer concrete columns. *Materials and structures,* 42, 715-724.

SHAYAN, A. 2013. Specification and Use of Geopolymer Concrete in the Manufacture of Structural and Non-Structural Components. Austroads Report, Austroads Project No. TS1835.

SOLTANINAVEH, K. 2008. *The properties of geopolymer concrete incorporating red sand as fine aggregate.* M.Sc., Curtin University of Technology.

SONEBI, M. 2006. Rheological properties of grouts with viscosity modifying agents as diutan gum and welan gum incorporating pulverised fly ash. *Cement and Concrete Research,* 36, 1609-1618.

SUMAJOUW, M. & RANGAN, B. V. 2006. Low-calcium fly ash-based geopolymer concrete: reinforced beams and columns. *Curtin University of Technology*.

TEMPEST, B. 2010. *ENGINEERING CHARACTERIZATION OF WASTE DERIVED GEOPOLYMER CEMENT CONCRETE FOR STRUCTURAL APPLICATIONS.* Ph.D., University of North Carolina at Charlotte.

URANIUM INFORMATION CENTER LTD. AUSTRALIA. 2005. Nuclear Energy Prospects in Australia. Retrieved 12 June 2006, from http://www.uic.com.au/nip44.htm.

VAN DAM, T. J. 2010. CPTP TechBrief: Geopolymer concrete, FHWA-HIF-10-014. Federal highway administration office of pavement technology.

VAN JAARSVELD, J. & VAN DEVENTER, J. 1999. Effect of the alkali metal activator on the properties of fly ash-based geopolymers. *Industrial & Engineering Chemistry Research,* 38, 3932-3941.

VAN JAARSVELD, J., VAN DEVENTER, J. & LORENZEN, L. 1997. The potential use of geopolymeric materials to immobilise toxic metals: Part I. Theory and applications. *Minerals Engineering,* 10, 659-669.

VAN JAARSVELD, J., VAN DEVENTER, J. & LUKEY, G. 2002. The effect of composition and temperature on the properties of fly ash-and kaolinite-based geopolymers. *Chemical Engineering Journal,* 89, 63-73.

VAN JAARSVELD, J., VAN DEVENTER, J. & LUKEY, G. 2003. The characterisation of source materials in fly ash-based geopolymers. *Materials Letters,* 57, 1272-1280.

VAN ZIJL, G. & WITTMAN, F. H. 2011. *Durability of Strain-Hardening Fibre-Reinforced Cement-Based Composites (SHCC)*, Springer Netherlands.

VECCHIO, F. 2000. Disturbed stress field model for reinforced concrete: formulation. *Journal of Structural Engineering,* 126, 1070-1077.

VOO, Y. L. & FOSTER, S. J. 2010. Characteristics of ultra-high performance 'ductile'concrete and its impact on sustainable construction. *The IES Journal Part A: Civil & Structural Engineering,* 3, 168-187.

WALLAH, S. & RANGAN, B. V. 2006a. Low-calcium fly ash-based geopolymer concrete: long-term properties. *Res. Report-GC2, Curtin University, Australia. pp,* 76-80.

WALLAH, S. & RANGAN, B. V. 2006b. Low-calcium fly ash-based geopolymer concrete: long-term properties. *Research Report-GC2, Curtin University, Australia.*

WANG, Q., LI, L., WU, C. P. & SUI, Z. T. Research on adaptability of slag-based geopolymer with superplasticizer. Key Engineering Materials, 2009. Trans Tech Publ, 129-134.

WANG, S. 2005. *Micromechanics based matrix design for engineered cementitious composites.* Ph.D., University of Michigan.

WANG, S. & LI, V. 27 LIGHTWEIGHT ENGINEERED CEMENTITIOUS COMPOSITES (ECC). PRO 30: 4th International RILEM Workshop on High Performance Fiber Reinforced Cement Composites (HPFRCC 4), 2003. RILEM Publications, 379.

WANG, S. & LI, V. C. 2007. Engineered cementitious composites with high-volume fly ash. *ACI Materials Journal-American Concrete Institute,* 104, 233-241.

WEIMANN, M. & LI, V. C. 2003. Hygral behavior of engineered cementitious composites (ECC). *International Journal for Restoration of Buildings and Monuments,* 9, 513-534.

WESCHE, K. 1991. *Fly ash in concrete: properties and performance*, RILEM Report of Technical Committee 67-FAB: E & FN Spon.

WORRELL, E., GALITSKY, C. & PRICE, L. 2008. Energy Efficiency Improvement Opportunities for the Cement Industry. Ernest Orlando Lawrence Berkeley National Laboratory, Berkeley, CA (US).

WU, H.-C., LI, V., LIM, Y. M., HAYES, K. & CHEN, C. 1996. Control of Cs leachability in cementitious binders. *Journal of materials science letters,* 15, 1736-1739.

XIE, Z. & XI, Y. 2001. Hardening mechanisms of an alkaline-activated class F fly ash. *Cement and Concrete Research,* 31, 1245-1249.

XU, H. & VAN DEVENTER, J. 2000. The geopolymerisation of alumino-silicate minerals. *International Journal of Mineral Processing,* 59, 247-266.

XU, H., VAN DEVENTER, J. & LUKEY, G. 2001. Effect of alkali metals on the preferential geopolymerization of stilbite/kaolinite mixtures. *Industrial & engineering chemistry research,* 40, 3749-3756.

XU, H. & VAN DEVENTER, J. S. 2002. Geopolymerisation of multiple minerals. *Minerals Engineering,* 15, 1131-1139.

YANG, E.-H. & LI, V. C. 2010. Strain-hardening fiber cement optimization and component tailoring by means of a micromechanical model. *Construction and building Materials,* 24, 130-139.

YANG, E.-H., WANG, S., YANG, Y. & LI, V. C. 2008. Fiber-bridging constitutive law of engineered cementitious composites. *Journal of advanced concrete technology,* 6, 181-193.

YANG, E.-H., YANG, Y. & LI, V. C. 2007. Use of high volumes of fly ash to improve ECC mechanical properties and material greenness. *ACI materials journal,* 104, 620-628.

ZHU, Y., YANG, Y. & YAO, Y. 2012. Use of slag to improve mechanical properties of engineered cementitious composites (ECCs) with high volumes of fly ash. *Construction and building materials,* 36, 1076-1081.

CHAPTER 3

EFFECT OF DIFFERENT SUPERPLASTICIZERS AND ACTIVATOR COMBINATIOINS ON WORKABILITY AND STRENGTH OF FLY ASH-BASED GEOPOLYMER

Note: This chapter is based on the paper "*Effect of different superplasticizers and activator combinations on workability and strength of fly ash based geopolymer*", by ***Nematollahi, B.*** and Sanjayan, J., published in ***Materials & Design***, 2014, 57, 667-672.

3.1 Introduction

As mentioned in Section 2.3.4 and also can be seen in Tables 2-1 and 2-2, it is common to use a small amount of SPs in typical SHCC mix proportion to adjust the workability and rheology of the mix. However, as mentioned in Section 2.4.4, SPs do not work the same on geopolymer systems than in OPC systems. In addition, the results of the previous studies on the effect of SPs on geopolymers are not yet conclusive about the effects of the nature and concentration of the activators used, type and dosage of SPs, time and temperature of heat curing, etc. Therefore, further research in this area is necessary. The objective of this chapter is to fill this knowledge gap by investigating the effect of different commercial SPs on the workability and strength of a low calcium fly ash-based geopolymer paste activated by two different activator combinations.

3.2 Materials

The low-calcium fly ash (Class F) used in this study was supplied from Gladstone power station in Queensland, Australia. Previous study revealed that among six types of Class F fly ashes obtained from six different Australian power stations, the low calcium fly ash supplied from Gladstone power station in Queensland, Australia exhibited the highest compressive strength due to the uniform distribution and similar pattern of SiO_2 and Al_2O_3 in the fly ash (Tennakoon et al., 2014). Table 3-1 presents the chemical composition and LOI of the fly ash determined by X-ray Fluorescence (XRF). The total does not sum up to 100% because of rounding-off of the percentages.

Previous studies reported that the type of alkaline activator plays an important role in the geopolymerisation process and has significant effect on the mechanical strength of geopolymer (Fernández-Jiménez and Palomo, 2005). As reported in Section 2.4.4, the effect of SPs on geopolymers directly depends on the type of activator and the pH of the alkaline solution. According to available literature, sodium hydroxide (NaOH) solution or a combination of NaOH and sodium silicate (Na_2SiO_3) solutions with Na_2SiO_3/NaOH mass ratio of 2.5 have been commonly used for production of fly ash-based geopolymers (Hardjito et al., 2004; Pan et al., 2011; Olivia and Nikraz, 2012; Sarker et al., 2013). Therefore, for the purpose of this study, two different activators with similar pH were used as follows:

1) NaOH solution (8.0 M concentration); pH=13.32 at 23°C
2) Multi-compound activator composed of NaOH and Na_2SiO_3 solutions with Na_2SiO_3/NaOH mass ratio of 2.5; pH=13.36 at 23°C

The NaOH solution was prepared with a concentration of 8.0 M using NaOH beads of 97% purity supplied by Sigma-Aldrich and tap water. The D Grade Na_2SiO_3 solution was supplied by PQ Australia with a specific gravity of 1.53 and a modulus ratio (Ms) equal to 2.0 (where Ms=SiO_2/ Na_2O, Na_2O=14.7% and SiO_2=29.4%). The NaOH and D Grade Na_2SiO_3 solutions were mixed together with Na_2SiO_3/NaOH mass ratio of 2.5 to prepare the multi-compound activator.

Six types of SPs investigated in this work were as follows: one melamine-based powder (M), two naphthalene-based (N1, N2), and three modified Polycarboxylate admixtures (PC1, PC2, PC3). According to Rixom and Maivaganam (1999), melamine-based and naphthalene based SPs are classified as the second generation of SPs where their fluidization mechanism is based on electrostatic inter-particle repulsion; whereas, modified Polycarboxylate SPs are considered as the third generation (the latest generation) of SPs where in addition to electrostatic repulsion benefits from steric repulsion produced by lateral ether chains on the SP's molecule. All these SPs are commercial products supplied by SIKA and BASF, Australia commonly used in conventional OPC concrete. The characteristics of the SPs used in this study are summarized in Table 3-2.

Table 3-1: Chemical composition of fly ash

Chemical	Component (wt. %)
Al_2O_3	25.56
SiO_2	51.11
CaO	4.3
Fe_2O_3	12.48
K_2O	0.7
MgO	1.45
Na_2O	0.77
P_2O_5	0.885
TiO_2	1.32
MnO	0.15
SO_3	0.24
LOI[1]	0.57

[1]Loss on ignition.

Table 3-2: Physical and chemical properties of the SPs

SP ID	Chemical base	Visual appearance	pH (20°C)	Density (g/cm^3)
PC1	modified Polycarboxylate	light brown liquid	6.5	1.05
PC2	modified Polycarboxylate	clear brown liquid	5.0±1.0	1.07
PC3	modified Polycarboxylate	light brown liquid	4.3±0.5	1.06
N1	Sodium naphthalene formaldehyde sulphonate	dark brown liquid	7.0±0.5	1.2
N2	Sodium naphthalene formaldehyde sulphonate	dark brown liquid	7.0	1.21
M	Sulphonated melamine methanol condensate	grey powder	8.0-10	0.80

3.3 Experimental Procedures

The experimental procedures in this study were divided into two parts. In the first part, the effect of different activators on workability and compressive strength of the fly ash-based geopolymer paste were investigated. The effect of different SPs on workability and compressive strength of the paste were investigated in the second part.

3.3.1 Effect of different activators

A constant activator to fly ash ratio of 0.3 was selected to prepare the mixtures. Activator was slowly added to fly ash and mixed in a Hobart mixer for 4 minutes. After the ingredients were thoroughly mixed to achieve the desired fresh state, flowability of the fresh paste was measured by mini-slump test, according to ASTM C1437 (2007). The fresh mixture was then cast in cylindrical molds (37 mm×74 mm) and sealed with aluminum foil and heat cured in the oven at 60°C for 24 hours. At the end of heat curing period, the specimens were removed from the oven and kept undisturbed until being cool and then removed from the molds and left in the laboratory at ambient temperature until the day of testing.

Compressive strength of each mixture was measured at 3 days after casting. Previous studies have shown that age does not have considerable effect on strength of geopolymers after completion of the heating curing period, thereby three-day compressive strength of geopolymer is equivalent to a typical OPC strength development after 28 days (Kong and Sanjayan, 2010; Hardjito et al., 2004). At least 6 cylindrical specimens for each mix were prepared and tested to check the variability under compression. Following AS 1012.9 (2014), the test rate was 20 MPa/min.

3.3.2 Effect of different SPs

To investigate the effect of different SPs on workability and strength of fly ash-based geopolymer paste, six different SPs (i.e. M, N1, N2, PC1, PC2 and PC3) were used in the case of using multi-compound activator (Na_2SiO_3/NaOH=2.5), whereas in the case of using sodium hydroxide solution (8.0 M concentration) only N1 was used because naphthalene-based SP is the only type of SP which is chemically stable in 8M NaOH solution (pH=13.32 at 23°C) which is an extremely high alkaline activator (Palacios and Puertas, 2004).

The fresh paste without SP was prepared as specified in Section 3.1.1 (Part I). Subsequently different SP with the dosage of 1% by mass of fly ash was added to the fresh paste and mixed for another 4 minutes. The flowability and compressive strength of the pastes were measured and compared with those of the pastes without using SP. Table 3-3 lists the various mixes prepared in this study using different activators and SPs.

Table 3-3: List of various mixes prepared using different activators and SPs

Mix ID		Type of activator	Type of superplasticizer
Part I	1	8 M NaOH solution	---
	2	Multi-compound activator	---
Part II	3	8 M NaOH solution	N1
	4	Multi-compound activator	PC1
	5	Multi-compound activator	PC2
	6	Multi-compound activator	PC3
	7	Multi-compound activator	N1
	8	Multi-compound activator	N2
	9	Multi-compound activator	M

3.4 Results and Discussion

3.4.1 Effect of different activators

The workability (in terms of relative slump value) and compressive strength of the mixtures without any SPs are presented in Table 3-4. As can be seen, both workability and compressive strength of the paste made by using only NaOH solution were 41% and 57%, respectively lower than those of the paste made by using multi-compound activator. However, through visual inspection it was noted that in the case of using only NaOH solution as the activator viscosity of the fly ash-based geopolymer paste was much lower than that of the paste made by using multi-compound activator. This seems to be due to much higher viscosity of D Grade Na_2SiO_3 solution (250-450 cps at 20°C) compared to that of the NaOH solution. It should be pointed out that previous studies proved that there is no relationship between slump and viscosity (Beaupré and Mindess, 1998; Tattersall and Banfill, 1983). According to Wallevik (2006), slump is influenced by the yield stress of the paste, not by the viscosity. It can be thereby said that the different workability of the mixtures is attributed to their different yield stress originated from their different type of activator.

The higher compressive strength of the paste made by using multi-compound activator solution is attributed to higher rate of geopolymerisation reaction in the paste, which is due to addition of Na_2SiO_3 solution to the NaOH solution which enhances the formation of geopolymer precursors upon contact between a mineral and the solution (Xu and van Deventer, 2000). Similar results were reported by other researchers for alkali-activated slag. For instance, Palacios and Puertas (2005) concluded that both the compressive and

flexural strengths of the slag-based mortars activated by NaOH solution (4% and 5% Na_2O by mass of slag) were much lower with respect to those of the mortar activated by multi-compound activator composed of NaOH solution (70% w/w) and Na_2SiO_3 (30% w/w) solution with SiO_2/Na_2O of 3.4.

It can be concluded that although the multi-compound activator resulted in a much more viscous paste, the workability and compressive strength of the paste made by the multi-compound activator were considerably higher than those of the paste made by only NaOH solution. In addition, using multi-compound activator results in some economical saving since the price of D Grade Na_2SiO_3 solution is cheaper than that of the NaOH solution.

Table 3-4: Workability and compressive strength of the fly ash-based geopolymer with different activators

Mix ID	Workability[a]	Compressive strength (MPa)	Type of activator
1	1.61 (161.5)	41.5±2.1	8 M NaOH solution
2	2.71 (192.5)	96.2±5.8	Multi-compound activator

[a] In terms of relative slump value of the fresh paste. The average diameter of the matrix flow (in millimeter) is shown in parenthesis.

3.4.2 Effect of different SPs

The workability (in terms of relative slump value) and compressive strength of the paste made by using only NaOH solution with and without using N1 (naphthalene-based SP) are presented in Table 3-5. As can be seen, workability of the paste with using N1 (a naphthalene-based SP) was 136% increased with respect to that of the paste without using any SP, while the compressive strength of the paste was not changed. It can be concluded that in the case of fly ash-based geopolymer activated by only NaOH solution (8.0 M concentration), N-based SPs (the second generation) are an effective type of SPs resulted in significant increase in the workability without having any negative effect on the compressive strength with reference to the paste without using any SP. Similar results were reported by Palacios and Puertas (2005) for slag-based paste activated by NaOH (4% and 5% Na2O by mass of slag). They concluded that the slump of the NaOH-activated slag paste was increased considerably during the full 60 min of the test with

using N based SP. Furthermore, N-based SP drastically reduced the activator to slag ratio causing significant improvement in mechanical strength (e.g. compressive strength) of the slag-based mortar compared to the mortar without using any SP. This is due to the fact that according to Palacios and Puertas (2004, 2005), N-based SP is the only type of SP which is chemically stable in NaOH solution (8.0 M concentration) with pH equals to 13.32 at 23°C.

Table 3-5: Effect of a naphthalene-based SP on workability and compressive strength of the fly ash-based geopolymer activated by only 8 M NaOH solution

Mix ID	Workability[a]	Compressive strength (MPa)	Type of SP
1	1.61 (161.5)	41.5±2.1	---
3	3.8 (219)	41.9±2.0	N1 (naphthalene-based)

[a] In terms of relative slump value of the fresh paste. The average diameter of the matrix flow (in millimeter) is shown in parenthesis.

The workability (in terms of relative slump value) and compressive strength of the paste made by using multi-compound activator with and without using different SPs are presented in Table 3-6. As can be seen, the workability of the pastes made by using modified Polycarboxylate-based SPs (i.e. PC1, PC2 and PC3) and naphthalene- based SPs (i.e. N1 and N2) increased with respect to that of the paste without using any SP. However, the workability of the paste made by using melamine-based powder (M) was decreased with respect to that of the paste without using any SP. The increase in workability was 45%, 41%, 39%, 6% and 8% for the pastes made by using PC1, PC2, PC3, N1, and N2, respectively with reference to the paste without using any SP. The workability of the paste made by using M-based SP was 3% lower than that of the paste without using any SPs. From the mini-slump test results, it can be concluded that each type of SPs influenced the fly ash-based geopolymer paste differently. This could be due to the instability of these commercial SPs in high basic media such as the multi-compound activator (Criado et al., 2009; Palacios and Puertas, 2004). In other words according to Palacios and Puertas (2004), all of the SPs used in this study were chemically unstable in multi-compound activator (Na_2SiO_3/NaOH=2.5) with pH equals to 13.36 at 23°C, thereby all of them experienced structural changes in contact with a very high alkaline solution, which resulted in loss of their plasticizing characteristics. In summary, it can be said that

in the case of fly ash-based geopolymer made by multi-compound activator (Na_2SiO_3/NaOH=2.5), PC based SPs (the latest generation) would be the most effective type of SPs resulted in 39% to 45% increase in relative slump value with reference to the paste without using any SP. It could be due to the fact that although PC-based SPs were also chemically unstable in multi-compound activator, existence of several lateral chains in its structure results in steric repulsion that compensates the tendency of particles to form complexes, therefore their plasticizing (fluidifying) ability would be greater than N-based SPs (Criado et al., 2009).

Similar results have been reported by Criado et al. (2009) for flow table spread in fly ash-based geopolymer mortar made by using M and PC based SPs. However, the effect of N-based SP on the workability of fly ash-based geopolymer mortar has not been investigated in their study. These researchers have also not investigated the effect of different SPs on strength of fly ash-based geopolymer.

Table 3-6: Effect of different SPs on workability and compressive strength of the fly ash-based geopolymer made by multi-compound activator

Mix ID	Workability[a]	Compressive strength (MPa)	Type of SP
2	2.71 (192.5)	96.2±5.8	---
4	3.93 (222)	68.0±3.8	PC1
5	3.82 (219.5)	81.3±4.6	PC2
6	3.77 (218.5)	80.8±4.4	PC3
7	2.88 (197)	55.6±3.2	N1
8	2.92 (198)	47.0±2.8	N2
9	2.63 (190.5)	55.1±3.1	M

[a] In terms of relative slump value of the fresh paste. The average diameter of the matrix flow (in millimeter) is shown in parenthesis.

According to Table 3-6, the compressive strength of the pastes made by using all types of SPs (i.e. N, M and PC based SPs) were decreased with respect to that of the paste without using any SP. The decrease in compressive strength was 29%, 15%, 16%, 42%, 51% and 43% for the pastes made by using PC1, PC2, PC3, N1, N2 and M, respectively with reference to the paste without using any SP. This reduction in compressive strength may be due to the instability of these SPs in multi-compound activator as a very high alkaline solution. Based on the compressive strength test results, N and M based SPs

resulted in significant (42% to 51%) reduction of compressive strength of the paste, while PC based SPs resulted in less (15% to 29%) reduction with reference to the paste without using any SP. As mentioned earlier, this could be due to the fact that although all of these SPs were chemically unstable in multi-compound activator, PC based SPs have several lateral chains in their structure causing steric repulsion in addition to electrostatic repulsion, therefore this type of SPs would have higher plasticizing (fluidifying) effect and less negative effect on the compressive strength compared to N and M based SPs (Criado et al., 2009). In summary, it can be said that in the case of fly ash-based geopolymer made by multi-compound activator, PC based SPs (the latest generation) would be the most effective type of SPs resulted in at most 29% decrease in compressive strength with reference to the paste without using any SP.

3.5 Conclusions

In this chapter the effects of two different activators (NaOH solution and multi-compound activator composed of NaOH and Na_2SiO_3 solutions with Na_2SiO_3/NaOH mass ratio of 2.5) and six different commercial SPs (three modified Polycarboxylate (PC) based, two naphthalene (N) based and one melamine (M) based) on workability and compressive strength of the fly ash-based geopolymer paste have been evaluated. The following conclusions are drawn:

1) Although the multi-compound activator resulted in a much more viscous paste, the workability and compressive strength of the paste made by the multi-compound activator were considerably higher than those of the paste made by only NaOH solution. The different workability of the pastes is due to their different yield stress originated from their different type of activator. The higher compressive strength of the paste made by using multi-compound activator solution is due to higher rate of geopolymerisation reaction in the paste, thanks to addition of Na_2SiO_3 solution to the NaOH solution which enhances the formation of geopolymer precursors upon contact between a mineral and the solution. The higher viscosity of the paste made by the multi-compound activator is due to considerably higher viscosity of the D Grade Na_2SiO_3 solution than the NaOH solution.

2) The effect of different SPs on the workability and compressive strength of fly ash-based geopolymer directly depends on the type of activator and SPs.

3) In the case of fly ash-based geopolymer paste activated by only NaOH solution (8.0 M concentration), the naphthalene (N) based SP (the second generation) was an effective type resulted in 136% increase in the relative slump value without having any negative effect on the compressive strength of the paste with reference to the paste without using any SP.

4) In the case of fly ash-based geopolymer paste activated by multi-compound activator, the modified Polycarboxylate (PC) based SP (the latest generation) was the most effective type resulted in 39% to 45% increase in the relative slump value and at most 29% decrease in the compressive strength of the paste with reference to the paste without using any SP.

In general, it can be said that with the current SPs technology, there is no commercial SP that exactly matches with geopolymer chemistry to be really effective in the geopolymer systems similar to the OPC-based system. In addition, possible detrimental effects of the available SPs on other properties of geopolymer (apart from the compressive strength) are still unknown. Therefore, in this doctoral research it was decided not to use any commercial admixtures (including SPs and viscosity modifying agents) in the mixture design of the SHGCs. Instead, the type and/or content of the activator, as well as the extra water in the mixture design were adjusted to control the workability and rheology of the mixture for uniform fiber dispersion.

3.6 References

AS 1012.9. 2014. Methods of testing concrete - Compressive strength tests - Concrete, mortar and grout specimens. Australia: Standards Australia.

ASTM C1437. 2007. Standard test method for flow of hydraulic cement mortar. United States: ASTM Standards.

BEAUPRÉ, D. & MINDESS, S. 1998. Rheology of fresh concrete: principles, measurement, and applications. *Materials Science of Concrete V,(Ed. Skalny, J. and Mindess, S.)*, 149.

CRIADO, M., PALOMO, A., FERNÁNDEZ-JIMÉNEZ, A. & BANFILL, P. 2009. Alkali activated fly ash: effect of admixtures on paste rheology. *Rheologica Acta,* 48, 447-455.

FERNÁNDEZ-JIMÉNEZ, A. & PALOMO, A. 2005. Composition and microstructure of alkali activated fly ash binder: effect of the activator. *Cement and concrete research,* 35, 1984-1992.

HARDJITO, D., WALLAH, S. E., SUMAJOUW, D. M. & RANGAN, B. V. 2004. On the development of fly ash-based geopolymer concrete. *ACI Materials Journal-American Concrete Institute,* 101, 467-472.

KONG, D. L. & SANJAYAN, J. G. 2010. Effect of elevated temperatures on geopolymer paste, mortar and concrete. *Cement and concrete research,* 40, 334-339.

OLIVIA, M. & NIKRAZ, H. 2012. Properties of fly ash geopolymer concrete designed by Taguchi method. *Materials & Design,* 36, 191-198.

PALACIOS, M. & PUERTAS, F. 2004. Stability of superplasticizer and shrinkage-reducing admixtures in high basic media. *Materiales de Construcción,* 54, 65-86.

PALACIOS, M. & PUERTAS, F. 2005. Effect of superplasticizer and shrinkage-reducing admixtures on alkali-activated slag pastes and mortars. *Cement and concrete research,* 35, 1358-1367.

PAN, Z., SANJAYAN, J. G. & RANGAN, B. V. 2011. Fracture properties of geopolymer paste and concrete. *Magazine of concrete research,* 63, 763-771.

RIXOM, M. & MAILVAGANAM, N. P. 1999. *Chemical admixtures for concrete,* ACI Education Bulletin E4-03, Taylor & Francis.

SARKER, P. K., HAQUE, R. & RAMGOLAM, K. V. 2013. Fracture behaviour of heat cured fly ash based geopolymer concrete. *Materials & Design,* 44, 580-586.

TATTERSALL, G. & BANFILL, P. 1983. The rheology of fresh concrete: Pitman Advanced Pub. *Program, London*.

TENNAKOON, C., NAZARI, A., SANJAYAN, J. G. & SAGOE-CRENTSIL, K. 2014. Distribution of oxides in fly ash controls strength evolution of geopolymers. *Construction and Building Materials,* 71, 72-82.

WALLEVIK, J. E. 2006. Relationship between the Bingham parameters and slump. *Cement and Concrete Research,* 36, 1214-1221.

XU, H. & VAN DEVENTER, J. 2000. The geopolymerisation of alumino-silicate minerals. *International Journal of Mineral Processing,* 59, 247-266.

PART I: HEAT CURED TWO-PART FLY ASH-BASED SHGCS

CHAPTER 4

DEVELOPMENT OF HEAT CURED TWO-PART FLY ASH-BASED SHGCS

Note: This chapter is based on the following papers:

1) "*Comparative deflection hardening behavior of short fiber reinforced geopolymer composites*", by ***Nematollahi, B.***, Sanjayan, J., and Shaikh, F.U.A., published in ***Construction and Building Materials***, 2014, 70, 54-64.

2) "*Tensile Strain Hardening Behavior of PVA Fiber-Reinforced Engineered Geopolymer Composite*", by ***Nematollahi, B.***, Sanjayan, J., and Shaikh, F.U.A., published in ***ASCE Journal of Materials in Civil Engineering***, 2015, 27(10), 04015001.

4.1 Introduction

Chapters 4 and 5 report the development of a short fiber-reinforced strain-hardening geopolymer composite (SHGC) with complete replacement of OPC binder by a fly ash-based geopolymer binder. The behavior of randomly oriented short fiber-reinforced composites such as fly ash-based SHGCs are governed by three groups of parameters. The first group involves matrix related parameters such as compressive and tensile strengths, fracture toughness, elastic modulus, while the second group consists of fiber related parameters such as fiber type, geometry and strength, and the third group comprises matrix-fiber interface related parameters such as the frictional and chemical bond strength (Li et al., 1995). Among these three groups, the focus of the research studies presented in Chapters 4, 5 and 6 is on the matrix-related parameters. The effects of fiber related and fiber-matrix interface related parameters on the tensile performance of the composite are discussed in Chapters 7 and 11, respectively.

The properties of the geopolymer matrix such as workability, density, compressive and tensile strengths, fracture toughness and elastic modulus are influenced by many factors such as type of fly ash, type of alkaline activator, activator to fly ash ratio, sand to fly ash ratio, temperature and duration of curing. Therefore, a series of systematic parametric studies were designed in Chapters 4 and 5 to investigate the quantitative influences of the geopolymer matrix-related parameters such as type of alkaline activator, water to geopolymer solids (W/GP solids) ratio, sand size and sand content on the matrix and

composite properties of fly ash-based SHGCs. It is essential to understand the quantitative influence of these parameters on the matrix and composite properties of fly ash-based SHGCs with the aim of selecting an appropriate type of geopolymer matrix to achieve desirable composite properties.

Previous studies revealed that the type of alkaline activator plays an important role in the geopolymerisation process and has significant effect on the mechanical strength of geopolymer (Fernández-Jiménez and Palomo, 2005). Therefore, the focus of this chapter is on the quantitative influences of type of activator, as one of the most significant factors in governing the characteristics of the geopolymer matrix, on the matrix and composite properties of fly ash-based SHGCs. Only fly ash was used in the matrix with no sand similar to the first generation of the SHCCs that only utilized OPC and silica fume with no sand in the SHCC matrix (Li et al., 1995; Kanda and Li, 1999). The effects of other matrix related parameters such as W/GP solids ratio (i.e. water content), sand size and sand content are studied in Chapter 5.

According to Rowles (2004), any strong alkali solution could be used as the alkaline activator to manufacture geopolymers. The alkaline activators can be liquid or solid, which needs water to be dissolved. Four different activator combinations including two sodium-based (Na-based) and one potassium-based (K-based) activator combinations in the form of solution and one lime-based activator combination in the form of powder were selected. A series of experiments including workability, density, compression, matrix fracture toughness, uniaxial tension and flexural tests were conducted to characterize the mechanical properties of the fly ash-based SHGCs manufactured with these activators.

4.2 Materials

The same low calcium (Class F) fly ash supplied from Gladstone power station in Queensland, Australia was used in this research. The chemical composition and LOI of the fly ash are presented in Table 3-1.

Four different activator combinations including two Na-based and one K-based activator combinations in the form of solution and one lime-based activator combination in the form of powder were used in this study. The first Na-based activator (Na-based-1) was

composed of 8.0 M sodium hydroxide (NaOH) and D Grade sodium silicate (Na_2SiO_3) solutions, while the second Na-based activator (Na-based-2) was only composed of 8.0 M NaOH solution. NaOH solution was prepared with a concentration of 8.0 M using NaOH beads of 97% purity supplied by Sigma-Aldrich and tap water. The D Grade Na_2SiO_3 solution was supplied by PQ Australia with a specific gravity of 1.51 and a modulus ratio (Ms) equal to 2.0 (where Ms=SiO_2/Na_2O, Na_2O=14.7% and SiO_2=29.4%). The NaOH and D Grade Na_2SiO_3 solutions were mixed together with Na_2SiO_3/NaOH mass ratio of 2.5 to prepare the Na-based-1 activator. The K-based activator was composed of 8.0 M potassium hydroxide (KOH) and KASIL2236 Grade potassium silicate (K_2SiO_3) solutions. KOH solution was prepared with a concentration of 8.0 M using KOH flakes of 90% purity supplied by Redox Australia and tap water. The KASIL2236 Grade K_2SiO_3 solution was supplied by PQ Australia with a specific gravity of 1.32 and a modulus ratio (Ms) equal to 2.23 (where Ms=SiO2/K_2O, K_2O=11.2% and SiO_2=24.8%). The KOH and K_2SiO_3 solutions were mixed together with K_2SiO_3/KOH mass ratio of 2.5 to prepare the K-based activator. Specifications of different grades of Na_2SiO_3 and K_2SiO_3 used in this study are summarized in Table 4-1.

Table 4-1: Specifications of different grades of Na_2SiO_3 and K_2SiO_3

Chemical grade	Density[1]	Viscosity[2]	Modulus ratio[3]	SiO_2[4]	Na_2O[4]	K_2O[4]	H_2O[4]
KASIL2236 Grade K_2SiO_3 solution	1.32	80	2.23	24.8	---	11.2	64.0
D Grade Na_2SiO_3 solution	1.51	350	2.0	29.4	14.7	---	55.9
GD Grade Na_2SiO_3 Powder	---	---	2.0	54.0	27.0	---	19.0[5]

[1]Average density (g/cc @ 20°C) reported by the supplier.

[2]Average viscosity (cps @ 20°C) reported by the supplier.

[3]M_s where M_s=SiO_2/ Na_2O or SiO_2/ K_2O.

[4]Average wt. % reported by the supplier.

[5]Chemically bound water in the powder which is released when dissolved in water.

All above activators were in the form of solution, while the lime-based activator was in the form of powder, composed of Supercalco 97 Grade calcium hydroxide ($Ca(OH)_2$) and GD Grade Na_2SiO_3 powders. The Supercalco 97 Grade $Ca(OH)_2$ powder was supplied by Redox Australia. The GD Grade Na_2SiO_3 powder was supplied by PQ Australia with a modulus ratio (Ms) equal to 2.0 (where $Ms=SiO_2/Na_2O$, $Na_2O=27.0\%$ and $SiO_2=54.0\%$). $Ca(OH)_2$ and Na_2SiO_3 powders were mixed together with $Ca(OH)_2/Na_2SiO_3$ mass ratio of 7.5 to prepare the lime-based activator. Table 4-2 presents properties of the PVA fiber with a surface oil coating of 1.2% by weight, supplied by Kuraray Co. Ltd., Japan.

Table 4-2: Properties of PVA fiber

Fiber type	Diameter (μm)	Length (mm)	Young's modulus (GPa)	Elongation (%)	Nominal Strength (MPa)	Density (g/cm^3)
RECS 15×8	40	8	41	6	1600	1.3

4.3 Mix Proportions

Table 4-3 presents the mix proportions of fly ash-based SHGCs used in this study. As can be seen, four fly ash-based SHGC mix proportions denoted as SHGC-Na-1, SHGC-Na-2, SHGC-K and SHGC-Lime employing the Na-based-1, Na-based-2, K-based and lime-based activator combinations, respectively were prepared through experiments using the principles of SHCC development. Previous studies revealed that water content plays an important role on the properties of geopolymer binders (Barbosa et al., 2000; Hardjito et al., 2004). Thus, in order to compare the effects of different activator combinations on the matrix and composite properties of fly ash-based SHGCs, a constant water to geopolymer solids (W/GP solids) ratio of 0.20 was selected to prepare the SHGC mixtures and the amounts of activators and/or water in the mixtures were adjusted accordingly to account for this constant W/GP solids ratio. This ratio was selected based on the results of various trial mixes, which indicated that fly ash-based geopolymer paste activated by the Na-based-1 activator with W/GP solids of 0.20 provided near optimum strength and workability. When the W/GP solids ratio was less than this figure, the workability of the geopolymer paste reduced, causing difficulties during compaction and loss of strength. It should be noted that a small amount of polycarboxylate ether (PCE) based

superplasticizer was used in SHCC-Lime mixture to achieve desirable rheology and workability for uniform fiber dispersion. According to Hardjito et al. (2004), for a given geopolymer binder, total mass of water in the mixture is taken as the sum of the mass of water in each of the activator solutions and the mass of extra water, if any, added to the mixture. The mass of geopolymer solids is the sum of the mass of fly ash and the mass of activator solids used to make each of the activator solutions.

Table 4-3: Mix proportions of fly ash-based SHGCs

Mix ID	Fly ash	OPC	Activator	Water	SP[6]	PVA fiber	W/GP solids ratio
SHGC-Na-1	1.0	---	0.35[1]	0.014[5]	---	0.02	0.20
SHGC-Na-2	1.0	---	0.29[2]	---	---	0.02	0.20
SHGC-K	1.0	---	0.35[3]	---	---	0.02	0.20
SHGC-Lime	1.0	---	0.093[4]	0.22	0.01	0.02	0.20

Note: All numbers are mass ratios of fly ash weight except W/GP solids ratios and fiber contents (volume fraction).

[1] Composed of the Na-based-1 activator combination.

[2] Composed of the Na-based-2 activator combination.

[3] Composed of the K-based activator combination.

[4] Composed of the lime-based activator combination.

[5] Extra water added to Na-based-1 activator combination.

[6] PCE based superplasticizer.

4.4 Mixing and Curing

All composites were prepared in a Hobart mixer. To prepare the fly ash-based geopolymer matrix in SHGC-Na-1, SHGC-Na-2 and SHGC-K mixtures, alkaline activators in the form of solution and extra water (if any) were added to the fly ash and mixed for about 4 minutes. However, in the case of the SHGC-Lime mixture, solid activators in the form of powder were added to the fly ash and dry mixed for approximately 3 minutes. Water was then gradually added to the mix and the mixing was continued for another 3 minutes. Subsequently, the PCE based superplasticizer (1% by mass of fly ash) was added to the mix and the mixing was continued for another 6 minutes to achieve proper workability of

the matrix. In each mix, after the matrix ingredients were thoroughly mixed to achieve the desired fresh state, the flowability of fresh geopolymer matrix (before addition of the fibers) was measured to ensure that the flowability was within the desired range for achieving good fiber dispersion. Finally, the PVA fibers (2% volume fraction) were gradually added to ensure uniform fiber dispersion. The whole mixing procedure for each mix generally took 15–25 minutes. The fresh geopolymer matrix and composite were cast into different molds and compacted using a vibrating table.

Heat curing was adopted for the fly ash-based SHGC mixtures. For heat curing, all molds were sealed to minimize moisture loss and placed in the oven at 60°C for 24 hours. At the end of heat curing period, the specimens were removed from the oven and kept undisturbed until being cool and then removed from the molds and left in the laboratory at ambient temperature (23°C ± 3°C) until the day of testing. Previous studies reported that age does not have considerable effect on strength of geopolymers after the completion of the heating curing period. Three-day compressive strength of geopolymer is thereby equivalent to a typical OPC strength development after 28-days of ambient temperature curing (Kong and Sanjayan, 2010; Hardjito et al., 2004). Therefore, the heat cured specimens were tested 3 days after casting.

4.5 Experimental Tests

4.5.1 Mini-slump test

In each mixture, the workability of fresh matrix (before addition of the fibers) was measured using mini-slump test also known as spread-flow test. According to ASTM C1437 (2007), a layer of the fresh matrix about 25 mm in thickness was poured into the truncated conical mold (top diameter=70 mm, bottom diameter=100 mm, height=50 mm) and tamped 20 times with tamper. Subsequently the conical mold was filled with the matrix and tamped as specified for the first layer. The top surface of the mold was leveled and the extra mixture was removed. After 1 min the conical mold was lifted vertically and diameter of the matrix spread was measured along two perpendicular directions. The relative slump value was derived from the following equation:

$$\Gamma p = (d/d_0)^2 - 1 \qquad (4.1)$$

where Γp is the relative slump, d is the average of two measured diameters of the matrix spread, and d_0 is the bottom diameter of the mini-slump cone equal to 100 mm in this study (Okamura and Ozawa, 1995).

4.5.2 Compression test

In each mixture, the compressive strength of matrix and composite was determined according to ASTM C109 (2007). For each mixture, a minimum of three 50 mm cube matrix specimens (before addition of the fibers) and three 50 mm cube composite specimens (after addition of the fibers) were prepared and tested.

4.5.3 Density test

In each mixture, the hardened density of matrix and composite was determined by weighing the cube specimens on the testing day before the compression tests.

4.5.4 Matrix fracture toughness test

In each mixture, the fracture properties of matrix including elastic modulus (E_m), fracture toughness (K_m) and crack tip toughness (J_{tip}) were determined using three-point bending tests on single edge notched beam specimens. The fracture toughness (i.e. the mode I critical intensity factor) is a measure of the magnitude of the stress concentration which exists in front of the crack tip when the crack starts to propagate (Petersson, 1980). For each mixture, at least four matrix prisms (before addition of the fibers) with the dimensions of 60 mm×60 mm×280 mm were prepared. Three-point bending tests with a fixed span to depth (l/d) ratio equal to 4 and an initial notch depth to beam depth (a/d) ratio equal to 0.5 were conducted under displacement control using MTS testing machine. A linear variable differential transducer (LVDT) was used to measure the deflection of the mid-span. Following Martin et al. (2007) and Sarker et al. (2013), the displacement control rate was 0.18 mm/min so that the maximum load for any specimen was achieved within the first 30–60 s. A schematic of the fracture toughness test setup is shown in Figure 4-1.

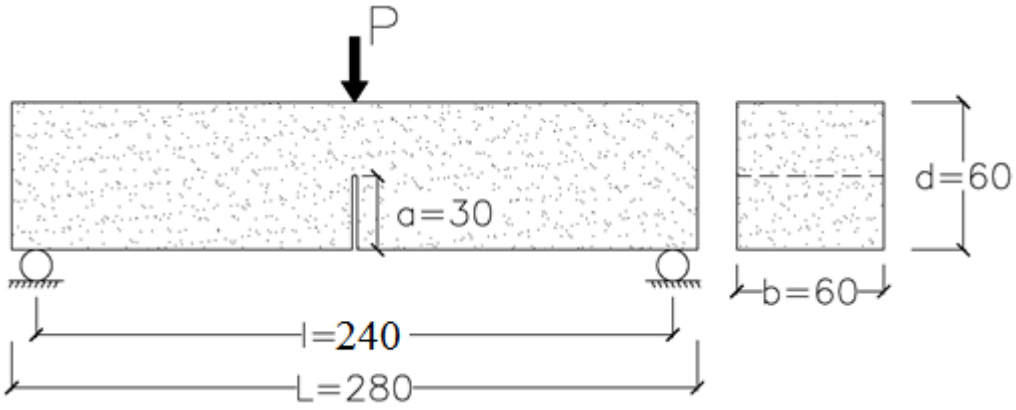

Figure 4-1: Schematic matrix fracture toughness test setup (all dimensions in mm)

According to the effective crack model (ECM) developed by (Karihaloo and Nallathambi, 1990), the E_m and K_m of each mixture were calculated from the following equations:

$$E_m = \frac{0.413P_i}{\delta_i}\left\{\frac{l^3(1+\frac{5\omega l}{8P_i})}{4bd^3(1-\frac{a}{d})^3}+\frac{1.17l}{1.68bd(1-\frac{a}{d})}\right\} \quad (4.2)$$

where E_m is the matrix elastic modulus, P_i is an arbitrary load level in the initial (linear) portion of the load-deflection plot and δ_i is its corresponding deflection, l, b and d are the span, width and depth of the specimen, respectively, a is the initial notch depth, and ω is the self-weight of the specimen per unit length.

$$K_m = \sigma_n\sqrt{a_e}Y(\alpha) \quad (4.3)$$

where K_m is the matrix fracture toughness, $\sigma_n=6M/(bd^2)$, $M=(P_{max}+\omega l/2)l/4$, a_e is the effective notch depth, which can be derived from Equation (3.2) by substituting the P_i and δ_i by the peak load (P_{max}) and its corresponding deflection (δ_p). Y(α) is the correction factor which can be determined as follows:

$$Y(\alpha)=\frac{1.99-\alpha(1-\alpha)(2.15-3.93\alpha+2.70\alpha^2)}{(1+2\alpha)(1-\alpha)^{1.5}} \quad (4.4)$$

where $\alpha=a_e/d$.

It should be noted that the ECM accounts for the pre-peak crack growth that occurs upon loading and the measured K_m does not to depend on the size and geometry of the test specimen, but on the mixture variables only (Karihaloo and Nallathambi, 1990).

Furthermore, Karihaloo and Nallathambi (1990) demonstrated that the predictions of the ECM are in very good agreement with those of two other non-linear models namely, the two parameter fracture model (TPFM) (Jenq and Shah, 1985), and the size effect law (Bažant et al., 1986).

According to Li et al. (1995), for small fiber volume fraction the J_{tip} can be approximated from the following equation:

$$J_{tip} = \frac{K_m^2}{E_m} \tag{4.5}$$

where K_m and E_m are the fracture toughness and elastic modulus of the matrix, respectively.

4.5.5 Uniaxial tension test

Uniaxial tension tests were conducted to evaluate the composite tensile performance under direct tension. For each mixture, at least three rectangular coupon specimens with the dimensions of 400 mm×75 mm×10 mm were prepared. All specimens were tested in uniaxial tension under displacement control using MTS testing machine with hydraulic wedge grips. Following Ahmed and Maalej (2009), the displacement rate was 0.25 mm/min. A schematic of the uniaxial tension test setup is shown in Figure 4-2. Aluminum plates were epoxy glued onto the grip region of the specimens to facilitate gripping and minimize stress concentration. Care was taken to ensure proper alignment of the specimen with the machine hydraulic grips. The MTS machine had a fully digital control panel and software to automatically run the test and collect the load and actuator displacement data. In addition, two LVDTs were also mounted parallel to the two side edges of the rectangular coupon specimen to measure the extension of the specimen between two points with a gauge length of 200 mm, as shown in Figure 4-2. Resulting uniaxial tensile load and displacement data were recorded to determine the ultimate tensile strength and tensile strain capacity and plot the tensile stress-strain curves of each mixture. The tensile first-crack strength of each mixture was estimated from the tensile stress-strain curves following the method proposed by Kanda and Li (2006). The tensile first-cracking point was taken as the point where the stress in tensile stress-strain curve drops significantly for the first time, or the point where a sudden change in slope of the curve occurs.

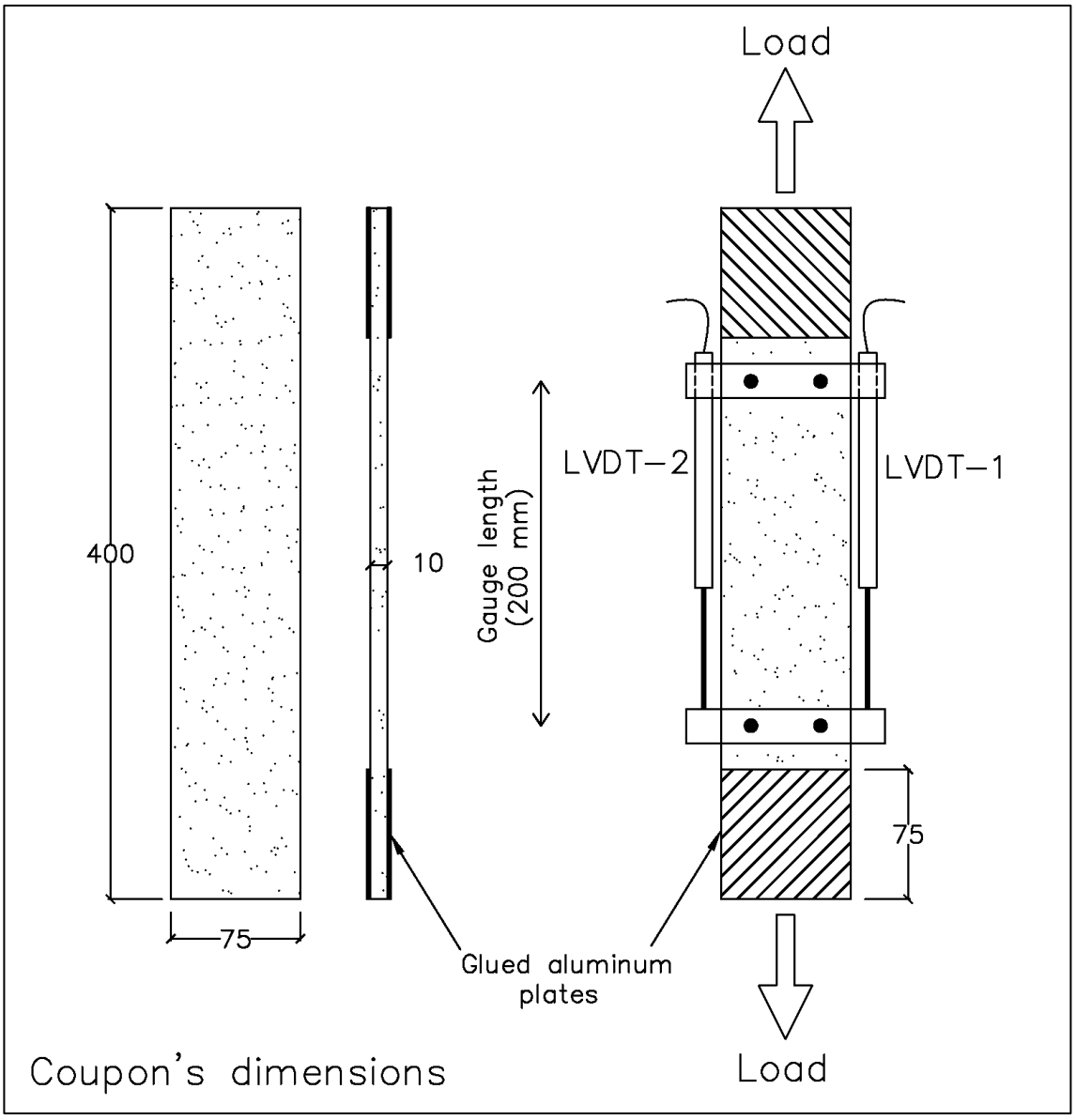

Figure 4-2: Schematic uniaxial tension test setup (all dimensions in mm)

4.5.6 Flexural test

Flexural tests using four-point bending test setup were conducted to evaluate the flexural performance of the composite. For each mixture, at least three rectangular coupon specimens with the dimensions of 400 mm×75 mm×10 mm were prepared. All specimens were tested in four-point bending test setup under displacement control with the mid-span measuring 100 mm. The displacement rate was 0.5 mm/min. Resulting load versus mid-span deflection data were recorded and flexural stress versus mid-span deflection curves were plotted. The flexural first-cracking point was defined as the point

where nonlinearity in the load–deflection curve becomes obvious. ASTM C1018 (1997) designates this point as limit of proportionality (LOP). However, ASTM C 1609 (2012) defines first peak point as a point in the load–deflection curve where the slope is zero. According to Kim et al. (2008), the first peak point cannot always be easily found in the initial portion of a load–deflection curve, if the bending behavior of the composite exhibits stable deflection-hardening behavior. Therefore, the LOP as defined in ASTM C1018 (1997) is more generally applicable and should be used instead of the first peak point as defined in ASTM C 1609 (2012).

In this study, the method proposed by Kim et al. (2008) is adopted to identify the LOP in the load-deflection curves. The load at LOP and its corresponding deflection are designated as P_{LOP} and δ_{LOP}, as shown in Figure 4-3. The ultimate flexural strength commonly known as modulus of rupture (MOR) is defined as the point where softening happens after the LOP. The load at MOR and its corresponding deflection are designated as P_{MOR} and δ_{MOR}, as shown in Figure 4-3. According to ASTM C1609 (2012), the flexural first-crack strength (f_{LOP}) and the modulus of rupture (MOR) of each mixture can be determined from the following equations:

$$f_{LOP} = \frac{P_{LOP} \times L}{b \times d^2} \tag{4.6}$$

$$MOR = \frac{P_{MOR} \times L}{b \times d^2} \tag{4.7}$$

where L=300 mm is the distance between the supporting rollers (span length), and b=75 mm and d=10 mm are the width and the height of the rectangular coupon specimen, respectively.

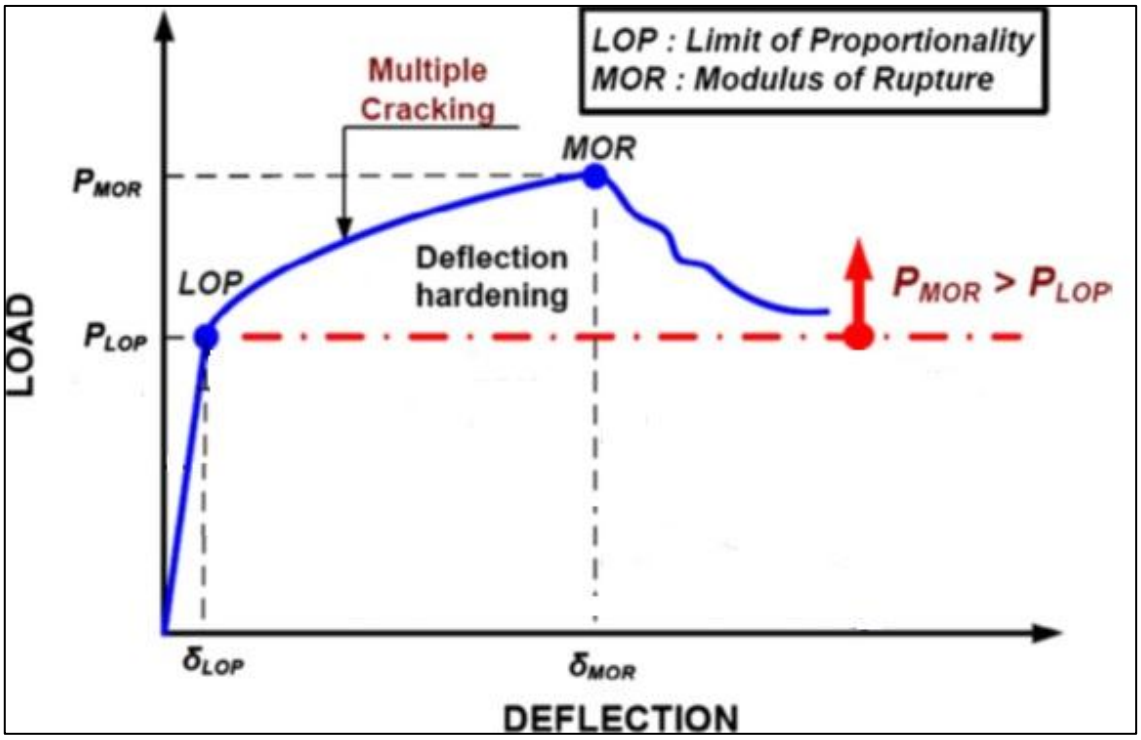

Figure 4-3: Typical load-deflection curve of a deflection-hardening composite (Source: Kim et al., 2008)

4.6 Results and Discussions

4.6.1 Workability, density and compressive Strength

The fresh matrix workability of each mix in terms of relative slump value is presented in Table 4-4. As can be seen, the type of activator had a significant effect on the flowability of the geopolymer matrix. SHGC-Lime and SHGC-Na-2 exhibited the highest and the lowest matrix workability, respectively. At the constant W/GP solids ratio of 0.20, the matrix workability of SHGC-K and SHGC-Lime were 59% and 135% higher, respectively than that of SHGC-Na-1. In addition, visual observation revealed that SHGC-K and SHGC-Lime matrices were less sticky and viscous than SHGC-Na-1 matrix. This may be attributed to the lower viscosity of KASIL 2236 Grade K_2SiO_3 solution than D Grade Na_2SiO_3 solution, as reported in Table 4-1. However, the matrix workability of SHGC-Na-2 was 91% lower than that of SHGC-Na-1.

Table 4-4: Workability, density and compressive strength results

Mix ID	Matrix workability[1]	Density; (kg/m^3)		Compressive strength; (MPa)	
		Matrix	Composite	Matrix	Composite
SHGC-Na-1	6.9 (281.5)	1859±14	1804±33	54.6±3.0	63.7±2.7
SHGC-Na-2	0.6 (126)	1894±16	1799±18	25.4±1.1	30.8±1.0
SHGC-K	11.0 (346)	1845±11	1829±20	32.3±1.4	37.3±1.3
SHGC-Lime	16.2 (415)	1827±10	1779±15	8.80±0.35	13.6±0.45

[1] In terms of relative slump value of the fresh matrix. The average diameter of the matrix flow (in millimeter) is shown in parenthesis.

It should be noted that previous studies proved that there is no relationship between slump and viscosity (Beaupré and Mindess, 1998; Tattersall and Banfill, 1983). According to Wallevik (2006), slump is influenced by the yield stress of the paste, not by the viscosity. Therefore, it can be said that the underlying reason for different matrix workability of fly ash-based SHGCs lies in their different yield stress of geopolymer matrix. It can be concluded that using the K-based and lime-based activator combinations resulted in a matrix with higher slump and lower viscosity the Na-based activator combinations. It should be pointed out that although the relative slump value of SHGC-Na-2 matrix was significantly lower than that of SHGC-Na-1, visual observations revealed that all SHGC matrices exhibited adequate workability and rheology to guarantee uniform fiber dispersion as being mixed and vibrated using a vibrating table, thanks to their thixotropic properties. Therefore, there was no problem in terms of casting and compaction of the specimens. It should be noted that the reported relative slump values are based on the mini-slump test without the 25 times tamping of the flow table.

The average density of each mixture is also presented in Table 4-4. As can be seen, the hardened densities of all fly ash-based SHGCs were almost comparable. In other words, the type of activator did not have a significant effect on the matrix and composite density of fly ash-based SHGCs. As can be seen in Table 4-4, the density of all composite, regardless of the type of binder and type of activator, was relatively lower than that of the corresponding SHGC and SHCC matrices. This may be attributed to increase of entrapped air due to the inclusion of micro-polymeric fibers (i.e. a fiber induced damage effect), which increased the porosity of the composite compared to the matrix material alone (Li and Mishra, 1992).

The average compressive strength of each mixture is also presented in Table 4-4. As can be seen, the compressive strength of all fly ash-based SHGCs was higher than that of the corresponding matrix, thanks to addition of the PVA fibers. This is true in all composites regardless of the type of activator. In addition, in all composite cubes tested under compression crack propagation was restrained due to the bridging mechanism of the PVA fibers. Thereby as shown in Figure 4-4, the composite cubes kept their original shapes after peak load in compression tests, resulting in a ductile failure mode in comparison to the brittle failure of the matrix cubes.

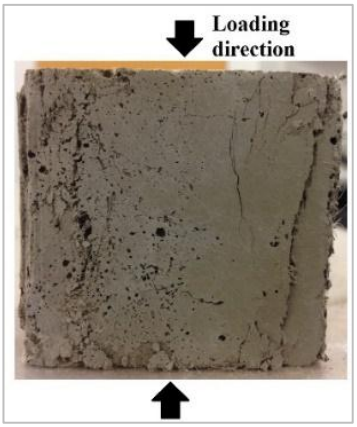

Figure 4-4: Ductile failure mode of composite cube under compression

It should be noted that although the concentration of the NaOH and KOH solutions was limited to 8.0 M to account for safety consideration, the compressive strength of all SHGCs, except SHGC-Lime, developed in this study was higher than that of the fly ash-based SHGCs developed by Ohno and Li (2014), which ranged from 17.4 MPa to 27.6 MPa by using 14.0 M NaOH solution. This could be mainly due to the longer heat curing period (i.e. 24 hours at 60° C) employed in this study. One advantage of reducing the concentration of NaOH solution is that it increases the safety in handling large quantities.

As can be seen in Table 4-4, the type of activator had a significant influence on the compressive strength of the geopolymer matrix and composite. SHGC-Na-1 and SHGC-Lime exhibited the highest and the lowest compressive strength, respectively. The composite compressive strength of SHGC-Na-2, SHGC-K and SHGC-Lime were 51.6%, 41.4%, and 78.6% lower, respectively than that of SHGC-Na-1. Fernández-Jiménez and

Palomo (2005) reported that in fly ash-based geopolymer, the main reaction product formed, regardless of the type of activator, is an alkaline aluminosilicate gel with low-ordered crystalline structure. However, the microstructure as well as the Si/Al and the Na/Al ratios of the aluminosilicate gel depend on the type of the activator used. It is thereby hypothesized that the geopolymer matrix microstructure of fly ash-based SHGCs are different, due to their different type of activator, which resulted in their different compressive strength. In other words, it can be said that the most prominent reason for different compressive strength of fly ash-based SHGCs lies in their different microstructure of the geopolymer matrices, due to their different type of activator.

As can be seen in Table 4-4, at the constant W/GP solids ratio of 0.20, both matrix workability and compressive strength of SHGC-Na-2 made by only 8.0 M NaOH solution significantly decreased with respect to those of SHGC-Na-1. Similar results were reported by Hardjito et al. (2004) for fly ash-based geopolymer concrete. This is attributed to the fact that the addition of Na_2SiO_3 solution to the NaOH solution improves the formation of geopolymer precursors upon contact between a mineral and the solution, the geopolymerisation reaction thereby occurs at a higher rate (Xu and van Deventer, 2000). In addition, using the Na-based-1 activator combination results in some economical saving, since the price of D Grade Na_2SiO_3 solution is much cheaper than that of the NaOH solution. Through visual inspection it was noted that viscosity of the geopolymer matrix made by the Na-based-2 activator was lower than that of SHGC-Na-1. This could to be due to much higher viscosity of D Grade sodium silicate solution (250–450 cps at 20 ˚C) than that of the 8.0 M NaOH solution.

As can be seen in Table 4-4, at the constant W/GP solids ratio of 0.20, although the matrix workability of SHGC-K was 59% higher than that of SHGC-Na-1, the compressive strength of K-based geopolymer matrix and composite was about 40% lower than that of Na-based geopolymer matrix and composite. In addition, the price of K_2SiO_3 and KOH solutions is higher than that of the NaOH and Na_2SiO_3 solutions. In general, it can be concluded that in fly ash-based SHGCs the use of the Na-based-1 activator combination is beneficial in terms of lower cost and higher compressive strength gain compared with the K-based and Na-based-2 activator combinations.

According to Tables 4-4, although the compressive strength of SHGC-Lime decreased by 78.6% with respect to that of SHGC-Na-1, its matrix workability significantly increased

by 90%. This translates to a much more workable and less viscous geopolymer matrix compared to that of SHGC-Na-1. A very important benefit of using solid activators such as the lime-based activator combination over the commonly used activator solutions is that in commercial application of geopolymer composites handling solid activators and just adding water similar to "traditional" cementitious composites would be safer and easier than handling large quantities of corrosive activator solutions. This significantly enhances the commercial viability of geopolymer composites. It should be noted that the geopolymerisation reaction only occurs when water is added to the "dry mix" geopolymer binder (combination of fly ash and lime-based activator in powder form), because reaction only occurs in solution form. In addition, using the lime-based activator combination results in some economical saving compared to the use of the Na-based-1 activator combination as the price of $Ca(OH)_2$ is much cheaper than that of the NaOH solution. The compressive strength of SHGC-Lime achieved in this study is relatively low and future work involves increasing the compressive strength. Development of "dry mix" based geopolymer matrix and composite is reported in Chapters 8 and 9.

4.6.2 Matrix fracture properties

The matrix fracture properties (without addition of the fibers) of each mixture including elastic modulus E_m, fracture toughness K_m and crack tip toughness J_{tip} are presented in Table 4-5. It should be pointed out that in this study the E_m of each mixture was not measured experimentally using cylindrical specimens in compression, instead the E_m of each mixture was derived indirectly based on ECM from the linear portion of the load-deflection curve of the notched beam specimen in three-point bending tests. The derived E_m values thereby should only be considered as relative values enabling us to compare the matrix elastic modulus of each mixture. SHGC-Na-1 exhibited the highest matrix elastic modulus. This is consistent with compressive strength results reported in Table 4-4, where SHGC-Na-1 exhibited the highest compressive strength among all SHGCs. The E_m of SHGC-Na-2, SHGC-K and SHGC-Lime were 32.9%, 38.8% and 78.8%, respectively lower than that of SHGC-Na-1, which correspond to their lower compressive strengths, as reported in Table 4-4.

Table 4-5: Matrix fracture properties

Mix ID	Matrix elastic modulus, E_m; (GPa)[a]	Matrix fracture toughness, K_m; ($MPa.m^{1/2}$)[b]	Crack tip toughness, J_{tip}; (J/m^2)[c]
SHGC-Na-1 matrix	8.5	0.436	22.4
SHGC-Na-2 matrix	5.7	0.312	17.1
SHGC-K matrix	5.2	0.237	10.8
SHGC-Lime matrix	1.8	0.086	4.1

[a] Following Equation (3.2) (Karihaloo and Nallathambi, 1990).

[b] Following Equation (3.3) (Karihaloo and Nallathambi, 1990).

[c] Following Equation (3.5) (Li et al., 1995).

With regards to matrix fracture toughness, as can be seen in Table 4-5, SHGC-Na-1 also exhibited the highest K_m among all SHGCs. The K_m of SHGC-Na-2, SHGC-K and SHGC-Lime were 28.4%, 45.6% and 80.3%, respectively lower than that of SHGC-Na-1. According to Pan et al. (2011), the fracture toughness of concrete is generally influenced by the microstructure of the paste and the size, texture and angularity of the coarse aggregates. Thus, it can be inferred that the different matrix fracture toughness of fly ash-based SHGCs is attributed to different microstructure of the geopolymer pastes, because no aggregate was used in the mixtures investigated in this study. As mentioned in Section 4.6.1, Fernández-Jiménez and Palomo (2005) demonstrated that the microstructure as well as the Si/Al and the Na/Al ratios of the aluminosilicate gel depend on the type of the activator used. Therefore, it is hypothesized that the microstructure of geopolymer pastes are different due to their different type of activator. As can be seen in Table 4-5, SHGC-Na-1 also exhibited the highest J_{tip} among all SHGCs, which corresponds to its higher K_m.

4.6.3 Uniaxial tensile performance

Tensile stress-strain responses of fly ash-based SHGCs are presented in Figures 4-5 to 4-8. As can be seen, all fly ash-based SHGCs, regardless of the type of activator, exhibited clear strain hardening behavior accompanied by multiple cracking process. The uniaxial tensile performance of fly ash-based SHGCs developed in this study are comparable to those of slag-based SHGCs developed by Lee et al. (2012). The uniaxial tension test results including the measured ultimate tensile strength and tensile strain capacity as well

as the estimated tensile first-crack strength are presented in Table 4-6. As can be seen, the type of activator had significant effects on the tensile performance of the developed fly ash-based SHGCs, which exhibited moderate to high ultimate tensile strength in the range of 1.7–4.7 MPa. At the same time, they exhibited moderate to very high tensile strain capacity in the range of 0.42−4.3%, which is about two orders of magnitude higher than that of brittle OPC-based or geopolymer concrete. Therefore, the development of SHGCs with fly ash-based geopolymer as the sole binder is experimentally established.

Table 4-6: Uniaxial tension test results

Mix ID	Tensile first-crack strength, σ_{fc}; (MPa)	Ultimate tensile strength, σ_{cu}; (MPa)	Tensile strain capacity, ε_{cu}; (%)	Stress-performance index
SHGC-Na-1	3.2 ± 0.21	4.7 ± 0.25	4.3 ± 0.14	1.5
SHGC-Na-2	3.7 ± 0.31	3.9 ± 0.40	0.42 ± 0.065	1.1
SHGC-K	1.4 ± 0.062	1.8 ± 0.21	2.0 ± 0.26	1.3
SHGC-Lime	1.3 ± 0.12	1.7 ± 0.10	1.1 ± 0.26	1.3

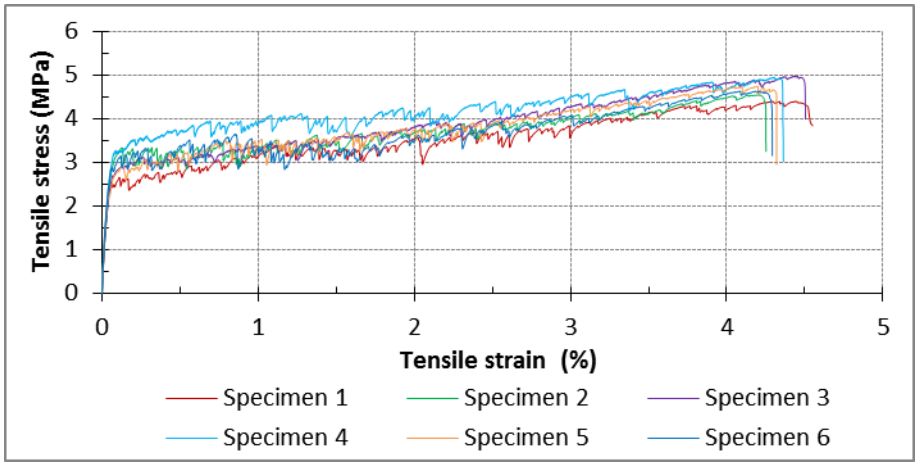

Figure 4-5: Tensile stress-strain responses of SHGC-Na-1

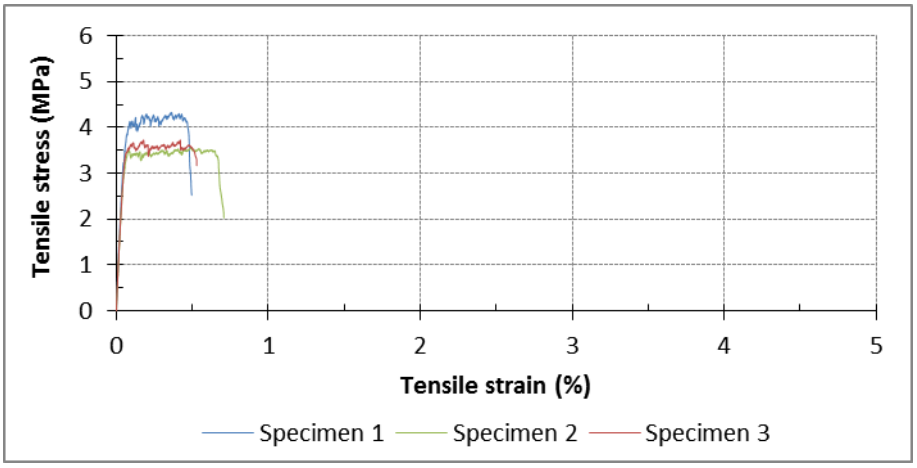

Figure 4-6: Tensile stress-strain responses of SHGC-Na-2

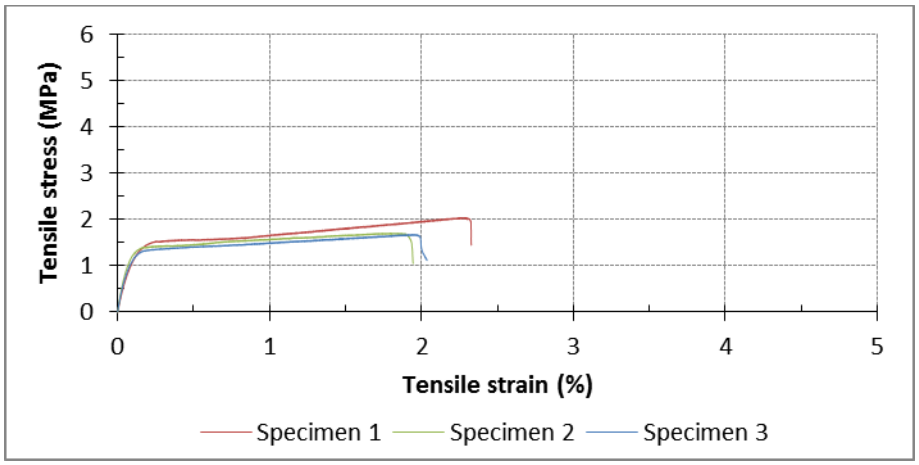

Figure 4-7: Tensile stress-strain responses of SHGC-K

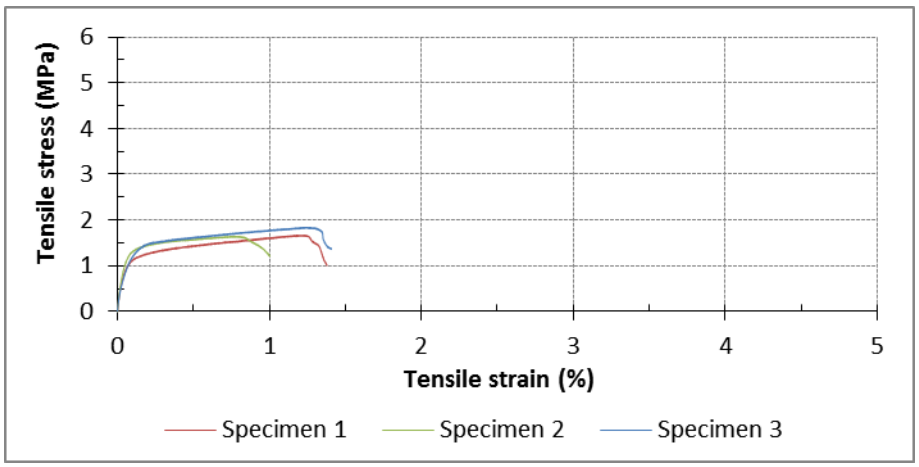

Figure 4-8: Tensile stress-strain responses of SHGC-Lime

It should be noted that the tensile strength of SHGC-Na-1 developed in this study is at least 38% higher than that of fly ash-based SHGCs developed by Ohno and Li (2014), where a combination of 14 M NaOH and Na_2SiO_3 solutions was used as the activator solution and the ultimate tensile strength of the developed composites ranged from 2.9 MPa to 3.4 MPa. This could be due to the interfacial properties (Lee et al., 2012). In other words, the fiber-matrix bond strength in SHGC-Na-1 developed in this study could be higher compared to that of the SHGCs developed by Ohno and Li (2014), resulting in higher fiber-bridging strength (Lee et al., 2012). The difference in fiber-matrix bond strength could be due to different oil-coating percentage of the PVA fibers, different mix proportions and concentration of the activators used in the two studies. The microscale investigation of fiber-matrix interface properties and mechanisms in fly ash-based SHGCs are investigated in Chapter 7.

Multiple cracking pattern of each composite under uniaxial tension is presented in Figure 4-9. After unloading, clear trace of all visible cracks was obtained by using a permanent marker. The average crack spacing was calculated by the gauge length divided by the number of visible cracks. As can be seen, crack distribution in SHGC-Na-1 was uniform and enormous micro-cracks with tightly controlled crack width (i.e. saturated cracking behavior) were observed, which corresponds to its very high tensile strain capacity (4.3%). On the other hand, the crack distribution in SHGC-K was not uniform and fewer number of cracks was observed (i.e. un-saturated cracking behavior), which corresponds to its lower tensile strain capacity (2.0%). While the crack spacing in SHGC-Na-1 was almost equal ranging from 2–3 mm, the crack spacing in SHGC-K was bigger ranging from 4–5 mm. In the case of SHGC-Lime and SHGC-Na-2, a few number of very fine and widely spaced cracks were observed and the crack distributions were not uniform (i.e. unsaturated cracking behavior), which correspond to their inferior tensile strain capacities (1.1% and 0.42%, respectively). It should be noted that in SHGC-Lime although the number of visible cracks on the unloaded specimen was fewer than that of SHGC-Na-2, but more micro-cracks were likely developed during loading of the specimen. This is because the tensile strain capacity of SHGC-Lime was higher than that of SHGC-Na-2 (1.1% versus 0.42%). Many of the micro-cracks developed during loading of the specimen were completely closed after unloading, it was thereby very difficult to be

distinguished by the naked eyes on the unloaded specimen. Similar pattern was reported by Kanda and Li (1999) for the SHCC mixtures investigated in their study.

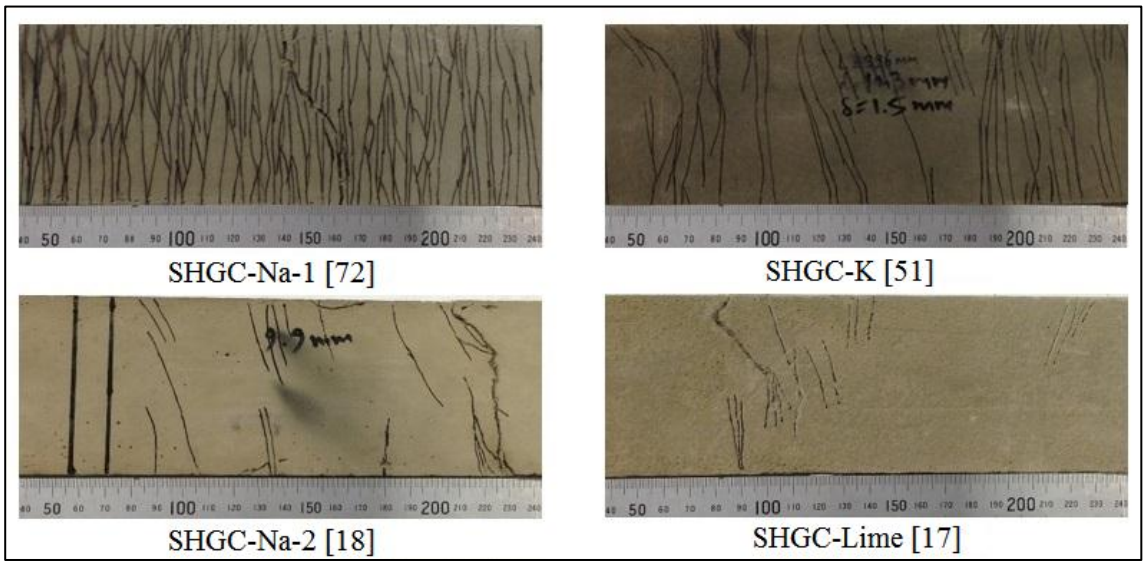

Figure 4-9: Typical multiple cracking pattern of each composite under uniaxial tension (The number of visible cracks is shown in square brackets [ ])

The average residual crack width and estimated loaded crack width of each composite are presented in Table 4-7. The residual crack width of each composite was measured using a microscope from the unloaded specimens after the uniaxial tension tests. The loaded crack width of each composite was estimated based on the tensile strain capacity, average crack spacing and the number of visible cracks. The loaded crack width of the coupon specimen during uniaxial tension tests is equivalent to the crack opening corresponding to maximum bridging stress in the fiber bridging curve of the composite (Lee et al., 2012). As can be seen in Table 4-7, the residual crack width of the coupon specimens after unloading is approximately 70% of the loaded crack width. This is due to the elastic recovery of the elongated PVA fibers bridging across the matrix cracks (Li et al. 2001). Similar results were reported by Li et al. (2001) regarding the SHCC mixtures investigated in their study. As can be seen in Table 4-7, although the crack width in SHGC-Na-2, SHGC-K and SHGC-Lime was smaller than that of SHGC-Na-1, unsaturated cracking behavior with non-uniform crack distribution was observed in these composites. It should be noted that the actual loaded crack width of each composite

should be smaller than the estimated values reported in Table 4-7. This is because, as mentioned earlier, the actual number of micro-cracks developed on the coupon specimen during loading was more than the number of visible cracks after unloading (Li et al., 2001).

Table 4-7: Average crack width of each composite

Mix ID	Average residual crack width; (μm)	Estimated loaded crack width; (μm)
SHGC-Na-1	83	119
SHGC-Na-2	34	48
SHGC-K	55	79
SHGC-Lime	48	69

As can be seen in Table 4-6, the tensile first-crack strength of SHGC-K and SHGC-Lime were 56%, and 66%, respectively lower than that of SHGC-Na-1, which corresponds to their lower matrix fracture toughness, as reported in Table 4-5 (Li et al., 2001). Although the matrix fracture toughness of SHGC-Na-1 was higher than that of SHGC-Na-2, the tensile first-crack strength of SHGC-Na-2 was 16% higher than that of SHGC-Na-1. This could be attributed to fiber-matrix interface properties. According to Yang and Li (2014), the tensile first-crack strength of the composite is generally governed by the matrix properties as well as fiber bridging properties, especially the chemical bond strength.

According to Table 4-6, SHGC-Na-1 made with 8.0 M NaOH solution (28.6% w/w) and Na_2SiO_3 solution (71.4% w/w) with a SiO_2/Na_2O ratio of 2.0 exhibited the highest ultimate tensile strength. The ultimate tensile strengths of SHGC-Na-2, SHGC-K, and SHGC-Lime were 17%, 61.7% and 63.8%, respectively lower than that of SHGC-Na-1. According to the micromechanics-based design theory of SHCC, the ultimate tensile strength of the composite is governed by fiber bridging capacity, which is further affected by the fiber characteristics and fiber-matrix interfacial properties (Huang et al., 2013). Therefore, it can be inferred that the higher ultimate tensile strength of SHGC-Na-1 is likely due to its higher fiber-matrix interface properties, resulting in its higher fiber bridging strength (Lee et al., 2012). The effects of type of activator on the microscale of fiber-matrix interface properties and mechanisms in fly ash-based SHGCs are investigated in Chapter 7.

The reasons for different tensile strain capacities of fly ash-based SHGCs are discussed below in terms of the two PSH performance indices, namely stress-performance index (σ_0 / σ_{fc}) and energy-performance index (J_b' / J_{tip}), proposed by Kanda and Li (2006). It should be noted that the ultimate tensile strength (σ_{cu}) coincides with σ_0 (maximum fiber bridging stress) of the composite when the composite exhibits the PSH behavior (Li et al., 1995).

According to the Table 4-6, SHGC-Na-1 exhibited the highest tensile strain capacity among all composites. The tensile strain capacity of SHGC-Na-2, SHGC-K and SHGC-Lime were 90%, 53% and 74%, respectively lower than that of SHGC-Na-1. One of the underlying reasons for different tensile strain capacities of fly ash-based SHGCs lies in their different stress-performance indices, as reported in Table 4-6. The higher the stress-performance index value, the greater the possibility of saturated PSH behavior, which results in higher tensile strain capacity of the composite (Kanda and Li, 2006). As can be seen in Table 4-6, SHGC-Na-1 and SHGC-Na-2 exhibited the highest and the lowest stress-performance indices, respectively. This pattern is well consistent with the tensile strain capacities of these composites, where SHGC-Na-1 and SHGC-Na-2 exhibited the highest and the lowest tensile strain capacities, respectively. The stress-performance indices of SHGC-K and SHGC-Lime were comparable, but lower than that of SHGC-Na-1. This is one of the reasons for the lower tensile strain capacities of these composites compared to that of SHGC-Na-1.

The second reason for different tensile strain capacities of fly ash-based SHGCs is associated with the energy-performance index of the composites. As reported in Table 4-5, the crack tip toughness J_{tip} of SHGC-Na-2, SHGC-K and SHGC-Lime were 24%, 52% and 82%, respectively lower than that of SHGC-Na-1. On the other hand, the lower ultimate tensile strength and loaded crack width of SHGC-Na-2, SHGC-K and SHGC-Lime (as reported in Tables 4-6 and 4-7, respectively) indicate that the complementary energy J_b' of these composites could be considerably lower than that of SHGC-Na-1 (Lee et al., 2012). Considering the ultimate tensile strength, loaded crack width, and J_{tip} of the composites, it can be inferred that although J_{tip} of SHGC-Na-2, SHGC-K and SHGC-Lime are lower than that of SHGC-Na-1, their considerably lower J_b' results in the substantially lower energy performance indices of these composites compared to that of SHGC-Na-1. This is another reason for the significantly higher tensile strain capacity of

SHGC-Na-1.Therefore, as expected from micromechanics-based design theory of SHCC, it is not surprising that SHGC-Na-1 with higher PSH performance indices exhibited significantly higher tensile strain capacity among all fly ash-based SHGCs investigated in this study. It should be noted that a detailed analysis of fly ash-based SHGCs is undertaken in Chapters 7 and 8 to quantify fiber-matrix interface properties (using single-fiber pullout tests) and J_b' (using a micromechanics-based model) to gain an in-depth understanding of fundamental fiber-matrix interactions and ascertain the satisfaction of the strength and energy criteria in these cement-less composites.

4.6.4 Flexural performance

The flexural stress versus mid-span deflection responses of fly ash-based SHGCs are presented in Figures 4-10 to 4-13. As can be seen, all fly ash-based SHGCs, regardless of the type of activator, exhibited clear deflection hardening behavior accompanied by multiple cracking process. The flexural performance of fly ash-based SHGCs developed in this study are comparable to those of slag-based SHGCs developed by Lee et al. (2012). The flexural test results including the measured MOR and deflection capacity as well as the estimated flexural first-crack strength are presented in Table 4-8. As can be seen, the type of activator had significant effects on the flexural performance of the composites. The developed fly ash-based SHGCs exhibited moderate to high MOR in the range of 4.92–11.5 MPa with moderate to very high deflection capacity in the range of 16.8−39.7 mm.

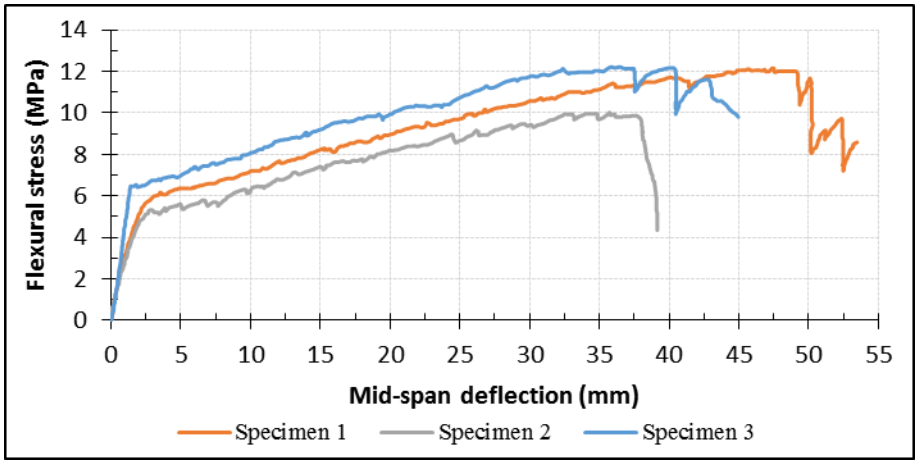

Figure 4-10: Flexural stress-mid span deflection responses of SHGC-Na-1

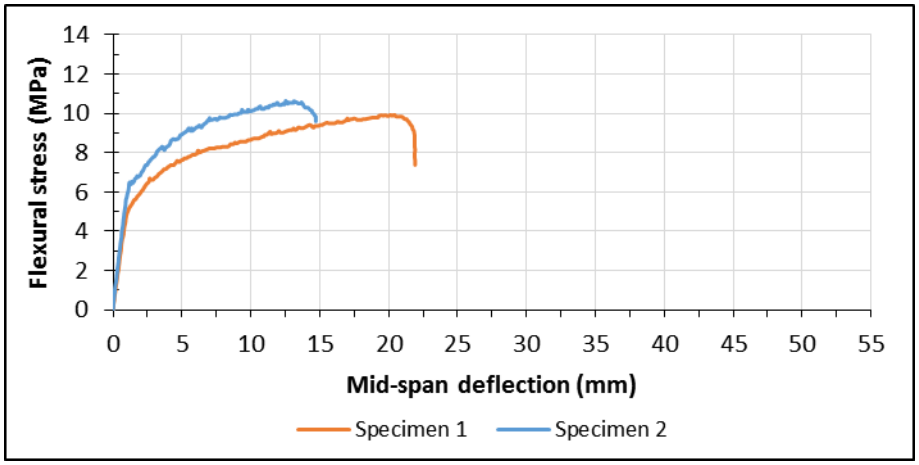

Figure 4-11: Flexural stress-mid span deflection responses of SHGC-Na-2

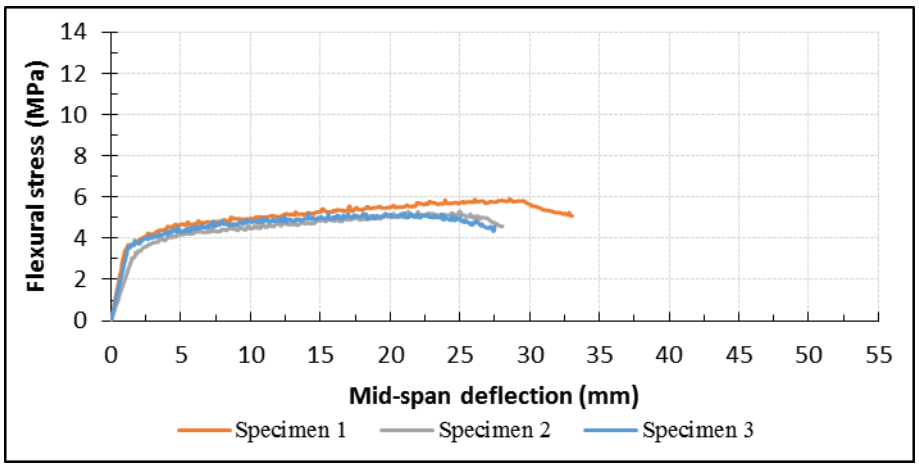

Figure 4-12: Flexural stress-mid span deflection responses of SHGC-K

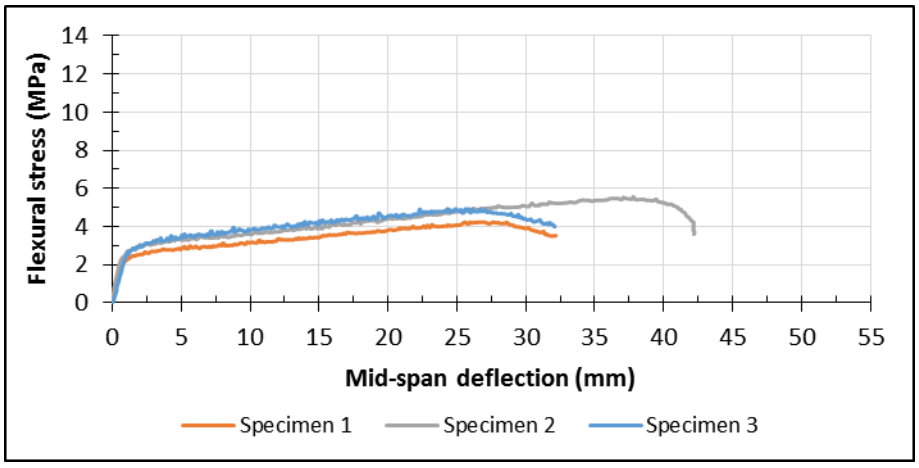

Figure 4-13: Flexural stress-mid span deflection responses of SHGC-Lime

Table 4-8: Flexural test results

Mix ID	Flexural first-crack strength, f_{LOP}; (MPa)	MOR; (MPa)	Deflection capacity, δ_{MOR}; (mm)
SHGC-Na-1	3.95±0.744	11.5±1.25	39.7±6.70
SHGC-Na-2	3.79±0.262	10.3±0.488	16.8±5.16
SHGC-K	3.28±0.212	5.47±0.377	23.6±4.25
SHGC-Lime	2.31±0.184	4.92±0.665	30.1±6.80

As can be seen in Table 4-8, the flexural first-crack strength of SHGC-Na-1 and SHGC-Na-2 were comparable. The flexural first-crack strength of SHGC-K and SHGC-Lime were 17%, and 42%, respectively lower than that of SHGC-Na-1, which corresponds to their lower matrix fracture toughness, as reported in Table 4-5 (Li et al., 2001). These results are in agreement with the tensile first-crack strength results reported in Table 4-6. According to Table 4-8, SHGC-Na-1 exhibited the highest MOR. The ultimate tensile strengths of SHGC-Na-2, SHGC-K, and SHGC-Lime were 10%, 52% and 57%, respectively lower than that of SHGC-Na-1. These results are well consistent with the ultimate tensile strength results reported in Table 4-6. As can be seen in Table 4-8, SHGC-Na-1 exhibited the highest deflection capacity. The deflection capacity of SHGC-Na-2, SHGC-K and SHGC-Lime were 58%, 41% and 24%, respectively lower than that of SHGC-Na-1. These results are also well consistent with the tensile strain capacity results reported in Table 4-6. In summary, it can be concluded that among all composites, SHGC-Na-1 exhibited the highest MOR and deflection capacity of up to 11.5 MPa and 39.7 mm, respectively, which corresponds well with its uniaxial tensile performance, where it also exhibited the highest tensile strength and tensile strain capacity of up to 4.7 MPa and 4.3%, respectively, as reported in Table 4-6.

Multiple cracking pattern of each composite under bending is presented in Figure 4-14. As can be seen, SHGC-Na-1 exhibited uniform crack distribution with enormous micro-cracks (i.e. saturated cracking behavior), which corresponds to its significantly high deflection capacity, as reported in Table 4-8. However, non-uniform crack distribution with fewer number of cracks (i.e. un-saturated cracking behavior) were observed in other composites, reflecting their lower deflection capacity, as reported in Table 4-8. The multiple cracking pattern of fly ash-based SHGCs in bending are comparable to their

multiple cracking pattern under uniaxial tension, as presented in Figure 4-9. Figure 4-15 presents the typical behavior of SHGC-Na-1 in bending, showing its very high deflection capacity.

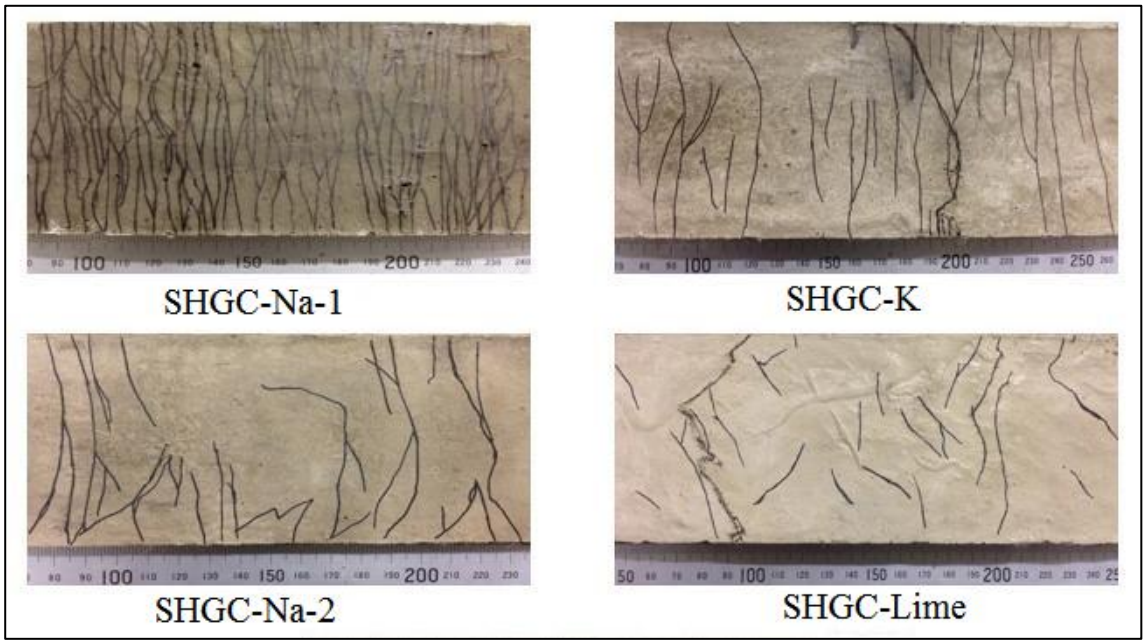

Figure 4-14: Typical multiple cracking pattern of each composite in bending

Figure 4-15: Very high ductile behavior of SHGC-Na-1 in bending

4.6.5 Toughness indices and residual strength factors

Hazards for structures subjected to dynamic loads, such as seismic, impact, and blast loads can be mitigated by using high energy absorbing materials. Hence, comparing

energy absorption capacity of the fly ash-based SHGCs developed in this study provides valuable information for such applications. One of the most important benefits of deflection hardening behavior is greater energy absorption capacity (i.e. toughness) of the composite compared to the composites that exhibit deflection softening behavior. According to the current ASTM C1609 (2012), specimen's toughness is defined as the area under the load-deflection curve up to a net deflection of 1/150 of the span. However, Kim et al. (2008) suggested that in deflection hardening composites especially in situations comprising large deformation in excess of 1/150 of the span, the toughness of the composite should be determined up to a net deflection of 1/100 and even 1/50 of the span, if the case justifies it. However, as can be seen in Table 4-8, very large deformations were observed in all fly ash-based SHGCs and the deflection at peak load is at least greater than 15 mm (i.e. equal to 1/20 of the span), which is far greater than 1/50 of the span. Thus, in this study according to ASTM C1018 (1997), toughness indices of I_5, I_{10} and I_{20} were determined which correspond to a net deflections of $3\delta_{LOP}$, $5.5\delta_{LOP}$ and $10.5\delta_{LOP}$, respectively.

According to ASTM C1018 (1997), the behavior of fiber reinforced composite up to the commencement of cracking in the matrix is characterized by the f_{LOP}, while the toughness indices represent the stiffness after first-crack up to particular end point deflections. Actual performance of a composite material can be compared with easily understood elastic-perfectly plastic material behavior through the toughness indices. Figure 4-16 defines the toughness indices in terms of multiples of first-crack deflection and elastic-plastic material behavior (ASTM C1018, 1997). As can be seen, values of 5.0, 10.0 and 20.0 in toughness indices (i.e. I_5, I_{10}, and I_{20}) represent the linear elastic material behavior up to first-crack and perfectly plastic behavior afterward. In other words, the values of I_5, I_{10}, and I_{20} for a linear elastic-perfectly plastic material are equal to 5.0, 10.0 and 20.0, respectively. The average level of strength maintained over specific deflection intervals after the first-crack as a proportion of the first-crack strength is characterized by the residual strength factors, which can be derived directly from the toughness indices. In other words, the residual strength factors represent the average post-crack load over a particular deflection interval as a percentage of the load at first-crack. Therefore, the residual strength factors equal to 100 represent the perfectly plastic behavior, whereas the lower values demonstrate inferior behavior. The residual strength factors of plain concrete are equal to zero.

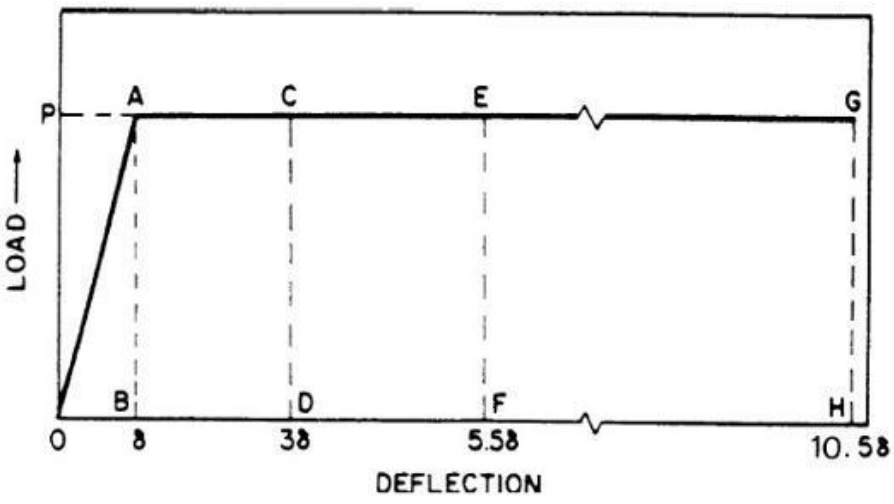

Area basis*	Toughness index designation	Deflection criterion	Values of toughness indices		
			Plain concrete	Elastic-Plastic material	Observed range for FRC
OACD	I_5	3δ	1.0	5.0	1 to 6
OAEF	I_{10}	5.5δ	1.0	10.0	1 to 12
OAGH	I_{20}	10.5δ	1.0	20.0	1 to 25

Note: *Indices calculated by dividing this area by the area to the first crack OAB.

Figure 4-16: Definition of the toughness indices in terms of multiples of first-crack deflection and elastic-plastic material behavior (Source: ASTM C1018, 1997)

The average toughness indices values of I_5, I_{10}, and I_{20} for each composite is presented in Figure 4-17. The average residual strength factors of each composite is presented in Table 4-9. The toughness indices of I_5, I_{10} and I_{20} of each composite were determined by dividing the area under the load-deflection curves up to the $3\delta_{LOP}$, $5.5\delta_{LOP}$ and $10.5\delta_{LOP}$ by the area up to the δ_{LOP}, respectively. Subsequently, the residual strength factors (i.e. $R_{5,10}$ and $R_{10,20}$) were obtained by calculating the values of $20 \times (I_{10} - I_5)$ and $10 \times (I_{20} - I_{10})$, respectively. As can be seen, in all fly ash-based SHGCs the I_5, I_{10}, and I_{20} values were greater than the set benchmark values (i.e. 5.0, 10.0 and 20.0 for I_5, I_{10} and I_{20}, respectively). In addition, the $R_{5,10}$ and $R_{10,20}$ values of all composites were also higher than 100, corresponding to perfectly plastic behavior. Therefore, it can be concluded that all fly ash-based SHGCs exhibited significantly improved post-cracking flexural performance, which is even superior to the perfectly plastic behavior. According to Naaman and Reinhardt (1995), $I_{20} > 20.0$ is an indication of deflection hardening behavior in fiber reinforced composites. As can be seen in Figure 4-17, the I_{20} values of all fly ash-based SHGCs were far bigger than 20.0. This is another indication that all composites, regardless of their type of activator, exhibited deflection hardening behavior.

As can be seen in Figure 4-17 and Table 4-9, the toughness indices and residual strength factors of SHGC-Na-1 were higher than those of SHGC-K and SHGC-Lime, which clearly indicate its higher non-elastic energy absorption capacity. However, the toughness indices and residual strength factors of SHGC-Na-1 were about 20% lower than those of SHGC-Na-2. This is due to the lower δ_{LOP} and f_{LOP} of SHGC-Na-2 compared to those of SHGC-Na-1.

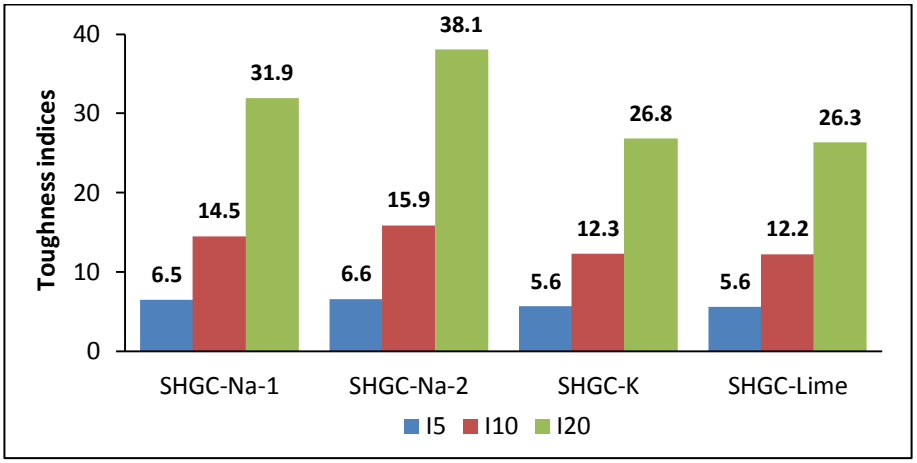

Figure 4-17: Toughness indices (I_5, I_{10} and I_{20}) of each composite

Table 4-9: Residual strength factors of each composite

Mix ID	$R_{5, 10}$	$R_{10, 20}$
SHGC-Na-1	159.5	174.8
SHGC-Na-2	186.2	221.8
SHGC-K	133.5	145.1
SHGC-Lime	132.8	141.2

4.7 Conclusions

In this chapter, four fly ash-based geopolymer composites incorporating four different activator combinations reinforced by randomly oriented short PVA fibers were manufactured. All composites exhibited moderate to high ultimate tensile strength in the range of 1.7–4.7 MPa depending on the type of activator. At the same time, they exhibited moderate to very high tensile strain capacity in the range of 0.42−4.3% depending on the type of activator, which is about two orders of magnitude higher than that of brittle OPC-

based or geopolymer concrete. Therefore, the development of SHGCs with fly ash-based geopolymer as the sole binder is experimentally established. The quantitative influences of type of activator on the matrix and composite properties of fly ash-based SHGCs, including workability, density, compressive strength, matrix fracture properties, uniaxial tensile and flexural behaviors were evaluated. The results indicated that the type of activator had significant effects on the matrix and composite properties, in particular on the uniaxial tensile and flexural performances of fly ash-based SHGCs. The following specific conclusions are drawn:

1) Among all fly ash-based SHGCs, SHGC-Na-1 made with NaOH and Na_2SiO_3 solutions exhibited the highest ultimate tensile strength and tensile strain capacity of up to 4.7 MPa and 4.3%, respectively. The higher ultimate tensile strength of SHGC-Na-1 is likely due to its higher fiber-matrix interface properties, resulting in its higher fiber bridging strength. SHGC-Na-1 also exhibited the highest stress-performance index among all composites. This is one of the reasons for the very high tensile strain capacity of SHGC-Na-1. In addition, the high ultimate tensile strength and loaded crack width of SHGC-Na-1 indicated that the complementary energy, and thereby the energy performance index of SHGC-Na-1 could be considerably higher than those of other composites. This is another reason for the significantly higher tensile strain capacity of SHGC-Na-1 compared to other composites. Therefore, as expected from micromechanics-based design theory of SHCC, it is not surprising that SHGC-Na-1 with higher PSH performance indices exhibited significantly higher tensile strain capacity among all fly ash-based SHGCs investigated in this study. Among all composites, SHGC-Na-1 also exhibited the highest MOR and deflection capacity of up to 11.5 MPa and 39.7 mm, respectively, which corresponds well with its superior uniaxial tensile performance.

2) Among all composites, crack distribution in SHGC-Na-1 was uniform and enormous micro-cracks with tightly controlled crack width (i.e. saturated cracking behavior) were observed, which corresponds to its very high tensile strain and deflection capacities. However, non-uniform crack distribution with fewer number of cracks (i.e. un-saturated cracking behavior) were observed in other composites, corresponding to their inferior tensile strain and deflection capacities.

3) The toughness indices and residual strength factors of SHGC-Na-1 were higher than those of SHGC-K and SHGC-Lime, which clearly indicate its higher non-elastic energy absorption capacity. However, the toughness indices and residual strength factors of SHGC-Na-1 were marginally lower than those of SHGC-Na-2 made with only NaOH solution. This is due to the lower δ_{LOP} and f_{LOP} of SHGC-Na-2 compared to those of SHGC-Na-1.

4) The type of activator had significant influences on the fracture toughness of the geopolymer matrix, and also on the compressive strength of the geopolymer matrix and composite. SHGC-Na-1 exhibited the highest matrix fracture toughness and compressive strength among all composites. The different matrix fracture toughness and compressive strength of fly ash-based SHGCs are attributed to different microstructure of the geopolymer pastes, due their different type of activator.

5) While the type of activator had a considerable influence on the workability of the geopolymer matrix, it did not have a significant effect on the matrix and composite density of fly ash-based SHGCs.

In summary, it can be concluded that in fly ash-based SHGCs, the use of Na-based activator combination composed of 8.0 M NaOH solution (28.6% w/w) and Na_2SiO_3 solution (71.4% w/w) with a SiO_2/Na_2O ratio of 2.0 is highly beneficial in terms of lower cost, higher compressive strength gain and matrix fracture properties, along with superior uniaxial tensile and flexural behaviors compared to the other three activator combinations investigated in this study. Therefore, the SHGC-Na-1 mix is used as the benchmark in the next chapter, which investigates the quantitative effects of other geopolymer matrix related parameters on the composite properties of fly ash-based SHGCs.

4.8 References

ASTM C1018. 1997. Standard Test Method for Flexural Toughness and First-Crack Strength of Fiber-Reinforced Concrete (Using Beam With Third-Point Loading). United States: ASTM Standards.

ASTM C109/C109M. 2007. Standard Test Method for Compressive Strength of Hydraulic Cement Mortars (Using 2-in. or [50-mm] Cube Specimens). United States: ASTM Standards.

ASTM C1437. 2007. Standard test method for flow of hydraulic cement mortar. United States: ASTM Standards.

ASTM C1609. 2012. Standard Test Method for Flexural Performance of Fiber-Reinforced Concrete (Using Beam With Third-Point Loading). United States: ASTM Standards.

AHMED, S. & MAALEJ, M. 2009. Tensile strain hardening behaviour of hybrid steel-polyethylene fibre reinforced cementitious composites. *Construction and Building Materials,* 23, 96-106.

BARBOSA, V. F., MACKENZIE, K. J. & THAUMATURGO, C. 2000. Synthesis and characterisation of materials based on inorganic polymers of alumina and silica: sodium polysialate polymers. *International Journal of Inorganic Materials,* 2, 309-317.

BAZANT, Z. P., KIM, J.-K. & PFEIFFER, P. A. 1986. Nonlinear fracture properties from size effect tests. *Journal of Structural Engineering,* 112, 289-307.

BEAUPRÉ, D. & MINDESS, S. 1998. Rheology of fresh concrete: principles, measurement, and applications. *Materials Science of Concrete V,(Ed. Skalny, J. and Mindess, S.),* 149.

FERNÁNDEZ-JIMÉNEZ, A. & PALOMO, A. 2005. Composition and microstructure of alkali activated fly ash binder: effect of the activator. *Cement and concrete research,* 35, 1984-1992.

HARDJITO, D., WALLAH, S. E., SUMAJOUW, D. M. & RANGAN, B. V. 2004. On the development of fly ash-based geopolymer concrete. *ACI Materials Journal-American Concrete Institute,* 101, 467-472.

HUANG, X., RANADE, R., ZHANG, Q., NI, W. & LI, V. C. 2013. Mechanical and thermal properties of green lightweight engineered cementitious composites. *Construction and Building Materials,* 48, 954-960.

JENQ, Y. & SHAH, S. P. 1985. Two parameter fracture model for concrete. *Journal of engineering mechanics,* 111, 1227-1241.

KANDA, T. & LI, V. C. 1999. New micromechanics design theory for pseudostrain hardening cementitious composite. *Journal of engineering mechanics,* 125, 373-381.

KANDA, T. & LI, V. C. 2006. Practical design criteria for saturated pseudo strain hardening behavior in ECC. *Journal of advanced concrete technology,* 4, 59-72.

KARIHALOO, B. & NALLATHAMBI, P. 1990. Effective crack model for the determination of fracture toughness (KICe) of concrete. *Engineering Fracture Mechanics,* 35, 637-645.

KIM, D. J., NAAMAN, A. E. & EL-TAWIL, S. 2008. Comparative flexural behavior of four fiber reinforced cementitious composites. *cement & concrete composites,* 30, 917-928.

KONG, D. L. & SANJAYAN, J. G. 2010. Effect of elevated temperatures on geopolymer paste, mortar and concrete. *Cement and concrete research,* 40, 334-339.

LEE, B. Y., CHO, C.-G., LIM, H.-J., SONG, J.-K., YANG, K.-H. & LI, V. C. 2012. Strain hardening fiber reinforced alkali-activated mortar–a feasibility study. *Construction and Building Materials,* 37, 15-20.

LI, V. & MISHRA, D. 1992. Micromechanics of Fiber Efect on the Uniaxial Compressive strength of Cementitious Composites. *Fibre Reinforced Cement and Concrete: Proceedings of the Fourth RILEM International Symposium.* University of Sheffield, UK, Sheffield: Taylor & Francis.

LI, V. C., MISHRA, D. K. & WU, H.-C. 1995. Matrix design for pseudo-strain-hardening fibre reinforced cementitious composites. *Materials and Structures,* 28, 586-595.

LI, V. C., WANG, S. & WU, C. 2001. Tensile strain-hardening behavior of polyvinyl alcohol engineered cementitious composite (PVA-ECC). *Materials Journal,* 98, 483-492.

MARTIN, J., STANTON, J., MITRA, N. & LOWES, L. N. 2007. Experimental testing to determine concrete fracture energy using simple laboratory test setup. *ACI Materials Journal,* 104, 575-584.

NAAMAN, A. & REINHARDT, H. W. 1995. Characterization of high performance fiber reinforced cement composites-HPFRCC. *The second international RILEM workshop on high performance fiber reinforced cement composites.* USA.

OHNO, M. & LI, V. C. 2014. A feasibility study of strain hardening fiber reinforced fly ash-based geopolymer composites. *Construction and Building Materials,* 57, 163-168.

OKAMURA, H. & OZAWA, K. 1995. Mix design for self-compacting concrete. *Concrete Library. JSCE,* 25, 107–120.

PAN, Z., SANJAYAN, J. G. & RANGAN, B. V. 2011. Fracture properties of geopolymer paste and concrete. *Magazine of concrete research,* 63, 763-771.

PETERSON, P. 1980. Fracture energy of concrete: method of determination. *Cement and Concrete research,* 10, 79-89.

ROWLES, M. R. 2004. *The structural nature of aluminosilicate inorganic polymers: a macro to nanoscale study.* Ph.D. Thesis, Curtin University of Technology.

SARKER, P. K., HAQUE, R. & RAMGOLAM, K. V. 2013. Fracture behaviour of heat cured fly ash based geopolymer concrete. *Materials & Design,* 44, 580-586.

TATTERSALL, G. & BANFILL, P. 1983. The rheology of fresh concrete: Pitman Advanced Pub. *Program, London*.

WALLEVIK, J. E. 2006. Relationship between the Bingham parameters and slump. *Cement and Concrete Research,* 36, 1214-1221.

XU, H. & VAN DEVENTER, J. 2000. The geopolymerisation of alumino-silicate minerals. *International Journal of Mineral Processing,* 59, 247-266.

CHAPTER 5

MATRIX DESIGN OF HEAT CURED TWO-PART FLY ASH-BASED SHGCS

Note: This chapter is based on the paper "*Matrix design of strain hardening fiber reinforced engineered geopolymer composite*", by ***Nematollahi, B.***, Sanjayan, J., and Shaikh, F.U.A., published in ***Composites Part B: Engineering***, 2016, 89, 253-265.

5.1 Introduction

The feasibility of developing a fiber-reinforced fly ash-based SHGC has been demonstrated in the previous chapter. The effect of different alkaline activators on the matrix and composite behavior of such SHGCs has also been evaluated. The results revealed that the fly ash-based SHGC, developed by using the suitable Na-based activator combination, exhibited the highest compressive and tensile strengths with very high tensile strain capacity over 60 MPa, 4.7 MPa and 4.3% on average, respectively. The Na-based activator was composed of 8.0 M NaOH solution (28.6% w/w) and Na_2SiO_3 solution (71.4% w/w) with a SiO_2/Na_2O ratio of 2.0. As a follow up investigation, this chapter is aimed to evaluate the quantitative influence of other geopolymer matrix related parameters such as water to geopolymer solids ratio, sand size and sand content on the tensile performance of the developed fly ash-based SHGC.

Only fly ash (with no sand) was used in the matrix of the fly ash-based SHGC developed in the previous chapter; this was similar to the first generation of the "conventional" SHCCs where only OPC and silica fume (with no sand) were used in the SHCC matrix (Li et al., 1995; Kanda and Li, 1999). The lack of sand in the matrix results in a composite with low elastic modulus (Li et al., 1995). Sand content can also alter matrix fracture toughness, pre-existing flaw size distribution and fiber/matrix interface properties (Lie et al., 2001; Yang et al., 2008). Few studies have evaluated the effect of aggregate type and size on ductility and mechanical properties of the "conventional" SHCCs (Li et al., 1995; Sahmaran et al., 2009). However, the quantitative effects of these parameters on the matrix and composite properties of the developed fly ash-based SHGC have not yet been evaluated. In addition, previous studies have also revealed that water content, viz. water to geopolymer solids ratio (W/GP solids), has a significant influence on the properties of

the geopolymer (Barbosa et al., 2000; Hardjito et al., 2004). The effect of the W/GP solids on the matrix and composite properties of the developed fly ash-based SHGC has not yet been evaluated either. Therefore, for the purpose of the current study, W/GP solids, sand size and sand content, i.e. sand to fly ash ratio (S/FA) were selected as the most significant parameters in governing the characteristics of the geopolymer matrix. A systematic experimental program was designed to evaluate the quantitative effects of these matrix-related parameters on the matrix and composite properties of the developed fly ash-based SHGC with the aim of selecting the appropriate type of geopolymer matrix to manufacture the fly ash-based SHGCs with enhanced elastic modulus, while maintaining the desirable tensile ductility behavior of the composite.

5.2 Materials

The same low calcium (Class F) fly ash supplied from Gladstone power station in Queensland, Australia was used in this research. The chemical composition and LOI of the fly ash are presented in Table 3-1. Based on the results of the previous chapter, the same Na-based-1 activator combination composed of 8.0 M NaOH solution (28.6% w/w) and D Grade Na_2SiO_3 solution (71.4% w/w) with a SiO_2/Na_2O ratio of 2.0 was also used in this research. Chemical and physical properties of the NaOH and Na_2SiO_3 solutions and the procedure for preparation of the activator combination are presented in Section 4.2 of Chapter 4. The same PVA fibers with a surface oil coating of 1.2% by weight, supplied by Kuraray Co. Ltd., Japan were used in this study. Properties of the PVA fibers are presented in Table 4-2. Sieve graded high silica purity sands with two different particle sizes were used in this study. The fine silica sand denoted as FS with maximum particle size of 212 μm was supplied by TGS Industrial Sand Ltd., Australia. The coarse silica sand denoted as CS with particle sizes between 1.18 mm and 600 μm was supplied by Sibelco, Australia. Both silica sands were used in saturated surface dry (SSD) condition.

5.3 Experimental Procedures

A systematic experimental program was designed in this study with the following two objectives. The first goal was to evaluate the effects of W/GP solids, sand size and sand content (S/FA) as the most important matrix related parameters on the mechanical properties of the geopolymer matrix including workability of the fresh matrix,

compressive strength and fracture properties in terms of elastic modulus, fracture toughness and crack tip toughness. The second objective was to identify the appropriate type of geopolymer matrix which can be used to design fly ash-based SHGCs with improved elastic modulus, while maintaining the desirable tensile ductility properties. Based on available literature, there have been only few studies that have accounted for the different mechanical characteristics of the geopolymer mixes with focus to achieve a desirable combination of properties. Nevertheless, there have been many studies which reported the effect of different geopolymer mix parameters on a particular property of the material such as compressive strength (Hardjito et al., 2004; Nematollahi and Sanjayan, 2014).

5.3.1 Mix proportions

Table 5-1 presents the mix proportions of fly ash-based SHGCs used in this study. As can be seen, two values of W/GP solids (0.20 and 0.23) and two different sand sizes (FS and CS) with two values of S/FA by mass (0.30 and 0.60) were selected. The SHGC mixtures were designated with their variable constituents in the mix. For example, SHGC23-FS-30 represents an SHGC mixture having a W/GP solids of 0.23 and containing FS sand with S/FA of 0.30. It should be noted that the SHGC20 mix shown in Table 5-1 is the same as SHGC-Na-1 mixture used in Chapter 4, which was used as the benchmark in this research.

5.3.2 Mixing, curing and testing of specimens

All mixtures were prepared in a Hobart mixer. To prepare the fly ash-based geopolymer matrix, fly ash and sand (if any) were dry mixed for about 3 minutes. Then alkaline solution and extra water (if any) were added and the mixing was continued for about 4 minutes. As mentioned in Chapter 3, after the matrix ingredients in each mixture were thoroughly mixed to achieve the desired fresh state, the flowability of fresh geopolymer matrix (before addition of the fibers) was measured to ensure that the flowability was within the desired range for achieving good fiber dispersion. Finally, the PVA fibers (2% volume fraction) were gradually added to ensure uniform fiber dispersion. The whole mixing procedure for each mixture generally took 20-25 minutes.

Table 5-1: Mix proportions of fly ash-based SHGCs

Mix designation	Fly ash	Activator	Water	Sand		PVA fiber	W/GP solids ratio
				FS[2]	CS[3]		
SHGC20[1]	1.0	0.35	0.014	---	---	0.02	0.20
SHGC23	1.0	0.45	---	---	---	0.02	0.23
SHGC23-FS-30	1.0	0.45	---	0.3	---	0.02	0.23
SHGC23-FS-60	1.0	0.45	---	0.6	---	0.02	0.23
SHGC23-CS-30	1.0	0.45	---	---	0.3	0.02	0.23
SHGC23-CS-60	1.0	0.45	---	---	0.6	0.02	0.23

Note: All numbers are mass ratios of fly ash weight except W/GP solids ratios and fiber contents (volume fraction).

[1] The same as SHGC-Na-1 mixture in Chapter 4, which was used as the benchmark in this study.

[2] Fine sand with maximum particle size of 212 μm.

[3] Coarse sand with particle sizes between 600 μm and 1.18 mm.

Heat curing was adopted in this chapter, based on the results presented in Chapter 4 which indicated that the heat curing enhances both strength and ductility properties of the fly ash-based SHGCs compared to the fly ash-based SHGCs developed by Ohno and Li (2014). The procedure for the heat curing is given in Section 4.4 of Chapter 4.

Mini-slump test also known as spread-flow test was conducted to determine flowability of the fresh geopolymer matrix. Details of the mini-slump test are given in Section 4.5 of Chapter 4. Compressive strength of matrix and composite in each mixture were measured. The procedure for compression test is given in Section 4.5 of Chapter 4. Three-point bending tests on single edge notched beam specimens were conducted to evaluate the matrix fracture properties including E_m, K_m and J_{tip} of the developed fly ash-based SHGCs. Details of the matrix fracture toughness test are given in Section 4.5 of Chapter 4. Uniaxial tension tests were conducted to evaluate the behavior of the developed fly ash-based SHGCs under direct tension. Details of the uniaxial tension test are given in Section 4.5 of Chapter 4.

5.4 Results and Discussions

5.4.1 Effect of W/GP solids on geopolymer matrix properties

The geopolymer matrix test results including average workability in terms of relative slump value, compressive strength (f'_{cm}), elastic modulus (E_m), fracture toughness (K_m) and crack tip toughness (J_{tip}) are presented in Table 5-2. As mentioned in Chapter 4, it should be noted that in this study the E_m of each mixture was derived indirectly based on ECM (Karihaloo and Nallathambi, 1990) from the linear portion of the load-deflection curve of the notched beam specimen in three-point bending tests. The derived E_m values thereby should only be considered as relative values enabling us to compare the matrix elastic modulus of each mixture. As can be seen in Table 5-2, the matrix workability of SHGC23 was 32% higher than that of SHGC20 due to its higher W/GP solids. Furthermore, as expected the workability of the mortar matrices was lower than that of SHGC23 (paste only mix with no sand), and the workability decreased with increase in the sand sizes and the sand contents in the mortar mixes.

Table 5-2: Geopolymer matrix test results

Mix designation	Workability	Compressive strength, f'_{cm} (MPa)	Elastic modulus, E_m (GPa)[b]	Fracture toughness, K_m ($MPa.m^{1/2}$)[c]	Crack tip toughness, J_{tip} (J/m^2)[d]
SHGC20	6.9 (281.5)	54.6±3.0	8.5	0.436	22.4
SHGC23	9.1 (318)	31.6±1.5	4.7	0.269	15.4
SHGC23-FS-30	8.8 (313)	36.4±0.9	5.6	0.402	28.9
SHGC23-FS-60	7.3 (287.5)	35.3±1.7	7.6	0.533	37.4
SHGC23-CS-30	9.0 (317)	34.8±1.6	6.4	0.377	22.2
SHGC23-CS-60	8.3 (305)	35.7±1.4	7.3	0.438	26.3

[a] In terms of relative slump value of the fresh matrix. The average diameter of the matrix flow (in millimeter) is shown in parenthesis.

[b] Following Equation (4.2) (Karihaloo and Nallathambi, 1990).

[c] Following Equation (4.3) (Karihaloo and Nallathambi, 1990).

[d] Following Equation (4.5) (Li et al., 1995).

The effect of W/GP solids (by mass) on the compressive strength and elastic modulus of the geopolymer matrix is presented in Figure 5-1. As can be seen, the increase in W/GP solids from 0.20 to 0.23 resulted in a considerable decrease in both compressive strength and elastic modulus of the geopolymer matrix. The compressive strength and elastic modulus of SHGC23 matrix were 42% and 45% lower, respectively compared to those of SHGC20 matrix. Similar trend was reported by other researchers for geopolymer paste and concrete (Hardjito et al., 2004, Barbosa et al., 2000). This trend is somewhat similar to the well-known effect of water to cement ratio (W/C) on the compressive strength and elastic modulus of the cement-based matrices (Hardjito et al., 2004), as reported by Li et al. (1995).

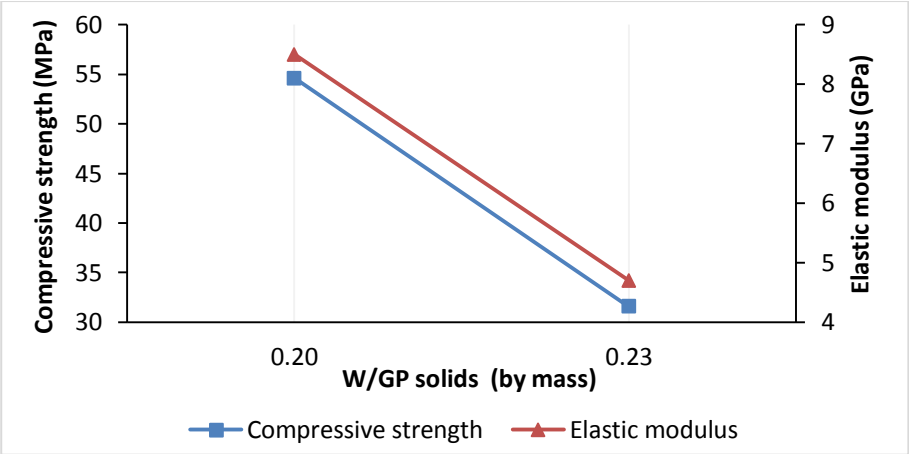

Figure 5-1: Effect of W/GP solids on compressive strength and elastic modulus of geopolymer matrix

The effect of W/GP solids (by mass) on the fracture toughness and crack tip toughness of the geopolymer matrix is presented in Figure 5-2. As can be seen, the increase in W/GP solids from 0.20 to 0.23 resulted in a considerable decrease in both fracture toughness and crack tip toughness of the geopolymer matrix. The fracture toughness and crack tip toughness of SHGC23 matrix were 38% and 31%, respectively lower compared to those of SHGC20 matrix. Similar trend was reported by other researchers regarding the effect of W/C on fracture toughness and crack tip toughness of the cement-based matrices (Li et al., 1995).

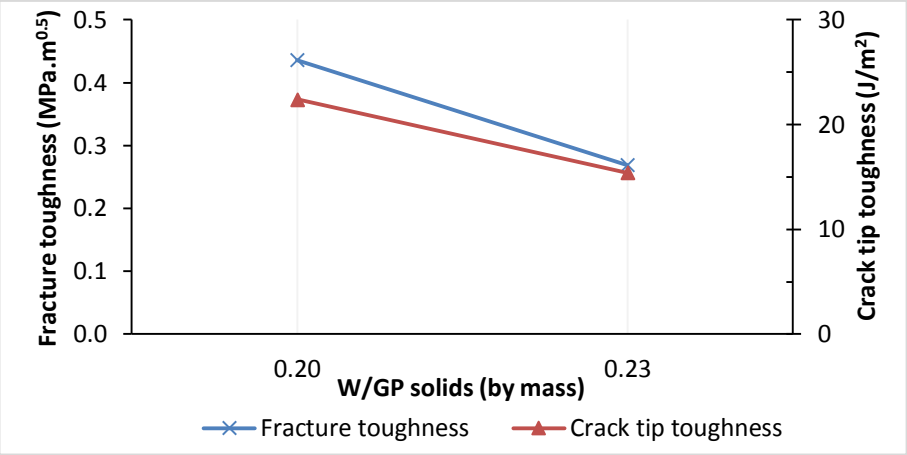

Figure 5-2: Effect of W/GP solids on fracture toughness and crack tip toughness of geopolymer matrix

5.4.2 Effect of sand size and sand content on geopolymer matrix properties

According to Table 5-2, the addition of sand, regardless of the sand size and content, increased the compressive strength and elastic modulus of the plain geopolymer paste. Similar trend was observed by other researchers regarding the effect of the addition of sand on the strength of the plain cement paste (Akkaya et al., 2000). The effect of sand size and sand content (S/FA) on the compressive strength of the geopolymer matrix is presented in Figure 5-3. As can be seen, the increase in S/FA from zero to 0.3, regardless of the sand size, resulted in 10−15% increase in the matrix compressive strength. However, no significant increase in the compressive strength of the mortar mixes was observed by increasing the S/FA from 0.3 to 0.6 (i.e. doubling the sand content), regardless of the sand size. In other words, the matrix compressive strengths of all mortar mixes, regardless of their sand size and content, were almost comparable. These results are in good agreement with those published by Temuujin et al. (2010), where the compressive strength of the fly ash-based geopolymer mortar mixes remained almost constant, while varying the sand content.

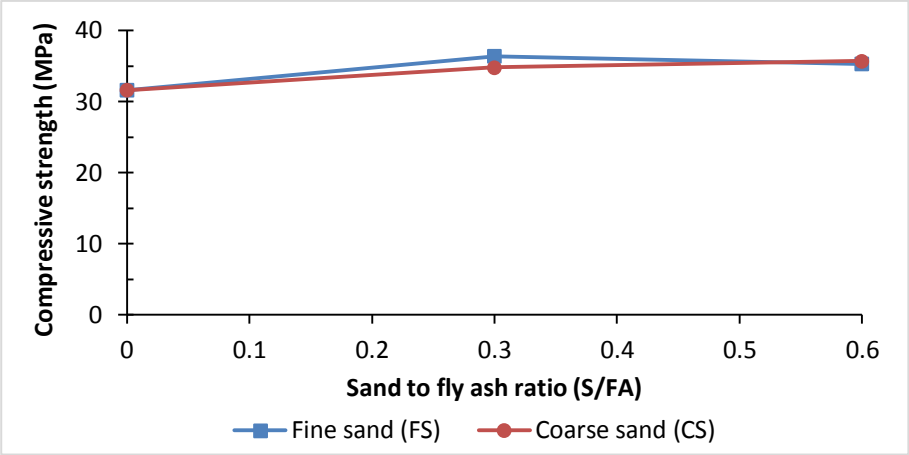

Figure 5-3: Effect of sand size and sand content on compressive strength of geopolymer matrix

The effect of sand size and sand content (S/FA) on the elastic modulus of the geopolymer matrix is presented in Figure 5-4. As can be seen, the increase in S/FA from zero to 0.3 resulted in 19−36% increase in the matrix elastic modulus, depending on the sand size. This is a considerable increase in the elastic modulus, considering that only a small amount of sand (S/FA=0.3) was used. In addition, the increase in S/FA from 0.3 to 0.6 (i.e. doubling the sand content) also resulted in 14−36% increase in the elastic modulus of the geopolymer matrix, depending on the sand size. Therefore, it can be said that the elastic modulus of the geopolymer mortar mixtures manufactured in this study (with S/FA=0.6) was significantly (up to 62%) higher than that of the geopolymer paste mixture with no sand (S/FA=0). Similar trend was reported by other researchers regarding the effect of sand content on elastic modulus of the cement-based matrices (Li et al., 1995).

It should be pointed out that comparison between the results obtained in this study regarding the effect of the addition of sand on elastic modulus of the geopolymer matrix with those of the cement-based matrix reported by Li et al. (1995) revealed that the effect of the addition of sand on elastic modulus of the geopolymer matrix was more pronounced than that of the cement-based matrix. This is due to the lower elastic modulus of the geopolymer paste compared to that of a comparable OPC paste. Pan et al. (2011) reported that the elastic modulus of fly ash-based geopolymer paste was approximately 27% lower than that of an OPC paste with similar compressive strength. According to a model proposed by Hashin (1962), the elastic modulus of a two-phase heterogeneous material

such as cement/geopolymer mortar (the two phases being cement/geopolymer paste and sand) can be expressed in terms of the elastic modulus of the sand and the cement/geopolymer paste as follows:

$$E_{mortar}=\left[\frac{(1+V_a)E_a+(1-V_a)E_p}{(1-V_a)E_a+(1+V_a)E_p}\right]E_p \quad (5.1)$$

where E_{mortar} is the elastic modulus of the mortar, E_p, V_p (=1-V_a) and E_a, V_a are the elastic modulus and volume fraction of the paste and aggregate, respectively. Silica sand has a much higher elastic modulus (72 GPa) than cement/geopolymer paste (Lide, 2004). Based on the Equation (5.1), for a constant volume fraction of sand (V_a), the rate of increase in the elastic modulus of a geopolymer mortar compared to that of a geopolymer paste is higher than the rate of increase in the elastic modulus of a cement mortar compared to that of a comparable cement paste. This is due the lower elastic modulus of the geopolymer paste than that of the OPC paste with similar compressive strength (Pan et al., 2011).

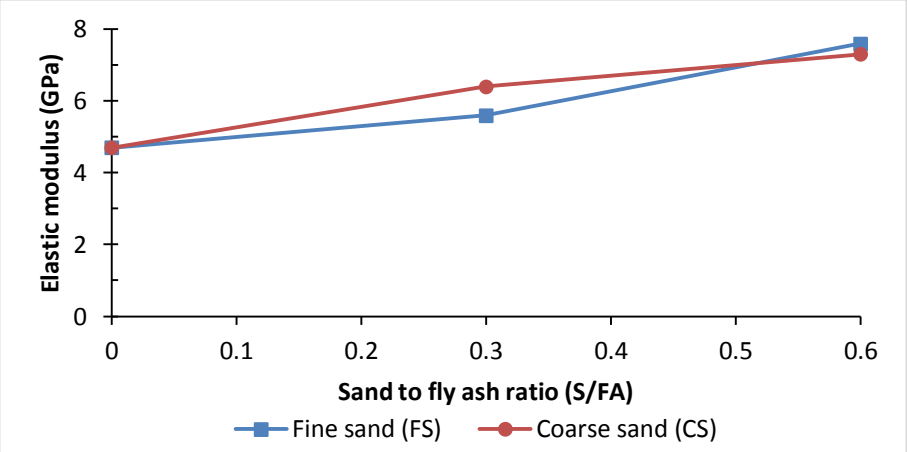

Figure 5-4: Effect of sand size and sand content on elastic modulus of geopolymer matrix

The effect of sand size and sand content (S/FA) on the fracture toughness of the geopolymer matrix is demonstrated in Figure 5-5. As can be seem, the increase in S/FA from zero to 0.3 resulted in 40−49% increase in the matrix fracture toughness. This is a substantial increase in the fracture toughness considering that only a small amount of sand (S/FA=0.3) was used. In addition, the increase in S/FA from 0.3 to 0.6 (i.e. doubling the

sand content) also resulted in 16−33% increase in the matrix fracture toughness. Therefore, it can be said that the fracture toughness of the geopolymer mortar mixtures prepared in this study (with S/FA=0.6) was significantly (up to 98%) higher than that of the geopolymer paste mixture with no sand (S/FA=0).

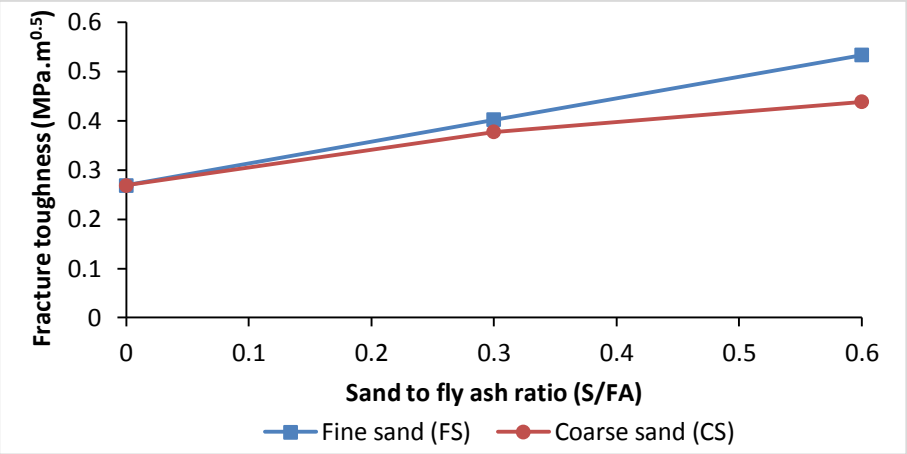

Figure 5-5: Effect of sand size and sand content on fracture toughness of geopolymer matrix

The increase in fracture toughness of the geopolymer mortar mixtures is attributed to the increase of energy consumption by the tortuous crack propagation path (Pan et al., 2011; Li et al., 2001). Similar trend was reported by other researchers regarding the effect of sand content on fracture toughness of the cement-based matrices (Li et al., 1995). With regards to sand size, as can be seen in Figure 5-5, at a constant S/FA, the fracture toughness of the geopolymer matrix containing coarse sand (CS) was 7−22% lower than that of the matrix containing fine sand (FS), depending on the sand content. This could be due to the fact that at a constant S/FA by mass, crack propagation in the matrix containing coarse sand (CS) is likely to be less tortuous, because of the smaller number of particles of coarse sand in the matrix compared to that of the fine sand of the same weight; thereby, consumes less energy compared to that of the matrix containing fine sand (FS). The visual observations of the fracture surface of the specimens also confirmed this trend. According to Pan et al. (2011), fracture toughness of concrete is generally influenced by the microstructure of the paste and the size, texture and angularity of the aggregates. Thus, in the current study, the sand content as well as the size, texture and

angularity of fine and coarse sands are the most prominent reasons for the different fracture toughness of the geopolymer matrices, because the other factors were kept the same for all mixtures.

The effect of sand size and sand content (S/FA) on crack tip toughness of geopolymer matrix is presented in Figure 5-6. As can be seen, the increase in S/FA from zero to 0.6 resulted in a significant increase (up to 143%) in the crack tip toughness, depending on the sand size. This corresponds to the considerable increase in the fracture toughness of the geopolymer mixtures due to addition of sand, as presented in Figure 5-5. This significant increase in crack tip toughness is not desirable, as it results in a significant reduction in the energy performance index (J_b'/J_{tip}) of the composite. In other words, the considerable increase in the crack tip toughness hinders the use of this geopolymer matrix to ensure saturated PSH behavior in the resulting composite. These results indicate that the sand content must be limited in the geopolymer matrix to maintain the desirable tensile ductility of the geopolymer composite. Similar results were reported by previous studies regarding the cement-based matrices (Li et al., 1995; Li et al., 2001).

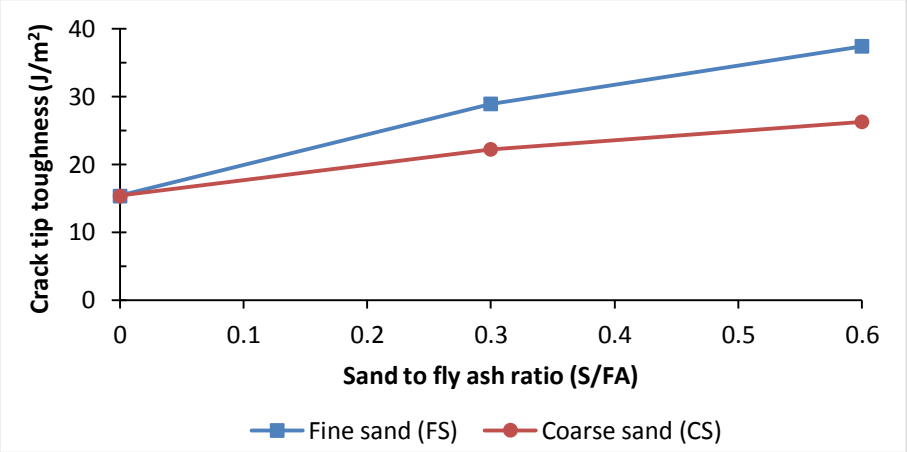

Figure 5-6: Effect of sand size and sand content on crack tip toughness of geopolymer matrix

5.4.3 Uniaxial tensile performance

The tensile stress-strain responses of the developed fly ash-based SHGCs are presented in Figures 5-7 to 5-12. As can be seen, all fly ash-based SHGCs exhibited clear PSH behavior with moderate to high ultimate tensile strength in the range of 3.9 MPa to 5.2 MPa and low to very high tensile strain capacity in the range of 1.0% to 4.3%, depending on their W/GP solids, sand size and sand content. The uniaxial tension test results including the measured ultimate tensile strength and tensile strain capacity, along with the estimated tensile first-crack strength are presented in Table 5-3. As can be seen, the ultimate tensile strength of all fly ash-based SHGCs developed in this study was higher than that of the fly ash-based SHGCs developed by Ohno and Li (2014) which ranged from 2.9−3.4 MPa. As mentioned in Chapter 4, this could be attributed to the fiber-matrix interfacial properties (Lee et al., 2012). In other words, the fiber-matrix bond strength in all fly ash-based SHGCs developed in this study could be higher compared to that of the composites developed by Ohno and Li (2014), leading to their higher fiber-bridging strength (Lee et al., 2012). The difference in fiber-matrix bond strength could be due to different oil-coating percentage of the PVA fibers, different mix proportions e.g. sand size, sand content, and type of fly ash) and concentration of the activators used in the two studies. The microscale investigation of fiber-matrix interface properties and mechanisms in fly ash-based SHGCs are investigated in Chapter 7.

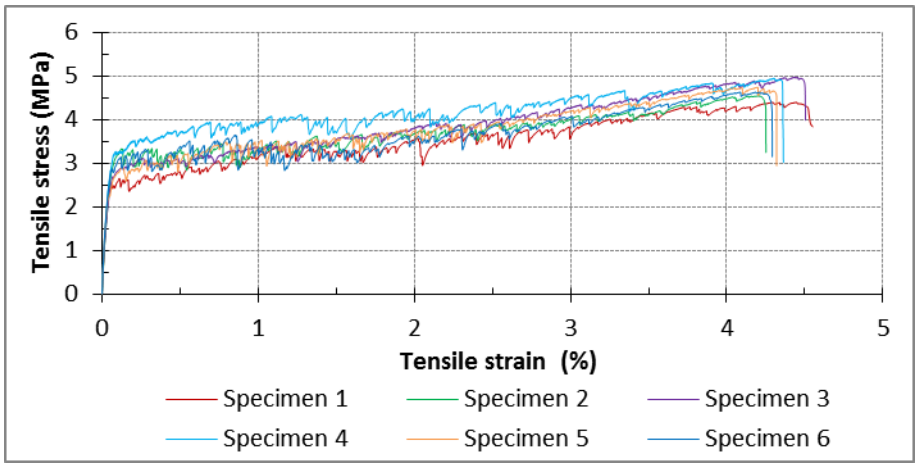

Figure 5-7: Tensile stress-strain responses of SHGC20

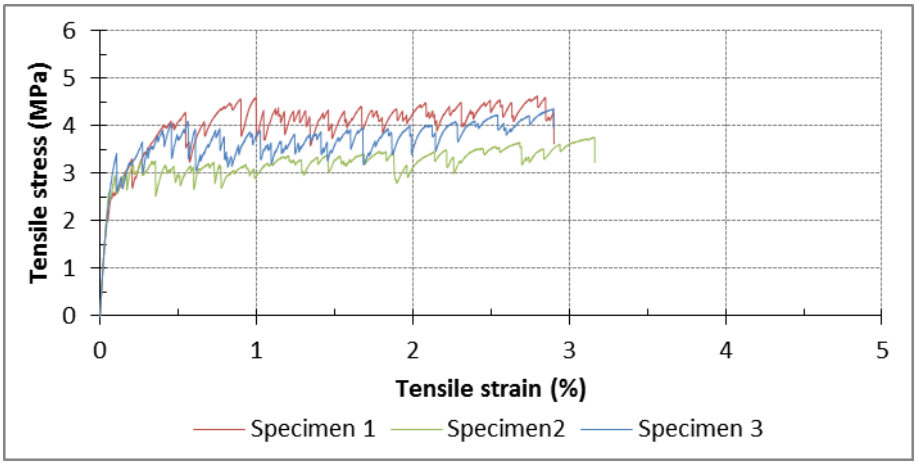

Figure 5-8: Tensile stress-strain responses of SHGC23

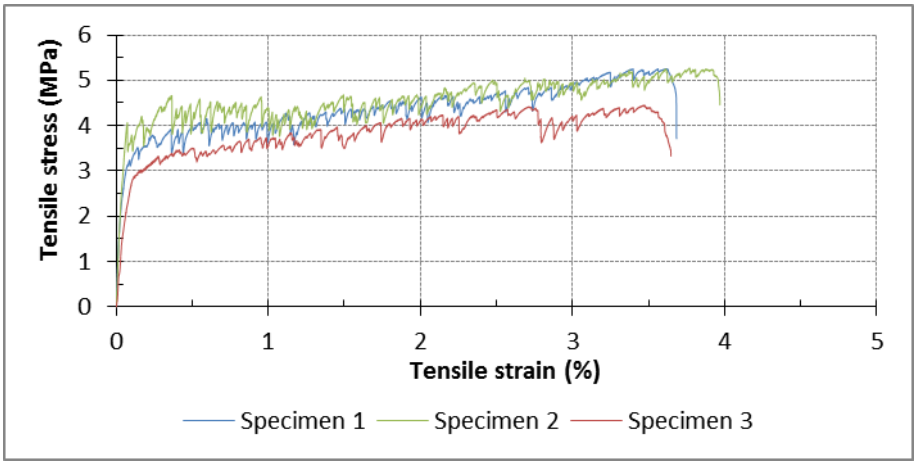

Figure 5-9: Tensile stress-strain responses of SHGC23-FS-30

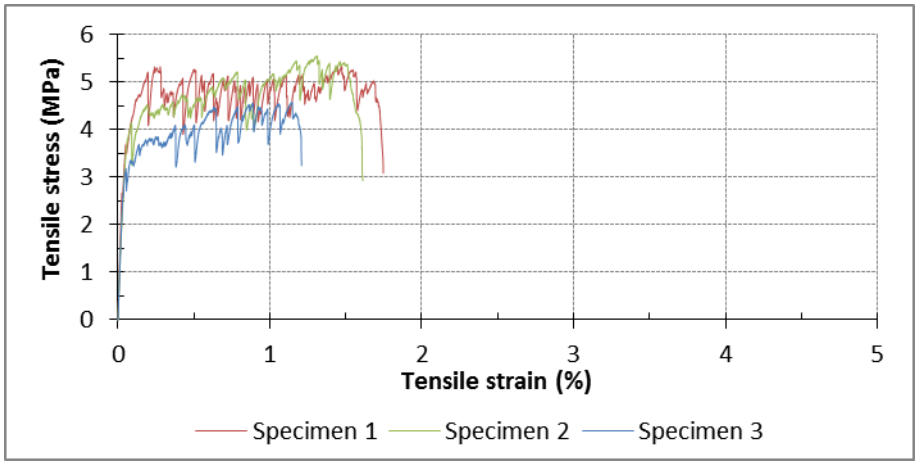

Figure 5-10: Tensile stress-strain responses of SHGC23-FS-60

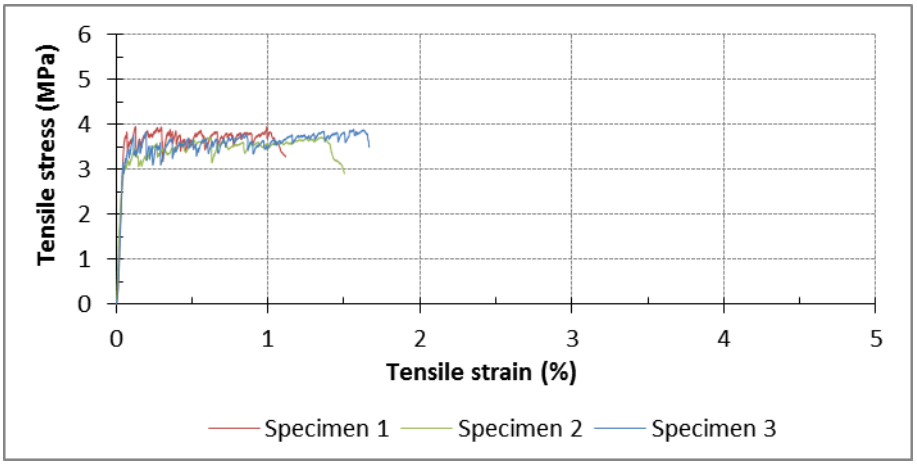

Figure 5-11: Tensile stress-strain responses of SHGC23-CS-30

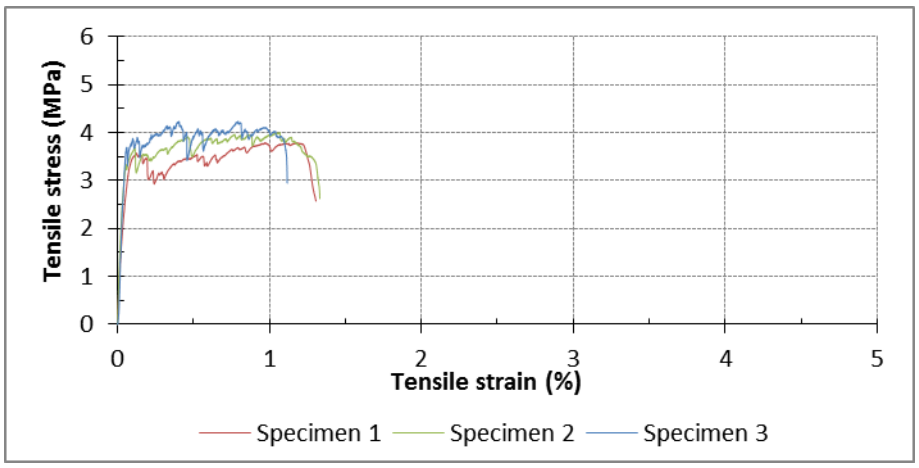

Figure 5-12: Tensile stress-strain responses of SHGC23-CS-60

Table 5-3: Uniaxial tension test results

Mix designation	First-crack strength, σ_{fc} (MPa)	Ultimate tensile strength, σ_{cu} (MPa)	Tensile strain capacity, ε_{cu} (%)	Stress-performance index
SHGC20	3.2 ± 0.21	4.7 ± 0.25	4.3 ± 0.14	1.5
SHGC23	2.8 ± 0.40	4.3 ± 0.45	3.0 ± 0.19	1.5
SHGC23-FS-30	3.4 ± 0.52	5.0 ± 0.47	3.6 ± 0.15	1.5
SHGC23-FS-60	3.7 ± 0.37	5.2 ± 0.51	1.3 ± 0.15	1.4
SHGC23-CS-30	3.3 ± 0.33	3.9 ± 0.12	1.3 ± 0.29	1.2
SHGC23-CS-60	3.5 ± 0.20	4.0 ± 0.23	1.0 ± 0.20	1.1

Multiple cracking pattern of each composite is presented in Figure 5-13. Table 5-4 presents the average crack spacing in each composite. As can be seen, the crack

distribution in SHGC20, SHGC23 and SHGC23-FS-30 was uniform with almost equal crack spacing in the range of 2.5−3.5 mm and enormous micro-cracks with tightly controlled crack width (i.e. saturated multiple cracking behavior) were observed, which correspond to their significantly high tensile strain capacities. However, the crack distribution in SHGC23-FS-60, SHGC23-CS-30 and SHGC23-CS-60 was not uniform and fewer visible cracks with un-even and wider crack spacing in the range of 4−11 mm were observed, which corresponds to their inferior tensile strain capacities (i.e. un-saturated multiple cracking behavior). Table 5-4 also presents the estimated loaded crack width of the coupon specimen during uniaxial tension tests, which corresponds to the crack opening at maximum bridging stress in the fiber bridging curve of the composite (Lee et al., 2012). As mentioned in Chapter 4, the average loaded crack width was estimated based on the tensile strain capacity, the average crack spacing and the number of visible cracks. According to Li et al. (2001), the actual loaded crack width should be smaller than the estimated values reported in Table 5-4, because the actual number of micro-cracks developed during loading of the coupon specimen was more than the number of visible cracks on the surface of the unloaded specimen. The effect of W/GP solids, sand size and sand content (S/FA) on the uniaxial tensile performance of the geopolymer composites are discussed below.

Table 5-4: Average crack spacing and estimated loaded crack width

Mix designation	Average crack spacing; (mm)	Estimated loaded crack width; (μm)
SHGC20	2.8 ± 0.23	119 ± 9.53
SHGC23	3.2 ± 0.46	94 ± 17
SHGC23-FS-30	2.8 ± 0.19	103 ± 3.63
SHGC23-FS-60	7.8 ± 2.0	107 ± 20.0
SHGC23-CS-30	5.3 ± 1.3	70 ± 24
SHGC23-CS-60	9.4 ± 1.6	93 ± 8.3

According to Table 5-3, the increase in W/GP solids from 0.20 to 0.23 resulted in 13% reduction in the first-crack strength of SHGC23 than that of SHGC20, which corresponds to the lower fracture toughness of SHGC23 matrix, as shown in Table 5-2 (Li et al., 2001). In addition, the increase in W/GP solids from 0.20 to 0.23 also resulted in 9% reduction in the ultimate tensile strength of SHGC23 than that of SHGC20, which could be due to

the interfacial properties (Lee et al., 2012). In other words, the fiber-matrix bond strength of SHGC23 is likely to be lower than that of SHGC20, resulting in the lower fiber bridging strength of the composite (Lee et al., 2012). The effects of W/GP solids on the microscale of fiber-matrix interface properties and mechanisms in fly ash-based SHGCs are investigated in Chapter 7.

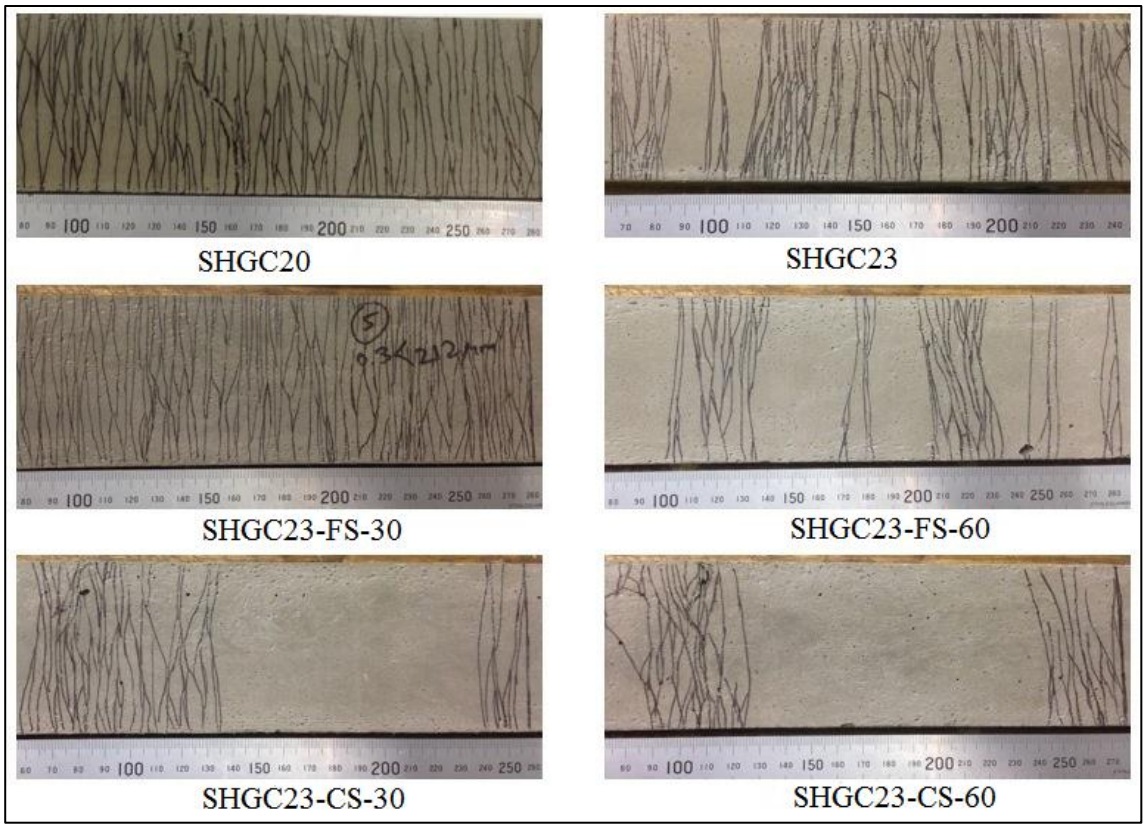

Figure 5-13: Typical multiple cracking pattern of each composite

As can be seen in Table 5-3, the increase in W/GP solids from 0.20 to 0.23, resulted in 30% reduction in the tensile strain capacity of SHGC23 than that of SHGC20. The reasons for different tensile strain capacities of SHGC20 and SHGC23 could be explained in terms of the two PSH performance indices, namely stress-performance index (σ_0/σ_{fc}) and energy-performance index (J_b'/J_{tip}), proposed by Kanda and Li (2006). It should be noted that the ultimate tensile strength (σ_{cu}) coincides with σ_0 (maximum fiber bridging stress) of the composite when the composite exhibits the PSH behavior (Li et al., 1995). The stress-performance index of SHGC23 and SHGC20 reported in Table 5-3 is comparable. With regards to the energy-performance index, as can be seen in Table 5-2,

the crack tip toughness J_{tip} of SHGC23 matrix was 31% lower than that of SHGC20 matrix. On the other hand, the lower ultimate tensile strength and loaded crack width of SHGC23 (as reported in Tables 5-3 and 5-4, respectively) suggest that the complementary energy J_b' of SHGC23 could be considerably lower than that of SHGC20 (Lee et al., 2012). It can be thereby inferred that the energy-performance index of SHGC23 could be lower than that of SHGC20, due to its considerably lower J_b' in spite of its lower J_{tip}. Therefore, as expected from micromechanics-based design theory of SHCC, while the stress-performance index of SHGC23 is comparable to that of SHGC20, the lower energy-performance index of SHGC23 results in its lower tensile strain capacity.

As can be seen in Table 5-3, the reduction in the tensile strain capacity of SHGC23 was quite considerable compared to that of SHGC20. Apart from the lower energy-performance index of SHGC23, the lower tensile strain capacity of SHGC23 could also be attributed to bundling of fibers, as some fiber bundles were observed in SHGC23 mixture during mixing. According to Li et al. (1990), fiber bundling is not desirable as it decreases the effectiveness of the fiber reinforcement and weak spots may be introduced by the fiber bundles, which adversely affect the composite tensile ductility. It should be noted that fiber-matrix interface properties should be determined to be able to quantify the complementary energy of each composite. As mentioned in Chapter 4, a detailed analysis of fly ash-based SHGCs is undertaken in Chapters 7 and 8 to quantify fiber-matrix interface properties (using single-fiber pullout tests) and J_b' (using a micromechanics-based model).

With regards to the effect of sand content on the uniaxial tensile performance of the geopolymer composite, as can be seen in Table 5-3, the ultimate tensile strength of SHGC23-FS-30 and SHGC23-FS-60 incorporating fine sand (FS) was 16% and 21%, respectively higher than that of SHGC23 with no sand. While the tensile strain capacity of SHGC-FS-30 (with S/FA of 0.3) was 20% higher than that of SHGC23 with no sand, the tensile strain capacity of SHGC23-FS-60 (with S/FA of 0.6) was 57% lower than that of SHGC23 with no sand. Similar result was reported by Ahmed and Maalej (2009) regarding the adverse effect of the excessive addition of fine sand on the PSH behavior of typical SHCCs. The undesirable effect of the excessive use of fine sand on the strain hardening behavior of the geopolymer composites could also be explained in terms of the two PSH performance indices of σ_0/σ_{fc} and J_b'/J_{tip}. The higher ultimate tensile strength

and loaded crack width of SHGC23-FS-60 (as reported in Tables 5-3 and 5-4, respectively) imply that complementary energy J_b' of the composite could be higher than that of SHGC23 with no sand. On the other hand, as reported in Table 5-2, the J_{tip} of SHGC23-FS-60 was significantly (143%) higher than that of SHGC23 with no sand, which is not desirable, as it results in a significant reduction in the energy performance index (J_b'/J_{tip}) of the composite. Therefore, it can be inferred that the energy-performance index of SHGC23-FS-60 could be significantly lower than that of SHGC23 with no sand, resulted in the inferior tensile strain capacity of the composite.

The second reason is associated with the stress-performance index of the composites. As can be seen in Table 5-3, the tensile first-crack strength of SHGC23-FS-60 was 32% higher than that of SHGC23 with no sand, which corresponds to the significant increase in the crack tip toughness of SHGC23-FS-60 matrix, as reported in Table 5-2. The increase in the first-crack strength of the composite is also not desirable, as it results in a reduction in the stress-performance index (σ_0/σ_{fc}) of the composite. As can be seen in Table 5-3, the stress-performance index of SHGC23-FS-60 was lower than that of SHGC23 with no sand. This is another reason for the significantly lower tensile strain capacity of SHGC23-FS-60 than that of SHGC23 with no sand. These results are in good agreement with those published by Li and Maalej (1996) regarding the "conventional" cement-based composites. It is well established that excessive use of sand in a cement-based matrix results in a matrix with high fracture toughness, which in turn increases the first-crack strength of the composite compared to the maximum bridging stress of the fibers and violates the conditions for saturated PSH behavior (Li and Maalej, 1996).

With regards to the effect of sand size on the uniaxial tensile performance of the composite, a similar trend was observed in the geopolymer composites containing coarse sand (CS). As can be seen in Table 5-3, the ultimate tensile strength of SHGC23-CS-30 and SHGC23-CS-60 incorporating coarse sand (CS) was 9% and 7%, respectively lower than that of SHGC23 with no sand. In addition, the ultimate tensile strength of SHGC23-CS-30 and SHGC23-CS-60 incorporating coarse sand was 22% and 23%, respectively lower than that of the corresponding composites containing fine sand (SHGC23-FS-30 and SHGC23-FS-60). This could be attributed to the interfacial properties. In other words, in the composites containing coarse sand (CS) the interactions between fiber-sand particle and fiber-pore adversely affected the fiber-matrix interfacial bond strength of the

composite, which resulted in lower fiber bridging strength in these composites (Akkaya et al., 2000).

In addition as can be seen in Tables 5-2 and 5-3, the addition of coarse sand (CS) to the geopolymer matrix also resulted in an increase in the crack tip toughness and first-crack strength of SHGC23-CS-30 and SHGC23-CS-60 compared to those of SHGC23 with no sand, which led to significant decrease in the tensile strain capacity of these composites, not only compared to that of SHGC23 with no sand, but also compared to that of the corresponding composites containing fine sand (SHGC23-FS-30 and SHGC23-FS-60). The reduction in the tensile strain capacity with the increase in the size of sand particles could be attributed to the fact that in fiber-reinforced cement-based materials the introduction of aggregates with particle size exceeding the average fiber spacing results in balling and greater interaction of fibers in the paste between the large aggregate particles, and as the maximum size of the aggregate increases this effect becomes more pronounced (De Koker and van Zijl, 2004). Hence, the greater the size of aggregate particles, the more clumping and interaction of fibers occurs, which makes it more difficult to achieve a uniform fiber dispersion (Sahmaran et al., 2009; Nagi and Hsu, 1992). The tensile behavior of the composite closely depends on the fiber distribution, flaw size distribution along with interfacial bond properties (Li and Wang, 2006). As mentioned earlier, non-uniform fiber dispersion in the form of fiber bundles and clumping decreases the efficiency of fiber reinforcement and introduces weak spots along certain fiber bundles, as the fiber bundles usually have low resistance to splitting, lower performance of the composite is thereby resulted (Li et al., 1990).

In summary, it can be concluded that the excessive use of fine sand and the use of coarse sand in the geopolymer matrix resulted in considerable increase in the crack tip toughness and first-crack strength of the geopolymer composite. Consequently, the two PSH performance indices (σ_0 / σ_{fc} and J_b' / J_{tip}) of the composite decreased significantly, which hindered the saturated PSH behavior in the geopolymer composite. These results are in good agreement with those published by other researchers regarding the "conventional" SHCCs, which indicate that the sand content must be limited in the matrix to maintain tensile ductility of the composite (Li et al., 1995; Li et al., 2001).

5.4.4 Compressive strength and elastic modulus of geopolymer composite

The compressive strength (f'_c) and estimated elastic modulus (E_c) of each geopolymer composite are presented in Table 5-5. Following Ahmed et al. (2007), E_c was estimated from the following equation:

$$E_c = E_m V_m + \eta_l \eta_\theta (E_f V_f) \quad (5.2)$$

where V_m ($=1-V_f$) and V_f are the volume fraction of matrix and fiber, respectively. E_m and E_f are elastic modulus of the matrix and fiber, respectively. η_l is the length efficiency factor for short fibers and η_θ is the orientation factor for randomly oriented short fibers. In this study, the values of 0.5 and 0.55 are chosen for η_l and η_θ, respectively (Nathan et al., 1977; Soroushian and Lee, 1990).

Table 5-5: Compressive strength and elastic modulus of geopolymer composites

Mix designation	Compressive strength, f'_c, (MPa)	Elastic modulus, E_c, (GPa)[a]
SHGC20	63.7±2.7	8.6
SHGC23	52.6±1.6	4.8
SHGC23-FS-30	56.8±1.9	5.7
SHGC23-FS-60	60.7±2.1	7.7
SHGC23-CS-30	51.2±1.5	6.5
SHGC23-CS-60	49.2±1.1	7.4

[a] Following Equation (5.2) (Ahmed et al., 2007).

According to Tables 5-5 and 5-3, the compressive strength of geopolymer composite in all mixtures was higher than that of the corresponding geopolymer matrix, due to the addition of the PVA fibers (2% v/v). In addition as mentioned in Chapter 4, the crack propagation in all composite cube specimens was restrained, thanks to the bridging mechanism of the PVA fibers; thereby, the composite specimens kept their original shape after peak load, leading to a ductile failure mode. It should be noted that although the concentration of the activator combination was limited to 8.0 M to consider safety concerns; as can be seen in Table 5-5 the compressive strength of all fly ash-based SHGCs developed in this study was significantly higher than that of the fly ash-based SHGCs developed by Ohno and Li (2014), which ranged from 17.4−27.6 MPa. This is mainly

attributed to the longer heat curing period (i.e. 24 hours at 60° C) applied in this study compared to the shorter heat curing period (maximum of 8 hours at 60° C) applied in Ohno and Li (2014)'s study.

As mentioned in Section 5.4.2, the compressive strength of geopolymer mortar matrices, regardless of the sand size and sand content, was higher than that of the geopolymer matrix with no sand (i.e. the geopolymer paste). In other words, when fibers were not present the addition of sand, regardless of the sand size and the sand content, increased the compressive strength of the geopolymer paste. However, in the presence of fibers an opposite trend was observed when coarse sand (CS) was used. In other words, as reported in Table 5-5, the compressive strength of SHGC23-CS-30 and SHGC23-CS-60 was slightly lower than that of SHGC23 with no sand. This could be attributed to the un-even dispersion of fibers and the increase in the size and number of fiber-free areas in the geopolymer composites with coarse sand, which in turn increased the total porosity and adversely affected the compressive strength of these composites (Akkaya et al., 2000). As can be seen in Table 5-5, the compressive strength of SHGC23-FS-30 and SHGC23-FS-60 was marginally higher than that of SHGC23 with no sand. This could be attributed to the relatively lower porosity, due to the better dispersion of the fibers in these composites compared to the geopolymer composites containing coarse sand (CS). These results are in good agreement with those published by other researchers regarding the effect of the addition of sand on the strength of the plain cement-based paste and the fiber-reinforced cement-based composites (Akkaya et al., 2000).

Among geopolymer composites made with sand, SHGC23-FS-60 exhibited the highest f'_c and E_c of 60.7 MPa and 7.7 GPa, respectively, as it contained the highest amount of fine sand (FS). The fact that SHGC20 without sand exhibited higher f'_c (63.7 MPa) and E_c (8.5 GPa) compared to that of SHGC23-FS-60 (with S/FA of 0.6) is attributed to their different W/GP solids ratio (0.20 versus 0.23). According to Table 5-5, in all mixtures the estimated E_c was comparable to the corresponding indirectly derived E_m, using ECM. Therefore, similar to the E_m, the E_c of SHGC23-FS-30 19% higher than that of SHGC23 with no sand. This is a considerable increase in the elastic modulus of the geopolymer composite, considering that only a small amount of fine sand (S/FA=0.3) was used. Doubling the S/FA in SHGC23-FS-60 resulted in 35% increase in its composite elastic modulus compared to that of SHGC23-FS-30. However, the tensile strain capacity of

SHGC23-FS-60 was significantly (64%) lower than that of SHGC23-FS-30. This pattern implies that for the fly ash-based SHGCs developed in this study the trade-off between elastic modulus and tensile strain capacity may be such that it is of little advantage to increase the sand content by a large amount compared to that used in SHGC23-FS-30. Similar trend was reported by other researchers regarding effect of the sand content on the elastic modulus and strain capacity of the "conventional" SHCCs (Li et al., 1995).

5.5 Conclusions

This chapter presents the results of an experimental research on the effect matrix properties on the composite performance of the fly ash-based SHGC developed in Chapter 4. Dependence of the matrix properties such as compressive strength, elastic modulus and fracture toughness on its mixture compositions governed by water to geopolymer solids ratio, sand size and sand content (sand to fly ash ratio) were experimentally evaluated. Special focus was placed on the effect of these matrix properties on the uniaxial tensile performance of the geopolymer composite. The results indicated that the use of lower water to geopolymer solids ratio and the addition of sand to the geopolymer matrix significantly enhanced the elastic modulus of the geopolymer matrix and composite in all cases. However, the excessive use of fine sand and the use of coarse sand in the geopolymer matrix resulted in the considerable increase of the matrix fracture toughness and the first-crack strength of the geopolymer composite. Consequently, the two PSH performance indices (σ_0 / σ_{fc} and J_b' / J_{tip}) of the geopolymer composite decreased significantly, which hindered the saturated PSH behavior of the geopolymer composite. Only the geopolymer matrices with suitable fracture toughness as defined by micromechanical principles maintained the desirable tensile ductility of the geopolymer composite. These findings are consistent with micromechanics-based design theory of typical SHCCs, which indicates that the sand content must be limited in the matrix to maintain tensile ductility of the composite.

As a result, a fly ash-based SHGC with appropriate amount of fine sand (i.e. the SHGC23-FS-30 mixture) was developed in this study, which exhibited higher elastic modulus, while maintaining the desirable PSH behavior with ultimate tensile strength and tensile strain capacity of up to 5.0 MPa and 3.6% on average, respectively. The pattern found in the experimental results indicates that for the fly ash-based SHGCs developed in this

study the trade-off between elastic modulus and tensile ductility may be such that it is of little advantage to increase the sand content by a large amount compared to that used in the SHGC23-FS-30 mixture. Therefore, the SHGC23-FS-30 mixture is used as the benchmark in the next chapter, which investigates the effects of three types of lightweight aggregates as complete replacement of micro-silica sand, on the thermal and mechanical properties of the geopolymer composite, with the aim of developing lightweight fly ash-based SHGCs.

5.6 References

AHMED, S. & MAALEJ, M. 2009. Tensile strain hardening behaviour of hybrid steel-polyethylene fibre reinforced cementitious composites. *Construction and Building Materials,* 23, 96-106.

AHMED, S. F., MAALEJ, M. & PARAMASIVAM, P. 2007. Analytical model for tensile strain hardening and multiple cracking behavior of hybrid fiber-engineered cementitious composites. *Journal of materials in civil engineering,* 19, 527-539.

AKKAYA, Y., PELED, A., PICKA, J. D. & SHAH, S. P. 2000. Effect of sand addition on properties of fiber-reinforced cement composites. *Materials Journal,* 97, 393-400.

BARBOSA, V. F., MACKENZIE, K. J. & THAUMATURGO, C. 2000. Synthesis and characterisation of materials based on inorganic polymers of alumina and silica: sodium polysialate polymers. *International Journal of Inorganic Materials,* 2, 309-317.

DE KOKER, D. & VAN ZIJL, G. Extrusion of engineered cement-based composite material. Proceedings of the 6th RILEM Symposium on Fiber-Reinforced Concretes (FRC), 2004. Citeseer, 20-22.

HARDJITO, D., WALLAH, S. E., SUMAJOUW, D. M. & RANGAN, B. V. 2004. On the development of fly ash-based geopolymer concrete. *ACI Materials Journal-American Concrete Institute,* 101, 467-472.

HASHIN, Z. 1962. The elastic moduli of heterogeneous materials. *Journal of Applied Mechanics,* 29, 143-150.

KANDA, T. & LI, V. C. 1999. New micromechanics design theory for pseudostrain hardening cementitious composite. *Journal of engineering mechanics,* 125, 373-381.

KANDA, T. & LI, V. C. 2006. Practical design criteria for saturated pseudo strain hardening behavior in ECC. *Journal of advanced concrete technology,* 4, 59-72.

KARIHALOO, B. & NALLATHAMBI, P. 1990. Effective crack model for the determination of fracture toughness (KICe) of concrete. *Engineering Fracture Mechanics,* 35, 637-645.

LEE, B. Y., CHO, C.-G., LIM, H.-J., SONG, J.-K., YANG, K.-H. & LI, V. C. 2012. Strain hardening fiber reinforced alkali-activated mortar–a feasibility study. *Construction and Building Materials,* 37, 15-20.

LI, V. C. & MAALEJ, M. 1996. Toughening in cement based composites. Part II: Fiber reinforced cementitious composites. *Cement and Concrete Composites,* 18, 239-249.

LI, V. C., MISHRA, D. K. & WU, H.-C. 1995. Matrix design for pseudo-strain-hardening fibre reinforced cementitious composites. *Materials and Structures,* 28, 586-595.

LI, V. C. & WANG, S. 2006. Microstructure variability and macroscopic composite properties of high performance fiber reinforced cementitious composites. *Probabilistic engineering mechanics,* 21, 201-206.

LI, V. C., WANG, S. & WU, C. 2001. Tensile strain-hardening behavior of polyvinyl alcohol engineered cementitious composite (PVA-ECC). *ACI materials Journal,* 98.

LI, V. C., WANG, Y. & BACKER, S. 1990. Effect of inclining angle, bundling and surface treatment on synthetic fibre pull-out from a cement matrix. *Composites,* 21, 132-140.

LIDE, D. R. 2004. *CRC handbook of chemistry and physics,* CRC press.

NAGI, M. & HSU, J.-W. 1992. Optimization of the use of lightweight aggregates in carbon fiber reinforced cement. *Materials Journal,* 89, 267-276.

NATHAN, G., PARAMASIVAM, P. & LEE, S. 1977. Tensile behavior of fiber reinforced cement paste. *JOURNAL OF FERROCEMENT-BANGKOK,* 7, 59-79.

NEMATOLLAHI, B. & SANJAYAN, J. 2014. Effect of different superplasticizers and activator combinations on workability and strength of fly ash based geopolymer. *Materials & Design,* 57, 667-672.

OHNO, M. & LI, V. C. 2014. A feasibility study of strain hardening fiber reinforced fly ash-based geopolymer composites. *Construction and Building Materials,* 57, 163-168.

PAN, Z., SANJAYAN, J. G. & RANGAN, B. V. 2011. Fracture properties of geopolymer paste and concrete. *Magazine of concrete research,* 63, 763-771.

ŞAHMARAN, M., LACHEMI, M., HOSSAIN, K. M., RANADE, R. & LI, V. C. 2009. Influence of aggregate type and size on ductility and mechanical properties of engineered cementitious composites. *ACI Materials Journal,* 106, 308-316.

SOROUSHIAN, P. & LEE, C.-D. 1990. Distribution and orientation of fibers in steel fiber reinforced concrete. *Materials Journal,* 87, 433-439.

TEMUUJIN, J., VAN RIESSEN, A. & MACKENZIE, K. 2010. Preparation and characterisation of fly ash based geopolymer mortars. *Construction and Building Materials,* 24, 1906-1910.

YANG, E.-H., WANG, S., YANG, Y. & LI, V. C. 2008. Fiber-bridging constitutive law of engineered cementitious composites. *Journal of advanced concrete technology,* 6, 181-193.

CHAPTER 6

THERMAL AND MECHANICAL PROPERTIES OF LIGHTWEIGHT FLY ASH-BASED SHGCS

Note: This chapter is based on the paper "*Thermal and Mechanical Properties of Sustainable Lightweight Strain Hardening Geopolymer Composites*", by **Nematollahi, B.**, Ranade, R., Sanjayan, J., and Ramakrishnan, S., published in ***Archives of Civil and Mechanical Engineering***, 2017, 17, 55-64.

6.1 Introduction

The fly ash-based SHGC with appropriate amount of normal weight micro-silica sand (the SHGC23-FS-30 mixture) developed in the previous chapter. SHGC23-FS-30 demonstrated comparable mechanical properties to typical SHCCs with compressive strength, ultimate tensile strength and tensile strain capacity of up to 56.8 MPa, 5.0 MPa and 3.6% on average, respectively. As a follow up investigation, this chapter is aimed to evaluate the effects of three types of lightweight aggregates as complete replacement of micro-silica sand on the thermal and mechanical properties of SHGC23-FS-30.

In the construction industry, the use of lightweight concrete (with a density less than 1850 kg/m^3 (ACI 213R, 2014)) instead of normal weight concrete (2400 kg/m^3) is favorable as it offers several advantages such as reduction in dead loads and section dimensions, enhanced thermal insulation, savings in steel reinforcement, ease of handling and transportation, and lower overall cost (Chandra and Berntsson, 2002). However, one of the major disadvantages of lightweight concrete is greater brittleness and lower fracture toughness compared to normal weight concrete of similar compressive strength (Chandra and Berntsson, 2002; Wang and Li, 2003). For instance, Hengst and Tressler (1983) reported that the fracture energy of lightweight foam concrete was significantly lower than that of normal weight concrete. According to Zhang and Gjorv (1991), the tensile to compressive strength ratio of high strength lightweight concrete was lower than that of high strength normal weight concrete. This is attributed to the use of lightweight aggregates, which are usually weaker than the cement matrix, which makes them susceptible to cracking (Wang and Li, 2003).

In past studies, different fibers have been introduced in the mixture design of lightweight concrete to enhance its tensile and flexural strengths, and the flexural toughness. However, these fiber-reinforced lightweight concretes, similar to conventional fiber-reinforced concrete, exhibit tension softening behavior (Gao et al., 1997; Park et al., 1999). Thus, although the lower density of lightweight concrete promotes its application as an alternative to normal weight concrete, the low tensile ductility and fracture toughness hinder the widespread structural applications of lightweight concrete in the construction industry.

The average density, compressive and tensile strengths, and tensile strain capacity of typical PVA-SHCC mix 45 (M45) are about 2077 kg/m^3, 52.6 MPa, 6 MPa and 2.7%, respectively, at the age of 28 days (Yang et al., 2007). Thus, the tensile ductility of typical SHCC M45 is several hundred times the ductility of conventional concrete in tension. Although the density of typical SHCC M45 is lower than that of normal weight concrete (2400 kg/m^3), it cannot be considered lightweight according to the definition of ACI Committee 213, which requires the density of concrete at 28 days to be less than 1850 kg/m^3 to qualify as lightweight concrete (ACI 213R, 2014).

Wang and Li (2003) attempted to develop lightweight SHCCs using four lightweight fillers including expanded perlite, hollow glass bubbles, polymeric microform, and air bubbles produced by air entrainment admixture. In that study, it was found that hollow glass bubbles were effective for lowering the density and improving the fiber dispersion and mechanical properties of SHCC (Wang and Li, 2003). The average density, compressive and tensile strengths, and tensile strain capacity of 1450 kg/m^3, 41.7 MPa, 4.31 MPa and 4.24%, respectively, were reported for the lightweight SHCC made by hollow glass bubbles with a mean size of 30 μm (Wang and Li, 2003). However, such lightweight SHCC uses high amount of cement and high temperature-processed hollow glass bubbles (Wang and Li, 2003), which results in high embodied energy and carbon footprint (Huang et al., 2013), lowering the environmental sustainability of the composite. Therefore, it is necessary to develop green and sustainable lightweight SHCCs with significantly lower environmental footprints.

Among the ingredients of SHCC M45, cement is a major contributor to the environmental impact accounting for 48.2% and 81.6% of total embodied energy and CO_2 emissions,

respectively (Huang et al., 2012). Several studies have focused on replacing cement in SHCC M45 with industrial wastes. For instance, normal weight green SHCCs have been developed by partial replacement of cement with fly ash (Yang et al., 2007), slag (Kim et al., 2007) and IOTs (Huang et al., 2012).

Recently, Huang et al. (2013) attempted to achieve the properties of lightweight and material greenness in SHCC, simultaneously. In that study, green lightweight SHCCs (GLSHCCs) were produced using IOTs, fly ash, and fly ash cenosphere as aggregates, mineral admixture, and lightweight filler, respectively (Huang et al., 2013). The density, compressive and tensile strengths, and tensile strain capacity in the range of 1649–1820 kg/m^3, 25.0–47.6 MPa, 4.8–5.9 MPa and 3.3–4.3%, respectively, were reported for the developed GLSHCCs at the age of 28 days, depending on the contents of IOTs, fly ash, and fly ash cenosphere (Huang et al., 2013). This chapter is aimed to develop lightweight SHGC, which is even more environmentally sustainable than the previously developed GLSHCCs, as the OPC binder in SHCC is completely replaced by fly ash-based geopolymer binder in SHGC.

According to the U.S. Department of Energy (2010), a major portion of the total energy consumption in buildings is associated with space heating and cooling. This energy demand can be significantly reduced by using construction materials with lower thermal conductivity (which means better insulating). Thus, using SHGCs with lower thermal conductivity in a building will be highly sustainable not only in terms of material greenness, but will also reduce the energy needs over the use phase of the building.

This research evaluates the mechanical and thermal properties of green lightweight SHGCs incorporating fly ash-based geopolymer as complete replacement of OPC and three types of lightweight aggregates including expanded perlite, microscopic hollow ceramic spheres and expanded recycled glass as complete replacement of micro-silica sand, to achieve the following three objectives: (1) to significantly reduce the environmental footprint, (2) to decrease the density of the composite, and (3) to reduce the thermal conductivity of the composite. A series of experiments including workability of the fresh matrix, density, compression, thermal conductivity and uniaxial tension tests were conducted as detailed in the following sections to characterize the thermal and mechanical properties of the developed green lightweight SHGCs.

6.2 Materials and Mix Proportions

The same low calcium (Class F) fly ash supplied from Gladstone power station in Queensland, Australia was used in this research. The chemical composition and LOI of the fly ash are presented in Table 3-1. As concluded in Chapter 4, the use of Na-based activator combination composed of 8.0 M NaOH solution (28.6% w/w) and Na_2SiO_3 solution (71.4% w/w) with a SiO_2 to Na_2O ratio of 2.0 is highly beneficial in the production of fly ash-based SHGCs. Thus, the same N-based activator combination was used in this research. The physical and chemical properties of NaOH and Na_2SiO_3 solutions and the procedure for preparation of the Na-based activator combination are given in Chapter 4. The same PVA fibers with a surface oil coating of 1.2% by weight, supplied by Kuraray Co. Ltd., Japan were used in this study. Properties of the PVA fibers are presented in Table 4-2. The same washed and sieve-graded micro-silica sands (denoted as FS in Chapter 5) with an average size of 165 μm, maximum size of 212 μm, and average specific gravity of 2.6 was used in this research. It is supplied by TGS Industrial Sand Ltd., Australia.

Reducing the composite density without sacrificing compressive and tensile strengths of the composite is one of the challenges of developing lightweight composites, since the weak lightweight aggregates act similar to flaws in the matrix (Wang and Li, 2003). From fracture mechanics, the largest existing flaw size determines the tensile strength of a brittle matrix such as geopolymer. However, the compressive strength is governed by a group of relatively large flaws (Wang and Li, 2003). Thus, in order to reduce the detrimental effect of using lightweight aggregates on the compressive and tensile strengths, Wang and Li (2003) recommended that the particle size of the lightweight aggregates should be much smaller than the most common pre-existing flaws (i.e. entrapped air bubbles with sizes more than 1 mm) in the composite. On the other hand, using lightweight aggregates with small particle size is also beneficial with respect to the workability of the composite, since aggregates with large particle size have negative impact on fiber dispersion (Wang and Li, 2003). Therefore, three types of small-size lightweight aggregates, as complete replacement of micro-silica sand, with the same volume percentage were used in this study.

(1) Lightweight expanded glass aggregates with granular sizes in the range of 40–125 μm and specific gravity of 1.4 was supplied by Dennert Poraver GmbH, Germany. The expanded glass aggregates are industrially manufactured from post-consumer recycled glass. Table 6-1 presents the chemical analysis of expanded recycled glass as reported by the manufacturer and determined by atomic emission spectrometric (AES).

(2) Grade SL125 is a fine grade white hollow ceramic microspheres, supplied by Envirospheres Pty Ltd., Australia, which has granular sizes in the range of 12–125 μm. The average particle size and specific gravity of Grade SL125 microspheres are about 80 μm and 0.85, respectively. The typical chemical properties of hollow ceramic microspheres, as reported by the manufacturer, are also given in Table 6-1.

(3) Grade AP20 expanded perlite is an ultra-lightweight and inert non crystalline siliceous volcanic mineral aggregate, with average particle size and specific gravity of 43 μm and 0.293, respectively (supplied by Ausperl Pty Ltd., Australia). In Grade AP20 expanded perlite, 90% of particles are smaller than 87 μm.

Table 6-1: Chemical composition of expanded recycled glass and hollow ceramic microspheres

Chemical	Component (wt. %)	
	Expanded recycled glass[2]	Hollow ceramic microspheres[2]
Al_2O_3	2.5	30–36
SiO_2	71.7	55–65
CaO	8.9	---
Fe_2O_3	0.4	1–2
K_2O	0.8	---
MgO	2.1	---
Na_2O	13.2	---
P_2O_5	---	---
TiO_2	0.1	0.5–1.0
MnO	0.0	---
SO_3	0.1	---
LOI[1]	0.3	---

[1]Loss on ignition.

[2] The values are reported by the manufacturer.

Table 6-2 presents the four green lightweight fly ash-based SHGC mix proportions investigated in this study. In all mixtures, the weight ratio of activator solution to fly ash was kept constant at 0.45, and volume fraction of the PVA fibers was fixed at 2%. It should be noted that the SHGC-S mix shown in Table 6-2 is the same as SHGC23-FS-30 mixture used in Chapter 5, which was used as the benchmark in this research. In the mixture SHGC-S, the weight ratio of micro-silica sand to fly ash was selected as 0.30. This dosage has been identified in Chapter 5 as the most suitable to promote optimum rheology and desirable mechanical properties (in particular uniaxial tensile performance) in fly ash-based SHGCs. In the other three mixtures, the weight ratios of lightweight aggregates to fly ash were calculated to maintain the same volume percentage as that of the micro-silica sand in the mixture SHGC-S.

Table 6-2: Mix proportions of green lightweight fly ash-based SHGCs

Mix ID	Fly ash	Act.[1]	Aggregates				PVA fiber
			Silica sand	Expanded glass	Ceramic microsphere	Expanded perlite	
SHGC-S[2]	1.0	0.45	0.30	---	---	---	0.02
SHGC-G	1.0	0.45	---	0.16	---	---	0.02
SHGC-M	1.0	0.45	---	---	0.10	---	0.02
SHGC-P	1.0	0.45	---	---	---	0.03	0.02

Note: All numbers are mass ratios of fly ash weight except fiber content (volume fraction).

[1] The Na-based activator combination.

[2]The same as SHGC23-FS-30 mixture used in Chapter 4, which was used as the benchmark in this research.

6.3 Mixing, Curing and Testing of Specimens

All mixtures were prepared in a 3 liter Hobart mixer. To prepare the fly ash-based geopolymer matrix, fly ash and aggregates were dry mixed for about 1 min at low speed. Then, the alkaline solution was gradually added and the mixing was continued for about 4 min. After the matrix ingredients were thoroughly mixed to achieve the desired fresh state, the flowability of fresh geopolymer matrix (before addition of the fibers) was

measured to ensure that the flowability was within the desired range for achieving good fiber dispersion. Finally, the PVA fibers (2% volume fraction) were gradually added to ensure uniform fiber dispersion. The whole mixing procedure for each mix generally took 15 min. The fresh geopolymer matrix and composite were cast into different molds and compacted using a vibrating table.

Heat curing was adopted in this research, based on the results in Chapter 4 and 5, which indicated that the heat curing enhances both strength and ductility properties of the fly ash-based SHGCs compared to fly ash-based SHGCs developed by Ohno and Li (2014). The procedure for heat curing is given in Chapter 4.

To determine flowability of fresh geopolymer matrix, mini slump test also known as spread-flow test was conducted. Details of the mini-slump test are given in Section 4.5 of Chapter 4. Compressive strength and hardened density of composite in each mixture were measured. The procedures for compression and density tests are given in Section 4.5 of Chapter 4. Uniaxial tension tests were conducted to evaluate the behavior of the developed green lightweight fly ash-based SHGCs under direct tension. It should be noted that the gauge length used in this research was about 80 mm. Details of the uniaxial tension test are given in Section 4.5 of Chapter 4.

Thermal conductivity measurements were conducted on the same coupon specimens that were used for the uniaxial tension tests. In this regard, an un-cracked area of 75 mm × 75 mm of each coupon specimen located within the wedge grips during the uniaxial tension tests was cut for the thermal conductivity measurements. As most residential or commercial buildings are subjected to air drying, thermal conductivity measurements were undertaken under air-dry state in the laboratory environment similar to field exposure. In this regard, the cut coupon specimens were kept in the laboratory environment (23 ± 3 °C) for about a month and thermal conductivity measurements were then conducted using a TCi thermal conductivity analyzer. The TCi developed by C-Therm Technologies Ltd. is a device that measures the thermal conductivity of a small sample, by using the Modified Transient Plane Source (MTPS) method (Cha et al., 2012). The experimental setup and data processing details can be found in Cha et al. (2012). After the test, the specimens were placed in an oven at 105 ° C for 24 hours to measure the moisture content.

6.4 Results and Discussions

6.4.1 Workability and density

The fresh matrix workability of each mix is given in Table 6-3. It should be pointed out that the reported relative slump values are based on the mini-slump test without the 25 times tamping of the flow table. From visual observations, based on past experience of mixing SHCC, all geopolymer matrices exhibited adequate workability and rheology to guarantee uniform fiber dispersion. As shown in Table 6-3, SHGC-S and SHGC-G exhibited the highest and lowest matrix workability, respectively. The relatively low matrix workability of SHGC-G may be attributed to the high water absorption of expanded glass particles (Poraver Technical Specifications, 2015). The matrix workability of SHGC-G, SHGC-M and SHGC-P containing lightweight aggregates were 24%, 16% and 19% lower than that of SHGC-S containing micro-silica sand, respectively.

Table 6-3: Workability, density and compressive strength results

Mix ID	Matrix workability[1]	Density; (kg/m^3)	Compressive strength; (MPa)
SHGC-S	8.8 (313)	1828±16	56.8±3.7
SHGC-G	6.7 (277)	1754±4	43.4±2.4
SHGC-M	7.4 (289)	1586±6	46.8±3.0
SHGC-P	7.1 (284.5)	1833±4	48.2±3.2

[1]Relative slump value of the fresh matrix. The average diameter of the matrix flow (in millimeter) is shown in parenthesis.

The average density of each mix is also presented in Table 6-3. The density of green lightweight SHGCs was in the range of 1586 kg/m^3 to 1833 kg/m^3, which is 24–34% less than that of a normal weight concrete with a density of 2400 kg/m^3 and meet the density requirement for lightweight concrete (below 1850 kg/m^3) (ACI 213R, 2014). It should be pointed out that even SHGC-S containing normal weight micro-silica sand (typically used in SHCC) exhibited an average density of 1828 kg/m^3, which can be classified as lightweight concrete. The density of SHGC-S is 12% less than that of typical SHCC M45

(2077 kg/m^3). This may be attributed to the lower specific density of fly ash (2.45 g/cm^3) than that of cement (3.15 g/cm^3). Therefore, replacing the OPC binder by fly ash-based geopolymer binder is beneficial for weight reduction of composite.

According to Table 6-3, the densities of SHGC-G and SHGC-M are 4% and 13%, respectively, lower than that of SHGC-S. The densities of SHGC-S and SHGC-P are comparable. Among the lightweight aggregates, hollow ceramic microspheres were the most effective in reducing the density of the composite. This may be attributed to the hollow and closed shell structure and the low particle density of microsphere particles (E-Sphere Technical Specifications, 2015). It should be noted that the density of the SHGC-M mixture (1586 kg/m^3) developed in this study is even lower than that of the lightest GLSHCCs (the mixture C6 with the average density of 1649 kg/m^3) developed by Huang et al. (2013), where fly ash to cement ratio was 4.4 and micro-silica sand was completely replaced by fly ash cenosphere.

6.4.2 Compressive strength

The average compressive strength of each mix is also presented in Table 6-3. The compressive strength of green lightweight SHGCs at 3 days after casting ranged from 43.4 MPa to 56.8 MPa, which is well above the compressive strength requirement of 17 MPa for structural lightweight concrete (ACI 213R, 2014). The compressive strength of SHGC-G, SHGC-M and SHGC-P containing lightweight aggregates were 24%, 18% and 15%, respectively lower than that of SHGC-S. This may be attributed to the fact that lightweight aggregates are usually weaker than micro-silica sand particles (Huang et al., 2013). Among the four SHGCs, the SHGC-S mixture containing micro-silica sand exhibited the highest compressive strength, comparable to typical SHCC M45. However, unlike typical SHCC M45, SHGC-S contains no cement, and therefore it has significantly lower environmental footprints compared to the typical SHCC M45 in which its cement content is still 1.5 times that of normal concrete (Yang et al., 2007).

Material sustainability indicators (MSI) in terms of embodied energy and CO_2 emission were computed in this study to compare the material sustainability of SHGC-S and typical SHCC M45 (Li et al., 2004). Table 6-4 presents the mix proportions of SHGC-S and typical SHCC M45 and the life cycle inventory data of the ingredients. The inventory data was obtained from relevant literature (Yang et al., 2007; Huang et al., 2012;

McLellan et al., 2011; Fawer et al., 1999; Yang et al., 2013; National Greenhouse Accounts Factors, 2014; Integrated Pollution Prevention and Control (IPPC), 2001). It should be noted that three assumptions were made in deriving the life cycle inventory data given in Table 6-4. First, the embodied energy and CO_2 emissions associated with fly ash are zero as it is a by-product of coal power station, most of which is disposed in landfills. Second, the embodied energy and CO_2 emissions associated with water are negligible relative to other ingredients. Third, the embodied energy and CO_2 emissions associated with the heat curing approach (24 hours at 60° C) adopted for production of SHGCs are derived from the data given in Yang et al. (2013) and National Greenhouse Accounts Factors (2014), considering the average emission factor for consumption of electricity from the grid in Australia to be 0.73 kg CO_2-e/kWh.

Table 6-4: Mix proportions of SHGC-S and typical SHCC M45 and life cycle inventory data of the ingredients used for calculating the MSI

Ingredients	SHCC M45[1] (kg/m^3)	SHGC-S (kg/m^3)	Embodied energy (MJ/kg)	CO_2 emissions (kg/kg)
OPC	571	---	5.06[2]	0.898[2]
Fly ash	685	1029.7	---	---
Micro-silica sand	456	308.9	0.175[2]	0.026[2]
Water	332	---	---	---
Activator solution[3]	---	463.4	4.26[5]	0.358[4]
Superplasticizer	6.8	---	36.76[2]	1.48[2]
PVA fiber	26	26	106.54[2]	3.6[2]
Heat curing	N/A	Applicable	0.0828[6]	0.017[6]

[1] The mix proportion of typical SHCC M45 is adopted from Yang et al. (2007).

[2] Derived from Huang et al. (2012) and Yang et al. (2007).

[3] The Na-based activator solution.

[4] Derived from McLellan et al. (2011).

[5] Derived from Fawer et al. (1999) and Integrated Pollution Prevention and Control (IPPC) (2001).

[6] Derived from Yang et al. (2013) and National Greenhouse Accounts Factors (2014).

Figure 6-1 presents the embodied energy and CO_2 emissions associated with production of a unit volume of SHGC-S and SHCC M45. The CO_2 emissions of SHGC-S is 52%

lower than that of SHCC M45. This is mainly attributed to the replacement of OPC binder, which is highly energy and carbon intensive with fly ash-based geopolymer binder. On the other hand, the embodied energy of SHGC-S is 17% lower than that of SHCC M45. The reason for the relatively less reduction in the embodied energy associated with SHGC-S over SHCC M45 is the fact that although the embodied energy associated with fly ash is considered to be zero, however high embodied energy is still required for production of the activator solution and the heat curing approach adopted for the manufacture of SHGC-S. It can be concluded that SHGC-S is a promising sustainable alternative to SHCC M45 in terms of carbon emission and energy consumption.

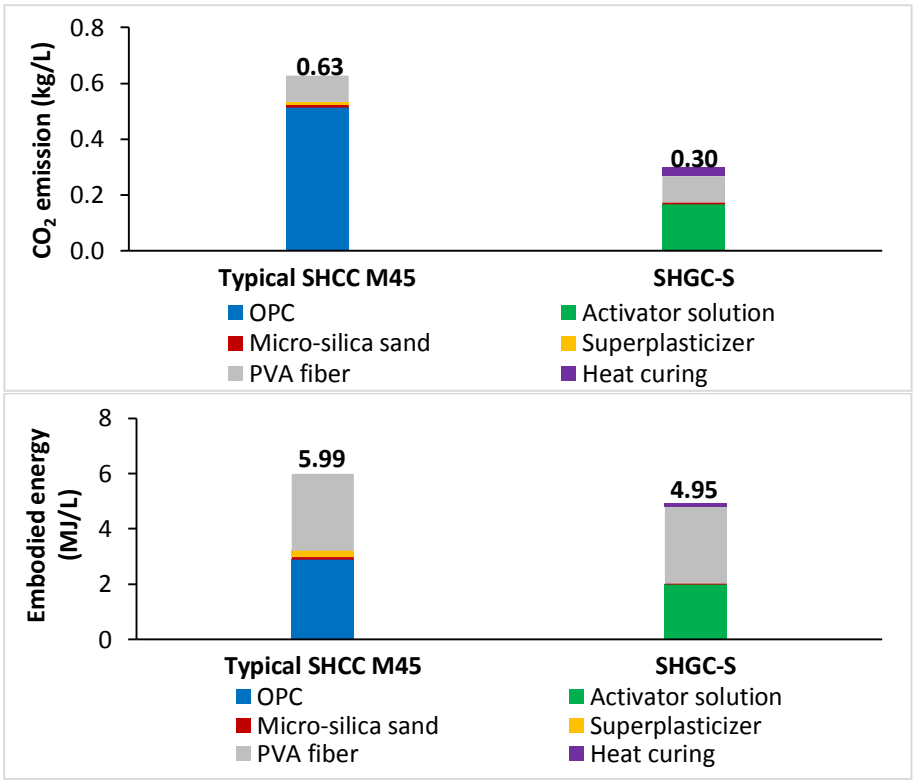

Figure 6-1: Material sustainability indicators of SHGC-S and typical SHCC M45

6.4.3 Uniaxial tensile performance

The uniaxial tensile stress-strain responses of the four green lightweight fly ash-based SHGCs developed in this study are presented in Figures 6-2 to 6-5. As can be seen, all lightweight fly ash-based SHGCs, regardless of the type of aggregate, exhibited clear

PSH behavior through multiple cracking process. The uniaxial tension test results including the average measured ultimate tensile strength (σ_{cu}) and tensile strain capacity (ε_{cu}) and the estimated tensile first-crack strength (σ_{fc}) are presented in Table 6-5. As can be seen, the developed lightweight fly ash-based SHGCs exhibited moderate to high ultimate tensile strength in the range of 3.4–5.0 MPa. At the same time, they exhibited very high tensile strain capacity in the range of 3.5−3.7%, which is about two orders of magnitude higher than that of brittle OPC-based or geopolymer concrete. Therefore, the development of green lightweight SHGCs with fly ash-based geopolymer as the sole binder is experimentally demonstrated.

Table 6-5: Uniaxial tension test results

Mix ID	First-crack strength, σ_{fc}; (MPa)	Ultimate tensile strength, σ_{cu} ; (MPa)	Tensile strain capacity, ε_{cu}; (%)	Stress-performance index (σ_{cu}/σ_{fc})
SHGC-S	3.4±0.62	5.0±0.47	3.6±0.15	1.5
SHGC-G	2.6±0.09	3.8±0.24	3.7±0.22	1.5
SHGC-M	2.5±0.17	3.4±0.32	3.5±0.43	1.4
SHGC-P	3.3±0.27	4.3±0.25	3.6±0.30	1.3

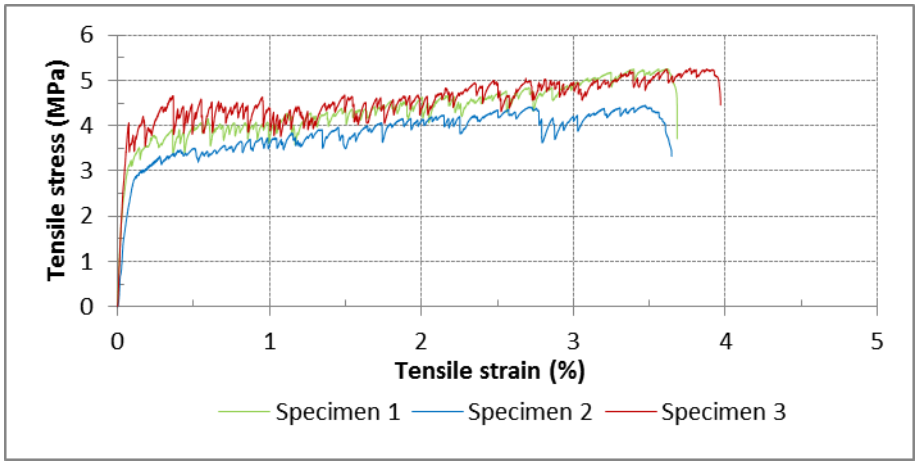

Figure 6-2: Tensile stress-strain responses of SHGC-S

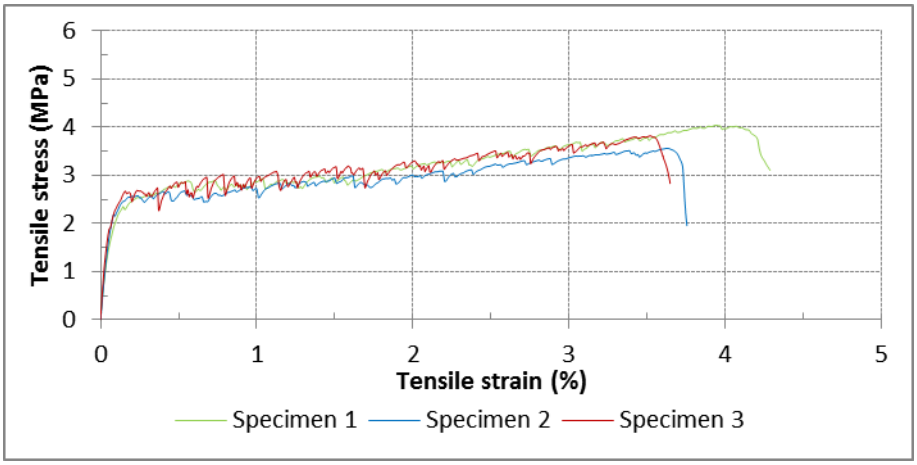

Figure 6-3: Tensile stress-strain responses of SHGC-G

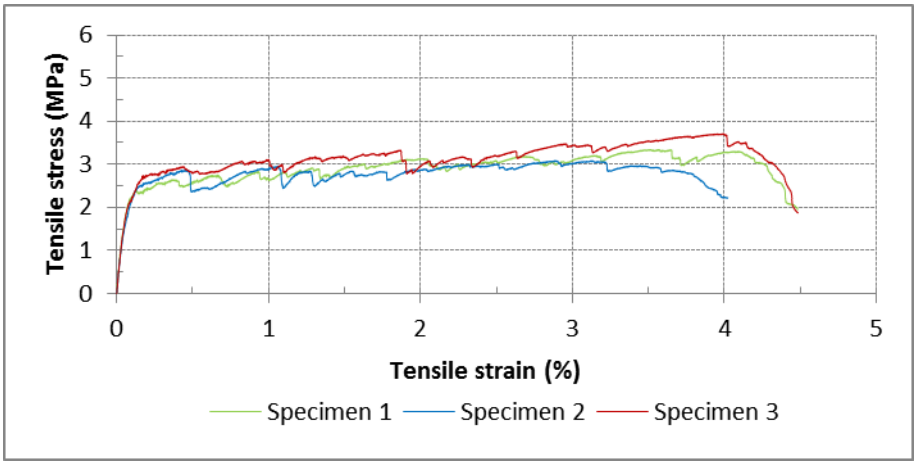

Figure 6-4: Tensile stress-strain responses of SHGC-M

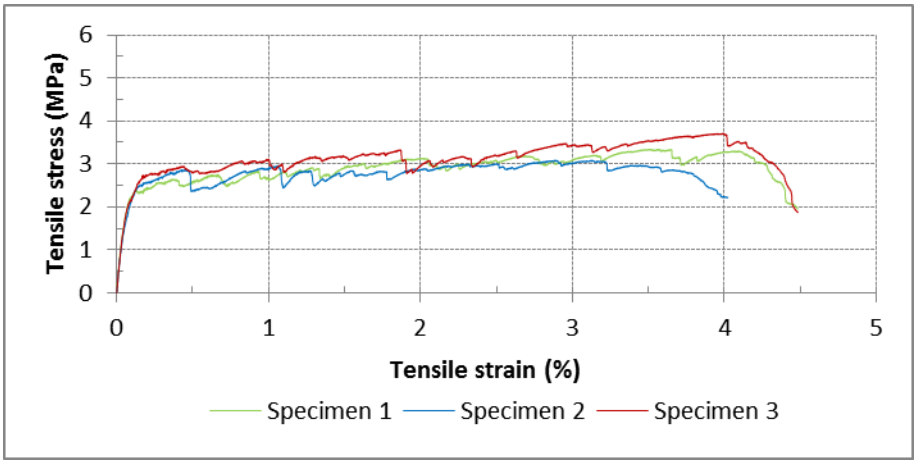

Figure 6-5: Tensile stress-strain responses of SHGC-P

Figure 6-6 presents the crack pattern of SHGC-S after unloading. The green lightweight fly ash-based SHGC clearly shows the multiple-cracking behavior with uniform crack distribution and a narrow crack spacing of 2–3 mm, representing saturated multiple cracking behavior, which corresponds to its significantly high tensile strain capacity. The average crack width of SHGC-S under load is estimated to be approximately 100 µm based on the tensile strain capacity, the average crack spacing and the number of visible cracks. It should be noted that the actual crack width under load should be smaller than the estimated value of 100 µm, because the actual number of micro-cracks formed during loading was more than the number of visible cracks after unloading. This is because many micro-cracks developed during loading completely closed after unloading, making them very difficult to be detected on the surface of the unloaded specimen (Li et al., 2001). Such a tight crack width indicates significant improvement in durability of green lightweight SHGC compared to cracked brittle lightweight concrete with crack width at the scale of several hundred microns to a few millimeters (Li, 2002).

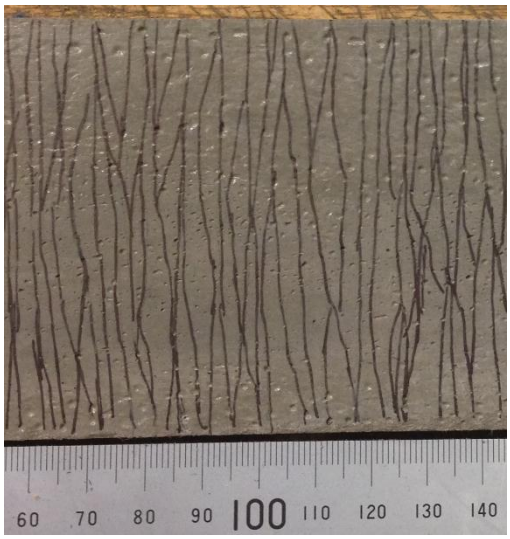

Figure 6-6: Crack pattern of SHGC-S

As observed in Table 6-5, the first-crack strength of SHGC-S and SHGC-P, and that of SHGC-G and SHGC-M are comparable. The first-crack strength of SHGC-S and SHGC-P are about 30% higher than that of SHGC-G and SHGC-M, due to their greater matrix fracture toughness (Li et al., 2001). This difference in matrix fracture toughness is likely due to the difference in the particle shape of the aggregates (Huang et al., 2013). While

the expanded recycled glass and hollow ceramic microspheres possess regular spherical shape (E-Sphere Technical Specifications, 2015; Poraver Technical Specifications, 2015), the micro-silica sand and expanded perlite particles are irregularly shaped (TGS Industrial sand Technical Specifications, 2015; Ausperl Technical Specifications, 2015). The irregular shape of the aggregates increases the tortuosity of the fracture path along the interface between geopolymer paste and aggregates, thereby resulting in higher fracture toughness and first-crack strength of SHGC-S and SHGC-P than SHGC-G and SHGC-M (Huang et al., 2013).

According to Table 6-5, SHGC-S containing normal weight micro-silica sand exhibited the highest ultimate tensile strength. The ultimate tensile strengths of SHGC-G, SHGC-M and SHGC-P containing lightweight aggregates were 24%, 32% and 14%, respectively, lower than that of SHGC-S. According to the micromechanics design theory of SHCC, the ultimate tensile strength of the composite is governed by fiber bridging capacity, which is further affected by the fiber characteristics and fiber-matrix interfacial properties (Huang et al., 2013). The lower ultimate tensile strength of the composites containing lightweight aggregates is likely due to their lower fiber-matrix bond. The relatively lower fiber/matrix frictional bond in SHGC-G and SHGC-M may be caused by the smooth spherical shape of the expanded recycled glass and hollow ceramic microspheres, compared to the irregularly shaped micro-silica sand and expanded perlite particles.

The tensile strain capacities of SHGCs are discussed below in terms of the two PSH performance indices, namely stress-performance index (σ_0 / σ_{fc}) and energy-performance index (J_b' / J_{tip}), proposed by Kanda and Li (2006). It should be noted that the ultimate tensile strength (σ_{cu}) coincides with σ_0 of the composite when the composite exhibits the PSH behavior (Li et al., 1995).

According to the Table 6-5, the tensile strain capacities of all SHGCs, regardless of the type of aggregate, were about 3.5–3.7%. The stress-performance index of each composite reported in Table 6-5 for various SHGCs is comparable (between 1.3 and 1.5). From Kanda and Li (2006), stress-performance index greater than 1.2 typically leads to saturated multiple cracking. This condition is true for all sustainable lightweight SHGCs in this study, and therefore leads to similar tensile strain capacity. This is one of the

reasons for the comparable tensile strain capacity of the composites. The second reason is associated with the energy-performance index of the composites. The relatively lower ultimate tensile strength of SHGC-G and SHGC-M suggests that the J_b' of these composites could be lower than that of SHGC-S and SHGC-P (Lee et al., 2012). At the same time, the relatively lower first-crack strength of SHGC-G and SHGC-M indicates that the matrix fracture toughness and J_{tip} of these composites could be lower than those of SHGC-S and SHGC-P (Li et al., 2001; Huang et al., 2013). Therefore, it is hypothesized that although the J_b' of SHGC-G and SHGC-M could be lower than that of SHGC-S and SHGC-P, however due to their lower J_{tip}, their energy-performance index would be comparable to that of SHGC-S and SHGC-P. Therefore, as expected from micromechanics-based design theory, it is not surprising that all sustainable lightweight SHGCs in this study with comparable PSH performance indices exhibited comparable tensile strain capacities.

6.4.4 Thermal conductivity

The thermal conductivity of concrete is typically sensitive to its moisture content. Greater moisture content results in greater thermal conductivity (Demirboğa and Gül, 2003). Although SHGCs are not cement-based, their thermal conductivity also depends on the moisture content. Therefore, the thermal conductivity measurements should be performed at the same moisture content for all SHGCs. In this study, all coupon specimens of various SHGCs were at stable moisture content of 5.6% at the time of thermal conductivity measurements.

The thermal conductivities of all SHGCs at ambient temperature (23 ± 3 °C) are reported in Figure 6-7. The SHGC-S containing normal weight micro-silica sand exhibited the highest thermal conductivity. The thermal conductivities of SHGC-G, SHGC-M and SHGC-P containing lightweight aggregates were 49%, 38% and 40%, respectively, lower than that of SHGC-S. The reduction in thermal conductivity of SHGCs incorporating lightweight aggregates is attributed to the lower thermal conductivity of the lightweight aggregates than that of the normal-weight micro-silica sand (Huang et al., 2013). The thermal conductivities of expanded recycled glass, ceramic microspheres, and expanded perlite are 0.07 W/m.K (Poraver Technical Specifications, 2015), 0.10 W/m.K (E-sphere

Technical Specifications, 2015), and 0.095 W/m.K (Ausperl Technical Specifications, 2015), respectively compared to 0.33 W/m.K of dry silica sand (Lasance, 2004).

According to Figure 6-7, expanded recycled glass was the most effective in reducing the thermal conductivity among the lightweight aggregates used in this study, which is meaningful because the expanded recycled glass has the least thermal conductivity among various aggregates investigated in this study. The relatively lower thermal conductivity of expanded recycled glass is due to its multicellular structure (Poraver Technical Specifications, 2015). It can be concluded that incorporation of lightweight aggregates can effectively reduce the thermal conductivity of the fly ash-based SHGCs, which can potentially benefit energy conservation in buildings constructed with the green lightweight fly ash-based SHGCs.

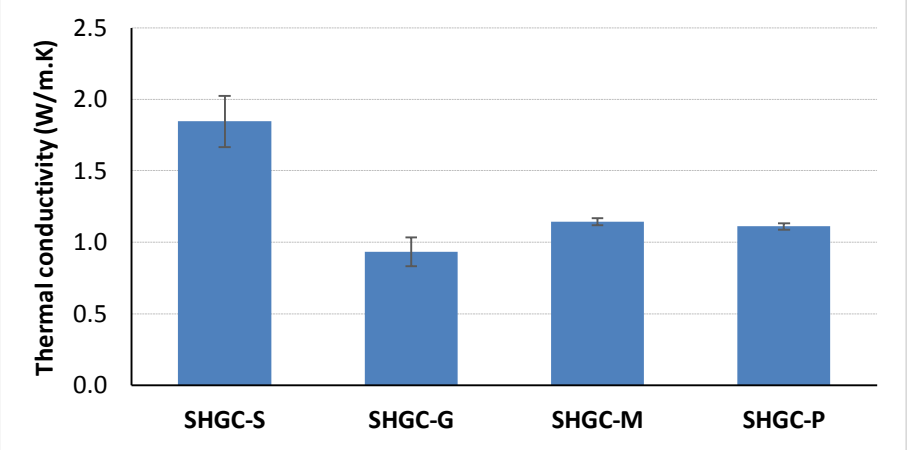

Figure 6-7: Thermal conductivities of sustainable lightweight fly ash-based SHGCs

6.5 Summary and Conclusions

This chapter presents the results of experimental determination of the mechanical and thermal properties of sustainable lightweight SHGCs exhibiting significant strain hardening behavior under uniaxial tension which are greener, lighter, and provides better thermal insulation than SHCC. The influences of replacing normal weight micro-silica sand with three types of lightweight aggregates on the mechanical and thermal properties of the developed fly ash-based SHGCs were experimentally evaluated. The sustainable lightweight fly ash-based SHGCs developed in this study exhibited density of 1586−1833

kg/m^3, compressive strength of 43.4−56.8 MPa, thermal conductivity of 1.845−0.934 W/m.K, tensile strength of 3.4−5.0 MPa, and tensile strain capacity of 3.5−3.7%, depending on the type of aggregates. The following specific conclusions are drawn:

1) The compressive strength and tensile performance of the fly ash-based SHGC containing normal weight micro-silica sand (SHGC-S) are comparable to those of typical SHCC M45. At the same time, SHGC-S is a cement-less and sustainable composite with 52% lower CO_2 emissions and 17% lower embodied energy compared to those of SHCC M45. In addition, SHGC-S with an average density of 1828 kg/m^3, unlike SHCC M45 (2077 kg/m^3), can be classified as lightweight concrete.

2) Among the lightweight aggregates investigated in this study, hollow ceramic microsphere was the most effective in reducing the density of the composite, with comparable tensile ductility and considerably (38%) lower thermal conductivity at the expense of 18% reduction in the compressive strength compared to those of the SHGC containing normal weight micro-silica sand.

3) The spherical shaped particles of expanded recycled glass and hollow ceramic microspheres cause reduction in the first-crack strength and ultimate tensile strength of the composite, compared to the SHGCs containing irregularly shaped micro-silica sand and expanded perlite particles. This may be due to lower matrix fracture toughness and fiber-matrix interfacial bond, when spherical aggregates are used. The tensile ductility of all sustainable lightweight fly ash-based SHGCs, regardless of the aggregate type, is very high (3.5–3.7%) due to high strength and energy performance indices resulting in saturated multiple cracking.

4) Among the lightweight aggregates used in this study, expanded recycled glass was the most effective in reducing the thermal conductivity of the composite compared to the SHGC containing normal weight micro-silica sand. It can be concluded that incorporation of lightweight aggregates can effectively (up to 49%) reduce the thermal conductivity of the composite, which can potentially reduce heat exchange and total energy consumption in buildings constructed with the sustainable lightweight fly ash-based SHGCs.

6.6 References

ACI 213R. 2014. Guide For Structural Lightweight-Aggregate Concrete. United States: American Concrete Institute.

ASTM C109/C109M. 2007. Standard Test Method for Compressive Strength of Hydraulic Cement Mortars (Using 2-in. or [50-mm] Cube Specimens). United States: ASTM Standards.

AUSPERL TECHNICAL SPECIFICATIONS [Online]. Australian Perlite Pty Limited (AUSPERL) Available: http://www.australianperlite.com/perlite/ [Accessed 20 February 2015].

CHA, J., SEO, J. & KIM, S. 2012. Building materials thermal conductivity measurement and correlation with heat flow meter, laser flash analysis and TCi. *Journal of Thermal Analysis and Calorimetry,* 109, 295-300.

CHANDRA, S. & BERNTSSON, L. 2002. Lightweight aggregate concrete: science, technology and applications. 2002, Norwich. New York, USA: William Andrew Publishing.

DEMIRBOĞA, R. & GÜL, R. 2003. The effects of expanded perlite aggregate, silica fume and fly ash on the thermal conductivity of lightweight concrete. *Cement and Concrete Research,* 33, 723-727.

E-SPHERES TECHNICAL SPECIFICATIONS [Online]. ENVIROSPHERES PTY LTD. Available: http://www.envirospheres.com/products_bl.asp [Accessed 10 February 2015].

FAWER, M., CONCANNON, M. & RIEBER, W. 1999. Life cycle inventories for the production of sodium silicates. *The International Journal of Life Cycle Assessment,* 4, 207-212.

GAO, J., SUN, W. & MORINO, K. 1997. Mechanical properties of steel fiber-reinforced, high-strength, lightweight concrete. *Cement and Concrete Composites,* 19, 307-313.

HENGST, R. & TRESSLER, R. 1983. Fracture of foamed Portland cements. *Cement and Concrete Research,* 13, 127-134.

HUANG, X., RANADE, R. & LI, V. C. 2012. Feasibility study of developing green ECC using iron ore tailings powder as cement replacement. *Journal of Materials in Civil Engineering,* 25, 923-931.

HUANG, X., RANADE, R., ZHANG, Q., NI, W. & LI, V. C. 2013. Mechanical and thermal properties of green lightweight engineered cementitious composites. *Construction and Building Materials,* 48, 954-960.

Integrated Pollution Prevention and Control (IPPC). 2001. Reference Document on Best Available Techniques in the Chlor-Alkali Manufacturing industry. *European IPPC Bureau*.

KANDA, T. & LI, V. C. 2006. Practical design criteria for saturated pseudo strain hardening behavior in ECC. *Journal of advanced concrete technology,* 4, 59-72.

KIM, J.-K., KIM, J.-S., HA, G. J. & KIM, Y. Y. 2007. Tensile and fiber dispersion performance of ECC (engineered cementitious composites) produced with ground granulated blast furnace slag. *Cement and Concrete Research,* 37, 1096-1105.

LASANCE, C. J. 2004. The thermal conductivity of silicon dioxide. *Electronics Cooling*.

LEE, B. Y., CHO, C.-G., LIM, H.-J., SONG, J.-K., YANG, K.-H. & LI, V. C. 2012. Strain hardening fiber reinforced alkali-activated mortar–a feasibility study. *Construction and Building Materials,* 37, 15-20.

LI, V. C. Reflections on the research and development of engineered cementitious composites (ECC). Proceedings of the JCI International Workshop on Ductile Fiber Reinforced Cementitious Composites (DFRCC)–Application and Evaluation, 2002. Citeseer, 1-21.

LI, V. C., MISHRA, D. K. & WU, H.-C. 1995. Matrix design for pseudo-strain-hardening fibre reinforced cementitious composites. *Materials and Structures,* 28, 586-595.

LI, V. C., WANG, S. & WU, C. 2001. Tensile strain-hardening behavior of polyvinyl alcohol engineered cementitious composite (PVA-ECC). *ACI materials Journal,* 98.

LI, Z., DING, Z. & ZHANG, Y. 2004. Development of sustainable cementitious materials. *International workshop on sustainable development and concrete technology, Beijing, China.*

MCLELLAN, B. C., WILLIAMS, R. P., LAY, J., VAN RIESSEN, A. & CORDER, G. D. 2011. Costs and carbon emissions for geopolymer pastes in comparison to ordinary Portland cement. *Journal of Cleaner Production,* 19, 1080-1090.

NATIONAL GREENHOUSE ACCOUNTS FACTORS. 2014. The Department of the Environment-Australian Government. Retrieved from http://www.environment.gov.au/.

PARK, S. B., YOON, E. S. & LEE, B. I. 1999. Effects of processing and materials variations on mechanical properties of lightweight cement composites. *Cement and Concrete Research,* 29, 193-200.

PORAVER TECHNICAL SPECIFICATIONS [Online]. Dennert Poraver GmbH. Available: http://www.poraver.com/us/products/technical-data/ [Accessed 20 February 2015].

TGS INDUSTRIAL SAND TECHNICAL SPECIFICATIONS [Online]. T.G.S Industrial Sands Pty. Ltd. Available: http://tgsindustrialsands.com.au/our-products/ [Accessed 20 February 2015].

U.S. DEPARTMENT OF ENERG. 2010. Buildings energy data book. Retrieved from <http:// buildingsdatabook.eren.doe.gov/docs%5CDataBooks%5C2010_BEDB.pdf>.

WANG, S. & LI, V. 27 LIGHTWEIGHT ENGINEERED CEMENTITIOUS COMPOSITES (ECC). PRO 30: 4th International RILEM Workshop on High Performance Fiber Reinforced Cement Composites (HPFRCC 4), 2003. RILEM Publications, 379.

YANG, E.-H., YANG, Y. & LI, V. C. 2007. Use of high volumes of fly ash to improve ECC mechanical properties and material greenness. *ACI materials journal,* 104, 620-628.

YANG, K.-H., SONG, J.-K. & SONG, K.-I. 2013. Assessment of CO 2 reduction of alkali-activated concrete. *Journal of Cleaner Production,* 39, 265-272.

ZHANG, M. H. & GJVORV, O. E. 1991. Mechanical properties of high-strength lightweight concrete. *Materials Journal,* 88, 240-247.

CHAPTER 7

MICROSCALE INVESTIGATION OF FIBER-MATRIX INTERFACE PROPERTIES OF FLY ASH-BASED SHGCS

Note: This chapter is based on the manuscript "*Microscale Investigation of Fiber-Matrix Interface Properties of Strain Hardening Geopolymer Composite*", by **Nematollahi, B.**, Qiu, J., Yang, E-H., and Sanjayan, J., being currently under review for publication in ***Journal of Composites Part B: Engineering***.

7.1 Introduction

Fly ash-based SHGC, similar to other randomly oriented discontinuous fiber-reinforced brittle matrix composites, is a heterogeneous material at micro and meso scales with multiple interacting phases, such as microscale fiber-matrix interactions (Rande, 2014). Micromechanics-based design of fly ash-based SHGCs particularly relies on beneficial tailoring of the interactions between the fiber and geopolymer matrix to achieve desired composite properties (Rande, 2014). Therefore, investigating the microscale fiber-matrix interaction properties and mechanisms is of primary importance in design and composite property tailoring of fly ash-based SHGCs.

This chapter reports the microscale investigation of the fly ash-based SHGCs to gain an in-depth understanding of the fundamental fiber-matrix interaction properties and mechanisms in these cement-less composites. The investigation involved experimental determination of the fiber-matrix interaction properties using single-fiber pullout tests. Dependence of the interface parameters on the geopolymer matrix composition mainly governed by the type of activator and W/GP solids was evaluated. Previous studies reported that the fiber surface oil coating can effectively tailor the interface properties in typical PVA-SHCC (Li et al., 2002). Thus, the quantitative influences of fiber surface oil coating on the interface properties of the fly ash-based SHGCs were also investigated by using both virgin (un-coated) and oil-coated PVA fibers in the single-fiber pullout tests. The quantitative effects of the measured interface properties on the crack bridging $\sigma(\delta)$ relation and tensile performance of the developed fly ash-based SHGCs were investigated using a micromechanics-based model.

7.2 Materials and mix proportions

The same low-calcium (Class F) fly ash supplied from Gladstone power station in Queensland, Australia was used in this research. The chemical composition and LOI of the fly ash are presented in Table 3-1. To investigate the effect of fiber surface oil coating on the fiber-matrix interface properties, both virgin and oil-coated PVA fibers, supplied by Kuraray Co. Ltd., Japan were used in this study. While virgin PVA fibers did not have any surface oil coating, oil-coated PVA fibers had a surface oil coating of 1.2% by weight. Properties of the PVA fibers are presented in Table 4-2. To study the effects of type of activator, the same Na-based-1 and K-based activator combinations used in Chapter 4, were used in this research. The Na-based-1 activator was composed of 8.0 M NaOH solution (28.6% w/w) and Na_2SiO_3 solution (71.4% w/w) with a SiO_2 to Na_2O ratio of 2.0. The K-based activator was composed of 8.0 M KOH solution (28.6% w/w) and K_2SiO_3 solution (71.4% w/w) with a SiO_2 to K_2O ratio of 2.23. The physical and chemical properties of NaOH, and Na_2SiO_3 solutions, as well as KOH and K_2SiO_3 solutions and the procedure for preparation of the Na-based-1 and K-based activator combinations are given in Chapter 4.

Table 7-1 presents the fly ash-based SHGC mix proportions used in this research. It should be noted that the SHGC-Na-20, SHGC-K-20 mixtures shown in Table 7-1 are the same as SHGC-Na-1 and SHGC-K mixtures used in Chapter 4. In addition, the SHGC-Na-23 mix shown in Table 7-1 is the same as SHGC23 mixture used in Chapter 5. The SHGC-Na-20 and SHGC-Na-23 mixtures were used to investigate the influence of the W/GP solids on the fiber-matrix interface properties. To investigate the effect of the type of activator on the interfacial properties, two different scenarios were considered. The SHGC-Na-20 and SHGC-K-20 mixtures compare the effect of type of activator on the same W/GP solids basis, whereas the SHGC-Na-23 and SHGC-K-20 mixtures compare it on the basis of the same compressive strength of the SHGC matrix. To evaluate the effects of fiber surface oil coating, both virgin and oil-coated PVA fibers were used in the single-fiber pullout tests.

Table 7-1: Mix proportions of the fly ash-based SHGCs

Mix ID	Fly ash (kg/m^3)	Act. (kg/m^3)	Extra Water (kg/m^3)	PVA fiber (kg/m^3)	W/GP solids ratio	Target compressive strength of SHGC matrix (MPa)
SHGC-Na-20	1.0	0.35[1]	0.014[3]	0.02	0.20	55
SHGC-Na-23	1.0	0.45[1]	---	0.02	0.23	32
SHGC-K-20	1.0	0.35[2]	---	0.02	0.20	32

Note: All numbers are mass ratios of fly ash weight except W/GP solids ratios, nominal compressive strength of SHGC matrix and fiber contents (volume fraction).

[1] Composed of the Na-based-1 activator combination.

[2] Composed of the K-based activator combination.

7.3 Mixing, Curing and Testing of Specimens

The mixtures were prepared following a typical SHGC mixing procedure explained in Chapter 4. Similar to the previous chapters, heat curing was adopted in this research. The procedure for the heat curing is given in Chapter 4.

Single-fiber pullout tests were conducted to measure the fiber-matrix interface properties, including chemical bond strength (G_d), frictional bond strength (τ_0), and slip-hardening coefficient (β). The specimen preparation and test set-up are illustrated in Figure 7-1. Three long PVA fibers were attached to the mold before casting. The one-part geopolymer matrix was then cast into the mold. Once the geopolymer matrix was hardened and cured, it was cut to make six single-fiber pullout specimens. For each mixture, at least four single-fiber pullout specimens were tested under displacement control at the rate of 0.03 mm/min. Further details of the test configuration, data processing, and calculation of the fiber-matrix interface parameters can be found in Redon et al. (2001) and Qiu and Yang (2015).

As mentioned in Chapter 4 and 5, a series of experiments including compression, matrix elastic modulus and fracture toughness, and uniaxial tension tests were also conducted to characterize the mechanical properties of the fly ash-based SHGC mixtures investigated in this chapter. The procedures for compression, matrix fracture toughness and uniaxial tension tests are given in Chapter 4. The results of these tests were adopted from Chapters 4 and 5 and re-presented in this chapter for better referencing and ease of comparison.

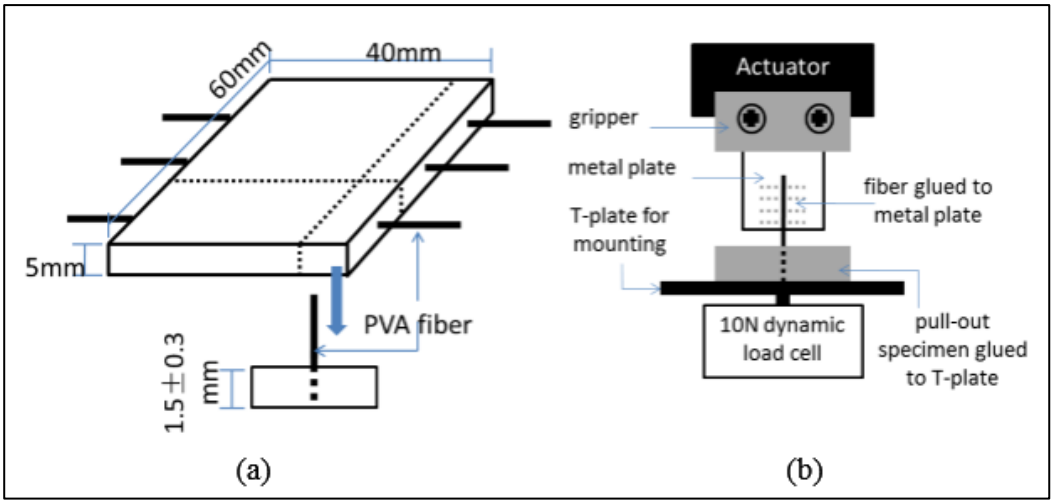

Figure 7-1: Illustration of (a) single-fiber pullout specimen preparation and (b) pullout test setup

7.4 Results and Discussions

7.4.1 Compressive strength

The compression test results were adopted from previous sections in Chapters 4 and 5 and re-presented in Table 7-2 for better referencing and ease of comparison. As can be seen, the type of activator had a significant influence on the compressive strength of the geopolymer matrix and composite. For the identical W/GP solids of 0.20, the compressive strength of K-based geopolymer matrix and composite was about 40% lower than that of the corresponding Na-based geopolymer matrix and composite. This could be attributed to the different microstructure of Na-based and K-based geopolymers. Fernández-Jiménez and Palomo (2005) reported that in fly ash-based geopolymer the type of activator has a significant effect on the microstructure of the aluminosilicate gel. It is interesting to note that while the compressive strength of the SHGC matrix in SHGC-Na-23 and SHGC-K-20 was comparable, the compressive strength of SHGC-Na-23 was 41% higher than that of SHGC-K-20. This could be attributed to the effect of type of activator on the fiber-matrix interface properties. As expected, the compressive strength of SHGC-Na-23 and its corresponding matrix was lower than that of SHGC-Na-20, thanks to its higher W/GP solids.

Table 7-2: Compression test results

Mix ID	Compressive strength; (MPa)	
	Matrix	Composite
SHGC-Na-20	54.6±3.0[a]	63.7±2.7[a]
SHGC-Na-23	31.6±1.5[b]	52.6±1.6[b]
SHGC-K-20	32.3±1.4[a]	37.3±1.3[a]

[a] Test results adopted from Chapter 4.

[b] Test results adopted from Chapter 5.

7.4.2 Matrix Fracture Properties

The matrix fracture properties test results were adopted from previous sections in Chapters 4 and 5 and re-presented in Table 7-3 for ease of comparison. It should be noted that in this chapter, the elastic modulus of the geopolymer matrix (E_m) was measured by performing the compression test on 100×200 mm cylinders in accordance with AS1012.17 (Standards Australia, 1997). However in Chapters 4 and 5, the E_m of each mixture was indirectly derived based on ECM from the linear portion of the load-deflection curve of the notched beam specimen in three-point bending tests. As mentioned in Chapter 4, these indirectly derived E_m values should only be considered as relative values enabling us to compare the matrix elastic modulus of each mixture. Nevertheless, it was found that these indirectly derived E_m values are lower than the absolute matrix elastic modulus values, measured by performing the compression tests on cylinders. The underestimation of E_m results in higher and un-reliable prediction of J_{tip}, and thereby the energy-performance index of the composite.

As expected and can be seen in Table 7-3, the fracture properties of SHGC-Na-23 matrix were lower than those of SHGC-Na-20, thanks to its higher W/GP solids. The type of activator had a significant effect on the fracture properties of the SHGC matrix. For the identical W/GP solids of 0.20, the crack tip toughness (J_{tip}) of K-based SHGC matrix was 61% less than that of Na-based SHGC matrix, due to a decrease in fracture toughness (K_m) and elastic modulus (E_m) of about 46% and 23%, respectively. The lower E_m of the K-based SHGC matrix corresponds to its lower compressive strength as reported in Table 7-2. The lower K_m of SHGC-K-20 matrix compared to SHGC-Na-20 matrix could be attributed to the different microstructure of Na-based and K-based geopolymers, because

all other parameters, except the type of activator, were kept constant for both SHGC matrices (Pan et al., 2011). As mentioned in Section 7.4.1, the geopolymer microstructures of the SHGC-Na-20 and SHGC-K-20 matrices are different, due to their different type of activator (Fernández-Jiménez and Palomo, 2005).

Table 7-3: Matrix fracture properties

Mix ID	Matrix elastic modulus, E_m; (GPa)[a]	Matrix fracture toughness, K_m; ($MPa.m^{1/2}$)	Crack tip toughness, J_{tip}; (J/m^2)
SHGC-Na-20 matrix	9.8	0.436[b]	19.4
SHGC-Na-23 matrix	7.5	0.269[c]	9.6
SHGC-K-20 matrix	7.5	0.237[b]	7.5

[a] Determined in accordance with AS1012.7 (1997) using 100×200 cylinders.

[b] Test results adopted from Chapter 4.

[c] Test results adopted from Chapter 5.

It is worth to note that the elastic modulus of SHGC-Na-23 and SHGC-K-20 matrices was identical, which corresponds to their comparable compressive strength as reported in Table 7-2. However, the K_m, and thereby J_{tip} of SHGC-Na-23 matrix were 14% and 28%, respectively higher than those of the SHGC-K-20 matrix. Similar to the above discussion, the different K_m of SHGC-Na-23 and SHGC-K-20 matrices is also attributed to their different geopolymer microstructures, due to their different type of activator (Fernández-Jiménez and Palomo, 2005). It is thereby concluded that the K-based activator increases the brittleness of the fly ash-based SHGC matrix.

7.4.3 Fiber-matrix interface properties

The fiber-matrix interface properties including G_d, τ_0, and β of each mix using virgin and oil-coated (1.2 wt.%) PVA fibers are summarized in Tables 7-4 and 7-5, respectively. The typical load-displacement curves from single-fiber pullout tests using virgin and oil-coated (1.2 wt.%) PVA fibers are shown in Figures 7-2 and 7-3, respectively. It should be noted that in these figures only one load-displacement curve from each mix is presented which is from a specimen which has interfacial properties close to the average. The SEM images of the typical pulled-out fiber of each mix are shown in Figures 7-4 to

7-7. In the following sections, the effects of the fiber surface oil coating, type of activator and W/GP solids on the fiber-matrix interface properties are discussed.

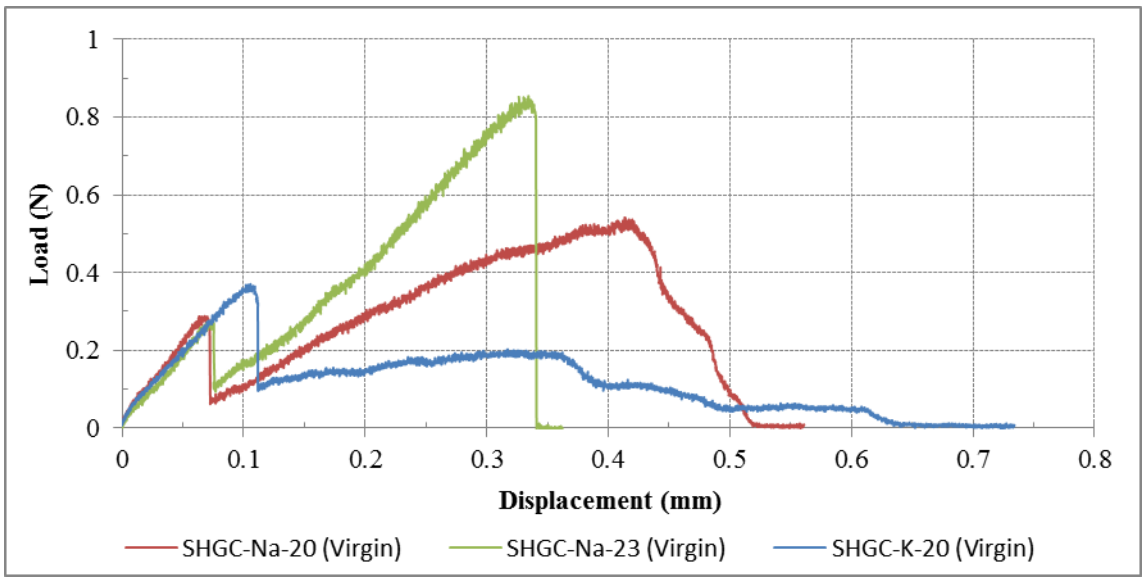

Figure 7-2: Typical load-displacement curves from single-fiber pullout tests using virgin (un-coated) PVA fiber

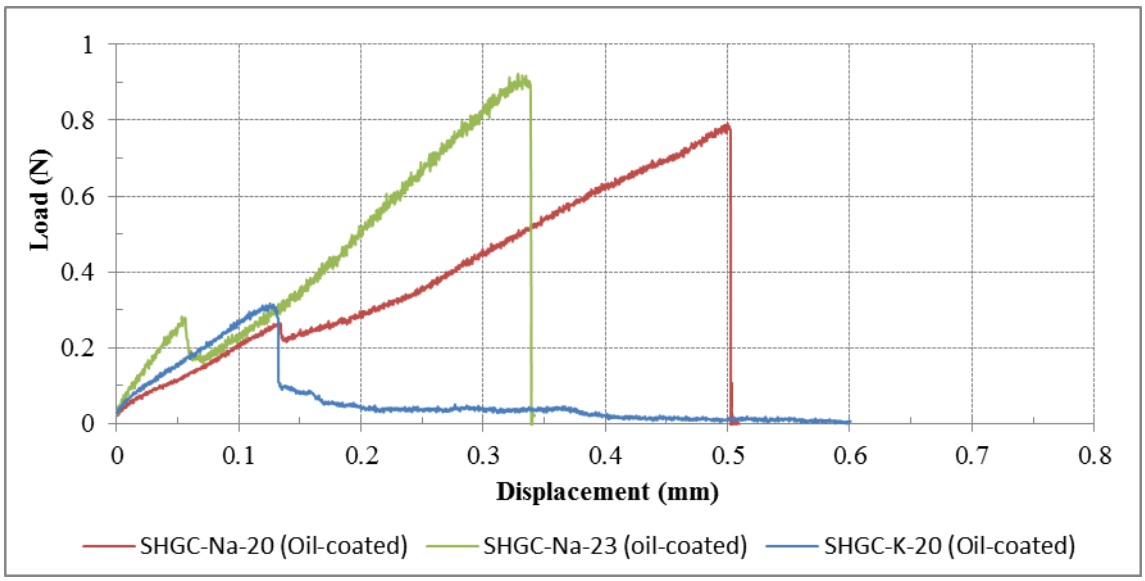

Figure 7-3: Typical load-displacement curves from single-fiber pullout tests using oil-coated (1.2 wt.%) PVA fiber

Table 7-4: Fiber-matrix interface properties using virgin (un-coated) PVA fibers

Mix ID	Chemical bond strength, G_d; (J/m^2)	Frictional bond strength, τ_0; (MPa)	Slip hardening coefficient, β
SHGC-Na-20	6.08±3.15	0.77±0.39	0.957±0.460
SHGC-Na-23	3.83±1.42	0.96±0.30	0.919±0.440
SHGC-K-20	8.89±3.48	0.80±0.35	0.380±0.250

Table 7-5: Fiber-matrix interface properties using oil-coated (1.2 wt.%) PVA fibers

Mix ID	Chemical bond strength, G_d; (J/m^2)	Frictional bond strength, τ_0; (MPa)	Slip hardening coefficient, β
SHGC-Na-20	1.31±1.05	1.30±0.77	0.499±0.295
SHGC-Na-23	0.59±0.67	1.73±0.51	0.463±0.200
SHGC-K-20	3.41±1.71	0.87±0.44	0.025±0.015

7.4.3.1 Effect of fiber surface oil coating on interface properties

As can be seen in Tables 7-4 and 7-5, the fiber surface oil coating had significant effects on the fiber-matrix interface properties of the developed fly ash-based SHGCs. The chemical bond strength and slip hardening coefficient of the oil-coated fiber were significantly lower than those of the virgin fiber. This trend is true in all fly ash-based SHGCs irrespective of the type of activator and W/GP solids of SHGC matrix. For instance in SHGC-Na-23, the chemical bond strength and slip hardening coefficient of the oil-coated fiber were 84% and 50%, respectively lower than those of the virgin fiber. It is interesting to note that the rate of reduction of the chemical bond strength due to the fiber surface oil coating was comparable in all fly ash-based SHGCs. However, the rate of reduction of the slip hardening coefficient in the K-based SHGC was significantly (about 2 times) higher than that of the Na-based SHGCs. As can be seen in Tables 7-4 and 7-5, in the K-based SHGC the slip hardening coefficient of the oil-coated fiber was 93% lower than that of the virgin fiber, whereas in the Na-based SHGCs the β of the oil-coated fiber was on average 49% lower than that of the virgin fiber.

In terms of the effect of fiber surface oil coating on the chemical bond strength, the trend observed in this study is similar to the previous observation in typical PVA-SHCC (Redon

et al., 2001; Li et al., 2002). Previous studies reported that the fiber surface oil coating can effectively reduce the hydrophilic nature of the PVA fibers, and hence reduce the interfacial chemical bond between the PVA fiber and the SHCC matrix (Redon et al., 2001). For instance, Redon et al. (2001) reported that in PVA-SHCC, the chemical bond strength of the oil-coated PVA fiber was 35% less than that of the virgin (un-coated) fiber. Fibers with hydrophilic nature such as PVA fibers generally exhibit strong chemical bond with the surrounding matrix (Kanda and Li, 1998). This high interface chemical bond is due to hydroxyl groups on the carbon backbone, which result in strong hydrophilic nature of the PVA fibers. The hydroxyl groups result in a strong hydrogen intermolecular bond, and hence lead to the high interfacial chemical bond between the PVA fiber and the matrix products (Kanda and Li, 1998; Akers et al., 1989).

On the other hand, the frictional bond strength of the oil-coated PVA fiber was higher than that of the virgin fiber. This trend is also true for all fly ash-based SHGCs, irrespective of the type of activator and W/GP solids of the SHGC matrix. It is interesting to note that in the Na-based SHGCs the rate of increase of the frictional bond strength due to the fiber surface oil coating was significantly (more than 8 times) higher than that of the K-based SHGC. As can be seen in Tables 7-4 and 7-5, in SHGC-Na-23 the τ_0 of the oil-coated fiber was 80% higher than that of the virgin fiber, whereas in SHGC-K-20 the τ_0 of the oil-coated fiber was only 9% higher than that of the virgin fiber. In terms of the effect of fiber surface oil coating on the frictional bond strength, the trend observed in this study is opposite to the previous observation in typical PVA-SHCC, in which fiber surface oil coating was reported to reduce the frictional bond strength of the PVA fibers (Redon et al., 2001; Li et al., 2002). For instance, Redon et al. (2001) reported that in PVA-SHCC, the frictional bond strength of the oil-coated fiber was 33% lower than that of the virgin fiber. It should be noted that in typical PVA-SHCC, debonding occurs along the fiber-matrix interface transition zone. In such scenario, the roughness of the new-formed interface, and hence the frictional bond is related to the chemical bond. As the fiber surface oil-coating reduces the chemical bond, the roughness of the new-formed interface, and thereby the frictional bond also decrease (Li et al., 2002).

In the developed fly ash-based SHGCs, however, two different types of debonding were observed. For the virgin PVA fiber in SHGC-Na-23 with very high chemical bond (G_d=3.83 J/m^2), as shown in Figure 7-4, the pulled-out fiber tip was severely scratched

and sharpened with a diameter of 20 to 35μm and no matrix debris can be seen on the surface of the virgin fiber. This was commonly believed to be caused by strong abrasion of soft fiber against hard matrix during slippage stage after complete debonding of the fiber from matrix, similar to those observed in virgin PVA-SHCC system (Li et al., 2002). However, such abrasion is generally associated with strong interface frictional bond, typically above 2 MPa (Li et al., 2002). In the current study, the interface frictional bond of the virgin PVA fiber in SHGC-Na-23 was much lower (τ_0=0.96 MPa), which suggests that the virgin fiber was not damaged during the slippage stage. It is plausible that the virgin PVA fiber may be weakened in the geopolymer matrix due to the presence of strong alkaline environment and may be damaged during the debonding stage when the tunnel crack propagates along the interface and branches into the virgin fiber, resulting in such delamination damage of fiber. In this scenario, the roughness of the new-formed interface, and thereby the frictional bond is no longer governed by the chemical bond, which indicates that the effect of fiber surface oil-coating is not truly reflected with τ_0. The delamination surface is relatively smooth as compared to the surface of the oil-coated fiber (Figure 7-5). This also explains low interface frictional bond of the virgin PVA-SHGC system. On the contrary, for the oil-coated PVA fiber in SHGC-Na-23 with low chemical bond (G_d=0.59 J/m^2), as shown in Figure 7-5, the pulled-out fiber tip is covered with matrix debris and its diameter is relatively un-changed as compared to the original fiber diameter (40μm). This suggests that tunnel crack propagates along the fiber-matrix interface transition zone and does not branch into the oil-coated fiber. Fiber surface oil coating may effectively protect the PVA fibers when they are in contact with strong alkaline solution in the geopolymer matrix.

In the current study, as can be seen in Tables 7-4 and 7-5, the slip-hardening coefficient of the virgin fibers was significantly higher than that of the oil-coated fibers. This trend is also true for all fly ash-based SHGCs, irrespective of the type of activator and W/GP solids of the SHGC matrix. The slip-hardening coefficient reflects the degree of friction enhancement during the fiber pullout (not the initial frictional bond τ_0), which results from the jamming effect at the new-formed interface (Redon et al., 2001). Virgin fibers induced more jamming effect probably because the scratched-off fibrils accumulated quickly between the fiber and the geopolymer matrix.

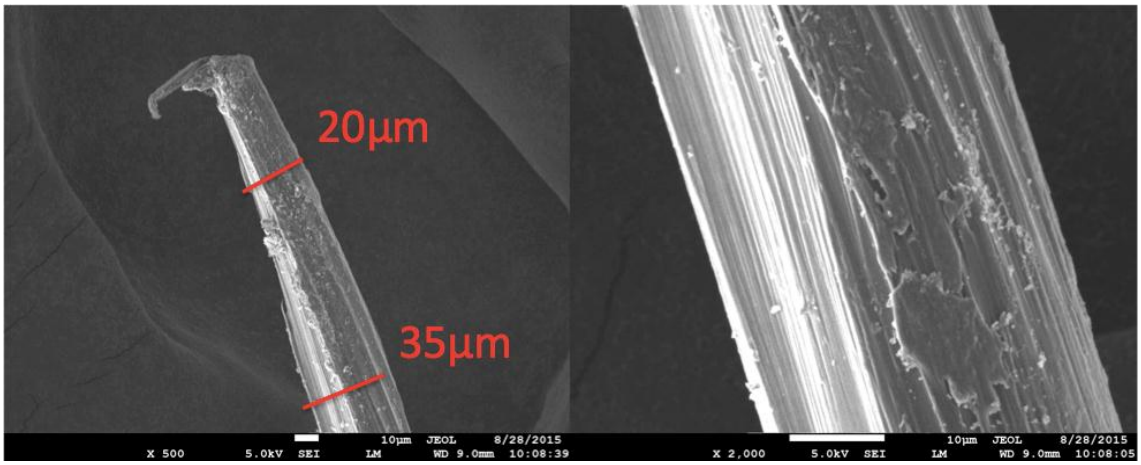

Figure 7-4: SEM images of SHGC-Na-23 using virgin PVA fiber

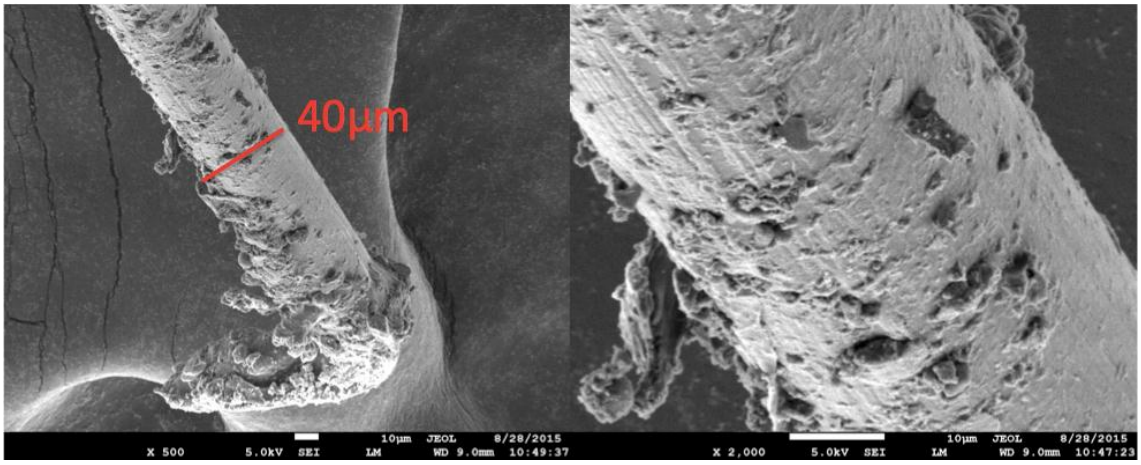

Figure 7-5: SEM images of SHGC-Na-23 using oil-coated PVA fiber

7.4.3.2 Effect of W/GP solids on interface properties

As can be seen in Tables 7-4 and 7-5, the increase of W/GP solids from 0.20 to 0.23 decreased the fiber-matrix interface chemical bond, but increased the interface frictional bond of the PVA fibers with the Na-based SHGC matrix. However, the increase in W/GP solids did not have any considerable effect on the slip hardening coefficient of the PVA fibers with the Na-based SHCG matrix. This trend is true for both virgin and oil-coated PVA fibers. For instance, the chemical bond strength of the oil-coated fiber in SHGC-Na-23 (Figure 7-5) was 55% lower, but its frictional bond strength was 33% higher than those of the oil-coated fiber in SHGC-Na-20 (Figure 7-6). The lower chemical bond in SHGC-Na-23 may be attributed to the higher W/GP solids (i.e. higher water content)

leading to a less densified matrix microstructure near the fiber. The higher W/GP solids also leads to lower pH and lower degree of geopolymerisation. As can be seen in Figures 7-5 and 7-6, different pulled-out fiber morphologies are observed for these two mixes. Despite both pulled-out fiber tips are covered with some matrix debris, the oil-coated fiber in SHGC-Na-23 is rougher than that of SHGC-Na-20, which explains its relatively higher frictional bond (1.73 MPa in SHGC-Na-23 compared to 1.30 MPa in SHGC-Na-20). As can be seen in Table 7-5, the slip-hardening coefficient of both mixes using oil-coated fiber was comparable, but significantly lower than that of the corresponding mixes using virgin fibers (Table 7-4). It is because for both mixes the debonding of the oil-coated fiber occurred along the fiber-matrix interface transition zone, and no significant jamming effect happened during fiber slippage. In terms of the effect of increase in W/GP solids on the frictional and chemical bond strengths, the trend observed in this study is opposite to the previous observation in typical PVA-SHCC, in which the increase in water to cement ratio (W/C) was reported to reduce the frictional bond strength of the PVA fibers, but the chemical bond strength was rather stable and not depended on the W/C of the SHCC matrix (Kanda and Li, 1998).

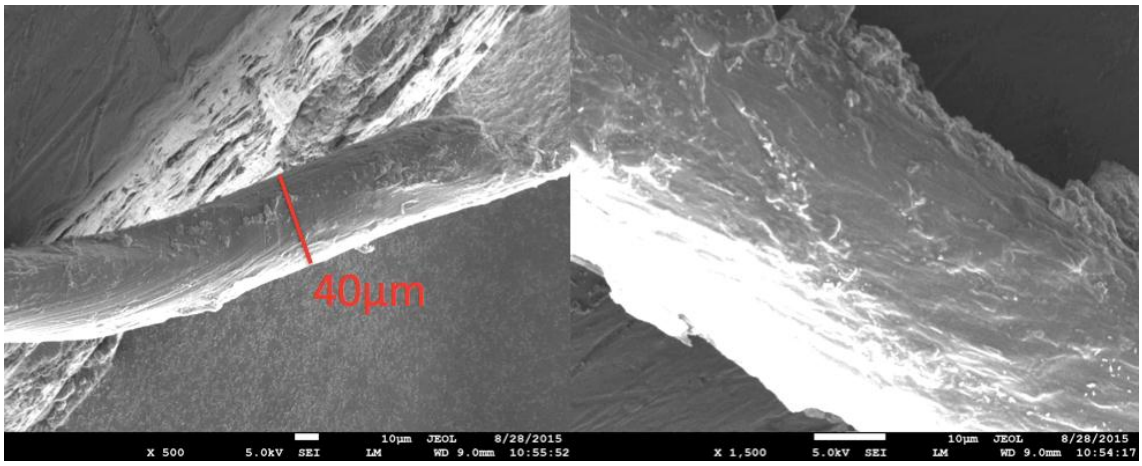

Figure 7-6: SEM images of SHGC-Na-20 using oil-coated PVA fiber

7.4.3.3 Effect of type of activator on interface properties

As can be seen in Tables 7-4 and 7-5, the type of activator had significant effects on the interface properties. The chemical bond strength of the PVA fibers with the Na-based SHGC matrix was lower than that of the K-based SHGC matrix. On the other hand, the

frictional bond strength and slip hardening coefficient of the PVA fibers with the Na-based SHGC matrix were higher than those of the K-based SHGC matrix. For instance, comparing SHGC-Na-23 and SHGC-K-20 with comparable compressive strength of the SHGC matrix, the chemical bond strength of the oil-coated fiber in SHGC-Na-23 was 83% lower than that of SHGC-K-20. On the other hand, the frictional bond and slip hardening coefficient of the oil-coated fiber in SHGC-Na-23 were significantly (about 2 times and more than 18 times, respectively) higher than those of the oil-coated fiber in SHGC-K-20. It should be noted that the similar trend was observed when comparing the interface properties of the oil-coated fibers in SHGC-Na-20 and SHGC-K-20 with constant W/GP solids of 0.20.

It can be said that the K-based activator significantly enhances the chemical bond between the PVA fiber and the SHGC matrix, similar to the effect of using virgin fiber (Section 7.4.3.1). As can be seen in Figures 7-5 and 7-7, surface morphology of the pulled-out fibers in SHGC-Na-23 and SHGC-K-20 is different. As mentioned in Section 7.4.3.1, in SHGC-Na-23 using oil-coated fiber (Figure 7-5), the pulled-out fiber tip is covered with matrix debris and its diameter is relatively un-changed as compared to the original fiber diameter (40μm). On the other hand, in SHGC-K-20 using oil-coated fiber (Figure 7-7), the pulled-out fiber tip was sharpened and the fiber surface was severely scratched, similar to that of the virgin fiber in SHGC-Na-23, as illustrated in Figure 7-4. This explains the significantly higher chemical bond strength of the oil-coated fiber in the K-based SHGC than the Na-based SHGCs. This may be attributed to greater attack of the K-based activator to the oil-coating agent on the surface of the PVA fiber. It has been reported that KOH solution can penetrate in oil molecules faster than NaOH solution due its higher alkalinity and solubility in water (Diphare and Muzenda, 2013). As a result, it is believed that KOH breaks the oil coating agent on the fiber surface quicker (Diphare and Muzenda, 2013), which causes the increase of chemical bond. Without the protection from the surface oil coating, oil-coated PVA fiber in the K-based SHGC matrix may also be weakened due to strong alkalinity of the matrix, and delamination damage of the fiber during debonding may occur, which results in the decrease of interface frictional bond, as shown in Table 7-5. As can be seen in Figure 7-7, the delamination surface of the oil-coated fiber in SHGC-K-20 is relatively smooth as compared to the surface of the oil-coated fiber in SHGC-Na-23 (Figure 7-5). This also explains the low interface frictional bond of the oil-coated fiber in the K-based SHGC than the Na-based SHGCs.

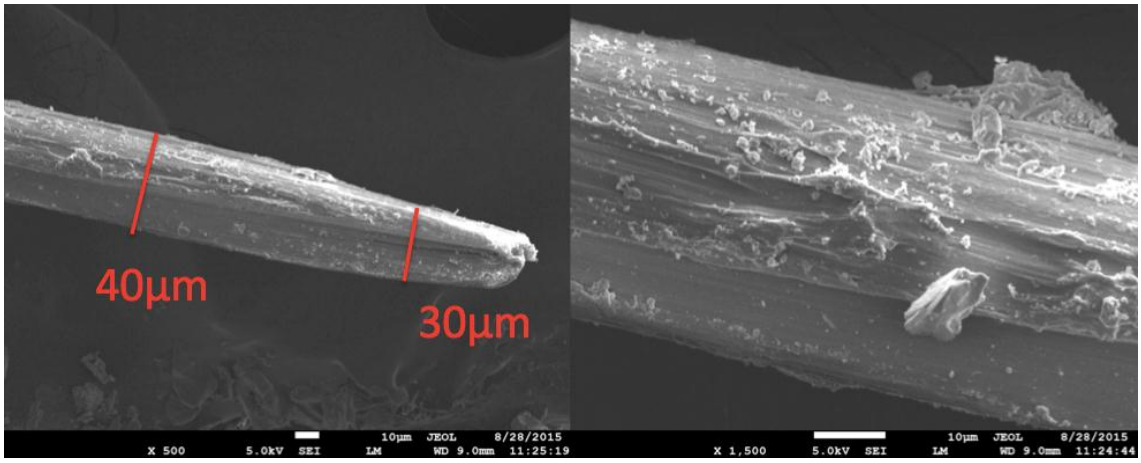

Figure 7-7: SEM images of SHGC-K-20 using oil-coated PVA fiber

It should be pointed out that the chemical bond strength of the virgin PVA fiber in SHGC-K-20 was also higher than that of the Na-based SHGCs. According to Kanda and Li (1998), the interfacial chemical bond of the PVA fiber with the matrix is primarily determined by the matrix chemistry and surface chemistry of the fiber. Therefore, the higher chemical bond of the virgin PVA fiber with the K-based SHGC matrix could be attributed to the geopolymer chemistry (microstructure) of the K-based SHGC matrix compared to that of the Na-based SHGC matrix, because the type of PVA fiber was identical in all mixes. As mentioned in Sections 7.4.1 and 7.4.2, the geopolymer microstructure of the Na-based and K-based SHGC matrices are different, due to their different type of activator. It is plausible that there may be a higher chemical adhesion between the K-based geopolymer matrix and the OH group on the surface of the virgin PVA fiber, resulting in its higher chemical bond strength.

7.4.4 Uniaxial tensile performance

The uniaxial tensile stress–strain curves of each mixture were adopted from previous sections in Chapters 4 and 5 and re-presented in Figures 7-8 to 7-10 for ease of comparison. As can be seen, all fly ash-based SHGCs, irrespective of the type of activator and W/GP solids demonstrated PSH behavior. The uniaxial tension test results of each mixture were adopted from previous sections in Chapters 4 and 5 and re-presented in Table 7-6 for ease of comparison. As can be seen, the type of activator had a significant effect on the uniaxial tensile behavior of fly ash-based SHGC. The Na-based SHGCs, irrespective of the W/GP solids, exhibited superior tensile performance to the K-based

SHGC. Comparing SHGC-Na-23 and SHGC-K-20 with comparable matrix compressive strength, the first-crack strength, ultimate tensile strength and tensile strain capacity of SHGC-K-20 were 52%, 58% and 33%, respectively lower than those of SHGC-Na-23. It should be noted that similar pattern was observed when comparing SHGC-Na-20 and SHGC-K-20 with constant W/GP solids. The lower first-crack strength of SHGC-K-20 corresponds to the lower fracture toughness of the K-based SHGC matrix, as reported in Table 7-3 (Li et al., 2001). The lower ultimate tensile strength of SHGC-K-20 is due to the significantly lower τ_0 and β of the oil-coated PVA fiber with the K-based SHGC matrix, as reported in Table 7-5, which led to its inferior fiber-bridging strength (Lee et al., 2012).

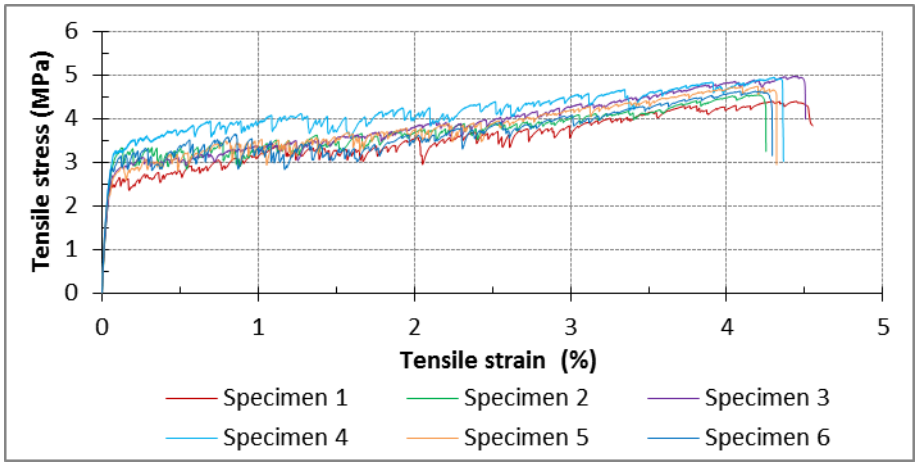

Figure 7-8: Tensile stress-strain responses of SHGC-Na-20

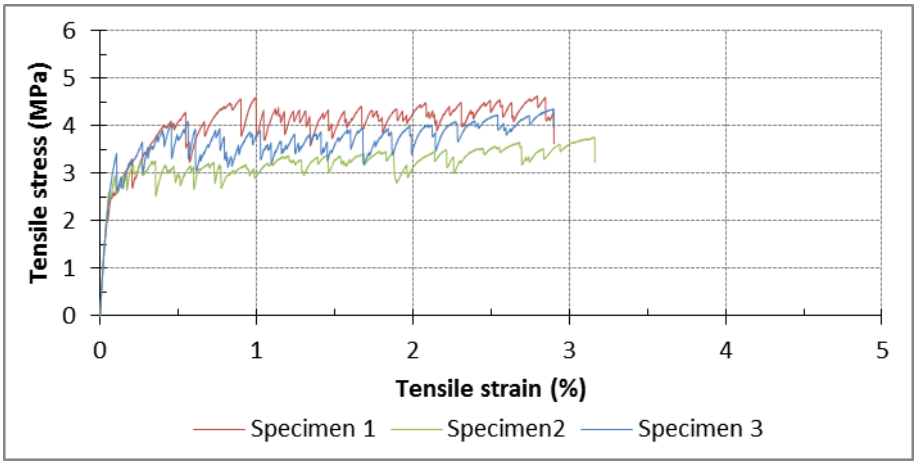

Figure 7-9: Tensile stress-strain responses of SHGC-Na-23

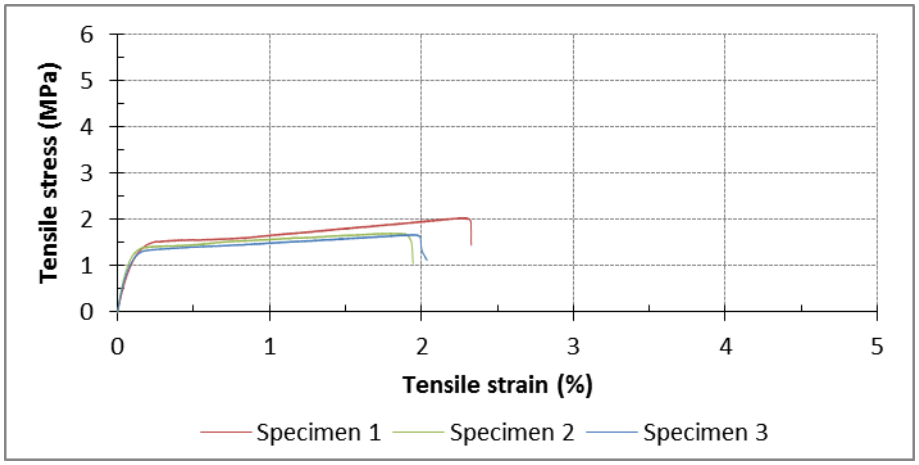

Figure 7-10: Tensile stress-strain responses of SHGC-K-20

Table 7-6: Uniaxial tension test results

Mix ID	First-crack strength, σ_{fc}; (MPa)[1]	Ultimate tensile strength, σ_{cu}; (MPa)	Tensile strain capacity, ε_{cu}; (%)
SHGC-Na-20	3.2 ± 0.21	4.7 ± 0.25[a]	4.3 ± 0.14[a]
SHGC-Na-23	2.8 ± 0.40	4.3 ± 0.45[b]	3.0 ± 0.19[b]
SHGC-K-20	1.4 ± 0.062	1.8 ± 0.21[a]	2.0 ± 0.26[a]

[a] Test results adopted from Chapter 4.

[b] Test results adopted from Chapter 5.

The underlying reasons for the lower tensile strain capacity of SHGC-k-20 could be explained in terms of the two PSH performance indices, namely stress-performance index (σ_0 / σ_{fc}) and energy-performance index (J_b' / J_{tip}), proposed by Kanda and Li (2006). The two PSH performance indices should be determined from the crack bridging relation of the composite. In this research, the micromechanics-based model developed by Yang et al. (2008) was used to compute the fiber-bridging constitutive law σ(δ) of fly ash-based SHGCs. The applicability of this micromechanics-based model to evaluate the tensile performance of SHGCs is demonstrated in Chapter 8. The resulting PSH performance indices are plotted in Figure 7-11. As can be seen, in all fly ash-based SHGCs both PSH performance indices are greater than. Thereby, it can be concluded that the necessary strength-based and energy-based conditions of steady-state flat crack propagation which result in sequential multiple cracking of geopolymer matrix are satisfied. Therefore, all fly ash-based SHGCs investigated in this study exhibited PSH behavior. In addition, as

can be seen in Figure 7-11, the PSH strength and energy indices of SHGC-K-20 were considerably lower than those of the Na-based SHGCs. As a result, it is not surprising that SHGC-K-20 with lower PSH performance indices exhibited inferior tensile ductility than that of the Na-based SHGCs.

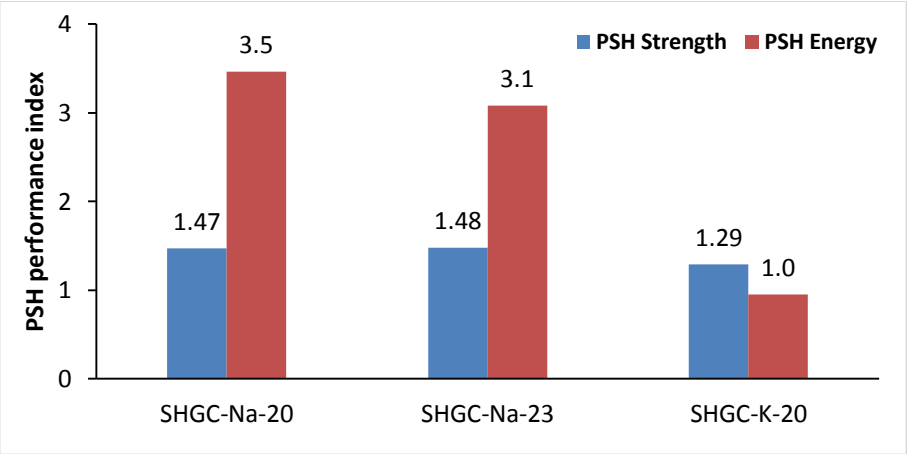

Figure 7-11: PSH performance indices of fly ash-based SHGCs

With regards to the influence of the W/GP solids on the tensile performance of the composite, as can be seen in Table 7-6, SHGC-Na-20 with lower W/GP solids exhibited superior tensile performance to SHGC-Na-23. The tensile strain capacity of SHGC-Na-20 was 43% higher than that of SHGC-Na-23. Similar to the above discussion, the reasons for the superior tensile ductility of SHGC-Na-20 could also be elucidated based on the two PSH performance indices. As can be seen in Figure 7-11, while the PSH strength index of SHGC-Na-20 and SHGC-Na-23 is comparable, the PSH energy index of SHGC-Na-20 is higher than that of SHGC-Na-23, which results in greater probability of saturated PSH behavior, and thereby higher tensile ductility of SHGC-Na-20.

The typical crack pattern in each mixture was adopted from previous sections in Chapters 4 and 5 and re-presented in Figure 7-12 for ease of comparison. As can be seen, enormous number of cracks with almost equal crack spacing ranging from 2.5 mm to 3.5 mm was observed in the Na-based SHGC specimens. The saturated multiple cracking behavior observed in the Na-based SHGC specimens corresponds to their superior tensile strain capacities, as reported in Table 7-6. The number of cracks on the surface of the SHGC-Na-20 specimen was more than that of the SHGC-Na-23 specimen corresponding to its

higher tensile strain capacity. In contrast, the lowest number of cracks with un-even spacing ranging from 4-11 mm was observed in the K-based SHGC specimen. The unsaturated multiple cracking behavior observed in the K-based SHGC specimen corresponds to its inferior tensile strain capacity, as reported in Table 7-6.

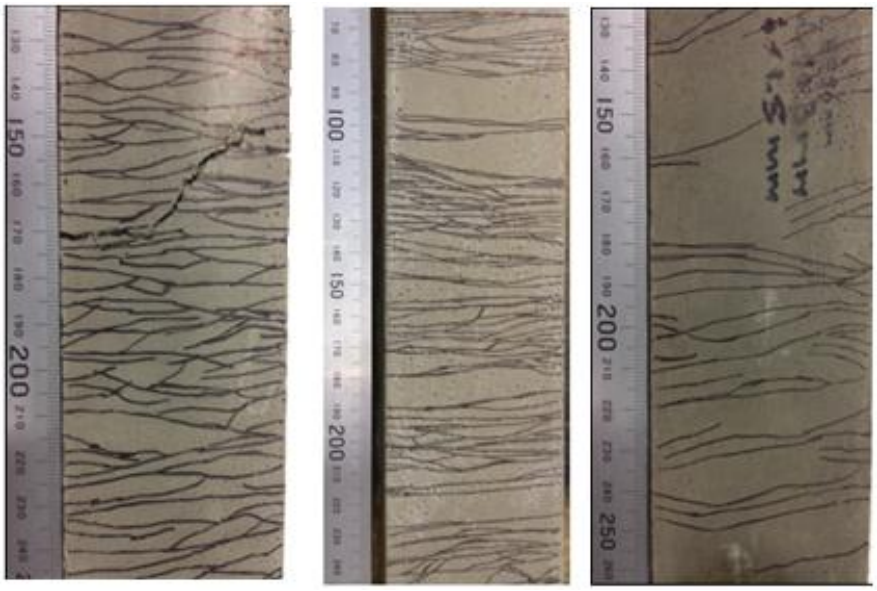

(a) (b) (c)

Figure 7-12: Typical multiple cracking pattern of (a) SHGC-Na-20 and (b) SHGC-Na-23 and (c) SHGC-K-20

7.5 Summary and Conclusions

A detailed micromechanics-based analysis of the fly ash-based SHGCs was performed in this chapter to determine the micro-scale fiber-matrix interface properties, which explain the experimentally observed macroscopic tensile performance of these cement-less composites. The following conclusions are drawn:

1) (a) The chemical bond and slip hardening coefficient between the oil-coated PVA fiber and the geopolymer matrix were significantly lower than those of the virgin (un-coated) fiber. (b) On the other hand, the frictional bond between the oil-coated fiber and the geopolymer matrix was higher than that of the virgin fiber. The behaviors (a) and (b) are true irrespective of the type of activator and water to geopolymer solids (W/GP solids) ratio. However, when compares to cement-based matrix, (a) is the same, but (b) is the opposite.

It is hypothesized that the virgin PVA fiber with very high chemical bond may be weakened in the geopolymer matrix due to the presence of strong alkaline environment and may be damaged during the debonding stage when the tunnel crack propagates along the interface and branches into the virgin fiber, resulting in delamination damage of fiber. The SEM images of the typical pulled-out fiber supported this hypothesis. The delamination surface of the pulled-out virgin fiber was relatively smooth as compared to the surface of the oil-coated fiber, which explains the low interface frictional bond of the virgin PVA-SHGC system.

On the contrary, for the oil-coated PVA fiber in the Na-based SHGC with low chemical bond, the pulled-out fiber tip is covered with matrix debris and its diameter is relatively un-changed as compared to the original fiber diameter. This suggests that, similar to PVA-SHCC, tunnel crack propagates along the fiber-matrix interface transition zone and does not branch into the oil-coated fiber. Fiber surface oil coating may effectively protect the PVA fibers when they are in contact with strong alkaline solution in the Na-based geopolymer matrix.

2) The fiber surface oil-coating does not provide much benefit when used with the K-based activator compared to the Na-based activator. The chemical bond of the oil-coated fiber in the K-based SHGC was considerably higher than that of the Na-based SHGCs. It can be said that the K-based activator significantly enhances the chemical bond between the PVA fiber and the geopolymer matrix, similar to the effect of using virgin fiber, which may result in delamination damage of the fiber during the debonding stage. On the other hand, the frictional bond and slip hardening coefficient of the oil-coated fiber in the K-based SHGC were considerably lower than those of the Na-based SHGCs, due to the relatively smooth delamination surface of the fiber.

3) The decrease in W/GP solids resulted in an increase in the chemical bond, but a decrease in the frictional bond of the PVA fiber with the Na-based geopolymer matrix. However, the slip hardening coefficient was relatively stable, independent of the W/GP solids ratio. This trend is true for both virgin and oil-coated PVA fibers. This is not the case in cement-based matrix, where the decrease in water to cement ratio (W/C) was reported to increase the frictional bond strength of the PVA fibers, but the chemical bond strength was relatively stable, independent of W/C.

4) Uniaxial tension test results indicated that the Na-based SHGCs exhibited superior tensile performance to the K-based SHGC, in spite of the higher fracture toughness of the Na-based SHGC matrix. This is due to the significantly higher complementary energy of the Na-based SHGCs, resulted from their beneficial fiber-matrix interface properties. In addition, the Na-based geopolymer matrix with lower W/GP solids enhanced the composite tensile ductility, due to the significant increase of the complementary energy of the composite, in spite of the increase of the matrix toughness.

5) The experimentally observed macroscopic composite tensile ductility corresponded well with the two PSH performance indices of the composite calculated based on the computed crack bridging relation of the fly ash-based SHGCs. It was found that the two PSH performance indices of the Na-based SHGCs were considerably higher than those of the K-based SHGC, thus providing a rational basis for the observed superior tensile performance of the Na-based SHGCs.

6) In summary it is concluded that the Na-based geopolymer matrix has advantageous properties in terms of the lower cost, higher compressive strength and fracture toughness, lower chemical bond, higher frictional bond and slip hardening coefficient with the PVA fibers, and thereby superior composite tensile performance compared to the K-based geopolymer matrix.

7.6 References

AKERS, S. A. S., STUDINKA, J. B., MEIER, P., DOBB, M. G., JOHNSON, D. J. & HIKASA, J. 1989. Long term durability of PVA reinforcing fibres in a cement matrix. *International Journal of Cement Composites and Lightweight Concrete,* 11, 79-91.

DIPHARE, M. & MUZENDA, E. 2013. Influence of Solvents on the Extraction of Oil from Waste Lubricating Grease: A Comparative Study. *2nd International Conference on Agricultural, Environment and Biological Sciences (ICAEBS'2013)*, Pattaya, Thailand.

FERNÁNDEZ-JIMÉNEZ, A. & PALOMO, A. 2005. Composition and microstructure of alkali activated fly ash binder: effect of the activator. *Cement and concrete research,* 35, 1984-1992.

KANDA, T. & LI, V. C. 1998. Interface property and apparent strength of high-strength hydrophilic fiber in cement matrix. *Journal of materials in civil engineering,* 10, 5-13.

KANDA, T. & LI, V. C. 2006. Practical design criteria for saturated pseudo strain hardening behavior in ECC. *Journal of advanced concrete technology,* 4, 59-72.

LI, V. C., WANG, S. & WU, C. 2001. Tensile strain-hardening behavior of polyvinyl alcohol engineered cementitious composite (PVA-ECC). *Materials Journal*, 98, 483-492.

LI, V. C., WU, C., WANG, S., OGAWA, A. & SAITO, T. 2002. Interface tailoring for strain-hardening polyvinyl alcohol-engineered cementitious composite (PVA-ECC). *Materials Journal*, 99, 463-472.

PAN, Z., SANJAYAN, J. G. & RANGAN, B. V. 2011. Fracture properties of geopolymer paste and concrete. *Magazine of concrete research*, 63, 763-771.

QIU, J. & YANG, E.-H. 2015. Micromechanics-based Study on Fatigue Failure of Engineered Cementitious Composites. *In: REINHARDT, H. W., ed. 7th RILEM Workshop on High Performance Fiber Reinforced Cement Composites*, Stuttgart, Germany.

RANADE, R. 2014. *Advanced cementitious composite development for resilient and sustainable infrastructure.* Ph.D., University of Michigan.

REDON, C., LI, V. C., WU, C., HOSHIRO, H., SAITO, T. & OGAWA, A. 2001. Measuring and modifying interface properties of PVA fibers in ECC matrix. *Journal of Materials in Civil Engineering*, 13, 399-406.

YANG, E.-H., WANG, S., YANG, Y. & LI, V. C. 2008. Fiber-bridging constitutive law of engineered cementitious composites. *Journal of advanced concrete technology,* 6, 181-193.

CHAPTER 8

MICROMECHANICS-BASED MODELLING AND OPTIMIZATION OF FLY ASH-BASED SHGCS

Note: This chapter is based on the manuscript "*Micromechanics Constitutive Modelling and Optimization of Strain Hardening Geopolymer Composite*", by **Nematollahi, B.**, Qiu, J., Yang, E-H., and Sanjayan, J., Accepted to be published in ***Ceramics International***, 2017.

8.1 Introduction

The results presented in the previous chapters demonstrated that the developed fly ash-based SHGC is highly promising as a sustainable alternative to typical SHCC. This is because the mechanical properties of the developed fly ash-based SHGC is comparable or superior to typical SHCC, yet its environmental footprints is significantly less than that of typical SHCC. The material sustainability evaluation results presented in Chapter 6 indicated that the developed fly ash-based SHGC offers 52% less carbon emissions and 17% less energy consumption compared to typical SHCC M45.

Although the cost of PVA fiber is considerably lower than that of high strength and high modulus PE fiber (Li et al., 2001), but the cost of oil-coated PVA fibers is still relatively high compared to other synthetic fibers. Therefore, it is essential and beneficial to understand how fly ash-based SHGCs can be designed to achieve optimal composite performance with the lowest volume fraction of the PVA fibers, and thereby the lowest cost. So far, several design models based on micromechanics have been proposed for design and optimization of SHCCs (Li and Leung, 1992; Lin et al., 1999; Yang et al., 2008). These micromechanics-based models link composite properties to material microstructures including fiber, matrix and interface. They can be used as powerful analytical tools to tailor the material constituents (Li et al., 2001). The first objective of this research is to verify applicability of the micromechanics model developed by Yang et al. (2008) for tensile performance evaluation of fly ash-based SHGCs. Subsequently, the second objective is using this model to address optimal mix composition of matrix, fiber and interface properties to achieve robust tensile ductility with minimum volume fraction of PVA fibers.

In the following sections, at first, the essence of fiber-bridging constitutive law and micromechanics-based modelling in randomly oriented short fiber-reinforced brittle matrix composite are reviewed. The fly ash-based SHGC-Na-20 mixture presented in Chapter 7 was selected as the benchmark in this study. The micromechanical parameters of the developed composite such as matrix fracture properties and fiber-matrix interface properties (reported in Chapter 7) were used as input parameters in the micromechanical model to compute crack bridging $\sigma(\delta)$ relation (the fiber-bridging constitutive law) of the composite. The computed $\sigma(\delta)$ relation of the composite was then compared with the uniaxial tension test results of the developed composite (reported in Chapter 7) to verify the applicability of the micromechanics-based model. Finally, it is demonstrated how this model guides towards composite optimization and component tailoring to achieve saturated strain hardening behavior with the lowest amount of PVA fiber.

8.2 Fiber-bridging constitutive law and micromechanics-based modelling of randomly oriented short fiber reinforced brittle matrix composite

The relationship between the fiber bridging stress (σ) transferred across a matrix crack and the opening of that crack (δ) can be expressed in terms of the fiber-bridging constitutive law $\sigma(\delta)$ of the composite (Yang et al., 2010). Understanding the $\sigma(\delta)$ relationship is of primary importance in development of strain hardening composite. It is because on one hand the $\sigma(\delta)$ relationship relates to material microstructure (micro-scale), and on the other hand governs the composite tensile performance (macro-scale) (Yang et al., 2010). The $\sigma(\delta)$ relationship is derived by using analytical tools of fracture mechanics, micromechanics, and probabilistics (Yang et al., 2010). The $\sigma(\delta)$ of the composite is expressed as a function of matrix, fiber and interface related micromechanical parameters.

The micromechanical parameters related to the fiber include fiber length (L_f), diameter (d_f), elastic modulus (E_f), tensile strength (σ_{fu}) and volume fraction (V_f). Matrix fracture toughness (K_m) and elastic modulus (E_m) are considered as the matrix-related micromechanical parameters. The fiber-matrix interface is characterized in terms of frictional bond strength (τ_0), chemical bond strength (G_d), slip-hardening coefficient (β), snubbing coefficient (f) and fiber strength reduction factor (f'). Frictional bond strength quantifies the interface friction force at the onset of fiber slippage. Chemical bond strength describes the fracture energy required for chemical debonding of the fiber from

surrounding matrix (Yang et al., 2010). Slip-hardening coefficient is to characterize the fiber sliding behavior, which can be either slip-hardening, constant friction or slip-softening (Yang et al., 2010). Snubbing coefficient is introduced to account for fiber orientation effect on the fiber pullout load (Li et al., 1995). The load needed to pull out an inclined fiber from a matrix crack can be higher than that of a straight fiber (with zero inclination). The increase in pullout load is attributed to the additional frictional snubbing force and the bending of the fiber at the corner of exit from the matrix (Li et al., 1990). Fiber strength reduction factor is introduced to account for reduction of fiber strength when pulled out at an inclined angle, which can be attributed to fiber surface abrasion, spalling of the matrix foundation and fiber bending, all of which are intensified with higher inclination angles (Kanda and Li, 1998). It has been reported that hydrophilic fibers, even with no inclination, exhibit lower tensile strength in a pulled-to-rupture test when embedded in a matrix than in the standard fiber strength test (i.e. the fixed-end strength test). In other words, the in-situ tensile strength of fiber embedded in a matrix (apparent fiber strength) is lower than the nominal strength of the fiber reported by the manufacturer (Kanda and Li, 1998).

Several micromechanics-based models have been developed so far to compute the $\sigma(\delta)$ relationship in brittle matrix composites reinforced with randomly oriented short fibers (Li and Leung, 1992; Lin et al., 1999). The micromechanics-based models quantify the synergistic interaction among fiber, matrix and interface and link the micromechanical parameters to the composite performance (Li et al., 2001). Yang et al. (2008) developed an analytical micromechanical model on the basis of the previous simplified model (Lin et al., 1999) with special focus on PVA-SHCC system, where the composite exhibits two-way fiber debonding-pullout, due to slip hardening behavior of the PVA fiber during the slippage regime. The accuracy of the crack opening prediction has been improved in Yang et al. (2008) model by considering a new mechanism of fiber-matrix interactions including fiber two-way debonding and pullout, matrix micro-spalling, and Cook-Gordon effect. In this regard, Yang et al. (2008) modelled two-way pullout behavior of a single PVA fiber from a matrix crack plane. Subsequently, the contributions of all PVA fibers with different embedment length and orientation across the crack plane were averaged to derive the fiber-bridging constitutive law of the composite. Probabilistics was introduced to account for the randomness of fiber location and orientation with respect to a crack plane (Yang et al., 2010). Details of the micromechanical analysis and the flow chart of

the numerical procedure to compute the σ(δ) relationship of typical PVA-SHCC can be found in Yang et al. (2008).

8.3 Comparison of model predictions with uniaxial tension test results

The micromechanical parameters used in the micromechanics-based model to calculate the fiber-bridging constitutive law σ(δ) of the developed fly ash-based SHGC-Na-1 are listed in Table 8-1. The fiber-related parameters reported in this table were adopted from Table 4-2 in Chapter 4. The interface-related and matrix-related parameters reported in this table were adopted from SHGC-Na-20 mixture in Tables 7-5 and 7-3 in Chapter 7, respectively. Following Yang et al. (2008), the value of snubbing coefficient is assumed to be f = 0.2. The value of strength reduction factor (f'= 0.21) was determined through single-fiber pullout test.

Table 8-1: Micromechanical parameters used in computing σ(δ) curve and model predictions against uniaxial tension test results

Fiber-related parameters	V_f (vol.%)	2	
	d_f (μm)	39	
	L_f (mm)	8	
	E_f (GPa)	41	
	σ_{fu} (MPa)	1070	
Interface-related parameters	G_d (J/m^2)	1.31	
	τ_0 (MPa)	1.30	
	β	0.499	
	f	0.20	
	f'	0.21	
Matrix-related parameter	E_m (GPa)	9.8	
	K_m (MPa.m$^{1/2}$)	0.436	
	J_{tip} (J/m^2)	19.4	
Model predictions	Fiber orientation	2D	3D
	σ_0 (MPa)	6.1	4.7
	δ_0 (μm)	125	99
	J_b' (J/m^2)	155.8	100.4
PSH indices	PSH energy (J'_b/J_{tip})	8.03	5.18
	PSH strength (σ_0/σ_{fc})	1.91	1.47
Exp. / Theo.	σ_0	0.77	1.00
	δ_0	0.95	1.20

Figure 8-1 presents the computed fiber bridging constitutive law σ(δ) of the developed fly ash-based SHGC with both 2D and 3D fiber orientation assumptions. The 3D fiber orientation assumption is applicable when all dimensions of the coupon specimen are greater than three times the fiber length. However, if the thickness of the specimen is less than the fiber length, fibers are more likely distributed in a 2D randomness manner (Yang et al., 2008). In this study, the fiber orientation is likely to be between 2D and 3D, as the thickness of the coupon specimen (=10−12 mm) is greater than the fiber length (= 8 mm), but less than 3 times the fiber length. The ultimate tensile strength and the corresponding crack opening measured experimentally from the uniaxial tension tests are also plotted in Figure 8-1 for comparison purpose. As can be seen, the peak point of the uniaxial tension test results (σ_{peak}^{test} = 4.7 MPa and δ_{peak}^{test} = 119 μm) are in good agreement with the peak points of the predicted σ(δ) curves. As a result, the applicability of the micromechanics-based model developed by Yang et al. (2008) in evaluating the tensile performance of the fly ash-based SHGC is therefore confirmed.

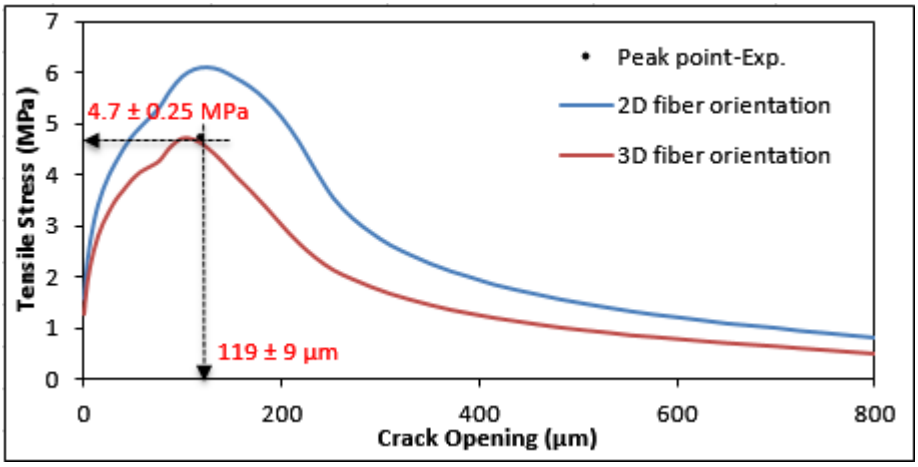

Figure 8-1: Comparison of σ(δ) relation between model prediction and uniaxial tension test result

The model predictions including the maximum fiber bridging stress σ_0 and its corresponding deflection δ_0, along with the ratio of the experimental to theoretical σ_0 and δ_0 are also presented in Table 8-1. As can be seen, the ratio of the experimental to the theoretical σ_0 was dependent on the fiber orientation assumption. In the case of 3D fiber orientation assumption, the predicted σ_0 was remarkably consistent with the ultimate tensile strength measured experimentally from the uniaxial tension tests ($\sigma_{peak}^{test} = \sigma_{peak}^{model}$

= 4.7 MPa). However, when 2D fiber orientation was assumed, the model overestimated the σ_0 by 23%. Similar results were reported by Yang et al. (2008) regarding the micromechanics-based modelling of typical SHCC. This inconsistency can be interpreted as follows. Multiple crack surfaces are generated during the strain hardening stage of the composite in uniaxial tension test. It is clear that the final failure plane is the one with the weakest bridging capacity (the lowest tensile strength capacity). In other words, damage localization in the composite takes place as soon as the weakest bridging plane reaches its peak bridging stress. Similar to typical SHCC, material inhomogeneity in fly ash-based SHGC is unavoidable; thereby the experimentally measured σ_{peak}^{test} = 4.7 MPa, actually represents the lowest peak fiber-bridging stress, which is 23% less than the estimated peak bridging stress (6.1 MPa). This is likely due to varying number of bridging fibers from one crack plane to another (Yang et al., 2008).

As can be seen in Table 8-1, the ratio of the experimental to the theoretical δ_0 was also dependent on the fiber orientation assumption. In the case of 3D fiber orientation assumption, the model underestimated the δ_0 by about 20%. However, when 2D fiber orientation was assumed, the predicted δ_0 (δ_0^{model} = 125 μm) was well consistent with the crack opening corresponding to ultimate tensile strength measured experimentally from the uniaxial tension tests (δ_0^{test} = 119 μm). The accuracy of the crack opening prediction with 3D fiber orientation assumption could be improved by considering the matrix spalling and Cook-Gordon effect (Yang et al., 2008).

As can be seen in Table 8-1, the PSH performance indices of the developed fly ash-based SHGC were also calculated based on the predicted complementary energy and peak bridging stress of the composite. Kanda and Li (2006) demonstrated experimentally that the PSH strength and energy indices greater than 1.3 and 2.7, respectively ensure saturated PSH behavior in typical PVA-SHCC. The PSH strength and energy performance indices of the developed composite were greater than 1.47 and 5.18, respectively. Thereby, it is not surprising that the developed cement-less composite exhibited saturated PSH behavior with very high tensile strain capacity (4.3%).

8.4 Optimization of fly ash-based PVA-SHGC by means of the micromechanical model

In the previous section, the applicability of the existing micromechanics-based model developed by Yang et al. (2008) to design fly ash-based SHGCs is confirmed. In this section, the focus is placed on illustration of how that micromechanical model can be used for systematic optimization of the fly ash-based PVA-SHGCs to achieve optimal composite tensile performance with the lowest volume fraction of PVA fibers. In this regard, a parametric study was performed using the verified model to evaluate the effects of fiber length, fiber surface oil-coating, and matrix fracture toughness (J_{tip}) on the critical volume fraction of fibers (V_{crit}^{f}). V_{crit}^{f} is the minimum volume fraction of fiber required to achieve saturated multiple cracking and tensile strain hardening behavior in the composite. The micromechanical parameters used for calculating V_{crit}^{f} graphs are summarized in Table 8-2. Following Kanda and Li (2006), the PSH strength index = 1.3 and PSH energy index = 2.7 were used in the following calculations to ensure saturated PSH behavior in fly ash-based PVA-SHGC.

Figure 8-2 shows the V_{crit}^{f} as a function of τ_0 for the virgin-short PVA fiber composite (V-S system) assuming 2D fiber orientation. The two curves shown in Figure 8-2-(a) were plotted by using all other micromechanical parameters given in Table 8-2 and plugging them into the energy-based condition and strength-based condition for the PSH behavior. As can be seen in Figure 8-2-(a), the V_{crit}^{f} computed from the strength-based condition sharply increases at the low τ_0 end ($\tau_0 < 0.6$ MPa), whereas it decreases when τ_0 increases and it almost approaches a constant value when $\tau_0 > 3.0$ MPa. Fiber-bridging strength depends on fiber volume fraction, fiber strength and fiber-matrix interfacial properties (Yang and Li, 2010). Fiber pullout prevails over fiber rupture when frictional bond is low; thereby the fiber-bridging strength is insensitive to the fiber strength and is governed by fiber volume fraction and τ_0. Therefore, high fiber volume fraction is needed to satisfy the strength-based condition (σ_0=5.85 MPa). On the other hand, when τ_0 increases, fiber rupture dominates over fiber pullout, and hence the fiber-bridging strength would be insensitive to τ_0. Since the fiber strength is known, the fiber volume fraction thereby approaches a constant value in order to meet the strength-based condition.

Table 8-2: Micromechanical parameters used in computing critical fiber volume of fly ash-based PVA-SHGC

Designation		V-S*	O-S#	O-L&	O-S-(low J_{tip})@
Fiber-related parameters	d_f (μm)	39	39	39	39
	L_f (mm)	8	8	16	8
	E_f (GPa)	41	41	41	41
	σ_{fu} (MPa)	1070	1070	1070	1070
Interface-related parameters	G_d (J/m^2)	6	1.5	1.5	1.5
	β	0.5	0.5	0.5	0.5
	f	0.20	0.20	0.20	0.20
	f'	0.21	0.21	0.21	0.21
Matrix-related parameter	E_m (GPa)	10	10	10	10
Energy-based condition	J_{tip} (J/m^2)	15	15	15	10
	J_b' (J/m^2)	40.5	40.5	40.5	27
Strength-based condition	σ_{fc} (MPa)	4.5	3.5	3.5	2.5
	σ_0 (MPa)	5.85	4.55	4.55	3.25

* V-S denotes virgin-short PVA-SHGC.

O-S denotes oil coated-short PVA-SHGC.

& O-L denotes oil coated-long PVA-SHGC.

O-S-(low J_{tip}) denotes oil coated-short PVA-SHGC with a low J_{tip}.

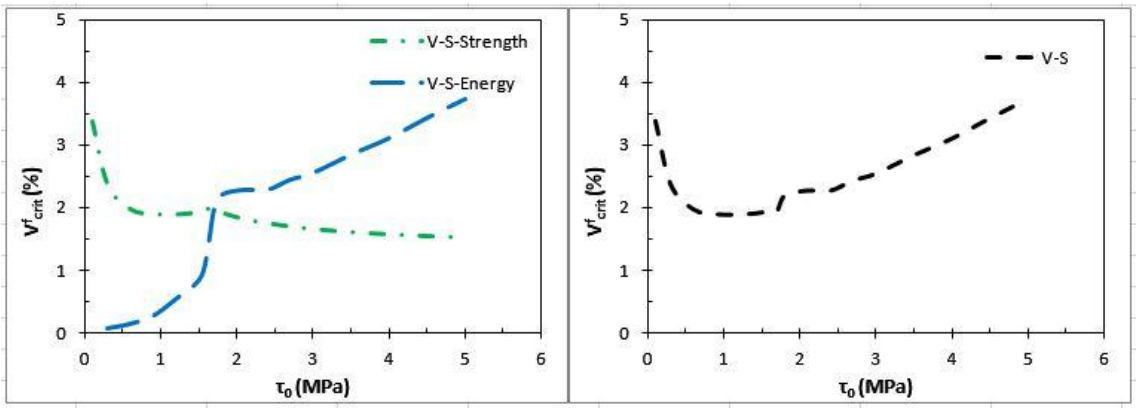

(a) (b)

Figure 8-2: Calculated critical volume fraction of fibers as a function of τ_0 for virgin-short PVA fiber composite (V-S system) determined by (a) the strength-based and energy-based conditions, and (b) the combined effect

With regards to the energy-based condition, as can be seen in Figure 8-2-(a), the V_{crit}^{f} significantly increases when τ_0 increases. This is because at higher interfacial friction the slope of the ascending branch of the fiber-bridging curve keeps rising, and hence resulting in a reduction in the J_b' of the composite (Li et al., 1997). Therefore, higher amount of fiber is needed to obtain the required complementary energy (J_b'=40.5 J/m^2) to satisfy the energy-based condition. Both energy-based and strength-based conditions must be satisfied to achieve the PSH behavior in the composite. Therefore, the V-S-Strength and V-S-Energy curves shown in Figure 8-2-(a) should be combined (whichever has higher V_{crit}^{f}) to determine the minimum amount of fiber required to achieve the saturated PSH behavior in the composite. According to the combined curve illustrated in Figure 8-2-(b), for the fly ash-based SHGC reinforced by virgin-short PVA fibers (V-S system) the optimum point falls in the range of 1.9% (v/v) with the interface frictional bond strength in the range of 0.9 MPa to 1.5 MPa.

The effects of the fiber surface oil coating on the V_{crit}^{f} of fly ash-based PVA-SHGC is shown in Figure 8-3. The micromechanical parameters used for calculating the strength-based and energy-based curves of the oil coated-short PVA fiber composite (O-S system) were identical with those of V-S system, except a lower G_d (6 → 1.5 MPa) was used, since the fiber surface oil coating reduces the chemical bond effectively, as reported in Chapter 7. In addition, σ_{fc} was also reduced (4.5 → 3.5 MPa), due to the lower G_d of the oil coated fiber (Yang and Li, 2014). A lower value of σ_0=4.55 MPa is thereby needed to achieve the same PSH strength index = 1.3 in O-S system. As can be seen in Figure 8-3-(a), the energy-based curve of the oil coated-short fiber composite (O-S-Energy curve) is below that of the virgin-short fiber composite (V-S-Energy curve) at all range of τ_0; in particular when τ_0 is beyond 1.5 MPa the V_{crit}^{f} in O-S system is significantly lower than that of V-S system. In addition, the strength-based curve of the oil coated-short fiber composite (O-S-Strength curve) is also below that of the virgin-short fiber composite (V-S-Strength curve) at all range of τ_0. This is due to the lower σ_{fc} of O-S system resulted from the lower G_d of the oil coated fiber. Therefore, lower volume fraction of the oil coated fiber is required to achieve σ_0=4.55 MPa in O-S system, compared to σ_0=5.85 MPa in V-S system. As can be seen in Figure 8-3-(b), the combined curve of the oil coated-short fiber composite (O-S curve) is also considerably below that of the virgin-short fiber composite (V-S curve) at all range of τ_0. For the fly ash-based SHGC reinforced by oil

coated-short PVA fibers (O-S system) the optimum point falls in the range of 1.4% to 1.5% (v/v) with the interface frictional bond strength in the range of 0.9 MPa to 2.4 MPa. This is well consistent with the single-fiber pullout and uniaxial tension test results, as reported in Chapter 7, respectively, where the fly ash-based SHGC with τ_0=1.3 MPa and 2% (v/v) of oil coated-short PVA fibers demonstrated strong PSH behavior. Therefore, it can be concluded that the fiber surface oil coating can efficiently reduce the V_{crit}^{f} needed to achieve the PSH behavior in fly ash-based SHGCs reinforced by PVA fibers.

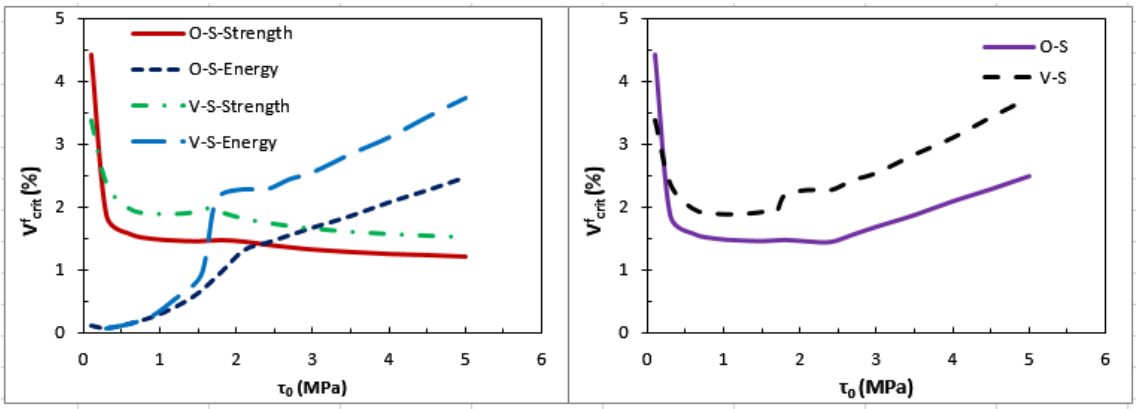

(a) (b)

Figure 8-3: Effect of fiber surface oil coating on critical volume fraction of fibers determined by: (a) the strength-based and energy-based conditions, and (b) the combined effect

The influence of the fiber length on V_{crit}^{f} of fly ash-based PVA-SHGC is demonstrated in Figure 8-4. The micromechanical parameters used for computing the strength-based and energy-based curves of oil coated-long fiber composite (O-L system) were exactly the same as those of the oil coated-short fiber composite (O-S system), except that the fiber length was increased from 8 mm to 16 mm. As can be seen in Figure 8-4-(a), the strength-based curve of the oil coated-long fiber composite (O-L-Strength curve) is dragged down at all range of τ_0; in particular at the low τ_0 end (τ_0 < 0.3 MPa) the reduction in V_{crit}^{f} is significant. In addition, when τ_0 is beyond 1.8 MPa the energy-based curve of the oil coated-long fiber composite (O-L-Energy curve) is also shifted down. As can be seen in Figure 8-4-(b), the combined curve of the oil coated-long fiber composite (O-L curve) is also shifted down at all range of τ_0. For the oil coated-long fiber composite (O-L system)

the minimum point of the combined curve is 1.19% (v/v) with τ_0=2.4 MPa; whereas the minimum point of the combined curve for the oil coated-short fiber composite is 1.43% (v/v) with τ_0=2.4 MPa. Therefore, it can be concluded that increase of the fiber length is advantageous for the fly ash-based SHGCs reinforced by oil-coated PVA fibers.

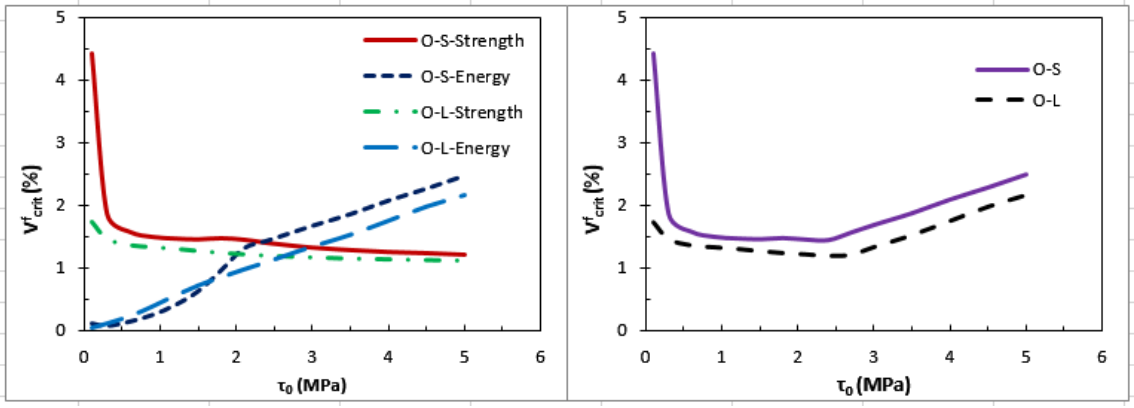

(a) (b)

Figure 8-4: Effect of fiber length on critical volume fraction of fibers determined by: (a) the strength-based and energy-based conditions, and (b) the combined effect

There are two approaches with regards to matrix modification of the composite, namely tailoring the matrix fracture toughness and manipulating the pre-existing flaw size distribution (Wang, 2005; Yang and Li, 2010). The latter approach can be achieved by introducing artificial defects into the matrix with prescribed size distribution (Wang, 2005 PhD thesis), whereas the former approach can be readily achieved by altering the water to geopolymer solids ratio and/or addition of micro-silica sand to the matrix, as reported in Chapter 5. In this study, only the effect of the matrix fracture toughness (J_{tip}) on the V^f_{crit} of the fly ash-based SHGCs is investigated, because it is easier to tailor the J_{tip} compared to introduction of artificial flaws into the matrix. The micromechanical parameters used for computing the strength-based and energy-based curves of oil coated-short fiber composite with low J_{tip} (O-S-(low J_{tip}) system) were identical with those of O-S system, except that the J_{tip} was lowered from 15 to 10 J/m^2 (due to lower matrix fracture toughness) and the σ_{fc} was also reduced from 3.5 to 2.5 MPa, due to lower J_{tip}. As can be seen in Figure 8-5, both strength-based and energy-based curves, as well as the

combined curve of the oil coated-short fiber composite with low J_{tip} (O-S-(lowJ_{tip}) system) are considerably shifted down at all ranges of τ_0. In O-S-(lowJ_{tip}) system the minimum point of the combined curve is only 0.99% (v/v) with τ_0=2.4 MPa; whereas the minimum point of the combined curve in O-S system is 1.43% (v/v) with τ_0=2.4 MPa. This translates to 30% reduction in the V_{crit}^{f} of the composite, which is really valuable due to relative high cost of the oil coated PVA fibers. Therefore, it can be concluded that the reduction of matrix fracture toughness is an effective approach to reduce the V_{crit}^{f} for the fly ash-based SHGCs reinforced by oil-coated PVA fibers. However, it should be noted that excessive reduction of J_{tip} might reduce the compressive strength of the composite, which is not usually advantageous (Yang and Li, 2010).

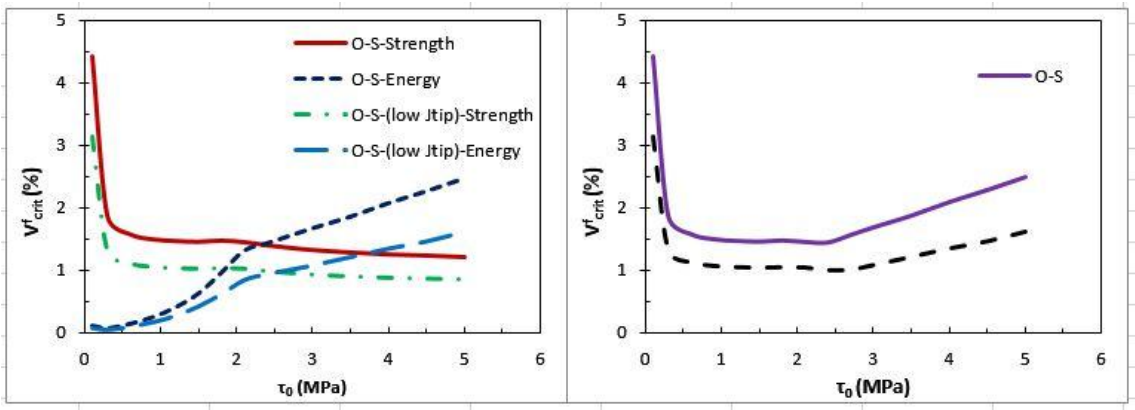

(a) (b)

Figure 8-5: Effect of matrix fracture toughness on critical volume fraction of fibers determined by: (a) the strength-based and energy-based conditions, and (b) the combined effect

8.5 Summary and Conclusion

The micromechanics-based modelling and optimization of fly ash-based SHGCs are presented in this chapter. The crack bridging σ(δ) relation of the developed fly ash-based SHGC was computed using the available micromechanics-based model for typical SHCCs. The computed σ(δ) relation of the composite was then compared with the uniaxial tension test results to verify the applicability of the model for evaluating the tensile performance of fly ash-based SHGCs. In general, the predicted peak bridging stress σ_0 and its corresponding deflection δ_0 was in good agreement with the ultimate

tensile strength and the corresponding crack opening measured experimentally from the uniaxial tension tests.

The ratio of the experimental to the theoretical σ_0 was dependent on the fiber orientation assumption. In the case of 3D fiber orientation assumption, the predicted σ_0 was remarkably consistent with the ultimate tensile strength measured experimentally from the uniaxial tension tests. However, when 2D fiber orientation was assumed, the model overestimated the σ_0 by 23%. The ratio of the experimental to the theoretical δ_0 was also dependent on the fiber orientation assumption. In the case of 3D fiber orientation assumption, the model underestimated the δ_0 by about 20%. However, when 2D fiber orientation was assumed, the predicted δ_0 was well consistent with the crack opening corresponding to ultimate tensile strength measured experimentally from the uniaxial tension tests. These results are consistent with those reported in the literature on micromechanics-based modelling of typical SHCCs.

In the second part of this chapter, a parametric study was performed using the verified model to evaluate the effects of fiber length, fiber surface oil-coating, and matrix fracture toughness on the critical volume fraction of fibers. It was demonstrated how the micromechanics-based model can effectively guide towards optimization of fly ash-based SHGCs by proper tailoring of the material constituents to achieve saturated PSH behavior with the lowest amount of fiber (V_{crit}^{f}= 1.0%), and thereby the lowest cost.

8.6 References

KANDA, T. & LI, V. C. 1998. Interface property and apparent strength of high-strength hydrophilic fiber in cement matrix. *Journal of materials in civil engineering*, 10, 5-13.

KANDA, T. & LI, V. C. 2006. Practical design criteria for saturated pseudo strain hardening behavior in ECC. *Journal of advanced concrete technology*, 4, 59-72.

LI, V. C., KANDA, T. & LIN, Z. Influence of Fiber/Matrix interface properties on complementary energy and composite damage tolerance. Key engineering materials, 1997. Trans Tech Publ, 465-472.

LI, V. C. & LEUNG, C. K. 1992. Steady-state and multiple cracking of short random fiber composites. *Journal of Engineering Mechanics,* 118, 2246-2264.

LI, V. C., MISHRA, D. K. & WU, H.-C. 1995. Matrix design for pseudo-strain-hardening fibre reinforced cementitious composites. *Materials and Structures*, 28, 586-595.

LI, V. C., WANG, S. & WU, C. 2001. Tensile strain-hardening behavior of polyvinyl alcohol engineered cementitious composite (PVA-ECC). *ACI materials Journal,* 98.

LI, V. C., WANG, Y. & BACKER, S. 1990. Effect of inclining angle, bundling and surface treatment on synthetic fibre pull-out from a cement matrix. *Composites,* 21, 132-140.

LIN, Z., KANDA, T. & LI, V. 1999. On interface property Characterization and performance of fiber-reinforced cementitious Composites. *Concrete Science and Engineering,* 1, 173-174.

LIN, Z. & LI, V. C. 1997. Crack bridging in fiber reinforced cementitious composites with slip-hardening interfaces. *Journal of the Mechanics and Physics of Solids,* 45, 763-787.

WANG, S. 2005. *Micromechanics based matrix design for engineered cementitious composites,* University of Michigan.

YANG, E.-H. & LI, V. C. 2010. Strain-hardening fiber cement optimization and component tailoring by means of a micromechanical model. *Construction and building Materials,* 24, 130-139.

YANG, E.-H. & LI, V. C. 2014. Strain-rate effects on the tensile behavior of strain-hardening cementitious composites. *Construction and Building Materials,* 52, 96-104.

YANG, E.-H., WANG, S., YANG, Y. & LI, V. C. 2008. Fiber-bridging constitutive law of engineered cementitious composites. *Journal of advanced concrete technology,* 6, 181-193.

PART II: AMBIENT TEMPERATURE CURED ONE-PART SHGCS

CHAPTER 9

SYNTHESIS OF HEAT AND AMBIENT TEMPERATURE CURED ONE-PART GEOPOLYMER MIXTURES

Note: This chapter is based on the paper "*Synthesis of heat and ambient cured one-part geopolymer mixes with different grades of sodium silicate*", by **Nematollahi, B.**, Sanjayan, J., and Shaikh, F.U.A., published in ***Ceramics International***, 2015, 41(4), 5696-5704.

9.1 Introduction

Geopolymer composite research is aimed to make sustainable alternatives to Portland cement-based composites. The high compressive and tensile strengths and the very high tensile ductility of the developed fly ash-based SHGC made by the suitable Na-based activator and the outstanding greenness potential of the geopolymer promote its application as a promising sustainable alternative to typical SHCC. To make the most of the remarkable mechanical properties and the environmental advantages of the developed fly ash-based SHGC, its widespread and large scale applications in the construction industry should be really taken into consideration. However, there are two main obstacles for commercialization and widespread application of the developed fly ash-based SHGC compared to typical SHCC. The first obstacle is the use of corrosive and often viscous alkaline solutions to manufacture fly ash-based SHGC. The second obstacle is the necessity of heat curing in the production of the developed fly ash-based SHGC, which limit its in-situ application.

This research is aimed to overcome the aforementioned two obstacles by developing an ambient temperature cured one-part SHGC as an alternative to the "traditional" heat cured two-part fly ash-based SHGC. Such ambient temperature cured one-part SHGC as a "dry mix" utilizes a small amount of solid activators as alternative to large quantities of commonly used alkaline solutions and eliminates the necessity of the heat curing. The micromechanics-based principles for strain hardening behavior in short fiber reinforced brittle matrix composites, combined with geopolymer technology principles led to the development of the ambient temperature cured one-part SHGC.

The first step for the development of the ambient temperature cured one-part SHGC is to manufacture a suitable ambient temperature cured one-part geopolymer matrix with desirable mechanical properties, moderate setting time and adequate rheology for uniform fiber dispersion. The focus of this chapter is to achieve this objective. In the next chapter, the best performing ambient temperature cured one-part geopolymer matrix is used to develop the ambient temperature cured one-part SHGC based on the micromechanics-based design principles of SHCC.

9.2 Research Significance

Conventionally, geopolymer is manufactured from a two-part mix, comprising of alkaline solutions and solid aluminosilicate precursors. These user-hostile activator solutions are frequently used to dissolve the aluminosilicate source materials and govern the mechanical properties of the geopolymer binder such as its compressive strength (Lee and van Deventer, 2002; Lee and van Deventer, 2003). There are several drawbacks with regards to the two-part mix formulations used in the synthesis of "traditional" geopolymers (Duxson and Provis, 2008). Handling large quantities of highly corrosive and often viscous alkaline solutions is difficult to be used for commercial and mass production of geopolymer materials, and thereby hinders the large-scale application of geopolymer. In addition, the rheology of the geopolymer can be complex and difficult to control as a result of formation of a sticky and thick paste, particularly in geopolymer systems where sodium is the source of alkali (Provis, 2009). Moreover, the two-part geopolymer system is sensitive to the ratio of alkali to available silicate, which can be challenging to control in practice where waste materials are used as a silica source (Criado et al., 2007). Lastly, as a result of movement of alkalis and water to the geopolymer surface during curing or in service, there can be a tendency toward efflorescence, and/or high permeability and water absorption, unless the water and alkali content of a two-part geopolymer mix are cautiously controlled (Najafi Kani et al., 2012; Provis et al., 2010). Thus, one of the main steps towards commercialization and large-scale application of geopolymer in the construction industry is developing a one-part "dry mix" geopolymer mixture as an alternative method which is more similar to the utilization of conventional Portland cement-based materials.

9.3 Review of Available Literature on One-Part Geopolymer Mixtures

Solid activators (e.g. solid silicates) can be used as alternatives to activator solutions (e.g. soluble silicate) to manufacture geopolymers (Rees et al., 2004). The use of solid activators in the manufacture of geopolymer enhances its commercial viability because it aids the development of a one-part "just add water" mixture, similar to the conventional cement-based materials. To date, few studies aimed to synthesize one-part geopolymer mixes using various source materials and solid activators. For instance, Kolousˇek et al. (2007) developed a one-part geopolymer mix by making a totally sodium silicate-free geopolymer system by calcination of kaolinite or halloysite together with powdered hydroxides, but this was reported to result in low strength development (7-days strengths of less than 1 MPa were reported).

Hajimohammadi et al. (2008, 2010 and 2011) attempted to provide an in-depth understanding of the chemistry of one-part geopolymer mixes. The effects of water content, high early silica, and high early alumina in the formation of one-part geopolymer mixes composed of geothermal silica and solid sodium aluminate as the solid silica, alkali, and alumina sources for geopolymerisation, with or without additional fly ash were evaluated. Geothermal silica is a waste residue and a source of solid amorphous silica which can potentially be used as a replacement for silicate solutions in geopolymerisation. Although the results of using geothermal silica and solid aluminate for geopolymerisation were encouraging in terms of possibilities for using the "just add water" concept in practice, however the method used to purify the raw geothermal silica was relatively complex. In addition, all geopolymer pastes were cured at 40°C in sealed molds for 2 weeks. These issues may limit the widespread application of this one-part geopolymer mix in the construction industry. Moreover, the focus of their studies was mainly on the chemistry and microstructure of the developed geopolymer and mechanical properties of the one-part geopolymer have not been reported.

Feng et al. (2012) studied the thermal activation (i.e. at elevated temperatures e.g. 850°C to 1150°C) of albite with sodium hydroxide (NaOH) or sodium carbonate (Na_2CO_3) powders for the synthesis of one-part mix geopolymers. Albite (sodium feldspar) is often one of the main components in mine tailings. Although the developed geopolymer exhibited acceptable compressive strength over 40 MPa after 28 days, however the

necessity of thermal activation of albite at elevated temperatures (e.g. 850°C to 1150°C) limit the common application of this one-part geopolymer in the construction industry.

To be useful in practice, the "just add water" concept needs to be applicable to fly ash and slag as the commonly used geopolymer source materials. In this regard, Yang et al. (2008) and Yang and Song (2009) attempted to develop one-part geopolymer mixes with fly ash and slag as the precursor and using either sodium silicate (Na_2SiO_3) powder or a combination of Na_2SiO_3 and NaOH powders as the solid activator. 100% fly ash or 100% slag were used individually as the source materials activated by only one grade of Na_2SiO_3 powder (i.e. Anhydrous Grade sodium metasilicate powder) as the solid activator. All fly ash and slag-based specimens were cured at ambient temperature (23°C±3°C). 100% Slag-based samples were removed from the molds after 1 day. In the case of using 100% slag as the source material and a combination of Na_2SiO_3 and NaOH powders as the solid activator, a maximum compressive strength of 49.6 MPa was achieved after 28 days. Where 100% slag as the source material was activated by Anhydrous Grade sodium metasilicate powder, a maximum compressive strength of 52.48 MPa after 28 days of curing was reported. Although the compressive strength and setting time of the developed one-part geopolymer mixes based on 100% slag as the source material were satisfactory, however their flow loss with time was significantly high which hinders the addition and uniform dispersion of fibers to make the composite, and thereby make them unsuitable mixes to be used as the one-part SHGC matrix.

100% fly ash-based specimens were de-molded after 3 days of casting, because they required more setting time. In the case of using 100% fly ash as the source material and Anhydrous Grade sodium metasilicate powder as the solid activator, a maximum compressive strength of 9.45 MPa after 28 days of curing was achieved. However, no meaningful compressive strength was reported where 100% fly ash and a combination of NaOH and Na_2SiO_3 powders were used as the source material and the solid activator, respectively (i.e. a maximum compressive strength of 3.5 MPa after 28 days of curing was reported). The developed one-part geopolymer mixes based on 100% fly ash as the source material are not suitable mixes to be used as the one-part SHGC matrix, due to their very long setting time and very low compressive strength. Thus, further research is required to increase the compressive strength of the one-part geopolymer mixes manufactured from fly ash and Na_2SiO_3 powder or a combination of NaOH and Na_2SiO_3

powders. The setting time of the fly ash-based mixes should also be accelerated so that these mixes can be de-molded after 1 day of casting similar to the OPC and slag-based specimens.

As mentioned above, there were several drawbacks with regards to each of the previously developed one-part geopolymer mixes which apparently made them not suitable to be used as the one-part geopolymer matrix for manufacture of the ambient temperature cured one-part SHGC. Therefore, a comprehensive and systematic experimental study as outlined in the following sections was conducted to synthesize a suitable ambient temperature cured one-part geopolymer matrix with desirable mechanical properties, moderate setting time and adequate rheology for uniform fiber dispersion.

9.4 Materials

9.4.1 Aluminosilicate source materials

A combination of fly ash, slag and calcium hydroxide with different weight percentages were used as the geopolymer precursor. The low calcium (Class F) fly ash and slag used in this study were supplied from Gladstone power station in Queensland, Australia and Independent Cement and Lime Pty Ltd, Australia, respectively. The chemical composition and LOI of slag determined by X-ray Fluorescence (XRF) are presented in Table 9-1. The total percentages do not sum up to 100% because of rounding errors. The chemical composition and LOI of fly ash are also re-presented in Table 9-1 for ease of comparison. Two different grades of calcium hydroxide ($Ca(OH)_2$) namely Supercalco 97 Grade and Industrial Grade were used in this study. The Supercalco 97 Grade is a laboratory grade $Ca(OH)_2$ powder supplied by Redox Australia, while the Industrial Grade is a hydrated lime powder commonly used in the construction industry supplied by Cement Australia.

9.4.2 Solid activators

Four different solid activators comprising three different grades of sodium silicate and a combination of sodium silicate and sodium hydroxide powders were used in this study. The first sodium silicate-based activator denoted as "Na_2SiO_3-Anhydrous" was composed of Anhydrous sodium metasilicate powder supplied by Redox Australia with a chemical composition of 51 wt.% Na_2O and 46 wt.% SiO_2 (balance H_2O). The second sodium

silicate-based activator denoted as "Na_2SiO_3-Penta" was composed of Penta sodium metasilicate powder supplied by Redox Australia with a chemical composition of 29 wt.% Na_2O and 28 wt.% SiO_2 (balance H_2O). The commonly used Na-based activator solution denoted as "NaOH+Na_2SiO_3-D" and composed of 8.0 M NaOH solution (28.6% w/w) and D Grade Na_2SiO_3 solution (71.4% w/w) was also used in this study for comparison purposes. The physical and chemical properties of NaOH and Na_2SiO_3 solutions and the procedure for preparation of "NaOH+Na_2SiO_3-D" activator are given in Chapter 4.

Table 9-1: Chemical composition of fly ash and slag

Chemical	Component (wt. %)	
	Fly ash	Slag
Al_2O_3	25.56	12.37
SiO_2	51.11	32.76
CaO	4.3	44.64
Fe_2O_3	12.48	0.54
K_2O	0.7	0.33
MgO	1.45	5.15
Na_2O	0.77	0.22
P_2O_5	0.885	0.014
TiO_2	1.32	0.51
MnO	0.15	0.37
SO_3	0.24	4.26
LOI[1]	0.57	0.09

[1]Loss on ignition.

The third sodium silicate-based activator denoted as "Na_2SiO_3-GD" was composed of GD Grade sodium silicate powder supplied by PQ Australia with a chemical composition of 27 wt.% Na_2O and 54 wt.% SiO_2 (balance H_2O). The last activator denoted as "NaOH+Na_2SiO_3-GD" and composed of NaOH and GD Grade sodium silicate powders was prepared as the counterpart to the commonly used Na-based activator solution (i.e. the "NaOH+Na_2SiO_3-D" activator) to evaluate the feasibility of developing a one-part geopolymer mix containing 100% fly ash as the source material and a combination of sodium silicate and sodium hydroxide powders as the solid activator instead of the commonly used NaOH and D Grade Na_2SiO_3 solutions. In this regard, NaOH powder (i.e. NaOH beads of 97% purity) and GD Grade Na_2SiO_3 powder were mixed together with GD Grade Na_2SiO_3 to NaOH mass ratio of 5.12 corresponding to the mass of NaOH and

Na_2SiO_3 solids used in "NaOH+Na_2SiO_3-D" activator. Table 9-2 presents specifications of different grades of sodium silicates used in this study.

Table 9-2: Specifications of different grades of sodium silicates

Chemical Name	Chemical form	Modules ratio (Ms=SiO_2/Na_2O)	SiO_2[&] (wt.%)	Na_2O[&] (wt.%)	H_2O (wt.%)
Na_2SiO_3-Anhydrous	Powder	0.9	46	51	3[*]
Na_2SiO_3-Penta	Powder	1.0	28	29	43[*]
Na_2SiO_3-GD	Powder	2.0	54	27	19[*]
Na_2SiO_3-D	Solution	2.0	29.4	14.7	55.9

[&]Average wt. % reported by the supplier.

[*] Chemically bound water in the powder which is released when dissolved in water.

9.5 Experimental procedures

The experimental program of this study was divided into two parts. In the first part of the experiment, twelve appropriate one-part geopolymer mix proportions employing the four different solid activators were designed to evaluate the properties of heat cured one-part geopolymer mixes. A conventional two-part geopolymer mix (i.e. the mixture M12) with the commonly used Na-based activator solution (i.e. the "NaOH+Na_2SiO_3-D" activator) was also made for comparison. Effects of the type and amount of the solid activator, the amount of fly ash replacement with slag and $Ca(OH)_2$ and water content on short term mechanical properties of the heat cured one-part geopolymer mixtures including workability of the fresh paste, density and compressive strength were evaluated. In the second part of the experiment, effects of ambient temperature curing on the properties of the developed one-part geopolymer mixes were also investigated. In this regard, three suitable one-part geopolymer mix proportions developed in the first part of the study exhibiting desirable mechanical properties were subjected to ambient temperature curing and the results were compared to those of the counterpart heat cured mixes.

9.5.1 Mix proportions

Table 9-3 presents details of the mix proportions used in this study. Previous studies revealed that the water content plays an important role on the properties of geopolymer

(Barbosa et al., 2000; Hardjito et al., 2004). Hence, in order evaluate the effect of water content in the mixture, water to geopolymer solids (W/GP solids) ratio as defined by Hardjito et al. (2004) was determined for each mixture. For a given geopolymer mix, the total mass of water in the mixture is taken as the sum of the mass of chemically bound water in the solid activator and the mass of water added to the mixture. The mass of geopolymer solids is the sum of the mass of geopolymer precursors (including fly ash, slag and $Ca(OH)_2$) and the mass of solid activator excluding the mass of its chemically bound water. Several trials were performed before achieving the final mixes. The mix variables were type and amount of the solid activator, the amount of fly ash replacement by slag and $Ca(OH)_2$ and the water content (i.e. the W/GP solids ratio).

The mixtures M1, M2 and M3 were designed by varying the amount of "Na_2SiO_3-GD" activator as 1.0 wt.%, 1.3 wt.% and 1.5 wt.% of the total geopolymer precursor, respectively and the other mix parameters such as $Ca(OH)_2$ and water contents were kept constant, but the amount of superplasticizer was adjusted to achieve an appropriate level of workability in these mixes. The effect of the W/GP solids ratio was evaluated by increasing the amount of water in the mixture M4 compared to that of the mixture M3, while the other parameters were kept constant. It should be noted that the amount of the superplasticizer in the mixture M4 was adjusted as its water content was increased with respect to that of the mixture M3. Effect of the type of solid activator was evaluated in the mixtures M4 and M5. In this regard, all mix parameters were kept constant except the type of the solid activator; in which "Na_2SiO_3-GD" activator was used in the mixture M4, while the mixture M5 was made by the "Na_2SiO_3-Penta" activator. It should be noted that the water content in the mixture M5 was adjusted to correspond to the constant W/GP solids ratio of 0.23 in both mixes.

In the mixtures M6, M7 and M8, fly ash was replaced by slag as 25 wt.% of the total geopolymer precursor. The mixtures M6 and M7 were designed by varying "Na_2SiO_3-Anhydrous" activator content as 10.2 wt.% and 12 wt.% of the total geopolymer precursor, respectively. The water content in the mixture M6 was adjusted to correspond to the constant W/GP solids ratio of 0.36 in both mixes. In the mixtures M7 and M8 all parameters except the water content were kept constant to evaluate the effect of the water content (i.e. the W/GP solids ratio) in these mixes.

Table 9-3: Mix proportions of one-part geopolymer mixes

Mix ID	Geopolymer precursor			Activator	Water	SP[&]	W/GP solids ratio
	Fly ash	Slag	$Ca(OH)_2$				
M1	0.89	----	0.11[*]	0.010[1]	0.203	0.009	0.20
M2	0.89	----	0.11[*]	0.013[1]	0.203	0.018	0.20
M3	0.89	----	0.11[*]	0.015[1]	0.203	0.018	0.20
M4	0.89	----	0.11[#]	0.015[1]	0.231	0.009	0.23
M5	0.89	----	0.11[#]	0.015[3]	0.227	0.009	0.23
M6	0.75	0.25	----	0.102[2]	0.394	----	0.36
M7	0.75	0.25	----	0.120[2]	0.400	----	0.36
M8	0.75	0.25	----	0.120[2]	0.300	----	0.27
M9	0.75	0.14	0.11[#]	0.120[2]	0.400	----	0.36
M10	0.75	0.14	0.11[#]	0.120[1]	0.375	0.027	0.36
M11	0.50	0.50	----	0.080[2]	0.350	----	0.33
M12	1.00	----	----	0.350[5]	0.050	----	0.23
M13	1.00	----	----	0.161[4]	0.239	----	0.23

Note: All numbers are mass ratios of geopolymer precursor weight except W/GP solids ratio.

[1] Composed of the "Na_2SiO_3-GD" activator (in powder form).

[2] Composed of the "Na_2SiO_3-Anhydrous" activator (in powder form).

[3] Composed of the "Na_2SiO_3-Penta" activator (in powder form).

[4] Composed of the "NaOH+Na_2SiO_3-GD" activator (in powder form).

[5] Composed of the "NaOH+Na_2SiO_3-D" activator (in solution form).

[*] Supercalco 97 Grade $Ca(OH)_2$ powder.

[#] Industrial Grade $Ca(OH)_2$ powder.

[&] PCE based superplasticizer.

25 wt.% of fly ash was replaced by slag in the mixture M7, whereas in the mixture M9 fly ash was replaced by slag and $Ca(OH)_2$ as 14 wt.% and 11 wt.% of the total geopolymer precursor, respectively and all other parameters were kept constant to evaluate the feasibility of using $Ca(OH)_2$ as partial replacement of slag in these mixes. Effect of the type of solid activator was also evaluated in the mixtures M9 and M10. In this regard, all the mix parameters were kept constant except the type of the solid activator, in which "Na_2SiO_3-Anhydrous" activator was used in the mixture M9, while the mixture M10 was made by "Na_2SiO_3-GD" activator. It should be noted that the water content in the mixture M10 was adjusted to correspond to the constant W/GP solids ratio of 0.36 in both mixes

and superplasticizer was also used in the mixture M10 to achieve a proper level of workability in that mix.

In the mixture M11, the amount of fly ash replacement with slag was increased to 50 wt.% of the total geopolymer source material while the amount of "Na_2SiO_3-Anhydrous" activator and the water content were reduced to 8 wt.% and 35 wt.% of the total geopolymer precursor, respectively compared to those of the mixture M7. The mixture M12 was prepared with the commonly used Na-based activator solution (i.e. "NaOH+Na_2SiO_3-D" activator) with the same W/GP solids ratio as that of the mixture M4 for comparison. The mixture M13, as the counterpart to the mixture M12, was prepared with "NaOH+Na_2SiO_3-GD" activator with the same W/GP solids ratio as that of the mixture M12 to evaluate the feasibility of developing a one-part geopolymer mix containing 100% fly ash as the source material and a combination of sodium silicate and sodium hydroxide powders as the solid activator, instead of the commonly used Na-based activator solution.

9.5.2 Mixing, curing and testing of specimens

All mixtures were prepared in a Hobart mixer. Solid ingredients, including fly ash, slag and calcium hydroxide (if any), and solid activator were added to the mixer and dry mixed for approximately 3 minutes. Water was then gradually added to the mix and the mixing was continued for another 3 minutes. Subsequently, a poly carboxylate ether (PCE) based superplasticizer (if any) was added to the mix and the mixing was continued for almost 6 minutes to achieve proper workability of the mixture. In the case of the "traditional" two-part geopolymer mix (the mixture M12), "NaOH+Na_2SiO_3-D" activator in the form of solution as well as extra water were added to fly ash and mixed for about 4 minutes.

As mentioned earlier, in the first part of the experiment the specimens were subjected to heat curing. However, in the second stage of the experiment, ambient temperature curing was adopted. The procedure for the heat curing is given in Chapter 4. For ambient temperature curing, the specimens were cured in air at ambient temperature (23°C ± 3°C) for 24 hours. The hardened specimens were then removed from the molds and cured in a water tank at ambient temperature (23°C ± 3°C) for 27 days after de-molding. The ambient temperature cured specimens were tested 28 days after casting, while the heat cured specimens were tested 3 days after casting.

To determine flowability of fresh geopolymer matrix, mini-slump test also known as spread-flow test was conducted. Details of the mini-slump test are given in Chapter 4. Compressive strength and hardened density of each mixture were measured. The procedures for compression and density tests are given in Chapter 4.

9.6 Results and Discussions

9.6.1 Heat cured one-part geopolymer mixes

Comparison of the workability (in terms of relative slump value), hardened density and compressive strength of the mixtures M1, M2, M3 and M4 are presented in Figure 9-1. As can be seen, the compressive strength of the mixture M3 significantly increased by 134% with respect to that of the mixture M1. However, the workability of the mixture M3 significantly decreased by 90% with respect to that of the mixture M1. In addition, the density of the mixture M3 was slightly lower than that of the mixture M1. Moreover, through visual inspection it was noted that surface tension of the mixture M3 was much higher than that of the mixture M1. Therefore, it can be concluded that for a constant $Ca(OH)_2$ and water contents (i.e. the W/GP solids ratio) the increase in the amount of the "Na_2SiO_3-GD" activator resulted in significant increase in the compressive strength and significant decrease in the workability of the one-part geopolymer mix.

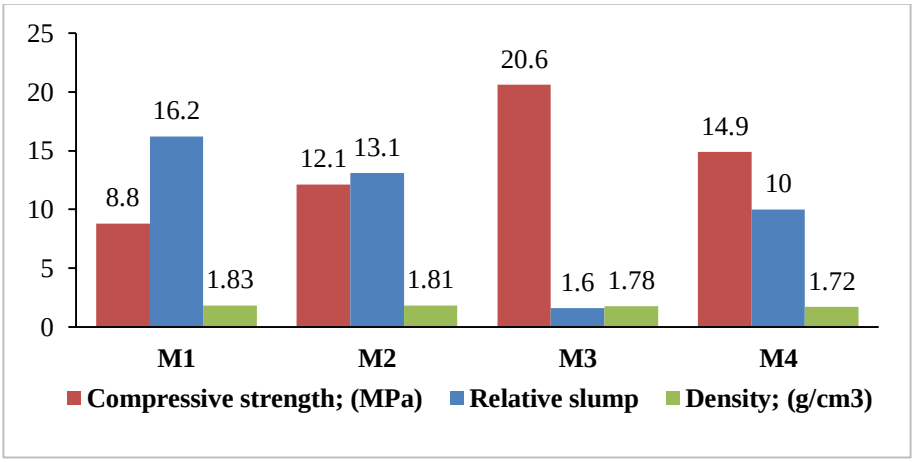

Figure 9-1: Properties of the mixtures M1, M2, M3 and M4

It should be noted that the Laboratory Grade $Ca(OH)_2$ (the Supercalco 97 Grade) was used in the initial mixtures (i.e. the mixture M1, M2 and M3) to avoid the effect of possible unknown contaminant in the Industrial Grade hydrated lime. However, in the mixtures M4 to M8, the Industrial Grade hydrated lime powder was used, which not only broadens the field applicability of the mixes, but also results in some economical saving as the price of the Industrial Grade hydrated lime is much cheaper than that of the Supercalco 97 Grade $Ca(OH)_2$. As can be seen Figure 9-1, the compressive strength of the mixture M4 decreased by 28% with respect to that of the mixture M3. However, the workability of the mixture M4 significantly increased by 525% with respect to that of the mixture M3. In addition, through visual inspection it was noted that surface tension of the mixture M4 was much lower than that of the mixture M3. Hence, it can be concluded that the increase in the water content (i.e. the W/GP solids ratio), with all other parameters being constant, led to significant increase in the workability and decrease in the compressive strength of the one-part geopolymer mix.

Comparison of the workability, hardened density and compressive strength of the mixtures M4, M12 and M13 are presented in Figure 9-2. As can be seen for a constant W/GP solids ratio, the compressive strength of the mixture M4, containing $Ca(OH)_2$ and "Na_2SiO_3-GD" activator as 11 wt.% and 1.5 wt.% of the total geopolymer precursor, respectively, decreased by 65% with respect to that of the "traditional" two-part mixture M12 containing the commonly used Na-based activator solution (i.e. the "NaOH+Na_2SiO_3-D" activator) as 35 wt.% of the mass of fly ash. However, the workability of the mixture M4 was comparable to that of the mixture M12. In addition, the density of the mixture M4 was 5% lower than that of the mixture M12.

As can be seen in Figure 9-2, for a constant W/GP solids ratio the compressive strength and workability of the mixture M13, as the counterpart to the "traditional" two-part mixture M12, decreased by 31% and 35%, respectively, compared to those of the mixture M12. Nevertheless, the developed one-part geopolymer mixture M13 possessed moderate compressive strength and good workability. In addition, the density of the one-part geopolymer mixture M13 was slightly lower than that of the mixture M12.

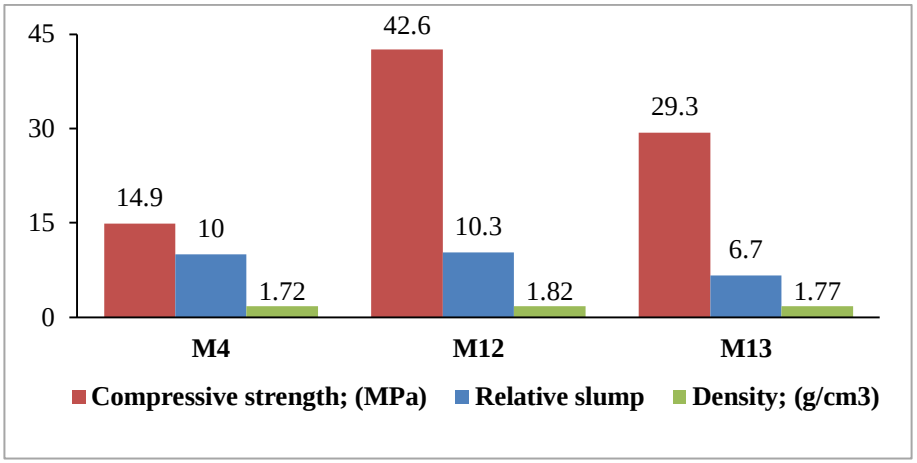

Figure 9-2: Properties of the mixtures M4, M12 and M13

It should be noted that the compressive strength of the mixture M13 developed in this study was significantly higher than that of the mixes developed by Yang and Song (2009), in which a maximum compressive strength of 3.5 MPa after 28 days of curing was achieved where 100% fly ash and a combination of NaOH and Na_2SiO_3 powders were used as the source material and the solid activator, respectively. Therefore, the development a one-part geopolymer mix containing 100% fly ash as the source material and a combination of NaOH and GD Grade Na_2SiO_3 powders as the solid activator with compressive strength over 29 MPa, instead of the commonly used Na-based activator solution (i.e. the "NaOH+Na_2SiO_3-D" activator) has been demonstrated to be feasible.

A much more important benefit of using solid activators such as "Na_2SiO_3-GD" activator in the mixture M4 and "NaOH+Na_2SiO_3-GD" activator in the mixture M13 over the commonly used Na-based activator solution (i.e. the "NaOH+Na_2SiO_3-D" activator) in the mixture M12 is that in commercial application of geopolymer handling a small amount of solid activators and just adding water similar to cementitious binders would be safer and easier than handling large quantities of corrosive activator solutions. Furthermore, using "Na_2SiO_3-GD" activator results in some economical saving compared to "NaOH+Na_2SiO_3-D" activator, as the price of Na_2SiO_3-GD powder is much cheaper than that of the NaOH solution and only a small amount of the "Na_2SiO_3-GD" activator (i.e. 1.5 wt.% of the total geopolymer precursor) would be required compared to the high amount of activator solution (i.e. 35 wt.% with respect to the mass of fly ash) used in the mixture M12.

Comparison of the workability, hardened density and compressive strength of the mixtures M4 and M5 are presented in Table 9-4. As can be seen for a constant W/GP solids ratio, the compressive strength of the mixture M5, containing "Na_2SiO_3-Penta" activator, significantly decreased by 65% with respect to that of the mixture M4 containing the "Na_2SiO_3-GD" activator. However, the workability of the mixture M5 increased by 27% with respect to that of the mixture M4. The density of both mixes was comparable. Hence, it can be concluded that in the case of using a combination of fly ash and hydrated lime as the geopolymer source materials, with all parameters being constant, the use of "Na_2SiO_3-GD" activator would be more effective resulting in good workability and moderate compressive strength compared to "Na_2SiO_3-Penta" activator.

Table 9-4: Properties of the mixtures M4 and M5

Mix ID	Relative slump value	Density; (g/cm^3)	Compressive strength; (MPa)
M4	10	1.72	14.9
M5	12.7	1.73	5.2

Comparison of the workability, hardened density and compressive strength of the mixtures M6, M7, M8 and M11 are presented in Figure 9-3. As can be seen, generally these one-part geopolymer mixes, in which a combination of fly ash and slag was used as the geopolymer source materials activated by "Na_2SiO_3-Anhydrous" powder, exhibited higher compressive strength compared to the previous mixes, in which a combination of fly ash and hydrated lime was used as the geopolymer source materials activated by "Na_2SiO_3-GD" powder.

As can be seen in Figure 9-3 for a constant W/GP solids ratio, the compressive strength of the mixture M7, containing "Na_2SiO_3-Anhydrous" activator as 12 wt.% of the total geopolymer precursor, significantly increased by 66% with respect to that of the mixture M6 containing the same activator as 10.2 wt.% of the total geopolymer precursor. In addition, the workability and density of the mixtures M6 and M7 were comparable. Therefore, it can be concluded that with all parameters being constant, the increase in the amount of "Na_2SiO_3-Anhydrous" activator resulted in significant increase in the compressive strength, with no negative effect on the workability of the mix.

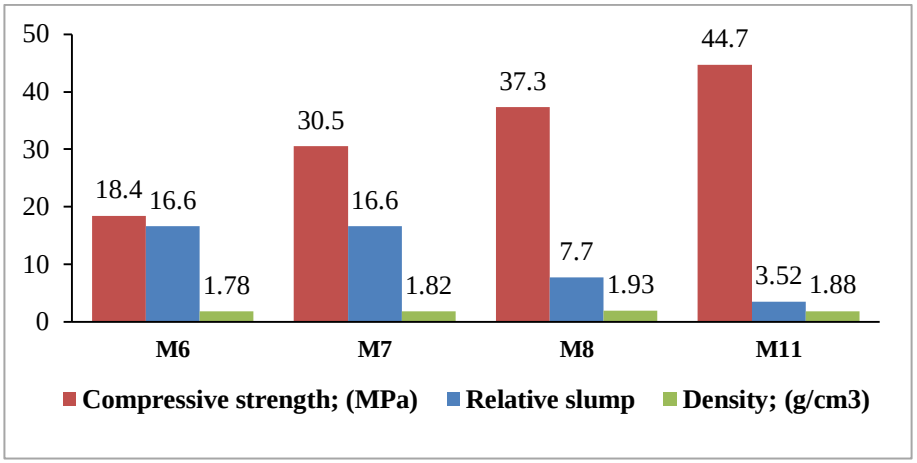

Figure 9-3: Properties of the mixtures M6, M7, M8 and M11

As can be seen in Figure 9-3, the compressive strength and density of the mixture M8, increased by 22% and 6%, respectively with respect to that of the mixture M7. However, the workability of the mixtures M8 significantly decreased by 54% with respect to that of the mixture M7. Thus, it can be said that although the decrease in the water content (i.e. the W/GP solids ratio) resulted in a moderate increase in the compressive strength, however the workability of the mix was significantly decreased.

As can be seen in Figure 9-3, the compressive strength of the mixture M11 containing 50 wt.% of slag and 8 wt.% of "Na_2SiO_3-Anhydrous" activator increased by 47% and 20% with respect to that of the mixture M7 and M8, respectively which contained 25 wt.% of slag and 12 wt.% of "Na_2SiO_3-Anhydrous" activator. However, the workability of the mixture M11 significantly decreased by 79% and 54% with respect to that of the mixture M7 and M8, respectively. It should be noted that visual inspection revealed that the setting time of the mixture M11 was higher than that of the mixtures M7 and M8. Hence, it can be concluded that in order to promote acceptable setting time and desirable mechanical properties, a lower dose of "Na_2SiO_3-Anhydrous" activator is required in the mixes formulated with at least 50 wt.% of slag compared to the mixes containing less than 50 wt.% of slag. In other words, 8 wt.% of "Na_2SiO_3-Anhydrous" activator was used in the mixture M11 containing 50 wt.% of slag, whereas the mixtures M7 and M8 containing 25 wt.% of slag were activated by using 12 wt.% of the activator. These results are in good agreement with those published by Ismail et al. (2013) for "traditional" two-part

geopolymer mortar and concrete mixes activated by Anhydrous Grade sodium metasilicate solution.

Comparison of the workability, hardened density and compressive strength of the mixtures M7, M9 and M10 are presented in Table 9-5. As can be seen for a constant W/GP solids ratio, the workability of the mixture M9 in which 11 wt.% of slag was replaced by hydrated lime, significantly decreased by 99% with respect to that of the mixture M7 containing 25 wt.% of slag (i.e. no hydrated lime). In addition, the compressive strength of the mixture M9 decreased by 31% with respect to that of the mixture M7. The density of both mixes was comparable. Hence, it can be concluded that partial replacement of slag by hydrated lime resulted in decrease in the workability and compressive strength of the mix.

Table 9-5: Properties of the mixtures M7, M9 and M10

Mix ID	Relative slump value	Density; (g/cm^3)	Compressive strength; (MPa)
M7	16.6	1.82	30.5
M9	0.2	1.78	21
M10	0.2	1.60	8.5

According to Table 9-5, for a constant W/GP solids ratio the compressive strength of the mixture M10, containing the "Na_2SiO_3-GD" activator, significantly decreased by 60% with respect to that of the mixture M9 containing the "Na_2SiO_3-Anhydrous" activator. In addition, the density of the mixture M10 decreased by 10% with respect to that of the mixture M9. The workability of both mixes was comparable. Hence, it can be concluded that in the case of using a combination of fly ash and slag or fly ash, slag and hydrated lime as the geopolymer source materials, the use of "Na_2SiO_3-Anhydrous" activator would be more effective resulting in moderate to high workability and compressive strength compared to "Na_2SiO_3-GD" activator. It should be pointed out that although the relative slump values of the mixtures M3, M9, M10 and M11 were relatively low compared to the other mixes, however these mixes yet exhibited adequate workability as being vibrated and compacted using a vibrating table, thanks to their thixotropic properties. In addition, it should be noted that the reported relative slump values are based

on the mini-slump tests without the 25 times tamping of the flow table. Hence, there was no problem in terms of casting and compaction of these specimens.

9.6.2 Ambient temperature cured one-part geopolymer mixes

As mentioned earlier, the effects of ambient temperature curing on the properties of the developed one-part geopolymer mixes were also investigated in this study. In this regard, the mixture M4 containing a combination of fly ash and hydrated lime as the geopolymer source material and the "Na_2SiO_3-GD" powder as the solid activator, as well as the mixtures M8 and M11 containing a combination of fly ash and slag as the geopolymer precursors and the "Na_2SiO_3-Anhydrous" powder as the solid activator were subjected to ambient temperature curing and their mechanical properties were compared to those of the counterpart heat cured mixes. Comparison of the hardened density and compressive strength of the ambient temperature cured and heat cured one-part geopolymer mixes are presented in Table 9-6. As can be seen, in the case of the mixture M4, the 7-days compressive strength of the mix was corresponding to 73% of the 28-days compressive strength. However, in the case of the mixtures M8 and M11 the 7-days compressive strength of the mix was on average equivalent to 90% of the 28-days compressive strength. In addition, the ambient temperature cured one-part geopolymer mixtures M8 and M11, in which combinations of fly ash and slag were used as the geopolymer source materials activated by the "Na_2SiO_3-Anhydrous" powder, exhibited significantly higher compressive strength than that of the ambient temperature cured one-part geopolymer mixture M4, in which a combination of fly ash and hydrated lime was used as the geopolymer source materials activated by the "Na_2SiO_3-GD" powder.

Table 9-6: Comparison of the properties of heat and ambient temperature cured one-part geopolymer mixes

Mix ID	Density; (g/cm^3)			Compressive strength; (MPa)		
	Ambient temperature cured		Heat cured	Ambient temperature cured		Heat cured
	7-days	28-days		7-days	28-days	
M4	1.89	1.87	1.72	10.4	14.2	14.9
M8	1.88	1.92	1.93	33.9	36.9	37.3
M11	1.86	1.90	1.88	42.1	48.6	44.7

According to Table 9-6, the 28-days compressive strength and density of the ambient temperature cured one-part geopolymer mixtures, regardless of the type of the activator and geopolymer source materials, were almost comparable to those of the counterpart heat cured one-part geopolymer mixes. This translates to the possibility of using the solid activators in practice without the necessity of heat curing, which provides the possibility of in-situ application for the developed one-part geopolymer mixes. Hence, it can be concluded that the results of using the "Na_2SiO_3-GD" and "Na_2SiO_3-Anhydrous" powders as the solid activators are encouraging in terms of possibilities for using the "just add water" concept in practice without the necessity of heat curing similar to the conventional cementitious materials. However, the compressive strength of the mixture M4 is relatively low and future work involves increasing its compressive strength to broaden its applications. It should be noted that the compressive strength of all ambient temperature cured one-part geopolymer mixtures developed in this study was significantly higher than that of the mixes developed by Yang et al. (2008), in which a maximum compressive strength of 9.45 MPa after 28 days of curing was achieved where 100% fly ash and the Anhydrous Grade metasilicate powder were used as the source material and the solid activator, respectively.

9.7 Summary and Conclusions

In this chapter, heat and ambient temperature cured one-part geopolymer mixes were synthesized by "just adding water" similar to the conventional cement-based materials. Twelve appropriate one-part geopolymer mixes were developed through the experiments. Different combinations of low- calcium (Class F) fly ash, slag and hydrated lime were used as the aluminosilicate source materials. Three different grades of sodium silicate and a combination of sodium silicate and sodium hydroxide powders were used as the solid activators. A conventional two-part geopolymer mix with the commonly used Na-based activator solution (i.e. NaOH and D Grade Na_2SiO_3 solutions) was also made for comparison. Effects of the type and amount of the solid activator, the amount of fly ash replacement with slag and hydrated lime and water content on short term mechanical properties of the heat cured one-part geopolymer mixtures comprising workability of the fresh mix, hardened density and compressive strength were evaluated. Effects of the ambient temperature curing on the properties of the developed one-part geopolymer mixes were also evaluated. The following specific conclusions are drawn:

1) The use of solid activators such as GD Grade sodium silicate or sodium metasilicate powders in the geopolymer mix verified the feasibility of developing a one-part mix or "bag" of geopolymer binder for the construction industry as an economical and user-friendly alternative to Portland cement binder.

2) GD Grade sodium silicate powder was the most effective type of solid activator in the case of using a combination of fly ash and hydrated lime as the geopolymer source materials. On the other hand, in the case of using a combination of fly ash and slag or fly ash, slag and hydrated lime as the aluminosilicate precursors, Anhydrous Grade sodium metasilicate powder was the most effective type of solid activator.

3) By using a small amount of GD Grade sodium silicate powder (e.g. 1.5 wt.%) in a (fly ash + lime) system, one-part geopolymer mixes with the compressive strength over 20 MPa were synthesized. Whereas, by using a relatively large amount of Anhydrous Grade sodium metasilicate powder (e.g. 8−12 wt.%) in a (fly ash + slag) or (fly ash + slag + lime) system, one-part geopolymer mixes with the compressive strength over 48 MPa were manufactured.

4) The feasibility of developing a one-part geopolymer mix containing 100% fly ash as the source material and a combination of NaOH and GD Grade Na_2SiO_3 powders as the solid activator with compressive strength over 29 MPa, instead of the commonly used NaOH and D Grade Na_2SiO_3 solutions was experimentally established.

5) The 28-days compressive strength of the ambient temperature cured one-part geopolymer mixtures, regardless of the type of activator and geopolymer source materials, were almost comparable to that of the counterpart heat cured one-part geopolymer mixes. This translates to the possibility of using the "just add water" concept in practice by using the solid activator without the heat curing requirement similar to the conventional cement based materials.

In summary, this study demonstrated that the ambient temperature cured one-part geopolymer is possible by using fly ash and slag as the commonly used geopolymer source materials and a small amount of the solid activator. This significantly enhances the commercial viability and large-scale in-situ application of the geopolymer by eliminating the difficulties associated with handling large quantities of user-hostile

alkaline solutions and the necessity for the heat curing. Furthermore, the use of a small amount of solid silicates could also results in some economical saving compared to large quantities of the commonly used NaOH and Na_2SiO_3 solutions, as the price of these solid activators are cheaper than that of the NaOH solution.

9.8 References

BARBOSA, V. F., MACKENZIE, K. J. & THAUMATURGO, C. 2000. Synthesis and characterisation of materials based on inorganic polymers of alumina and silica: sodium polysialate polymers. *International Journal of Inorganic Materials,* 2, 309-317.

CRIADO, M., FERNÁNDEZ-JIMÉNEZ, A., DE LA TORRE, A., ARANDA, M. & PALOMO, A. 2007. An XRD study of the effect of the SiO 2/Na 2 O ratio on the alkali activation of fly ash. *Cement and Concrete Research,* 37, 671-679.

DUXSON, P. & PROVIS, J. L. 2008. Designing precursors for geopolymer cements. *Journal of the American Ceramic Society,* 91, 3864-3869.

FENG, D., PROVIS, J. L. & DEVENTER, J. S. 2012. Thermal Activation of Albite for the Synthesis of One-Part Mix Geopolymers. *Journal of the American Ceramic Society,* 95, 565-572.

HAJIMOHAMMADI, A., PROVIS, J. L. & VAN DEVENTER, J. S. 2008. One-part geopolymer mixes from geothermal silica and sodium aluminate. *Industrial & Engineering Chemistry Research,* 47, 9396-9405.

HAJIMOHAMMADI, A., PROVIS, J. L. & VAN DEVENTER, J. S. 2010. Effect of alumina release rate on the mechanism of geopolymer gel formation. *Chemistry of Materials,* 22, 5199-5208.

HAJIMOHAMMADI, A., PROVIS, J. L. & VAN DEVENTER, J. S. 2011. The effect of silica availability on the mechanism of geopolymerisation. *Cement and Concrete Research,* 41, 210-216.

HARDJITO, D., WALLAH, S. E., SUMAJOUW, D. M. & RANGAN, B. V. 2004. On the development of fly ash-based geopolymer concrete. *ACI Materials Journal-American Concrete Institute,* 101, 467-472.

ISMAIL, I., BERNAL, S. A., PROVIS, J. L., SAN NICOLAS, R., BRICE, D. G., KILCULLEN, A. R., HAMDAN, S. & VAN DEVENTER, J. S. 2013. Influence of fly

ash on the water and chloride permeability of alkali-activated slag mortars and concretes. *Construction and Building Materials,* 48, 1187-1201.

KANI, E. N., ALLAHVERDI, A. & PROVIS, J. L. 2012. Efflorescence control in geopolymer binders based on natural pozzolan. *Cement and Concrete Composites,* 34, 25-33.

KOLOUŠEK, D., BRUS, J., URBANOVA, M., ANDERTOVA, J., HULINSKY, V. & VOREL, J. 2007. Preparation, structure and hydrothermal stability of alternative (sodium silicate-free) geopolymers. *Journal of Materials Science,* 42, 9267-9275.

LEE, W. & VAN DEVENTER, J. 2002. Structural reorganisation of class F fly ash in alkaline silicate solutions. *Colloids and Surfaces A: Physicochemical and Engineering Aspects,* 211, 49-66.

LEE, W. & VAN DEVENTER, J. 2003. Use of infrared spectroscopy to study geopolymerization of heterogeneous amorphous aluminosilicates. *Langmuir,* 19, 8726-8734.

PROVIS, J. 2009. Activating solution chemistry for geopolymers. *Geopolymers: Structures, Processing, Properties and Industrial Applications,* 50-71.

PROVIS, J. L., DUXSON, P. & VAN DEVENTER, J. S. 2010. The role of particle technology in developing sustainable construction materials. *Advanced Powder Technology,* 21, 2-7.

REES, C., LUKEY, G. & VAN DEVENTER, J. Characteristics of geopolymers derived from flyash and solid-silicate wastes. Chemeca 2004: 32nd Australasian Chemical Engineering Conference: Sustainable Processes, 2004. Engineers Australia, 173.

YANG, K.-H. & SONG, J.-K. 2009. Workability loss and compressive strength development of cementless mortars activated by combination of sodium silicate and sodium hydroxide. *Journal of materials in Civil Engineering,* 21, 119-127.

YANG, K.-H., SONG, J.-K., ASHOUR, A. F. & LEE, E.-T. 2008. Properties of cementless mortars activated by sodium silicate. *Construction and Building Materials,* 22, 1981-1989.

CHAPTER 10

DEVELOPMENT OF AMBIENT TEMPERATURE CURED ONE-PART SHGCS

Note: This chapter is based on the manuscript "*Micromechanics-based Investigation of a Sustainable Ambient Temperature Cured One-Part Strain Hardening Geopolymer Composite*", by **Nematollahi, B.**, Sanjayan, J., Qiu, J., and Yang, E-H., published in ***Construction and Building Materials***, 2017, 131, 552-563.

10.1 Introduction

This chapter reports the development of an ambient temperature cured one-part SHGC as an alternative to the heat cured two-part fly ash-based SHGC. Such ambient temperature cured one-part SHGC as a "dry mix" uses a small amount of solid activator as alternative to the commonly used alkaline solutions and eliminates the necessity for heat curing. The experimental results presented in Chapter 9 indicated that the best performing ambient temperature cured one-part geopolymer mixture that promotes good mechanical properties, moderate setting time and adequate rheology for uniform fiber dispersion was composed of fly ash (50% w/w) and slag (50% w/w) as the geopolymer precursor and anhydrous sodium metasilicate powder as the solid activator. The water to the precursor (fly ash + slag) ratio was 0.35 and the solid activator to the precursor ratio was 0.08. Therefore, the same one-part geopolymer composition was used in this chapter for the development of the ambient temperature cured one-part SHGC.

The objectives of this chapter are as follows:

(1) To evaluate the quantitative influences of curing condition and type of slag on the matrix and composite properties of the developed one-part SHGCs, comprising density, workability, compressive strength and uniaxial tensile performance.

(2) To perform a micromechanics-based investigation to explain the experimentally observed macroscopic tensile performance of the composites. The investigation included determination of the matrix fracture properties and fiber-matrix interface properties using

fracture toughness tests and single fiber pullout tests, respectively and computing the crack-bridging relation of the composites via a micromechanics-based model.

(3) To compare the material sustainability of the ambient temperature cured one-part SHGC developed in this chapter with the "traditional" heat cured "two-part" fly ash-based SHGC previously developed in Chapter 3, and the typical SHCC M45 (Yang et al., 2007) using material sustainability indicators (MSIs) (Li et al., 2004).

10.2 Materials and Mix Proportions

The low-calcium fly ash (Class F) used in this research was supplied from Gladstone power station in Queensland, Australia. Two types of slags denoted as "typical" slag and "gypsum-free" slag were used in this research. The "typical" slag is a typical Australian slag which contains 2% gypsum, whereas the "gypsum-free" slag contains no gypsum. Table 10-1 presents the chemical composition and LOI of the slags determined by X-ray Fluorescence (XRF). The total does not sum up to 100% because of rounding-off of the percentages. The chemical composition and LOI of fly ash are also re-presented in Table 10-1 for ease of comparison.

Table 10-1: Chemical composition of fly ash and slags

Chemical	Component (wt. %)		
	Fly ash	"Typical" slag	"Gypsum-free" slag
Al_2O_3	25.56	12.37	13.8
SiO_2	51.11	32.76	34.2
CaO	4.3	44.64	43.1
Fe_2O_3	12.48	0.54	0.4
K_2O	0.7	0.33	0.4
MgO	1.45	5.15	5.4
Na_2O	0.77	0.22	0.1
P_2O_5	0.885	0.014	---
TiO_2	1.32	0.51	---
MnO	0.15	0.37	---
SO_3	0.24	4.26	0.8
LOI[1]	0.57	0.09	1.8

[1]Loss on ignition.

Figure 10-1 presents the particle size distribution of the fly ash and slags used in this study determined by using a CILAS particle size analyzer model 1190. The passing percentages of particle size distribution are summarized in Table 10-2. The anhydrous sodium metasilicate powder used in this study was supplied by Redox, Australia with a chemical composition of 51 wt.% Na_2O and 46 wt.% SiO_2 (balance H_2O). The same PVA fiber as that used in Chapter 4 with a surface oil coating of 1.2% by weight was used in this research. Properties of the PVA fiber supplied by Kuraray Co. Ltd., Japan are presented in Table 4-2.

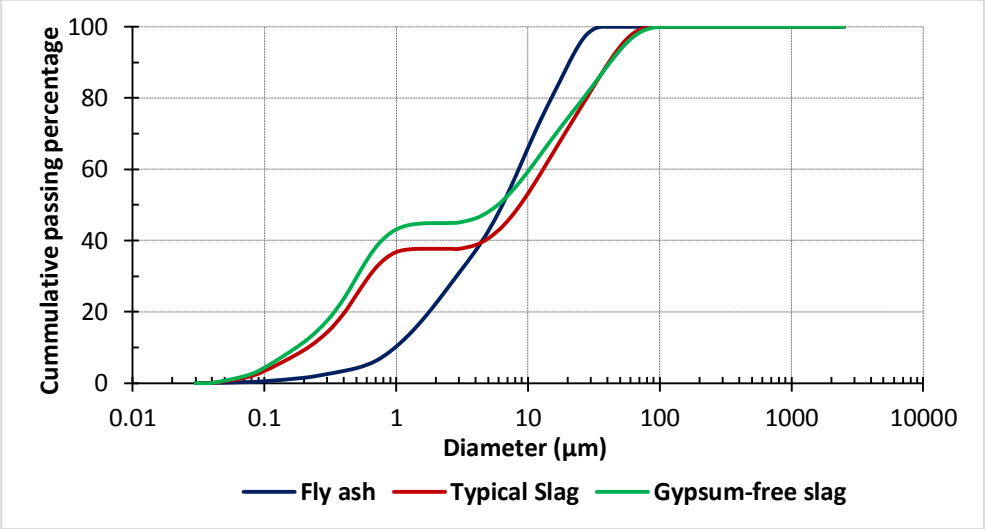

Figure 10-1: Particle size distribution of fly ash and slags

Table 10-2: Particle size distribution of fly ash and slags

Material	90%[a] (µm)	50% [a] (µm)	10% [a] (µm)	Mean diameter (µm)
Fly ash	20.59	6.39	0.98	8.66
"Typical" slag	41.09	8.73	0.21	14.70
"Gypsum-free" slag	42.06	5.89	0.17	13.77

[a] The passing percentage.

Table 10-3 presents mix proportions of the one-part "dry mix" SHGCs investigated in this study. It should be noted that the amorphous contents of fly ash and slag are considered as reactive components, while the crystalline contents are unreacted components acting as filler in the one-part geopolymer matrix. Therefore, unlike typical

SHCC M45 (Yang et al., 2007), micro-silica sand was not used in the one-part SHGC mixtures investigated in this study. The Gladstone fly ash has an amorphous content of 66% (w/w) and crystalline content of 34% (w/w), compared to 92% (w/w) and 8% (w/w), respectively for the "typical" slag (Tennakoon et al., 2014).

Table 10-3: Mix proportions of one-part "dry mix" SHGCs

Mix ID	One-part "dry mix" geopolymer binder				Water[2]	PVA fiber
	Fly ash	"Typical" slag	"Gypsum-free" slag	Solid activator[1]		
One-part SHGC-T	0.50	0.50	---	0.08	0.35	0.02
One-part SHGC-GF	0.50	---	0.50	0.08	0.35	0.02

Note: All numbers are mass ratios of the precursor weight (fly ash + slag) except fiber content (volume fraction).

[1] Composed of anhydrous sodium metasilicate powder.

[2] Added to the one-part "dry mix" geopolymer binder.

10.3 Mixing, Curing and Testing of Specimens

To prepare the one-part geopolymer matrix, fly ash, slag and solid activator in the form of powder were added to a Hobart mixer and dry mixed for approximately 3 minutes. Tap water was then gradually added to the mix and the mixing was continued for another 8 minutes. After the matrix ingredients were thoroughly mixed to achieve the desired fresh state, the flowability of fresh one-part geopolymer matrix (before addition of the fibers) was measured to ensure that the flowability was within the desired range for achieving good fiber dispersion. Finally, the PVA fibers (2% v/v) were gradually added and mixed, taking care to ensure uniform fiber dispersion. The whole mixing procedure generally took 20 minutes. The fresh one-part geopolymer matrix and composite were cast into different molds and compacted using a vibrating table.

To evaluate the effect of curing condition on the matrix and composite properties of the developed one-part SHGCs, the matrix and composite specimens were divided into two groups and subjected to two different curing conditions, namely heat curing and ambient

temperature curing. The procedures for the heat and ambient temperature curing are given in Chapters 4 and 9, respectively.

Mini-slump test also known as spread-flow test was conducted to determine flowability of the fresh one-part geopolymer matrix. In this regard, the one-part geopolymer matrix (without addition of the fibers) was prepared as stated above but the mixing was continued for 20 minutes after adding water. The mini-slump test was then conducted. Details of the mini-slump test are given in Chapter 4. To evaluate the effect of elapsed time on the fresh matrix workability, the fresh one-part geopolymer matrix was left undisturbed for 10 minutes and the mini-slump test was conducted again. This procedure was repeated 4 times and the mini-slump test was conducted with time intervals of 10 minutes.

Compressive strength and hardened density of matrix and composite in each mixture were measured. The Procedures for compression and density tests are given in Chapter 4. Uniaxial tension tests were conducted to evaluate the behavior of the developed one-part SHGCs under direct tension. It should be noted that the gauge length used in this study was about 80 mm. Details of the uniaxial tension test are given in Chapter 4. Three-point bending tests on single edge notched beam specimens were conducted to evaluate the matrix fracture properties including E_m, K_m and J_{tip} of the developed one-part SHGCs. Details of the matrix fracture toughness test are given in Chapter 4. Single-fiber pullout tests were conducted to measure fiber-matrix interfacial properties, including chemical bond G_d, τ_0, and β. Details of the single-fiber pullout test are given in Chapter 7.

10.4 Results and Discussions

10.4.1 Workability, density and compressive strength

Figure 10-2 presents the average workability of the fresh one-part SHGC matrices, in terms of relative slump values. It should be noted that the reported relative slump values are based on the mini-slump test without the 25 times tamping of the flow table. As expected and can be seen in Figure 10-2, the workability, regardless of the type of slag, was decreased over time when the fresh one-part SHGC matrices were left undisturbed. In terms of the effect of type of slag on the fresh matrix workability, as can be seen in Figure 10-2, the initial relative slump value (measured 20 minutes after adding water to the one-part geopolymer binder) of the one-part SHGC-T matrix (made with “typical”

slag) was slightly lower than that of the one-part SHGC-GF matrix (made with "gypsum-free" slag). However, the reduction rate of relative slump value over time in the one-part SHGC-T matrix was considerably higher than that of the one-part SHGC-GF matrix. In other words, the final relative slump value (measured 60 minutes after adding water to the one-part geopolymer binder) of the one-part SHGC-T matrix was 32% lower than that of the one-part SHGC-GF matrix. This could be due to the fact that the "typical" slag contains 2% gypsum.

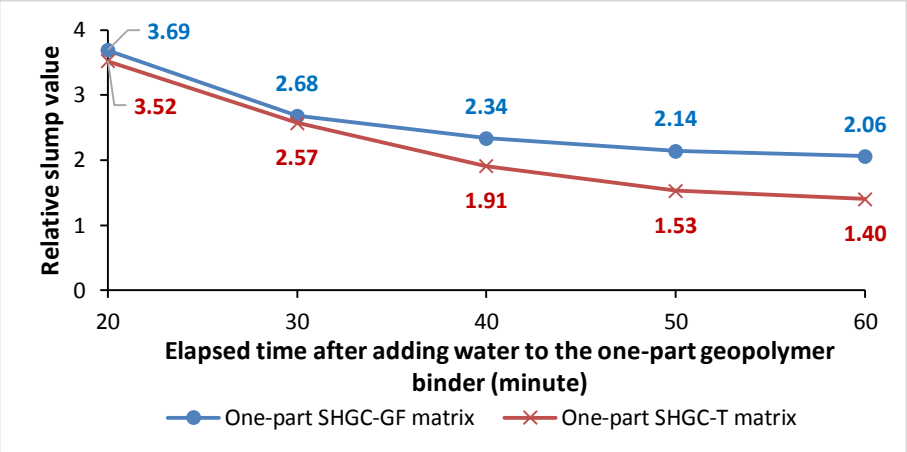

Figure 10-2: Workability of the fresh one-part SHGC matrices

As can be seen in Figure 10-2, 60 minutes after adding water to the one-part geopolymer binder, the measured relative slump values of the one-part SHGC-T and one-part SHGC-GF matrices (without the 25 times tamping of the flow table) were 1.40 and 2.06, respectively. Immediately after the last measurement of the spread diameter, the flow table was tamped 25 times in 15 seconds and the spread diameters were measured again. The measured relative slump values of the one-part SHGC-T and one-part SHGC-GF matrices after the 25 times tamping of the flow table were 4.27 and 3.95, respectively. This translates to 205% and 92% increase in the relative slump values of the one-part SHGC-T and one-part SHGC-GF matrices, respectively, due to the 25 times tamping of the flow table. This indicates that while both fresh one-part SHGC matrices, regardless of the type of slag, exhibited thixotropic properties, the thixotropic property of the one-part SHGC-T matrix was significantly (more than 2 times) higher than that of the one-part SHGC-GF matrix. Visual observations revealed that both fresh one-part SHGC

matrices exhibited sufficient workability to ensure uniform fiber dispersion, thanks to their thixotropic properties. According to the mini-slump test results and visual observations, the rheology (i.e. workability and setting time) of the one-part SHGC mixtures developed in this study were appropriate in a way that it was possible to work with the fresh mixtures for at least more than one hour after adding water, without any difficulty during mixing and casting of the specimens.

The average hardened density of each mix is presented in Table 10-4. The density of one-part SHGCs was in the range of 1800 kg/m^3 to 1874 kg/m^3, which is 22–25% less than that of a normal weight concrete with a density of 2400 kg/m^3 and meet the density requirement for lightweight concrete (below 1850 kg/m^3) (ACI 213R, 2014). It is interesting to note that the density of ambient temperature cured one-part SHGCs is 10−11% less than that of typical SHCC M45 (2077 kg/m^3) (Yang et al., 2007). This may be attributed to the lower specific density of fly ash (2.45 g/cm^3) and slag (2.85 g/cm^3) than that of cement (3.15 g/cm^3) and exclusion of micro-silica sand from the one-part SHGC mixtures. As can be seen in Table 10-4, the type of slag did not have any noticeable effect on the density of the developed one-part SHGCs and their corresponding one-part SHGC matrices. The density of the developed one-part SHGCs, regardless of the curing condition and type of slag, was relatively lower than that of the corresponding one-part SHGC matrices. This may be attributed to increase of entrapped air due to the addition of micro-polymeric fibers, which results in a composite with higher porosity compared to the matrix material alone (Li and Mishra, 1992).

Table 10-4: Density and compressive strength results

Mechanical property		One-part SHGC-T		One-part SHGC-GF	
		Heat cured	Ambient temperature cured	Heat cured	Ambient temperature cured
Density; (kg/m^3)	Matrix	1880±12	1895±9	1898±2	1895±12
	Composite	1816±7	1849±14	1800±11	1874±17
Compressive strength; (MPa)	Matrix	44.7±4.1	48.6±4.1	45.3±1.8	48.2±5.3
	Composite	47.4±6.7	48.7±4.1	43.3±1.3	52.5±5.6

As shown in Table 10-4, the density of the ambient temperature cured one-part SHGCs and their corresponding ambient temperature cured one-part SHGC matrices, regardless

of the type of slag, were slightly higher than that of the counterpart heat cured one-part SHGCs. This could be attributed to the different moisture content of the specimens due to their different curing conditions. In fact, as mentioned in Chapter 9, the ambient temperature cured specimens were stored in the water tank at a temperature of 23°C ± 3°C for 27 days after de-molding. It is, thereby, inferred that the ambient temperature cured specimens were in saturated surface dry (SSD) condition at the day of testing. However, the heat cured specimens were supposed to be in almost dry condition at the day of testing as they were placed in the oven at 60°C for 24 hours immediately after casting. Previous studies revealed that in fly ash-based geopolymer, large amount (almost 89%) of the water present in the mixture released after the geopolymerisation reaction and evaporated during the heat curing period and the resulting geopolymer compounds contained only a small amount (almost 11%) of non-evaporable/combined water which may have been entrapped in discontinuous gel pores and has remained combined in the geopolymer products (Fang and Kayali, 2013).

The average compressive strength of each mix is also presented in Table 10-4. The compressive strength of the one-part SHGCs ranged from 43.3 MPa to 52.5 MPa, which is well above the compressive strength requirement of 17 MPa for structural lightweight concrete (ACI 213R, 2014). Among all one-part SHGC mixes, the ambient temperature cured one-part SHGC-GF exhibited the highest compressive strength, comparable to typical SHCC M45 (52.6 MPa) (Yang et al., 2007). However, unlike typical SHCC M45, the ambient temperature cured one-part SHGC-GF contains no cement, and therefore it has significantly lower environmental footprints compared to the typical SHCC M45, in which its cement content is still 1.5 times that of normal concrete (Yang et al., 2007).

As can be seen in Table 10-4, the curing condition, regardless of type of slag, did not have significant effect on the compressive strength of the one-part SHGC matrices. In addition, the curing condition did not have considerable effect on the compressive strength of the one-part SHGCs made with “typical” slag. However, the compressive strength of the ambient temperature cured one-part SHGC-GF was 21% higher than that of the counterpart heat cured one-part SHGC-GF. According to Table 10-4, the type of slag, regardless of the curing condition, did not have significant effect on the compressive strength of the one-part SHGCs and their corresponding one-part SHGC matrices.

While it is not the focus of this study, it is interesting to note that the compressive strength of the ambient temperature cured one-part SHGCs developed in this study, regardless of the type of slag, were significantly (180−202%) higher than that of the "traditional" ambient temperature cured two-part fly ash-based SHGC developed by Ohno and Li (2014), in which not only possessed the low compressive strength of 17.4 MPa, but also the common user-hostile activator solutions were used for its manufacture rather than the solid activator used in this study.

10.4.2 Matrix fracture properties

Elastic modulus (E_m), fracture toughness (K_m) and crack tip toughness (J_{tip}) of the developed one-part SHGC matrices (without addition of the fibers) are presented in Table 10-5. As mentioned in Chapter 4, it should be noted that in this research, the E_m was not measured experimentally using cylindrical specimens in compression, instead the E_m of each mix was derived based on ECM (Karihaloo and Nallathambi, 1990) from the linear portion of the load-deflection curve of the notched beam specimen in three-point bending tests. The E_m values thereby reported in Table 10-5 should only be considered as relative values enabling us to compare the matrix elastic modulus of each mix.

Table 10-5: Matrix fracture test results

Matrix fracture property	One-part SHGC-T matrix		One-part SHGC-GF matrix	
	Heat cured	Ambient temperature cured	Heat cured	Ambient temperature cured
Elastic modulus E_m; (GPa)[a]	4.8	5.3	4.3	4.1
Fracture toughness, K_m; ($MPa.m^{1/2}$)[a]	0.287	0.316	0.237	0.251
Crack tip toughness, J_{tip}; (J/m^2)[b]	17.2	18.8	13.1	15.4

[a] Following ECM (Karihaloo and Nallathambi, 1990).

[b] $J_{tip} = \frac{K_m^2}{E_m}$ (Li et al., 1995).

As can be seen in Table 10-5, the curing condition, regardless of the type of slag, did not have significant effect on the matrix elastic modulus. This is consistent with the compressive strength results reported in Table 10-4. In terms of the effect of type of slag

on the matrix elastic modulus, as can be seen in Table 10-5, the E_m of the one-part SHGC-T matrices, regardless of the curing condition, were 12−29% higher than the corresponding one-part SHGC-GF matrices.

With regards to the effect of the curing condition on the matrix fracture toughness, the K_m of the ambient temperature cured one-part SHGC matrices, regardless of the type of slag, were slightly higher than that of the corresponding heat cured one-part SHGC matrices. This indicates that crack propagation in the ambient temperature cured one-part SHGC matrices is likely to be more tortuous; thereby, consumes more energy compared to that of the heat cured one-part SHGC matrices. The visual observations of the fracture surface of the specimens confirmed this trend. According to Pan et al. (2011), the fracture toughness of concrete is mainly affected by the microstructure of the paste and the size, texture and angularity of the coarse aggregates. Thereby, it can be inferred that the most prominent reason for the difference in the K_m of the heat cured and ambient temperature cured one-part SHGC matrices, regardless of the type of slag, lies in their different geopolymer microstructures, because all parameters, except the curing condition, were kept constant.

It is thereby hypothesized that the microstructure of the heat cured and ambient temperature cured one-part SHGC matrices would be different due to their different curing condition. In other words, the reaction products in the ambient temperature cured one-part SHGC matrices are likely to be coarser than those of the heat cured one-part SHGC matrices, resulting in a more tortuous crack propagation in the ambient temperature cured one-part SHGC matrices, and hence leading to their slightly higher matrix fracture toughness. Consequently, as can be seen in Table 10-5, the J_{tip} of the ambient temperature cured one-part SHGC matrices, regardless of the type of slag, were 9−18% higher than that of the corresponding heat cured one-part SHGC matrices. This corresponds to the higher K_m of the ambient temperature cured one-part SHGC matrices. It is thereby concluded that ambient curing reduces brittleness of the one-part SHGC matrix.

With regards to the effect of type of slag on the matrix fracture toughness, the K_m of the one-part SHGC-GF matrices (made with “gypsum-free” slag), regardless of the curing condition, were 17−21% lower than that of the corresponding one-part SHGC-T matrices

(made with "typical" slag). Similar to the above discussion, it is hypothesized that the microstructure of the one-part SHGC-GF and one-part SHGC-T matrices would be different due to their different type of slag. In other words, the reaction products in the one-part SHGC-GF matrices are likely to be finer than those of the one-part SHGC-T matrices, resulting in a less tortuous crack propagation in the one-part SHGC-GF matrices, and hence leading to their lower matrix fracture toughness. Consequently, as can be seen in Table 10-5, the crack tip toughness of the one-part SHGC-GF matrices, regardless of the curing condition, were 18−24% lower than that of the corresponding one-part SHGC-T matrices. This corresponds to the lower K_m of the one-part SHGC-GF matrices. It is thereby concluded that using "gypsum-free" slag increases brittleness of the one-part SHGC matrix.

10.4.3 Fiber-matrix interface properties

The fiber-matrix interface properties including G_d, τ_0, and β of the one-part SHGCs are presented in Table 10-6. Frictional bond strength is considered to follow a Coulomb-type friction law, which can be explained by a fiber-matrix friction coefficient and residual normal shrinkage stress of matrix onto the fiber surface (Li and Stang, 1997). Lang et al. (1993) reported that there is a positive correlation between fracture surface roughness and fracture toughness. As fracture toughness increases, fracture surface roughness increases. Therefore, it can be inferred that in the one-part SHGCs when the PVA fiber is fully debonded from the surrounding matrix, the fracture surface roughness in the fiber-matrix interfacial zone depends on the fracture toughness of the one-part SHGC matrix. As fracture toughness of the one-part SHGC matrix increases, the fracture surface roughness in the fiber-matrix interfacial zone, and thereby the contact surface between the fiber and the matrix during the fiber slippage increases. This results in the higher frictional bond of the PVA fiber with the one-part SHGC matrix.

In this study as can be seen in Table 10-6, the τ_0 increased from heat cured one-part SHGC-GF to ambient temperature cured one-part SHGC-GF, and then to heat cured one-part SHGC-T, and finally to ambient temperature cured one-part SHGC-T. Such trend is well consistent with the measured matrix fracture toughness, as reported in Table 10-5. The ambient temperature cured one-part SHGC-T with the highest K_m exhibited the highest τ_0 (2.14 MPa), whereas the heat cured one-part SHGC-GF with the lowest K_m

exhibited the lowest τ_0 (1.14 MPa). It is concluded that there is a positive correlation between the frictional bond strength of the one-part SHGC and the fracture toughness of the one-part SHGC matrix. The higher the fracture toughness of the one-part SHGC matrix, the higher the value of τ_0.

Table 10-6: Fiber-matrix interfacial properties

Fiber-matrix interfacial property	One-part SHGC-T		One-part SHGC-GF	
	Heat cured	Ambient temperature cured	Heat cured	Ambient temperature cured
Chemical bond strength, G_d; (J/m^2)	0.85±0.47	1.03±0.34	0.91±0.70	0.46±0.37
Frictional bond strength, τ_0; (MPa)	1.47±1.30	2.14±0.62	1.14±0.82	1.31±0.29
Slip hardening coefficient, β	0.021±0.0048	0.041±0.0070	0.049±0.012	0.040±0.0059

With regards to chemical bond strength, as can be seen in Table 10-6, the ambient temperature curing increased the G_d when "typical slag" was used in the one-part SHGC mixture, whereas an opposite trend is observed when "gypsum-free" slag was used (i.e. the G_d of the heat cured one-part SHGC-GF was higher than that of the counterpart ambient temperature cured composite). Kanda and Li (1998) reported that the PVA fibers are expected to exhibit a strong chemical bond with the cement matrix, of which strength is primarily determined by the cement chemistry and surface chemistry of the fibers. In this study, the type of PVA fiber was identical in all composites. It is thereby hypothesized that the main prominent reason for the different G_d of the one-part SHGCs may be due to the different geopolymer chemistry (i.e. microstructure) of the one-part SHGC matrices. As mentioned in Section 10.4.2, it is hypothesized that the matrix microstructure of the developed one-part SHGCs may be different due to their different curing condition and type of slag.

10.4.4 Uniaxial tensile performance

Tensile stress-strain responses of the developed one-part SHGCs are presented in Figures 10-3 to 10-6. As can be seen, the developed one-part SHGCs, regardless of the curing condition and type of slag, exhibited strong strain hardening behavior. The uniaxial

tension test results including the average measured ultimate tensile strength (σ_{cu}) and tensile strain capacity (ε_{cu}) and the estimated first-crack strength (σ_{fc}) are presented in Table 10-7. As can be seen, the developed one-part SHGCs exhibited high ultimate tensile strength in the range of 4.3−4.6 MPa, with very high tensile strain capacity in the range of 2.6−4.2%, which is several hundred times that of conventional geopolymer concrete.

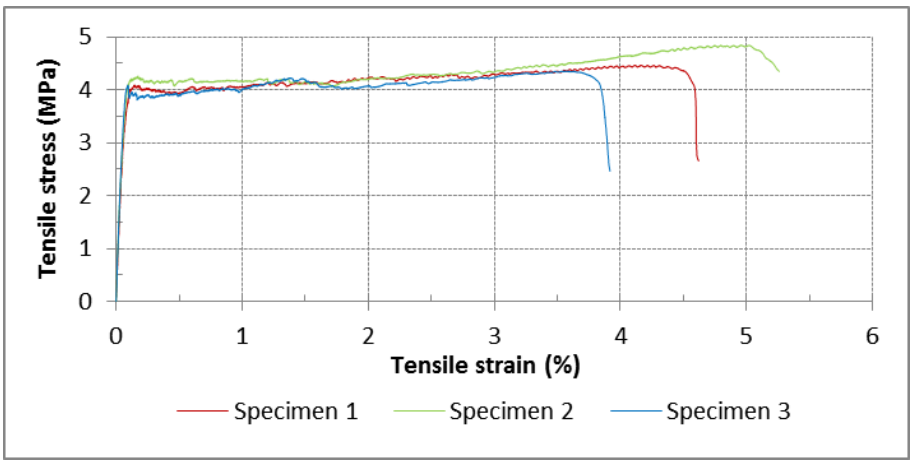

Figure 10-3: Tensile stress-strain curves of ambient temperature cured one-part SHGC-T

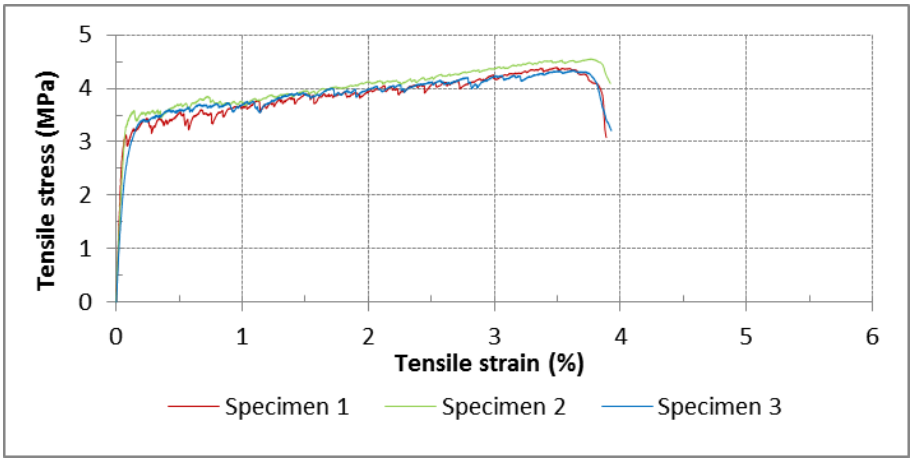

Figure 10-4: Tensile stress-strain responses of heat cured one-part SHGC-T

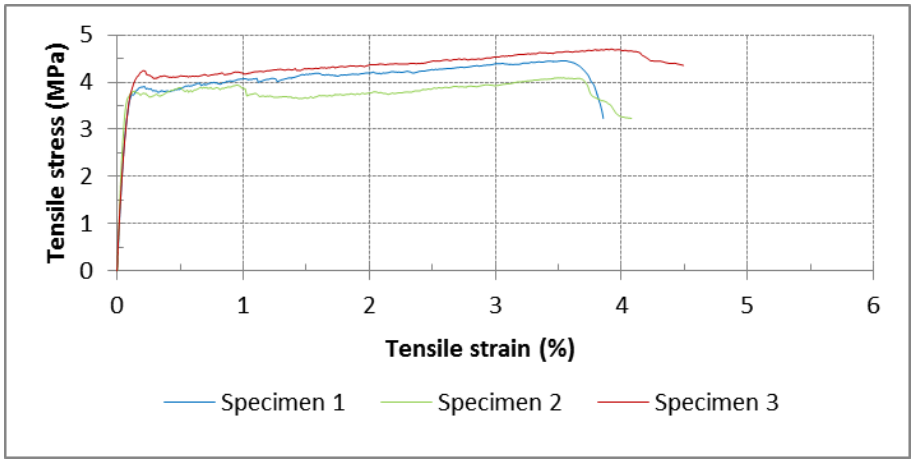

Figure 10-5: Tensile stress-strain responses of ambient temperature cured one-part SHGC-GF

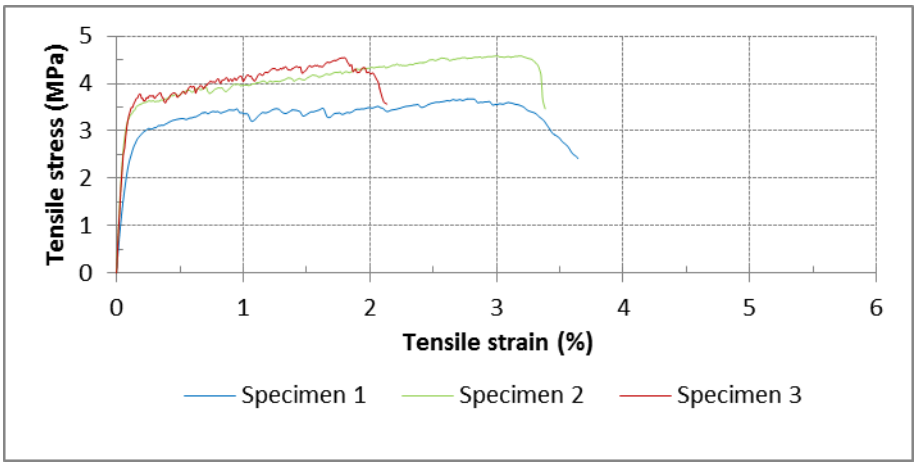

Figure 10-6: Tensile stress-strain responses of heat cured one-part SHGC-GF

Table 10-7: Uniaxial tension test results

Composite property	One-part SHGC-T		One-part SHGC-GF	
	Heat cured	Ambient temperature cured	Heat cured	Ambient temperature cured
First-crack strength, σ_{fc}; (MPa)	3.3±0.15	4.1±0.10	3.4±0.37	3.9±0.26
Ultimate tensile strength, σ_{cu} ; (MPa)	4.4±0.11	4.6±0.26	4.3±0.51	4.4±0.31
Tensile strain capacity, ε_{cu}; (%)	3.6±0.14	4.2±0.71	2.6±0.72	3.7±0.23

While it is not the focus of this study, it is interesting to note that the ultimate tensile strength and tensile strain capacity of the ambient temperature cured one-part SHGCs

developed in this study, regardless of type of slag, were significantly (52−59% and 37−56%, respectively) higher than those of the "traditional" ambient temperature cured two-part fly ash-based SHGC developed by Ohno and Li (2014), in which the common activator solutions were used for its production rather than the solid activator used in this study and possessed the ultimate tensile strength and tensile strain capacity of 2.9 MPa and 2.7%, respectively.

Figure 10-7 presents the typical multiple cracking pattern of the ambient temperature cured one-part SHGC-T. It should be pointed out that the real number of micro-cracks formed during loading of the specimens was more than the number of visible cracks on the surface of the unloaded specimens. This is because many of the micro cracks formed during loading completely closed after unloading, which make them very difficult to be detected on the surface of the unloaded specimens (Li et al., 2001).

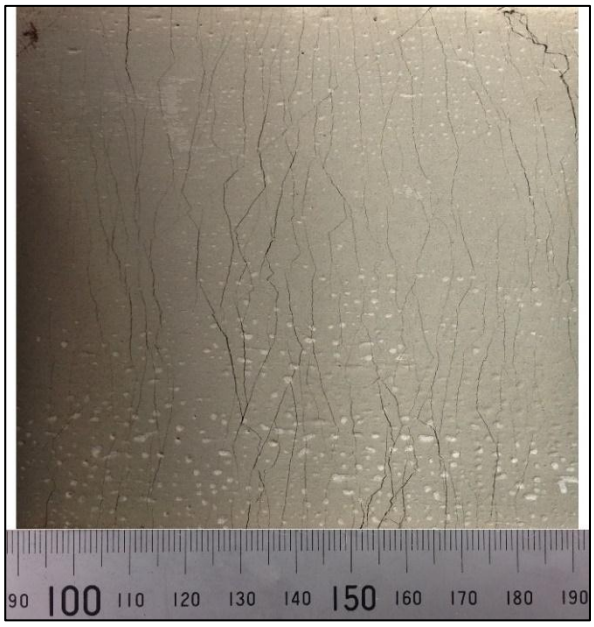

Figure 10-7: Typical multiple cracking pattern of ambient temperature cured one-part SHGC-T

As can be seen in Figure 10-7, enormous micro-cracks with tightly controlled crack width and almost equal crack spacing in the range of 2–3 mm were observed, which represent saturated multiple cracking behavior. This multiple cracking pattern corresponds to the very high tensile strain capacity of the composite. The tight crack width indicates

significant improvement in durability of the developed ambient temperature cured one-part SHGC compared to cracked brittle geopolymer concrete with crack width in the range of several hundred microns to a few millimeters (Li, 2002).

With regards to the effect of the curing condition on the tensile performance, as can be seen in Table 10-7, the ambient temperature cured one-part SHGCs, regardless of the type of slag, exhibited superior uniaxial tensile performance to the counterpart heat cured composites. The first-crack strength and tensile strain capacity of the ambient temperature cured one-part SHGCs, regardless of the type of slag, were 15−24% and 17−42%, respectively higher than those of the counterpart heat cured composites. The higher first-crack strength of the ambient temperature cured one-part SHGCs could be attributed to the higher fracture toughness of the ambient temperature cured one-part SHGC matrices as shown in Table 10-5 (Li et al., 2001). The ultimate tensile strength of the ambient temperature cured and heat cured one-part SHGCs, regardless of the type of slag, were comparable.

The underlying reasons for the higher tensile strain capacity of the ambient temperature cured one-part SHGCs could be explained in terms of the two PSH performance indices proposed by Kanda and Li (2006), which could be calculated based on the micromechanics modeling of fiber-bridging behavior. In this study, the micromechanics-based model developed by Yang et al. (2008) was used to predict the fiber-bridging constitutive law $\sigma(\delta)$ of the developed one-part SHGCs. The applicability of this micromechanics-based model to evaluate the tensile performance of SHGCs is demonstrated in Chapter 8. The resulting PSH performance indices are plotted in Figure 10-8. As can be seen, in all developed composites both PSH performance indices exceed unity, and hence it can be concluded that the necessary micromechanics-based strength and energy conditions of steady-state flat crack propagation are satisfied, which result in sequential development of matrix multiple cracking. Therefore, all one-part SHGCs developed in this study exhibited strain hardening behavior. In addition, as can be seen in Figure 10-8, while the PSH strength indices of the ambient temperature cured and heat cured one-part SHGCs, regardless of the type of slag, are comparable, the PSH energy index of the ambient temperature cured one-part SHGCs, regardless of the type of slag, is 14−20% higher than that of the corresponding heat cured composites, which results in

greater possibility of saturated multiple cracking, and thereby higher tensile strain capacity of the ambient temperature cured one-part SHGCs.

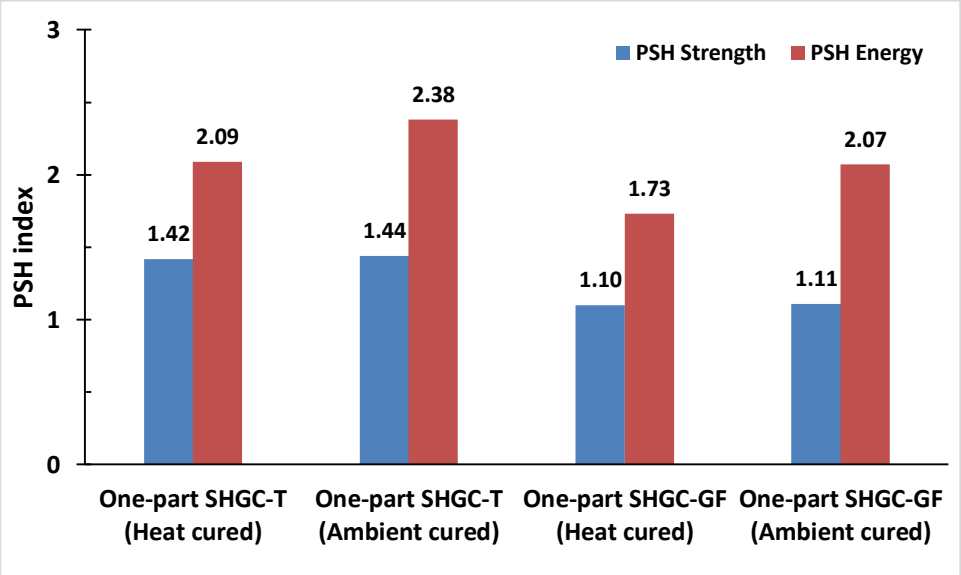

Figure 10-8: PSH performance indices of one-part SHGCs

In terms of the effect of the type of slag on the tensile performance, as can be seen in Table 10-7, the one-part SHGC-T mixes, regardless of the curing condition, exhibited superior uniaxial tensile performance to the corresponding one-part SHGC-GF mixes. The tensile strain capacity of the one-part SHGC-T mixes, regardless of the curing condition, was 14−38% higher than that of the corresponding one-part SHGC-GF mixes. Similar to the above discussion, the reasons for the superior tensile ductility of the one-part SHGC-T mixes could also be explained in terms of the two PSH performance indices. As can be seen in Figure 10-8, the PSH strength and energy indices of the one-part SHGC-T mixes, regardless of the curing condition, are 29−30% and 15−21%, respectively higher than those of the corresponding one-part SHGC-GF mixes, which result in greater possibility of saturated multiple cracking, and thereby higher tensile strain capacity of the one-part SHGC-T mixes.

10.4.5 Environmental performance

MSIs in terms of embodied energy and CO_2 emission were calculated in this study to quantitatively compare the material greenness of the ambient temperature cured one-part SHGC developed in this study with the "traditional" heat cured two-part fly ash-based

SHGC previously developed in Chapter 5, and the typical SHCC mix 45 (M45) (Yang et al., 2007). Table 10-8 presents the mix proportions of different composites and the life cycle inventory data of the ingredients. The inventory data was obtained from relevant literature (Yang et al., 2007; Huang et al., 2012; McLellan et al., 2011; Fawer et al., 1999; Yang et al., 2013; National Greenhouse Accounts Factors, 2014; Integrated Pollution Prevention and Control (IPPC), 2001).

Table 10-8: Mix proportions of different composites and life cycle inventory data of the ingredients

Ingredients	Typical SHCC M45[1] (kg/m^3)	Heat cured two-part SHGC[2] (kg/m^3)	Ambient temperature cured one-part SHGC; (kg/m^3)	Embodied energy (MJ/kg)	CO_2 emissions (kg/kg)
OPC	571	---	---	5.06[3]	0.898[3]
Fly ash	685	1029.7	637.4	---	---
slag	---	---	637.4	---	---
Micro-silica sand	456	308.9	---	0.175[3]	0.026[3]
Water	332	---	446.2	---	---
Activator solution[4]	---	463.4	---	4.26[6]	0.358[5]
Solid activator[7]	---	---	102	10.57[8]	0.57[8]
Superplasticizer	6.8	---	---	36.76[3]	1.48[3]
PVA fiber	26	26	26	106.54[3]	3.6[3]
Heat curing	N/A	Applicable	N/A	0.0828[9]	0.017[9]

[1] The mix proportion of typical SHCC M45 is adopted from Yang et al. (2007).

[2] The mix proportion of "traditional" heat cured two-part fly ash-based SHGC is adopted from Chapter 5.

[3] Derived from Huang et al. (2012) and Yang et al. (2007).

[4] Commonly used Na-based activator solution.

[5] Derived from McLellan et al. (2011).

[6] Derived from Fawer et al. (1999) and Integrated Pollution Prevention and Control (IPPC) (2001).

[7] Composed of anhydrous sodium metasilicate powder.

[8] Derived from Fawer et al. (1999).

[9] Derived from Yang et al. (2013) and National Greenhouse Accounts Factors (2014).

It should be noted that three assumptions were made in deriving the life cycle inventory data given in Table 10-8. First, the embodied energy and CO_2 emissions associated with fly ash and slag are zero as they are considered as by-products of coal power station and iron industry, respectively. Second, the embodied energy and CO_2 emissions associated with water are negligible relative to other ingredients. Third, the embodied energy and CO_2 emissions associated with the heat curing approach (24 hours at 60° C) adopted for manufacture of the "traditional" heat cured two-part fly ash-based SHGC are derived from the data given in Yang et al. (2013) and National Greenhouse Accounts Factors (2014), considering the average emission factor for consumption of electricity from the grid in Australia to be 0.73 kg CO_2-e/kWh.

Figure 10-9 presents the embodied energy and CO_2 emissions associated with production of a unit volume of different composites. As can be seen, the embodied energy and CO_2 emissions associated with manufacture of the SHGCs, regardless of the curing condition and type of geopolymer matrix (i.e. one-part or two-part formulations), are lower than those of the typical SHCC M45. This is because the high carbon and high energy intensive cement binder in typical SHCC M45 was completely replaced by the geopolymer binder in the SHGCs. It should be noted that the reductions obtained with regards to manufacture of the ambient temperature cured one-part SHGC developed in this study are more pronounced. This is due to the fact that although the embodied energy and CO_2 emissions associated with production of a unit weight of the solid activator are higher than those of production of a unit weight of the activator solution, but the amount of solid activator used in manufacture of the ambient temperature cured one-part SHGC is significantly (78%) lower than that of the activator solution used in manufacture of the "traditional" heat cured two-part fly ash-based SHGC. In addition, the embodied energy and CO_2 emissions associated with the heat curing approach are eliminated in production of the ambient temperature cured one-part SHGC.

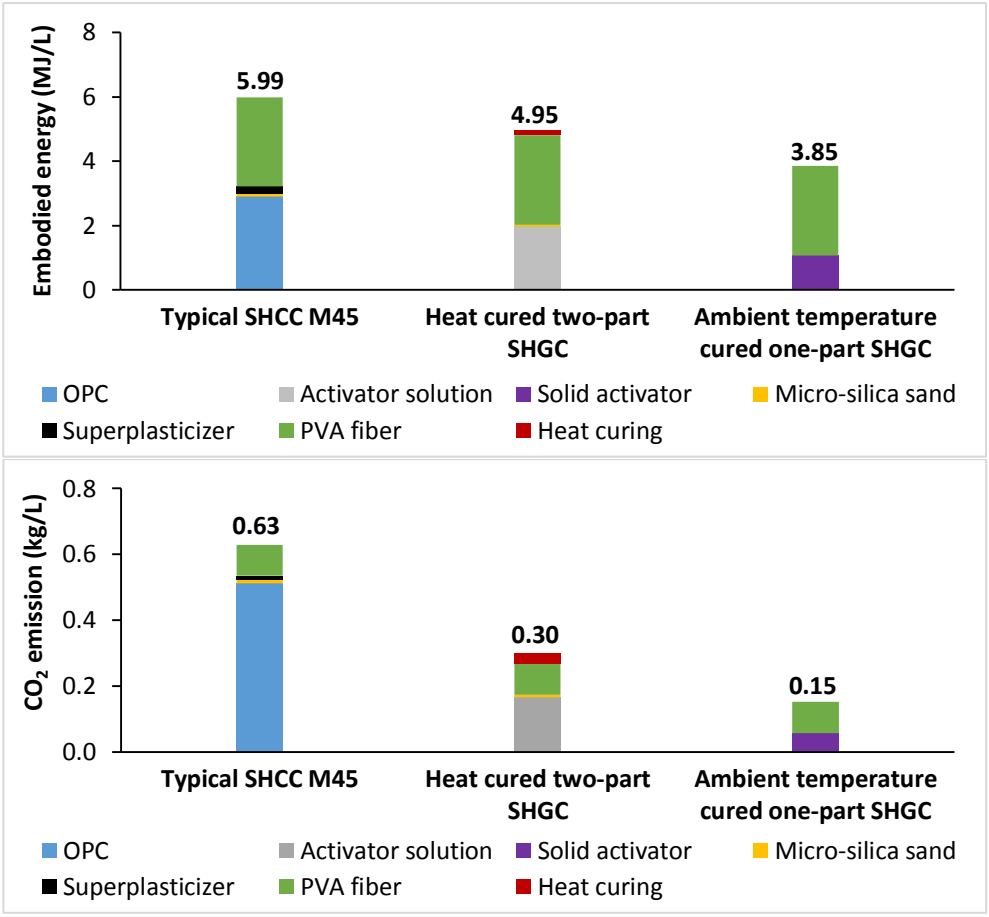

Figure 10-9: Material sustainability indicators of different composites

The CO_2 emissions associated with production of the developed ambient temperature cured one-part SHGC are 50% and 76% lower than those of the "traditional" heat cured two-part fly ash-based SHGC and the typical SHCC M45, respectively. On the other hand, the embodied energy for production of the developed ambient temperature cured one-part SHGC is 22% and 36% lower than that of the "traditional" heat cured two-part fly ash-based SHGC and the typical SHCC M45, respectively. As can be seen, the reductions obtained in terms of the embodied energy are relatively lower than the reductions obtained with regards to the CO_2 emissions. This is because of the fact that although the embodied energy associated with fly ash and slag are considered to be zero, relatively high embodied energy is still required for production of the activator solution or the solid activator. It can be concluded that the developed ambient temperature cured one-part SHGC is highly promising as a sustainable alternative to typical SHCC M45 in terms of carbon emission and energy consumption. Although MSIs provide a simple platform to compare the material sustainability of different composite designs, it should

be noted that MSIs are partial life cycle analysis based on the constituent materials only, and true assessment of sustainability should be based on full life cycle analysis of a specific type of infrastructure (Yang et al., 2007; Keoleian et al., 2005).

10.5 Summary and Conclusions

A new ambient temperature cured one-part SHGC with comparable mechanical properties to typical SHCC, yet with added advantage of significantly lower environmental footprints was developed in this chapter. A small amount of sodium metasilicate powder was used to synthesize the ambient temperature cured "dry mix" geopolymer binder ("bag" of geopolymer). This eliminates the difficulties associated with handling large quantities of user-hostile alkaline solutions. In addition, the developed ambient temperature cured one-part SHGC eliminates the necessity for the heat curing, which provides possibility of in-situ application. The developed ambient temperature cured one-part SHGC significantly enhances the commercial viability of the SHGCs, and facilitates their widespread application in the construction industry.

The influences of the curing condition and type of slag on the matrix, interface and composite properties of the developed one-part SHGC were evaluated. The one-part SHGCs developed in this study exhibited density of 1800−1874 kg/m^3, compressive strength of 43.4−52.5 MPa, tensile strength of 4.3−4.6 MPa, and tensile strain capacity of 2.6−4.2%, depending on the curing condition and type of slag. The following specific conclusions are drawn:

1) The ambient temperature cured one-part SHGCs, regardless of the type of slag, exhibited superior uniaxial tensile performance to the corresponding heat cured composites. This is due to the higher PSH energy index of the ambient temperature cured one-part SHGCs than that of the corresponding heat cured composites, which results in greater possibility of saturated multiple cracking, and thereby higher tensile strain capacity of the ambient temperature cured one-part SHGCs.

2) The one-part SHGCs made with "typical" slag (which contains 2% gypsum), regardless of the curing condition, exhibited superior uniaxial tensile performance to the corresponding composites made with "gypsum-free" slag (which contains no gypsum). This is due to the higher PSH strength and energy indices of the one-part SHGCs made

with “typical” slag than those of the corresponding composites made with “gypsum-free” slag, which result in greater possibility of saturated multiple cracking, and thereby higher tensile strain capacity of the one-part SHGCs made with “typical” slag.

3) The curing condition and type of slag had significant effects on the fiber-matrix interface properties. The ambient temperature curing increased the chemical bond strength (G_d) when “typical slag” was used in the one-part SHGC composition, whereas an opposite trend was observed when “gypsum-free” slag was used. The main prominent reason for the different G_d of the one-part SHGCs is attributed to the different geopolymer chemistry (i.e. microstructure) of the one-part SHGC matrices, resulting from their different curing condition and type of slag. It was concluded that there is a positive correlation between the frictional bond strength (τ_0) of the one-part SHGC and the fracture toughness of the one-part SHGC matrix. The higher the fracture toughness of the one-part SHGC matrix, the higher the value of τ_0. This is due to the increase in the contact surface between the fiber and the matrix during the fiber slippage.

4) The heat curing condition and using “gypsum-free” slag reduced the fracture toughness and crack tip toughness of the one-part SHGC matrix. In other words, it was concluded that the heat curing condition and using “gypsum-free” slag increased brittleness of the one-part SHGC matrix.

5) The compressive strength and tensile performance of the ambient temperature cured one-part SHGC developed in this study are comparable to those of typical SHCC M45. At the same time, the developed ambient temperature cured one-part SHGC is a sustainable composite with 76% lower CO_2 emissions and 36% lower embodied energy compared to those of typical SHCC M45. In addition, the ambient temperature cured one-part SHGC with an average density of 1849 kg/m^3, unlike typical SHCC M45 (2077 kg/m^3), can be classified as lightweight composite.

In summary, it is concluded that the developed ambient temperature cured one-part SHGC is a promising sustainable alternative to typical SHCC. Therefore, it is expected to promote sustainability of the infrastructures through simultaneous improvements of material greenness and infrastructure durability via ultra-high ductility and tight crack width control.

10.6 References

ACI 213R. 2014. Guide For Structural Lightweight-Aggregate Concrete. United States: American Concrete Institute.

FANG, Y. & KAYALI, O. 2013. The fate of water in fly ash-based geopolymers. *Construction and Building Materials,* 39, 89-94.

FAWER, M., CONCANNON, M. & RIEBER, W. 1999. Life cycle inventories for the production of sodium silicates. *The International Journal of Life Cycle Assessment,* 4, 207-212.

HUANG, X., RANADE, R. & LI, V. C. 2012. Feasibility study of developing green ECC using iron ore tailings powder as cement replacement. *Journal of Materials in Civil Engineering,* 25, 923-931.

Integrated Pollution Prevention and Control (IPPC). 2001. Reference Document on Best Available Techniques in the Chlor-Alkali Manufacturing industry. *European IPPC Bureau*.

KANDA, T. & LI, V. C. 1998. Interface property and apparent strength of high-strength hydrophilic fiber in cement matrix. *Journal of materials in civil engineering,* 10, 5-13.

KANDA, T. & LI, V. C. 2006. Practical design criteria for saturated pseudo strain hardening behavior in ECC. *Journal of advanced concrete technology,* 4, 59-72.

KARIHALOO, B. & NALLATHAMBI, P. 1990. Effective crack model for the determination of fracture toughness (KICe) of concrete. *Engineering Fracture Mechanics,* 35, 637-645.

KEOLEIAN, G. A., KENDALL, A., DETTLING, J. E., SMITH, V. M., CHANDLER, R. F., LEPECH, M. D. & LI, V. C. 2005. Life cycle modeling of concrete bridge design: Comparison of engineered cementitious composite link slabs and conventional steel expansion joints. *Journal of infrastructure systems,* 11, 51-60.

LANGE, D. A., JENNINGS, H. M. & SHAH, S. P. 1993. Relationship between fracture surface roughness and fracture behavior of cement paste and mortar. *Journal of the American Ceramic Society,* 76, 589-597.

LI, V. & MISHRA, D. 1992. MICROMECHANICS OF FIBER EFFECT ON THE UNIAXIAL COMPRESSIVE STRENGTH OF CEMENTITIOUS COMPOSITES. *Fibre Reinforced Cement and Concrete: Proceedings of the Fourth RILEM International Symposium*. University of Sheffield, UK, Sheffield: Taylor & Francis.

LI, V. C. Reflections on the research and development of engineered cementitious composites (ECC). Proceedings of the JCI International Workshop on Ductile Fiber Reinforced Cementitious Composites (DFRCC)–Application and Evaluation, 2002. Citeseer, 1-21.

LI, V. C. & STANG, H. 1997. Interface property characterization and strengthening mechanisms in fiber reinforced cement based composites. *Advanced cement based materials,* 6, 1-20.

LI, V. C., WANG, S. & WU, C. 2001. Tensile strain-hardening behavior of polyvinyl alcohol engineered cementitious composite (PVA-ECC). *ACI materials Journal,* 98.

LI, Z., DING, Z. & ZHANG, Y. Development of sustainable cementitious materials. Proceedings of international workshop on sustainable development and concrete technology, Beijing, China, 2004. 55-76.

MCLELLAN, B. C., WILLIAMS, R. P., LAY, J., VAN RIESSEN, A. & CORDER, G. D. 2011. Costs and carbon emissions for geopolymer pastes in comparison to ordinary Portland cement. *Journal of Cleaner Production,* 19, 1080-1090.

NATIONAL GREENHOUSE ACCOUNTS FACTORS. 2014. The Department of the Environment-Australian Government. Retrieved from http://www.environment.gov.au/.

OHNO, M. & LI, V. C. 2014. A feasibility study of strain hardening fiber reinforced fly ash-based geopolymer composites. *Construction and Building Materials,* 57, 163-168.

PAN, Z., SANJAYAN, J. G. & RANGAN, B. V. 2011. Fracture properties of geopolymer paste and concrete. *Magazine of concrete research,* 63, 763-771.

TENNAKOON, C., NAZARI, A., SANJAYAN, J. G. & SAGOE-CRENTSIL, K. 2014. Distribution of oxides in fly ash controls strength evolution of geopolymers. *Construction and Building Materials,* 71, 72-82.

YANG, E.-H., YANG, Y. & LI, V. C. 2007. Use of high volumes of fly ash to improve ECC mechanical properties and material greenness. *ACI Materials Journal,* 104.

YANG, K.-H., SONG, J.-K., ASHOUR, A. F. & LEE, E.-T. 2008. Properties of cementless mortars activated by sodium silicate. *Construction and Building Materials,* 22, 1981-1989.

YANG, K.-H., SONG, J.-K. & SONG, K.-I. 2013. Assessment of CO_2 reduction of alkali-activated concrete. *Journal of Cleaner Production,* 39, 265-272.

CHAPTER 11

MICROMECHANICS-BASED INVESTIGATION OF HIGH DUCTILE POLYETHYLENE FIBER-REINFORCED ONE-PART SHGCS

Note: This chapter is based on the manuscript "*High Ductile Behavior of a Polyethylene Fiber-Reinforced One-Part Geopolymer Composite: A Micromechanics-based Investigation*", by **Nematollahi, B.**, Sanjayan, J., Qiu, J., and Yang, E-H., published in ***Archives of Civil and Mechanical Engineering***, 2017, 17, 555-563.

11.1 Introduction

The results achieved in the previous chapters clearly revealed that SHGCs reinforced by PVA fibers (PVA-SHGCs) can be successfully manufactured with comparable or superior tensile performance to that of "conventional" PVA-SHCCs. However, the behavior of the SHGCs reinforced with other types of fibers such as polypropylene and polyethylene fibers has received less attention. Therefore, this research is aimed to evaluate the tensile performance of a one-part SHGC reinforced by ultra-high-molecular-weight polyethylene (UHMWPE, henceforth referred to as PE) fibers. The quantitative influences of curing condition, namely heat and ambient temperature curing, on the macroscale properties of the matrix and composite including workability, density, compressive strength, and uniaxial tensile performance were evaluated.

The results of the ambient temperature cured one-part PVA-SHGC-T developed in Chapter 10 are used as the benchmark, enabling us to also investigate the quantitative influences of type of fiber, viz. hydrophilic PVA fiber and hydrophobic PE fiber, on the macroscale properties of the matrix and composite. A micromechanics-based investigation was performed to explain the experimentally observed macroscopic high tensile ductility of the developed one-part PE-SHGCs. The investigation involved determination of the matrix fracture properties and the fiber-matrix interface properties using fracture toughness tests and single-fiber pullout tests, respectively. The fiber-bridging constitutive law of the composites was computed via a micromechanics-based model to link the material microstructures to macroscopic composite tensile performance.

11.2 Materials and mix proportions

The low-calcium (Class F) fly ash and slag used in this study were supplied from Gladstone power station in Queensland, Australia and Independent Cement and Lime Pty Ltd, Australia, respectively. It should be noted that only one type of slag (i.e. "typical" slag which is a typical Australian slag containing 2% gypsum) is used in this chapter. This is because the results presented in Chapter 10 indicated that using "typical" slag is beneficial compared to the "gypsum-free" slag in terms of the fiber-matrix interface properties and thereby the tensile performance of the composite. The chemical composition and LOI of the fly ash and "typical" slag used in this chapter are presented in Table 10-1. The particle size distribution of the fly ash and "typical" slag and the passing percentages of particle size distribution are presented in Figure 10-1 and Table 10-2, respectively. The anhydrous sodium metasilicate powder used in this study was the same as that used in Chapter 10. Properties of the PE fibers used in this study supplied by Toyobo Co. Ltd., Japan are presented in Table 11-1. Properties of the PVA fibers are also re-presented in Table 11-1 for ease of comparison.

Table 11-1: Properties of the PVA and PE fibers

Fiber type	Diameter (μm)	Length (mm)	Young's modulus (GPa)	Elongation (%)	Density (g/cm^3)	Nominal Strength (MPa)
PVA-RECS 15	40	8	41	6	1.3	1600
PE-SK71	12	12	123	3-5	0.97	3500

Table 11-2 presents the one-part SHGC mix proportions investigated in this study. As mentioned in Introduction, the ambient temperature cured one-part PVA-SHGC-T mixture proportion was also used in this chapter as the benchmark. As mentioned in Chapter 10, unlike typical SHCC mixture (Yang et al., 2007), micro-silica sand was not used in the one-part SHGC mixtures investigated in this research, since the crystalline contents of fly ash and slag are unreacted components acting as filler in the one-part geopolymer matrix. The Gladstone fly ash and "typical" slag have a crystalline content of 44% (w/w) and 8% (w/w), respectively (Tennakoon et al., 2014).

Table 11-2: Mix proportion of one-part SHGCs

Mix ID	One-part "dry mix" geopolymer binder			Water[2]	PVA fiber	PE fiber	Curing condition
	Fly ash	Slag	Solid activator[1]				
One-part PE-SHGC-H	0.50	0.50	0.08	0.35	---	0.02	Heat curing
One-part PE-SHGC-A	0.50	0.50	0.08	0.35	---	0.02	Ambient temperature curing
One-part PVA-SHGC-A	0.50	0.50	0.08	0.35	0.02	---	Ambient temperature curing

Note: All numbers are mass ratios of the precursor weight (fly ash + slag) except fiber content (volume fraction).

[1] Composed of anhydrous sodium metasilicate powder.

[2] Added to the one-part "dry mix" geopolymer binder.

11.3 Mixing, curing and testing of specimens

The procedures for mixing, curing and testing of the specimens are similar to those mentioned in Section 10.3 of Chapter of 10.

11.4 Results and Discussions

11.4.1 Workability, density and compressive strength

The workability of the fresh one-part SHGC matrix is given in Table 11-3. As mentioned in Chapter 10, it should be noted that the reported relative slump value is based on the mini-slump test without the 25 times tamping of the flow table. Visual observations revealed that the one-part SHGC matrix exhibited thixotropic properties. In other words, the fresh one-part SHGC matrix exhibited adequate workability to guarantee uniform fiber dispersion as being mixed and vibrated, thanks to its thixotropic properties.

The average density of each mix is also presented in Table 11-3. As can be seen, the curing condition and type of fiber did not have any significant effect on the density of the developed one-part SHGCs and their corresponding one-part SHGC matrices. The density of the developed one-part SHGCs, regardless of the curing condition and type of

fiber, was relatively lower than that of the corresponding one-part SHGC matrices. This could be due to a fiber-induced air entrapping effect, leading to a composite with higher porosity than the matrix material alone (Li and Mishra, 1992). The density of the developed one-part PE-SHGCs was in the range of 1837 kg/m^3 to 1844 kg/m^3, which is 23% less than that of a normal weight concrete with a density of 2400 kg/m^3 and meet the density requirement for lightweight concrete (below 1850 kg/m^3) (ACI 213R, 2014).

Table 11-3: Workability, density and compressive strength results

Mix ID	Matrix workability[1]	Density; (kg/m^3)		Compressive strength; (MPa)	
		Matrix	Composite	Matrix	Composite
One-part PE-SHGC-H	3.52 (212.5)	1880	1837	44.7±4.1	33.9±3.7
One-part PE-SHGC-A		1895	1844	48.6±4.1	44.3±2.2
One-part PVA-SHGC-A		1895	1849	48.6±4.1	48.7±4.1

[1]In terms of relative slump value of the fresh matrix. The average diameter of the matrix flow (in millimeter) is shown in parenthesis.

The average compressive strength of each mix is also given in Table 11-3. As can be seen, the compressive strength of the ambient temperature cured one-part PE-SHGC-A and its corresponding matrix was higher than that of the counterpart heat cured matrix and composite. With regards to the type of fiber, the compressive strengths of the one-part PE-SHGCs, regardless of the curing condition, were 9−24% lower than that of the corresponding one-part SHGC matrices. As mentioned earlier, this could be attributed to the higher porosity of the composite specimens than that of the matrix specimens, due to the fiber induced damage effect (Li and Mishra, 1992). Nevertheless, the compressive strength of the ambient temperature cured one-part PVA-SHGC-A was comparable to that of the ambient temperature cured one-part SHGC matrix. In addition, the compressive strength of the ambient temperature cured one-part PVA-SHGC-A was slightly higher than that of the ambient temperature cured one-part PE-SHGC-A. This could be due to the lower aspect ratio of the PVA fibers than that of the PE fibers, which suggests that the PVA fibers may induce less fiber damage effect (air entrapping effect) in the composite compared to the PE fibers.

The compressive strength of the developed one-part SHGCs ranged from 33.9 MPa to 48.7 MPa, which is well above the compressive strength requirement of 17 MPa for structural lightweight concrete (ACI 213R, 2014). Among all one-part SHGCs, the ambient temperature cured one-part PVA-SHGC-A exhibited the highest compressive strength, comparable to typical SHCC M45 (52.6 MPa) (Yang et al., 2007). However, unlike typical SHCC M45, the ambient temperature cured one-part PVA-SHGC-A contains no cement, and therefore it has significantly lower environmental footprints compared to the typical SHCC M45, in which its cement content is still 1.5 times that of normal concrete (Yang et al., 2007).

11.4.2 Matrix fracture properties

Fracture properties of the developed one-part SHGC matrices (without addition of the fibers) are presented in Table 11-4. As mentioned in Chapter 10, it should be noted that the E_m values reported in Table 11-4 were not experimentally measured using cylindrical specimens in compression, instead they were derived based on ECM (Karihaloo and Nallathambi, 1990) from the linear portion of the load-deflection curve of the notched beam specimen in three-point bending tests. Therefore, they should only be considered as relative values enabling us to compare the elastic modulus of the one-part SHGC matrices. As can be seen in Table 11-4, the curing condition did not have significant effect on the matrix elastic modulus. This is consistent with the compressive strength results reported in Table 11-3.

Table 11-4: Matrix fracture test results

Mix ID	Matrix elastic modulus [a], E_m; (GPa)	Matrix fracture toughness [a], K_m; (MPa.m$^{1/2}$)	Crack tip toughness [b], J_{tip}; (J/m^2)
Heat cured one-part SHGC matrix	4.8	0.287	17.2
Ambient temperature cured one-part SHGC matrix	5.3	0.316	18.8

[a] Following ECM (Karihaloo and Nallathambi, 1990).

[b] $J_{tip} = \frac{K_m^2}{E_m}$ (Li et al., 1995).

As can be seen in Table 11-4, the fracture toughness of the ambient temperature cured one-part SHGC matrix was higher than that of the heat cured matrix. This indicates that crack propagation in the ambient temperature cured one-part SHGC matrix is likely to be more tortuous; thereby, consumes more energy than that of the heat cured matrix. This trend is confirmed by visual observations of the fracture surface of the specimens. According to Pan et al. (2011), the fracture toughness of concrete is mainly affected by the size, texture and angularity of the coarse aggregates, as well as the microstructure of the paste. It can be thereby conferred that the main reason for the difference in the fracture toughness of the one-part SHGC matrices lies in their geopolymer microstructures, because all other parameters, except the curing condition, were kept constant for both matrices. As can be seen in Table 11-4, the J_{tip} of the ambient temperature cured one-part SHGC matrix was also higher than that of the heat cured matrix, which corresponds to its higher K_m. It is thereby concluded that ambient temperature curing reduces the brittleness of the one-part SHGC matrix.

11.4.3 Fiber-matrix interface properties

The fiber-matrix interface properties of each mix are summarized in Table 11-5. With regards to effect of the curing condition on the interface properties, both τ_0 and β of the ambient temperature cured one-part PE-SHGC-A were higher than those of the counterpart heat cured composite. This could be due to the higher matrix fracture toughness of the ambient temperature cured one-part SHGC matrix. Lang et al. (1993) reported that there is a positive correlation between fracture surface roughness and fracture toughness. As fracture toughness increases, fracture surface roughness increases. Therefore, it can be inferred that in the ambient temperature cured one-part PE-SHGC-A the fracture surface roughness in the fiber-matrix interfacial zone is higher, due to its higher matrix toughness, as shown in Table 11-4. This increases the contact surface between the fiber and the matrix in the interfacial zone during the fiber slippage, and thereby leading to the higher frictional bond strength in the ambient temperature cured one-part PE-SHGC-A. Similarly, due to the higher matrix fracture toughness, and thereby rougher fracture surface in the fiber-matrix interfacial zone in the ambient temperature cured one-part PE-SHGC-A, the fiber is more likely to be abraded during fiber slippage and a jamming effect is more likely to occur, leading to the relatively higher β value of the ambient temperature cured one-part PE-SHGC-A.

Table 11-5: Fiber-matrix interface properties

Mix ID	Chemical bond strength, G_d; (J/m^2)	Frictional bond strength, τ_0; (MPa)	Slip hardening coefficient, β
One-part PE-SHGC-H	---	1.32±0.49	0.014±0.0013
One-part PE-SHGC-A	---	1.36±0.40	0.019±0.0015
One-part PVA-SHGC-A	1.03±0.34	2.14±0.62	0.041±0.0070

With regards to effect of the type of fiber on the interface properties, unlike PE fiber, as expected the PVA fiber due to its hydrophilic nature exhibited a chemical bond with the ambient temperature cured one-part SHGC matrix (Kanda and Li, 1998). In addition, the τ_0 and β of the ambient temperature cured one-part PVA-SHGC-A were significantly higher than those of the counterpart composite reinforced by the PE fibers. The higher frictional bond strength of the PVA fibers with the surrounding one-part SHGC matrix is also attributed to its hydrophilic characteristics (Kanda and Li, 1998). The significantly higher β of the PVA fibers is due to its lower elastic modulus (Redon et al., 2001). As shown in Table 11-1, the elastic modulus of the PVA fibers is 3 times less than that of the PE fibers. According to Redon et al. (2001), the lower the fiber hardness than that of the surrounding matrix, the higher the possibility of fiber damage and jamming effect in the slippage regime, resulting in higher β value.

11.4.4 Uniaxial tensile performance

Tensile stress-strain responses of the developed one-part SHGCs are presented in Figures 11-1 to 11-3. As can be seen, all one-part SHGCs, regardless of the curing condition and type of fiber, exhibited strong strain hardening behavior. The uniaxial tension test results including the average measured ultimate tensile strength (σ_{cu}) and tensile strain capacity (ε_{cu}) and the estimated first-crack strength (σ_{fc}) are summarized in Table 11-6. As can be seen, the developed one-part PE-SHGCs exhibited moderate to high ultimate tensile strength in the range of 3.3−4.2 MPa and very high tensile ductility in the range of 4.9−5.5%, whereas the ambient temperature cured one-part PVA-SHGC-A exhibited high ultimate tensile strength and very high tensile ductility of up to 4.6 MPa and 4.2%, respectively.

Table 11-6: Uniaxial tension test results

Mix ID	first-crack strength, σ_{fc}; (MPa)	Ultimate tensile strength, σ_{cu} ; (MPa)	Tensile strain capacity, ε_{cu}; (%)
One-part PE-SHGC-H	2.1±0.24	3.3±0.50	5.5±0.52
One-part PE-SHGC-A	2.8±0.66	4.2±0.66	4.9±0.68
One-part PVA-SHGC-A	4.1±0.095	4.6±0.26	4.2±0.71

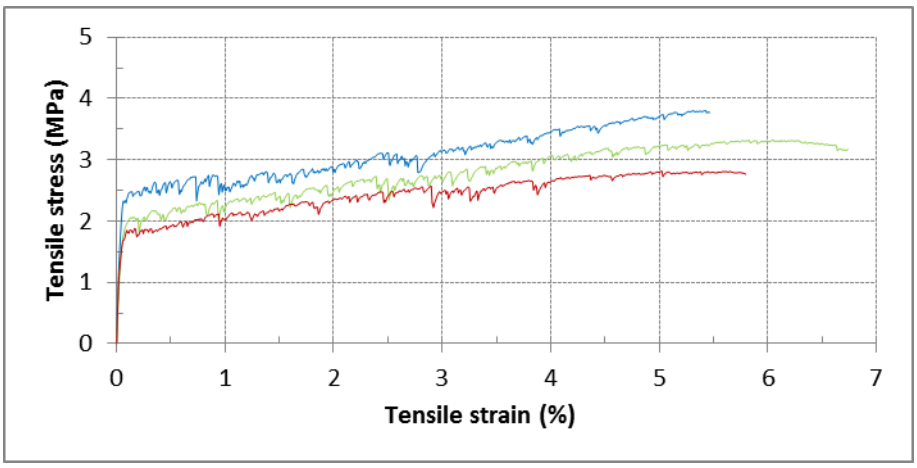

Figure 11-1: Tensile stress-strain responses of heat cured one-part PE-SHGC-H

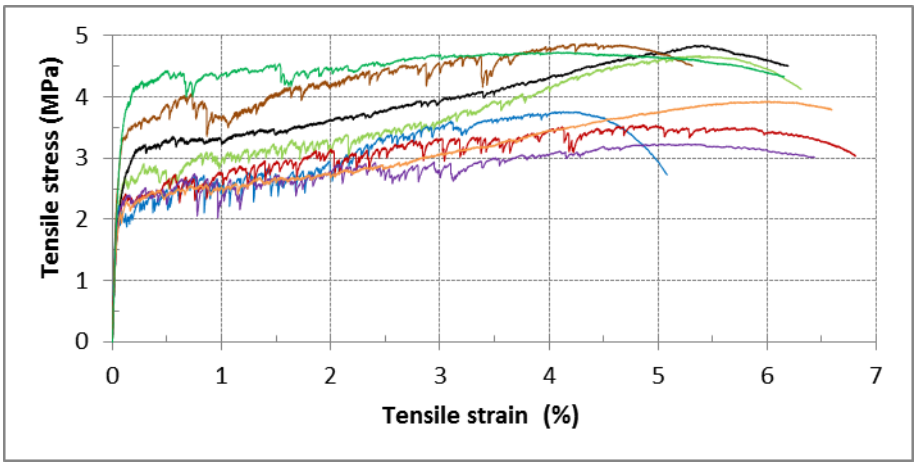

Figure 11-2: Tensile stress-strain responses of ambient temperature cured one-part PE-SHGC-A

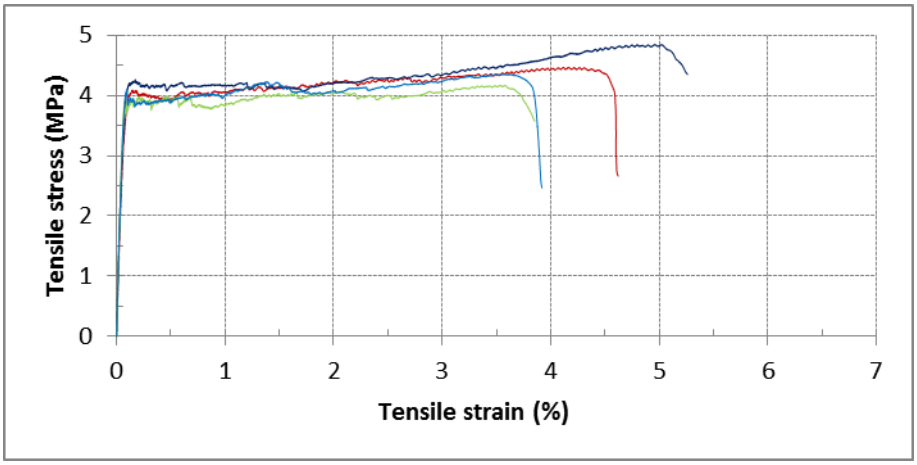

Figure 11-3: Tensile stress-strain responses of ambient temperature cured one-part PVA-SHGC-A

In terms of the effect of the curing condition on the tensile performance of the one-part PE-SHGCs, as can be seen in Table 11-6, the first-crack strength and the ultimate tensile strength of the ambient temperature cured one-part PE-SHGC-A were 33% and 27% higher, respectively than those of the counterpart heat cured composite. The higher first-crack strength of the ambient temperature cured one-part PE-SHGC-A corresponds to its higher matrix fracture toughness, as shown in Table 11-4 (Li et al., 2001). The higher ultimate tensile strength of the ambient temperature cured one-part PE-SHGC-A is attributed to the fiber-matrix interface properties. In other words as shown in Table 11-5, the τ_0 and β of the ambient temperature cured one-part PE-SHGC-A were higher than those of the counterpart heat cured composite, resulting in its higher fiber bridging strength.

On the other hand, the tensile strain capacity of the ambient temperature cured one-part PE-SHGC-A was 11% lower than that of the counterpart heat cured composite. The reasons for different tensile ductility of the heat cured and ambient temperature cured one-part PE-SHGCs can be described in terms of the two PSH performance indices proposed by Kanda and Li (2006), which could be calculated based on the micromechanics modeling of fiber-bridging behavior.

In this study, the micromechanical model developed by Yang et al. (2008) was used to compute the fiber-bridging constitutive law $\sigma(\delta)$ of the developed one-part SHGCs. The applicability of this micromechanics-based model to evaluate the tensile performance of

SHGCs is demonstrated in Chapter 8. The resulting PSH performance indices are plotted in Figure 11-4. As can be seen, in all composites both PSH performance indices exceed unity, and hence it can be concluded that the necessary strength and energy-based conditions for the PSH behavior are satisfied. Therefore, all one-part SHGCs developed in this study exhibited strain hardening behavior. In addition, the PSH strength and energy indices of the heat cured one-part PE-SHGC-H were 5% and 21%, respectively higher than those of the counterpart ambient temperature cured composite. As a result, it is not surprising that the heat cured one-part PE-SHGC-H with higher PSH performance indices exhibited higher tensile strain capacity than that of the counterpart ambient temperature cured composite.

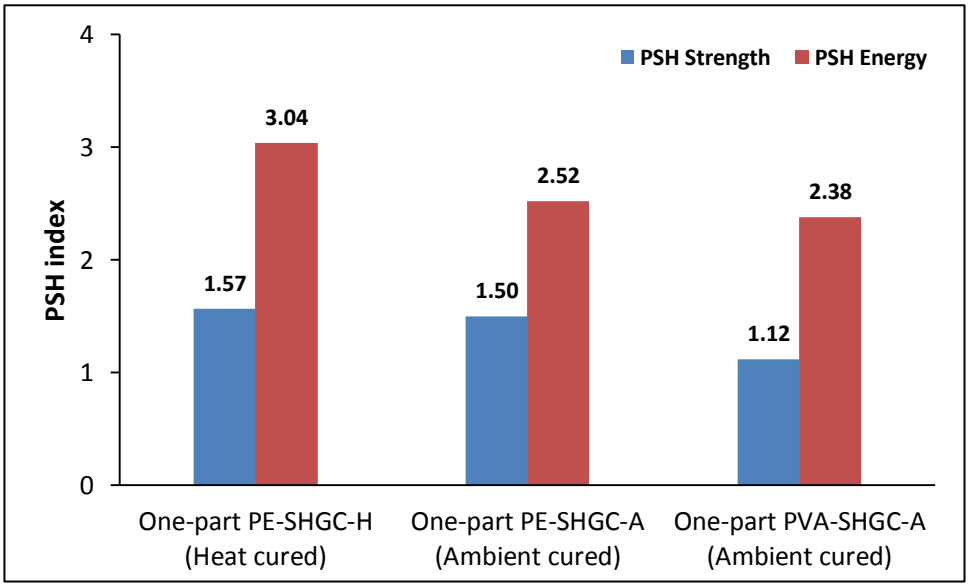

Figure 11-4: PSH indices of the developed one-part SHGCs

With regards to the effect of the type of fiber on the tensile performance of the one-part SHGCs, as shown in Table 11-6, the first-crack strength and the ultimate tensile strength of the ambient temperature cured one-part PVA-SHGC-A were 46% and 10% higher, respectively than those of the ambient temperature cured one-part PE-SHGC-A. The higher first-crack strength of the ambient temperature cured one-part PVA-SHGC-A is attributed to its higher fiber-matrix interface properties, especially the strong chemical bond of the PVA fibers with the one-part SHGC matrix, as shown in Table 11-5. In general, the first-crack strength of the composite is governed by the matrix properties, as

well as fiber bridging properties, especially the chemical bond strength (Yang and Li, 2014). The higher ultimate tensile strength of the ambient temperature cured one-part PVA-SHGC-A is attributed to the significantly higher τ_0 and β of the PVA fibers as shown in Table 11-5, resulting in its higher fiber bridging strength.

On the other hand, the tensile strain capacity of the ambient temperature cured one-part PVA-SHGC-A was 14% lower than that of the ambient temperature cured one-part PE-SHGC-A. Similar to the above discussion, the reasons for the lower tensile ductility of the ambient temperature cured one-part PVA-SHGC-A could also be described based on the two PSH performance indices. As can be seen in Figure 11-4, the PSH strength and energy indices of the ambient temperature cured one-part PVA-SHGC-A were 25% and 6%, respectively lower than those of the ambient temperature cured one-part PE-SHGC-A. This can be attributed to the strong chemical bond and higher frictional bond and slip hardening coefficient of the PVA fiber with the ambient temperature cured SHGC matrix, as well as the lower strength of the PVA fiber, which result in lower complimentary energy of the composite. Therefore, the tensile strain capacity of the ambient temperature cured one-part PVA-SHGC-A was lower than that of the ambient temperature cured one-part PE-SHGC-A.

The crack pattern of each composite is presented in Figure 11-5. As can be seen, uniform crack distribution with almost equal crack spacing was observed in all developed one-part SHGCs, regardless of the curing condition and type of fiber. Numerous micro-cracks with tightly controlled crack width (i.e. saturated multiple cracking behavior) were observed on the surface of the coupon specimens, which correspond to the very high tensile strain capacity of the developed composites. It should be pointed out that the actual number of micro-cracks formed during loading of the specimens was more than the number of visible cracks on the surface of the unloaded specimens, which illustrated in Figure 11-5. This is because many of the micro-cracks appeared during loading, completely closed after unloading which make them very hard to be detected on the surface of the unloaded specimens (Li et al., 2001).

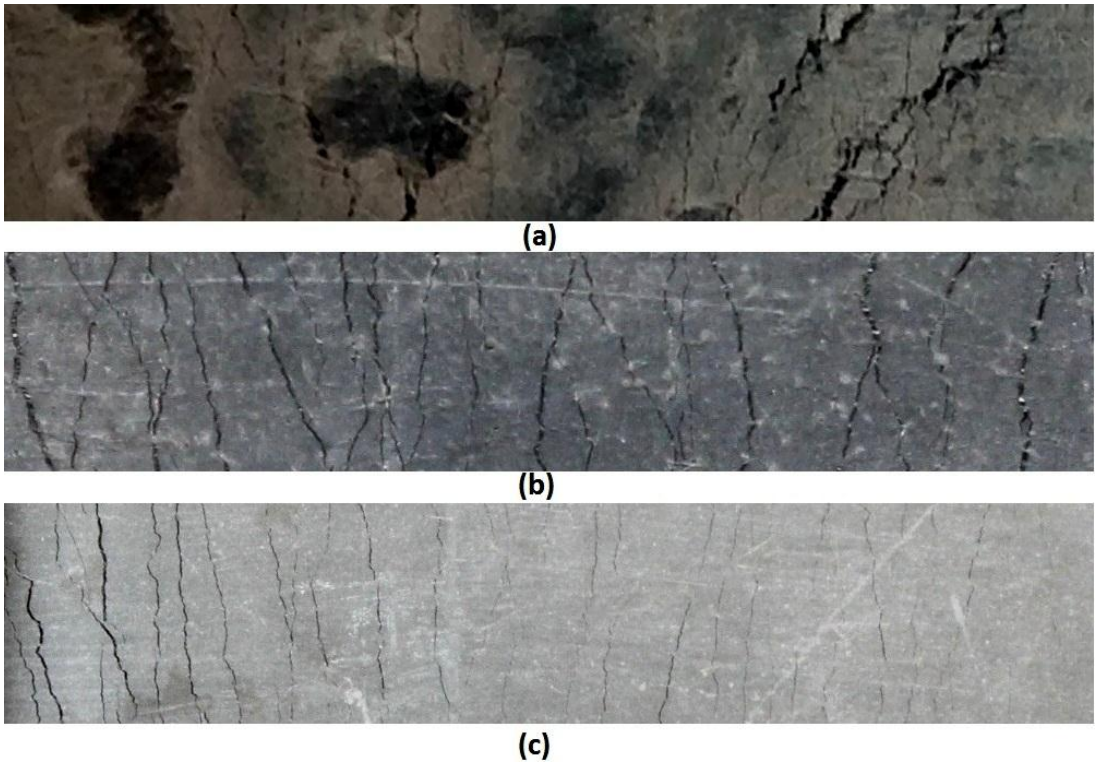

Figure 11-5: Typical multiple cracking pattern of (a) ambient temperature cured one-part PE-SHGC-A, (b) heat cured one-part PE-SHGC-H, and (c) ambient temperature cured one-part PVA-SHGC-A

11.5 Conclusions

A detailed micromechanics-based investigation was conducted in this chapter to fully explain the experimentally observed high ductile behavior of a one-part SHGC reinforced by high strength and high modulus PE fibers. The quantitative effects of curing condition and type of fiber on the matrix and fiber-matrix interface properties, along with their consequent quantitative influences on the macroscale properties of the developed one-part SHGCs were experimentally evaluated. The crack bridging relation and the PSH performance indices of the composites were computed using the existing micromechanical model to elucidate the experimentally observed macroscopic tensile performance of the developed one-part SHGCs. The following conclusions are drawn:

1) The ambient temperature curing condition increased the micro-scale fiber-matrix interface properties (frictional bond τ_0 and slip hardening coefficient β) of the PE fiber with the one-part SHGC matrix. This is attributed to the higher fracture toughness of the

ambient temperature cured one-part SHGC matrix, in which increases the roughness of the fracture surface in the fiber-matrix interfacial zone, and thereby increases the contact surface between the fiber and matrix in the interfacial zone during the fiber slippage.

2) The ambient temperature curing condition marginally increased the compressive strength, elastic modulus and fracture toughness of the one-part SHGC matrix. It is thereby concluded that ambient temperature curing condition reduces the brittleness of the one-part SHGC matrix.

3) The first-crack strength of the ambient temperature cured one-part PE-SHGC was considerably higher than that of the counterpart heat cured composite. This corresponds the higher fracture toughness of the ambient temperature cured one-part SHGC matrix. In addition, the ultimate tensile strength of the ambient temperature cured one-part PE-SHGC was also noticeably higher than that of the counterpart heat cured composite. This is attributed to the higher τ_0 and β of the PE fiber with the ambient temperature cured one-part SHGC matrix. On the other hand, the tensile strain capacity of the heat cured one-part PE-SHGC was higher than that of the counterpart ambient temperature cured composite. This result is well consistent with the calculated PSH performance indices of the composites, where both PSH strength and energy indices of the heat cured one-part PE-SHGC were relatively higher, resulting in the higher tensile ductility of the heat cured composite.

4) The type of fiber had significant effects on the microscale fiber-matrix interface properties, and thereby on the macroscopic tensile performance of the composite. The first-crack strength of the ambient temperature cured one-part PVA-SHGC was significantly higher than that of the ambient temperature cured one-part PE-SHGC. This is due to the higher interface properties, especially the strong chemical bond (G_d) of the PVA fiber with the one-part SHGC matrix. In addition, the ultimate tensile strength of the ambient temperature cured one-part PVA-SHGC was also higher. This is due to the significantly higher τ_0 and β of the PVA fiber with the one-part SHGC matrix, resulting in the higher fiber bridging strength of the composite. However, the tensile strain capacity of the ambient temperature cured one-part PVA-SHGC was lower than that of the ambient temperature cured one-part PE-SHGC. This result is also in good agreement with the computed PSH performance indices of the composites, where both PSH strength and

energy indices of the ambient temperature cured one-part PVA-SHGC were relatively lower. This is attributed to the strong G_d and higher τ_0 and β of the PVA fiber with the one-part SHGC matrix, along with the lower strength of the PVA fiber, which result in lower complimentary energy of the ambient temperature cured one-part PVA-SHGC.

11.6 References

ACI 213R. 2014. Guide For Structural Lightweight-Aggregate Concrete. United States: American Concrete Institute.

KANDA, T. & LI, V. C. 1998. Interface property and apparent strength of high-strength hydrophilic fiber in cement matrix. *Journal of materials in civil engineering,* 10, 5-13.

KANDA, T. & LI, V. C. 2006. Practical design criteria for saturated pseudo strain hardening behavior in ECC. *Journal of advanced concrete technology,* 4, 59-72.

KARIHALOO, B. & NALLATHAMBI, P. 1990. Effective crack model for the determination of fracture toughness (KICe) of concrete. *Engineering Fracture Mechanics,* 35, 637-645.

LANGE, D. A., JENNINGS, H. M. & SHAH, S. P. 1993. Relationship between fracture surface roughness and fracture behavior of cement paste and mortar. *Journal of the American Ceramic Society,* 76, 589-597.

LI, V. & MISHRA, D. 1992. MICROMECHANICS OF FIBER EFFECT ON THE UNIAXIAL COMPRESSIVE STRENGTH OF CEMENTITIOUS COMPOSITES. *Fibre Reinforced Cement and Concrete: Proceedings of the Fourth RILEM International Symposium.* University of Sheffield, UK, Sheffield: Taylor & Francis.

LI, V. C., WANG, S. & WU, C. 2001. Tensile strain-hardening behavior of polyvinyl alcohol engineered cementitious composite (PVA-ECC). *ACI materials Journal,* 98.

PAN, Z., SANJAYAN, J. G. & RANGAN, B. V. 2011. Fracture properties of geopolymer paste and concrete. *Magazine of concrete research,* 63, 763-771.

REDON, C., LI, V. C., WU, C., HOSHIRO, H., SAITO, T. & OGAWA, A. 2001. Measuring and modifying interface properties of PVA fibers in ECC matrix. *Journal of Materials in Civil Engineering,* 13, 399-406.

TENNAKOON, C., NAZARI, A., SANJAYAN, J. G. & SAGOE-CRENTSIL, K. 2014. Distribution of oxides in fly ash controls strength evolution of geopolymers. *Construction and Building Materials,* 71, 72-82.

YANG, E.-H. & LI, V. C. 2014. Strain-rate effects on the tensile behavior of strain-hardening cementitious composites. *Construction and Building Materials,* 52, 96-104.

YANG, E.-H., WANG, S., YANG, Y. & LI, V. C. 2008. Fiber-bridging constitutive law of engineered cementitious composites. *Journal of advanced concrete technology,* 6, 181-193.

YANG, E.-H., YANG, Y. & LI, V. C. 2007. Use of high volumes of fly ash to improve ECC mechanical properties and material greenness. *ACI Materials Journal,* 104.

CHAPTER 12

DEVOPMENT OF A SUSTAINABLE LIGHTWEIGHT PRECAST COMPOSITE FLOOR INCORPORATING ONE-PART SHGCS

12.1 Introduction

The "conventional" composite floor is composed of steel beams and a concrete slab interconnected with shear connectors. The steel beams are made of structural steel. The concrete slab is normally either a solid slab (without a haunch) or a composite slab incorporating profiled steel sheeting (AS 2327.1, 2003). Nowadays, the composite slab is commonly used in Australia. The major types of profiled steel sheeting used in Australia are BONDEK II, CONDECK HP, and COMFORM. According to AS 2327.1 (2003), the minimum cover slab thickness is 65 mm. Therefore, the minimum overall slab depth of a composite slab is nominally 120 mm for BONDEK II and CONDECK HP, and 125 mm for COMFORM (Design Booklet DB1.1, 2001). This translates to a self-weight of 300 kg/m^2 for the composite slab.

The motivation for this research arose from an industry challenge in the potential replacement of "conventional" precast composite floor with a sustainable lightweight precast composite floor. The challenge was to substantially reduce the weight of the precast composite floor, while maintaining the strength, stiffness and ductility. In the construction industry, the use of lighter weight and high strength materials and structural members are advantageous as the reduction of dead load, together with increase in load capacity, can offer considerable cost reductions. However, low tensile strength and strain capacity, and low fracture toughness have been the key obstacles for the use of lightweight concrete in civil engineering applications. The one-part PVA-SHGC developed in Chapter 10 exhibited high tensile strength and very high tensile ductility comparable to those of "conventional" SHCC with added advantages of significantly lower environmental impact and the lower weight. Therefore, the developed one-part PVA-SHGC can be an ideal option to tackle the aforementioned obstacles, due to its significantly enhanced post-cracking flexural performance, tensile ductility and non-elastic energy absorption capacity.

In this study, a sustainable lightweight precast composite floor composed of a thin concrete slab and lightweight C-section purlins interconnected with shear connectors is presented. At first, the sustainable lightweight composite floor was designed based on the first principles in conjunction with Recommendations for Design and Construction of High Performance Fiber Reinforced Cement Composites with Multiple Fine Cracks (HPFRCC) (2008) and the relevant Australian standards. Push-out shear tests on small scale specimens were conducted to evaluate the load-slip behavior and ascertain the adequacy of the proposed configuration of the shear connectors. Subsequently, large scale specimens were manufactured and tested in a four-point bending test setup to evaluate the flexural behavior of the sustainable lightweight composite floor.

12.2 Design of Sustainable Lightweight Precast Composite Floor

12.2.1 The design concept

The reinforced concrete slab in the "conventional" composite floor is replaced by a 40 mm thick slab made of one-part PVA-SHGC in the proposed sustainable lightweight precast composite floor. The 4 m long lightweight C-section purlins spaced 450 mm center to center are used, which play the role of the structural steel beams in the "conventional" composite floor. Self-drilling metal screws are used as shear connectors to interconnect the thin concrete slab and the lightweight C-section purlins to ensure the composite action. All-thread rods spaced at 950 mm center to center with a diameter of 12 mm are used to connect the mid-height of the C-section purlins together to provide lateral support during the construction of the composite floor. Schematic drawings of the proposed sustainable lightweight precast composite floor are shown in Figure 12-1. It should be noted that the width of the composite floor is selected to be 900 mm so that the specimen can fit the available testing machine for experimental testing. Figure 12-2 shows dimensions of the lightweight C-section purlins (denoted as C20015) used in the design stage of the composite floor. The C-section purlins are roll-formed from high strength zinc-coated steel with minimum yield stress of 450 MPa, and the standard zinc coating class of Z350 (350 g/m^2 minimum coating mass). The C-section purlins are supplied with standard elongated punched holes (18×22 mm) spaced 130 mm center to center on top and bottom flanges to provide continuity of concrete when the flange is buried inside the concrete slab. Details of the punched holes are also shown in Figure 12-2.

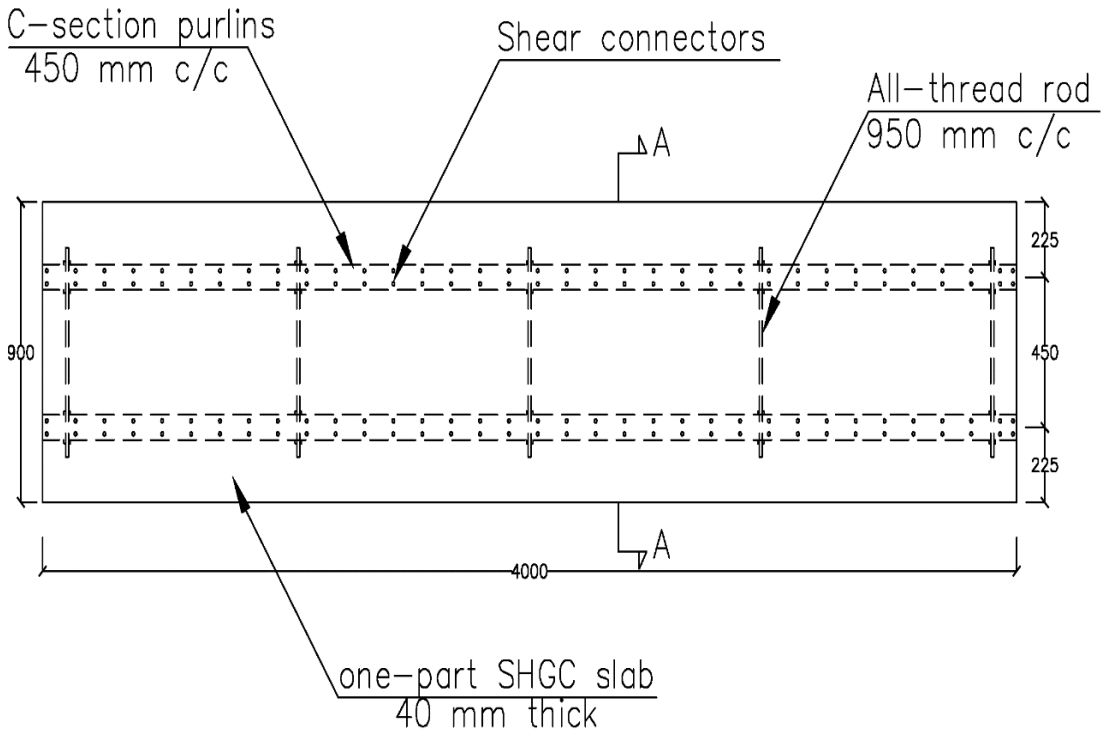

(a): Plan view

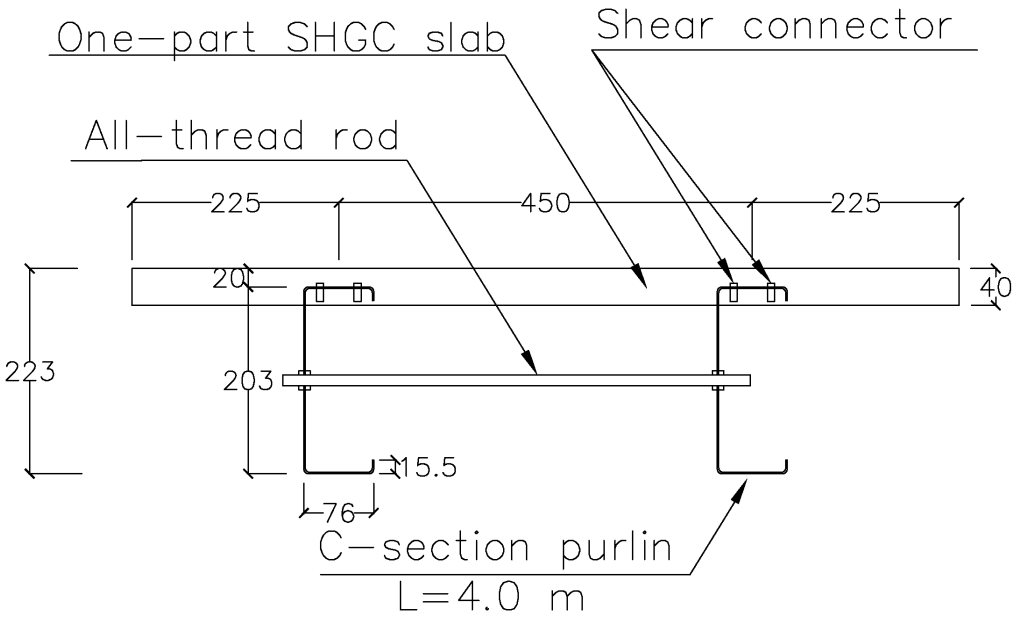

(b): Cross section A-A

Figure 12-1: Schematic drawings of sustainable lightweight precast composite floor (all dimensions in mm)

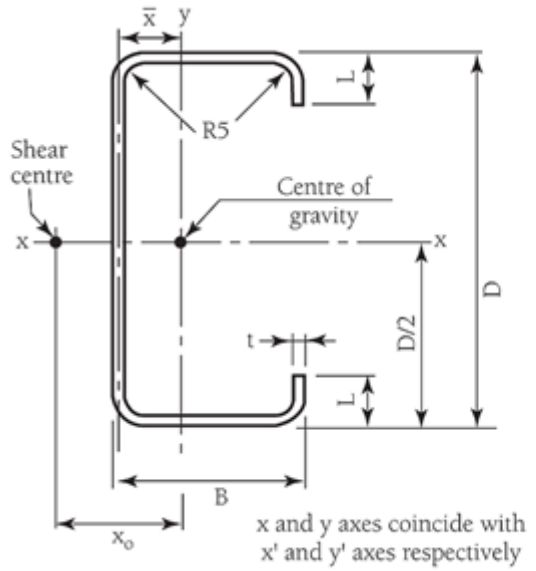

Dimensions of C20015	
t (mm)	1.5
D (mm)	203
B (mm)	76
L (mm)	15.5
Mass per unit length (kg/m)	4.49

(a) Dimensions of C20015 section purlin used in the design stage

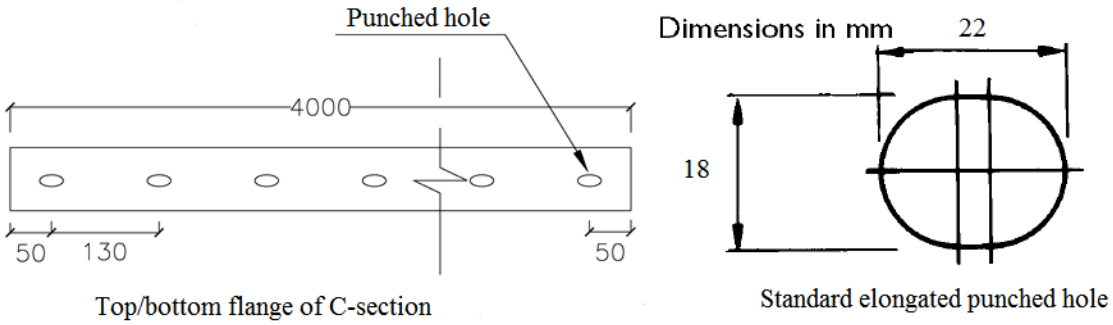

(b) Details of the punched holes on top and bottom flanges of the C-sections

Figure 12-2: Dimensions of C20015 section purlin used in the design stage, and details of the punched holes on top and bottom flanges

12.2.2 Flexural design

The details of flexural design procedure of the proposed composite floor are summarized in the following:

Self-weight of the one-part SHGC slab = $0.9 \times 0.04 \times 1850 = 66.60$ kg/m

Self-weight of the C-sections $= 2 \times 4.49 = 8.98$ kg/m

Self-weight of the composite floor = 66.60 + 8.98 = 75.6 kg/m ≈ 0.76 kN/m

Table 12-1 summarizes the loads adopted in the analysis and design of the composite floor. The design load, design bending moment and design shear force acting on the composite floor under serviceability limit state (SLS) and ultimate limit state (ULS) conditions are summarized in Table 12-2.

Table 12-1: The loads adopted in the design stage

Type of loading	Nominal value (kN/m)	SLS factor	ULS factor	Design value under SLS (kN/m)	Design value under ULS (kN/m)
Self-weight	0.76	1.0	1.2	0.76	0.91
Dead load (1.5 kPa)	1.35	1.0	1.2	1.35	1.62
Live load (2 kPa)	1.8	0.4	1.5	0.72	2.7

Table 12-2: The design actions adopted in the design stage

Design actions	Under SLS condition	Under ULS condition
Design load, W^* (kN/m)	2.83	5.23
Design bending moment, M^* (kN.m)	5.7	10.5
Design shear force, V^* (kN)	5.7	10.5

The design bending moment capacity (ϕM_u) of the composite floor under ULS condition can be calculated using the equilibrium equations in conjunction with AS 2327.1 (2003) and Recommendations for Design and Construction of High Performance Fiber Reinforced Cement Composites with Multiple Fine Cracks (HPFRCC) (2008). In order to derive the nominal moment capacity (M_u), the stress and strain diagrams for the cross section A-A are presented in Figure 12-3. Table 12-3 presents the material characteristics of the one-part SHGC used for calculation of the M_u of the cross section. The calculation procedure to determine the M_u of the composite floor is summarized in the following:

It is assumed that neutral axis (N.A.) is located in the one-part SHGC slab. In addition, it is assumed that the C-section purlins are in yield condition. It should be noted that the tensile force in the portion of the C-section purlins which are not yielded is ignored in the calculation. According to Figure 12-3, the following equations for the forces acting on the cross section can be written:

$$C = 0.85 \times f'_{ck} / \gamma_c \times d_n \times 900 \quad (12.1)$$

$$T_F = f_{tyk} / \gamma_c \times (40 - d_n) \quad (12.2)$$

$$T_S = f_{sy} \times A_s \quad (12.3)$$

$$A_S = 2 \times \{(223-1.75\ d_n) \times 1.5 + (76-1.5) \times 1.5 + (15.5-1.5) \times 1.5\} \quad (12.4)$$

By substituting the values of f'_{ck}, f_{tyk} and γ_c given in Table 12-3, the Equations (12.1) and (12.2) can be re-written as follows:

$$C = 21420\ d_n \quad (12.5)$$

$$T_F = 2111.54 \times (40 - d_n) \quad (12.6)$$

Considering that f_{sy} = 450 MPa for the C-section purlins used in this study, the Equation (12.3) can be simplified as follows:

$$T_S = 420525 - 2362.5\ d_n \quad (12.7)$$

The depth of the neutral axis (d_n) can be determined from force equilibrium equation ($C = T_S + T_F$). Subsequently, the values of C, T_S and T_F can be calculated. ε_{st} can also be determined from the following equation:

$$\varepsilon_{st} = (223-d_n) \times 0.003 / d_n \quad (12.8)$$

The values of d_n, C, T_S and T_F, as well as ε_{st} are summarized in Table 12-4. Based on the results summarized in Table12-4, the assumption that the N.A. is located in in the one-part SHGC slab is correct. In addition, the assumption of yielding of the C-section purlins is also correct ($\varepsilon_{st} > \varepsilon_{sy} = 0.00225$).

Subsequently, M_u of the cross section can be determined by taking moment about top extreme fiber as follows:

$$M_u = T_S \times \{(223-1.75\ d_n) / 2 + 1.75\ d_n\} + T_F \times \{(40-d_n) / 2 + d_n\} - C \times d_n / 2 \quad (12.9)$$

By substituting the values of d_n, C, T_S and T_F in the Equation (12.9), M_u will be equal to 45.3 kN.m. According to AS2327.1 (2003), the capacity reduction factor ϕ for bending is equal to 0.9. Therefore, the design bending moment capacity of the cross section of the composite floor will be equal to $\phi M_u = 0.9 \times 45.3 = 40.8$ kN.m. Since the design bending

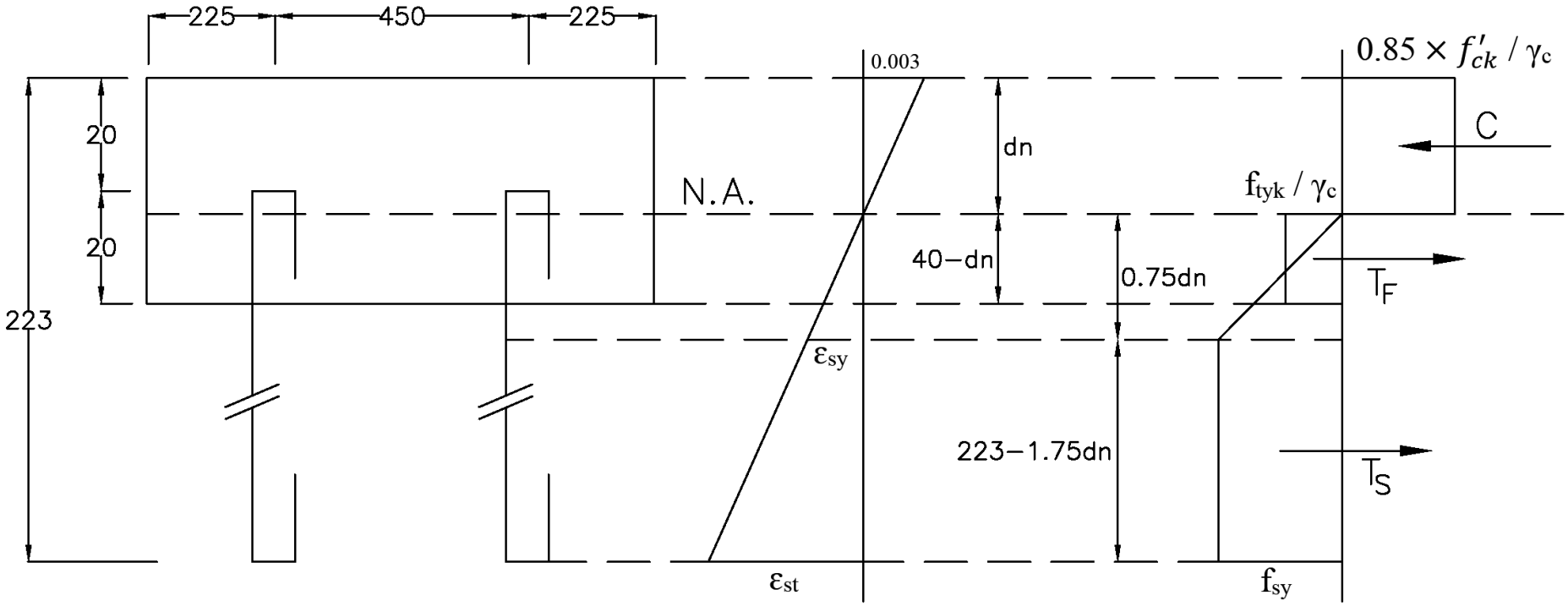

Figure 12-3: Stress and strain diagrams of cross section A-A of sustainable lightweight composite floor

moment (M^* = 10.5 kN.m) is less than the design bending moment capacity (ϕM_u = 40.8 kN.m), therefore the proposed composite floor is satisfactory in terms of bending under ULS.

Table 12-3: Material characteristics of one-part SHGC used to derive M_u

Mean value of cube compressive strength[1], f_c' (MPa)	47.4
Characteristic compressive strength[2], f_{ck}' (MPa)	36.4
Mean value of tensile first-crack strength[3], σ_{fc} (MPa)	3.3
Characteristic tensile yield strength[4], f_{tyk} (MPa)	3.05
Material factor; γ_c[5]	1.3

[1] According to Table 10-4 for the heat cured one-part SHGC-T mixture.

[2] $f_{ck}' = f_c' - 1.645\times$ S.D. in accordance with Recommendations for Design and Construction of High Performance Fiber Reinforced Cement Composites with Multiple Fine Cracks (HPFRCC) (2008); the standard deviation (S.D.) is equal to 6.7 MPa according to Table 10-4 for the heat cured one-part SHGC-T mixture.

[3] According to Table 10-7 for the heat cured one-part SHGC-T mixture.

[4] $f_{tyk} = \sigma_{fc} - 1.645\times$ S.D. in accordance with Recommendations for Design and Construction of High Performance Fiber Reinforced Cement Composites with Multiple Fine Cracks (HPFRCC) (2008); the S.D. is equal to 0.15 MPa according to Table 10-7 for the heat cured one-part SHGC-T mixture.

[5] According to Recommendations for Design and Construction of High Performance Fiber Reinforced Cement Composites with Multiple Fine Cracks (HPFRCC) (2008).

Table 12-4: The values of d_n, C, T_S and T_F as well as ε_{st}

d_n (mm)	C (kN)	T_S (kN)	T_F (kN)	ε_{st}
19.5	417.7	374.4	43.3	0.0313

12.2.3 Vertical shear design

According to Clause 5.11 of AS4100 (1998), it is assumed that all vertical shear force is to be resisted by the web of the C-section purlins (i.e. the one-part SHGC slab is ignored in the calculation of the design vertical shear capacity of the cross section).

Because the C-section purlins are subjected to combined shear and bending, and the bending moment is assumed to be resisted by the whole cross-section, the C-section purlins shall be designed for combined bending and shear, and shall satisfy Clause 5.12.3 of AS4100 (1998) as follows:

$$V^* \leq \phi V_{vm} \tag{12.10}$$

$$\text{Where } V_{vm} = V_v \text{ for } M^* \leq 0.75\,\phi M_s \tag{12.11}$$

Where V_v is the nominal shear capacity of a web in shear alone, determined in accordance with Clause 5.11.1 of AS4100 (1998), and M_s is the nominal section moment capacity, determined in accordance with Clause 5.2 of AS4100 (1998), where $M_s = f_y Z_{ex}$. According to AS2327.1 (2003), the capacity reduction factor ϕ for vertical shear is equal to 0.9. As reported by the supplier, $Z_{ex} = 24.1\times 10^3$ mm^3 for C20015 section purlins. Therefore, $0.75\,\phi M_s$ for two C-section purlins shall be determined as follows:

$$0.75\,\phi M_s = 0.75 \times 0.9 \times 450 \times 24.1 \times 10^3 \times 2 = 14.6 \text{ kN.m} \tag{12.12}$$

As calculated in Section 12.2.2, $M^* = 10.5$ kN.m, which is less than 14.6 kN.m, therefore Equation (12.11) is satisfied. Therefore, Equation (12.10) shall be re-written as follows:

$$V^* \leq \phi V_v \tag{12.13}$$

Where V_v is the nominal shear capacity of the web. According to Clause 5.11.2 of AS4100 (1998), V_v of a web where the shear stress distribution is approximately uniform shall be taken as

$$V_v = V_u \tag{12.14}$$

Where V_u is the nominal shear capacity of a web with a uniform shear stress distribution. According to Clause 5.11.2 of AS4100 (1998), since the maximum web panel depth to

thickness ratio (d_p / t_w = 200 / 1.5 = 133.33) is bigger than 82 / $\sqrt{\frac{f_y}{250}}$ = 82 / $\sqrt{\frac{450}{250}}$ = 61.1, the nominal shear capacity (V_u) of the web shall be taken as

$$V_u = V_b \quad (12.15)$$

Where V_b is the nominal shear buckling capacity of the web determined in accordance with Clause 5.11.5 of AS4100 (1998).

According to Clause 5.11.5 of AS4100 (1998), the nominal shear buckling capacity (V_b) for an unstiffened web shall be calculated as follows:

$$V_b = \alpha_v V_w \leq V_w \quad (12.16)$$

Where α_v can be calculated as follows:

$$\alpha_v = \{ \frac{82}{\frac{d_p}{t_w} \times \sqrt{\frac{f_y}{250}}} \}^2 \quad (12.17)$$

and V_w is the nominal shear yield capacity of a web determined in accordance with Clause 5.11.4 of AS4100 (1998) as follows:

$$V_w = 0.6\, f_y\, A_w \quad (12.18)$$

where A_w is the gross sectional area of the web.

The values of α_v, A_w, V_w, V_b, V_u, V_v, ϕ and V^* are summarized in Table 12-5. As can be seen, $V^* \leq \phi V_v$, therefore the proposed composite floor is satisfactory in terms of the vertical shear force.

Table 12-5: Values of α_v, A_w, V_w, V_b, V_u, V_v, ϕ and V^*

α_v	A_w[1] (mm^2)	V_w (kN)	V_b (kN)	V_u (kN)	V_v (kN)	ϕ	ϕV_v (kN)	V^* (kN)
0.21	600	162	34.02	34.02	34.02	0.9	30.6	10.5

[1] Based on using two C20015 purlin sections.

12.2.4 Deflection control under SLS condition

According to Table C1 of Appendix C of AS1170.0 (2002), the mid-span deflection of a specialist floor system due to (1.0 G + 0.4 Q) under SLS condition should be limited to span / 600. Assuming that the span (clear spacing between the supports) of the proposed composite floor is 4.0 m; thereby, the mid-span deflection should be limited to 6.67 mm. The mid-span deflection of a simply-supported member under uniformly distributed load (UDL) can be determined from the following equation:

$$\delta_{max} = 5\ \omega\ L^4 / 384\ E\ I \qquad (12.19)$$

Where ω is the UDL, L is the clear span, E and I are the elastic modulus and second moment of area of the member, respectively. To be able to use the Equation (12.19), the transformed area of the composite floor cross section should be determined. In this regard, concrete area is transformed to steel area (i.e. concrete area of A_c is equivalent to steel area of nA_c), where $n = E_c / E_s$. E_c and E_s are the elastic modulus of concrete and steel, respectively. Thereby, the transformed area will be equal to ($A_s + nA_c$). Subsequently, the second moment of area of the transformed area can be determined. The section properties of C20015 section and transformed area are summarized in Table 12-6. Using ω = 2.83 kN/m as determined in Table 12-2, the δ_{max} can be determined as follows:

$$\delta_{max} = \frac{5 \times 2.83 \times (4 \times 1000)^4}{384 \times 200000 \times 13.8 \times 10^6} = 3.42 \text{ mm} \qquad (12.20)$$

Since 3.42 mm < 6.67 mm, thereby the deflection of the proposed lightweight composite floor under SLS condition seems to be satisfactory.

With regards to vibration control of the floor, according to Table C1 of Appendix C of AS1170.0 (2002), if the static mid-span deflection due to Q = 1.0 kN is less than 1 or 2 mm, then it can be said that the proposed floor may not have vibration problems. The mid-span deflection of a simply-supported member under concentrated load can be determined from the following equation:

$$\delta_{max} = P\ L^3 / 48\ E\ I \qquad (12.21)$$

Where P is the concentrated load, L is the clear span, E and I are the elastic modulus and second moment of area of the member, respectively. Thereby, the static mid-span deflection due to Q = 1.0 kN can be calculated as follows:

$$\delta_{max} = \frac{1000 \times (4 \times 1000)^3}{48 \times 200000 \times 13.8 \times 10^6} = 0.48 \text{ mm} \quad (12.22)$$

Since 0.48 mm < 1 mm, thereby it can be said that the proposed lightweight composite floor may not have vibration problems.

Table 12-6: Section properties of C20015 section and the transformed area

Section properties		C20015 section	Transformed area
Area, A(mm^2)		555	2586
Second moment of area, I_x (10^6 mm^4)		3.53	13.8
Distance from natural axis (mm)	Top, y_t	101.5	63.6
	Bottom, y_b	101.5	159.4

Note: Concrete area $A_c = 900 \times 40 = 36000$ mm^2.

Considering that $E_c = 8200$ MPa; thereby, $n = 8200 / 200000 = 0.041$.

The transformed area is $A_s + n A_c = 2 \times 555 + 0.041 \times 36000 = 2586$ mm^2.

12.2.5 Longitudinal shear design

One of the most important steps in designing the lightweight composite floor is the design of shear connection to ensure composite actions. The composite action is the interaction between the C-section purlins and the one-part SHGC slab, which enables the two components to act together as a single structural member (Design Booklet DB1.1, 2001). The shear connection mainly resist interface slip, and causes the one-part SHGC slab and the C-section purlins to interact, leading to having the lightweight composite floor with much greater bending strength and stiffness, otherwise the two components act separately, resulting a non-composite member.

In this study, Buildex® 14-20 × 22 3/8 Hex Washer Teks® self-drilling screws supplied by Buildex® Australia, which are suitable for fixing metal to metal, are used as mechanical shear connectors. The basic size of the thread outside diameter of the screws

is 6.3 mm (i.e. the screws are 14 gauge). The length of the shank is 22 mm. The screw has 22 threads per inch (TPI). The screws have a 3/8 Hex drive head with an outside diameter of 14.7 mm and the height of 6.8 mm. The screws are made of Carbon Steel SAE 1022 with heat treatment in accordance to AS 3566.1 (2002) and have Climaseal®4 finish which provides superior corrosion performance complies with Class 4 of AS3566.2 (2002). According to the supplier, the Teks® point is suitable for drilling into steel while ensuring maximum pullout strength and a high strip torque. Schematic drawing of the self-drilling screw is shown in Figure 12-4.

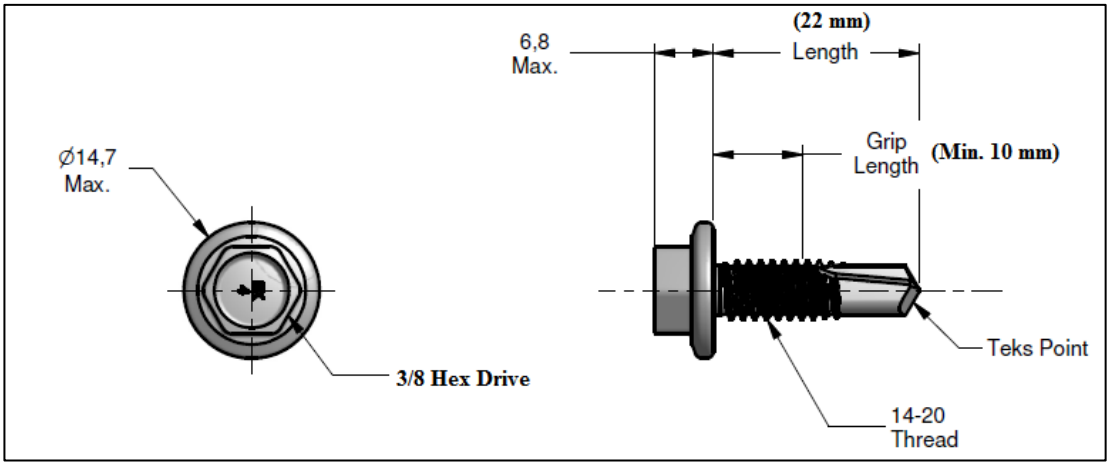

Figure 12-4: Schematic drawing of self-drilling screws used as shear connectors

As can be seen in Figure 12-5, at the interface of the concrete slab and the C-section purlins the shear flow (q) (i.e. the longitudinal shear force per unit length of the member) can be determined as follows:

$$q = \frac{C}{2000} = \frac{T_S + T_F}{2000} \tag{12.23}$$

where $C = T_S + T_F = 417.7$ kN as given in Table 12-4; thereby, q = 208.85 N/mm. The q at the interface should be resisted by the shear connectors located on the two C-section purlins. Thereby, the shear connectors on each C-section should resist q / 2 = 104.4 N/mm. The single shear strength of the screws (the shear load required to break the screw) is 2.8 kN, as reported by the supplier. According to AS2327.1 (2003), the capacity reduction factor ϕ for shear connectors is equal to 0.85. Assuming two rows of screws are located

on both sides of the punched holes, the maximum spacing of the screws (S) can be determined as follows:

$$S = 0.85 \times 2.8 \times 1000 / (104.4 / 2) = 45.6 \text{ mm} \quad (12.24)$$

Thereby, the spacing of the screws is selected to be 43 mm. As can be seen in Figure 12-6, the shear connectors were arranged such that two rows of screws were equally spaced between the punched holes.

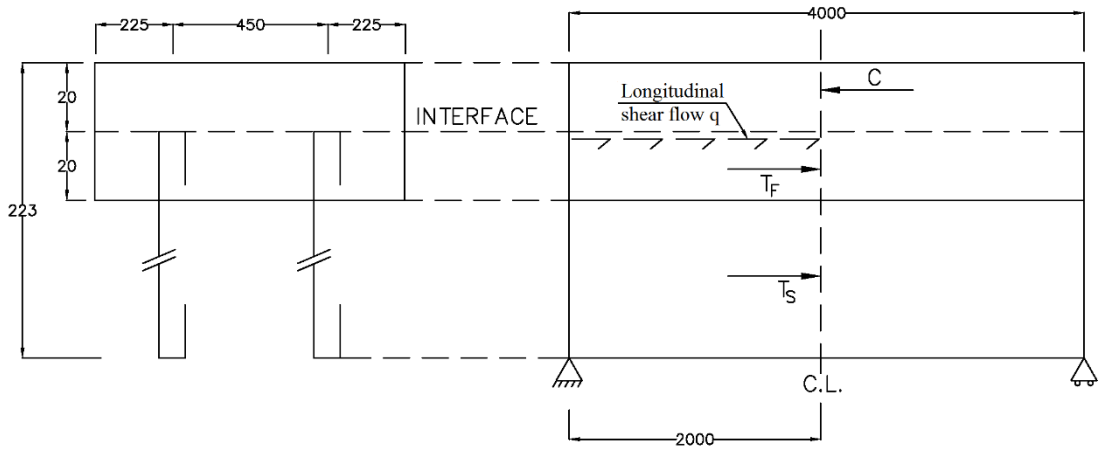

Figure 12-5: Schematic drawing to determine longitudinal shear flow at the interface

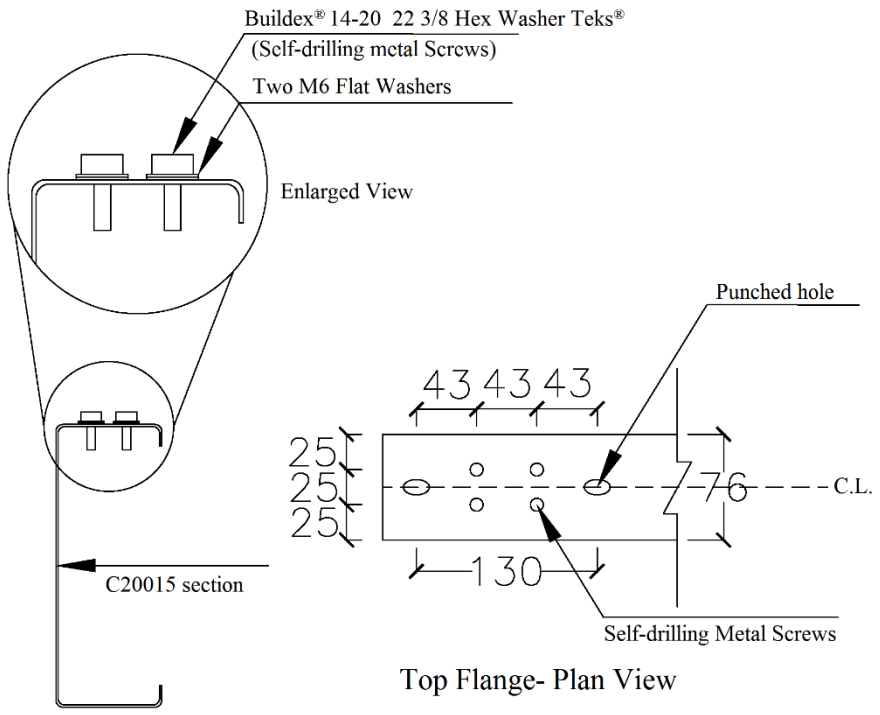

Figure 12-6: Schematic configuration of shear connectors

12.3 Push-out shear test

Push-out shear tests on small-scale specimens have been conducted to determine the load-slip behavior and ascertain the adequacy of the proposed configuration of the shear connectors. At least two specimens composed of a one-part SHGC slab with the dimensions of 450 mm × 450 mm, and one C20015 section purlin placed in the center of the slab were prepared. The materials, mix proportion, mixing and curing of the one-part SHGC mixture used for casting the pushout specimens are the same as those of "one-part SHGC-T" mixture presented in Sections 10-2 and 10-3 of Chapter 10. A schematic drawings of the specimens for the push-out shear test are shown in Figure 12-7. As can be seen, a polystyrene foam is placed inside the mold before casting; thereby, the end of the bottom flange of the C-section purlin was exposed and during the test the loading plate was easily placed on it. Photographs of the mold and different views of the push-out specimen are shown in Figure 12-8. The push-out shear test with and without the self-drilling screws were conducted under displacement control using MTS testing machine. The displacement control rate was 0.1 mm/min. A linear variable differential transducer (LVDT) was used to measure the displacement of the specimen. Figure 12-9 shows the photographs taken from different views of the push-out shear test setup.

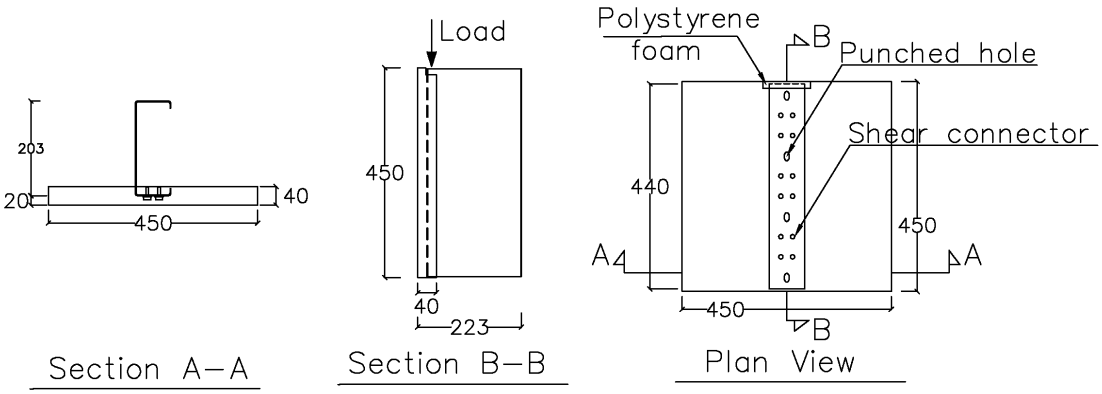

Figure 12-7: Schematic drawings of the small-scale specimen used for push-out shear test

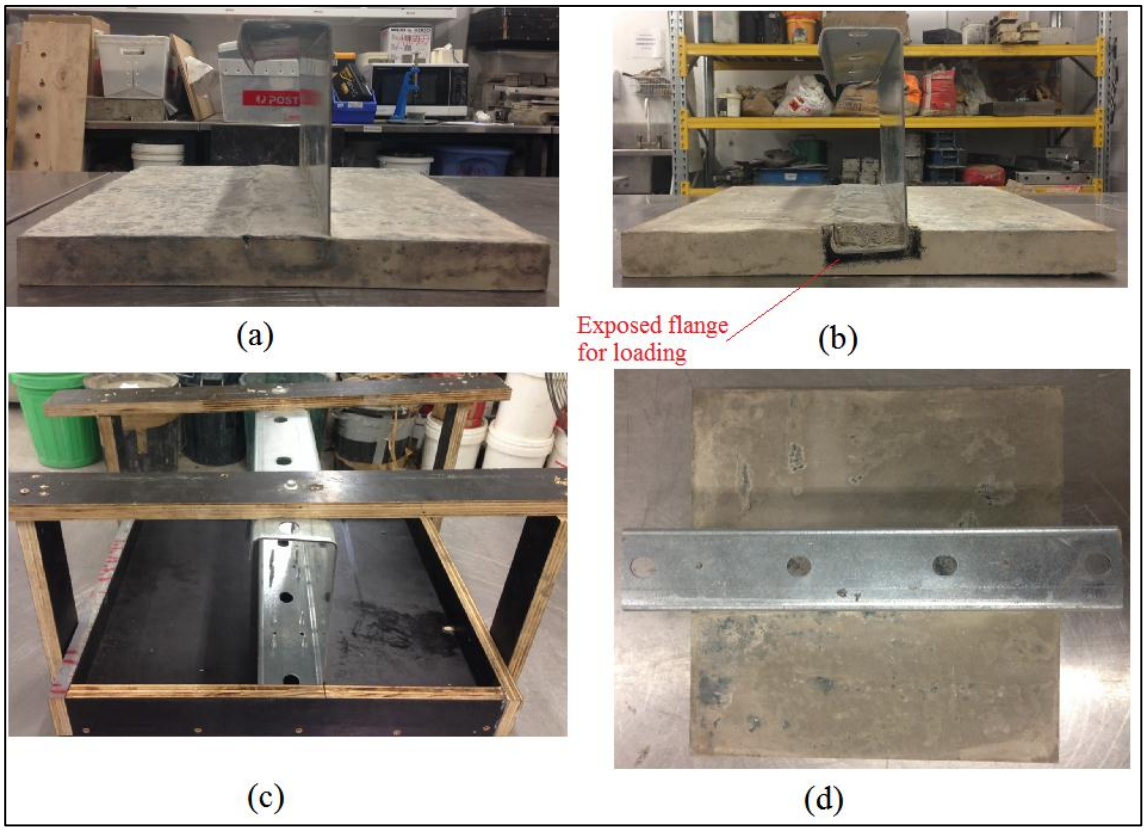

Figure 12-8: Photographs of the small-scale specimen used for push-out shear test: (a) and (b): side views, (c) the mold before casting and (d) top view

The shear load-displacement responses of the push-out specimens without and with shear connectors are presented in Figures 12-10, 12-11, respectively. The maximum shear force, and its corresponding displacement, as well as the experimental and theoretical values of the shear flow are summarized in Table 12-7. As can be seen, the ratio of average experimental shear flow to the theoretical shear flow is 1.09; thereby, the proposed configuration of the shear connectors seems to be satisfactory. In addition, the average experimental shear flow of the specimens with shear connectors is more than 5 times than that of the specimens without shear connectors (i.e. with the punched holes alone). Figure 12-12 shows the photographs taken from different views of the specimen after the push-out shear test. As can be seen, 75% of the screws (9 out of 12) were sheared, while the other screws remained intact.

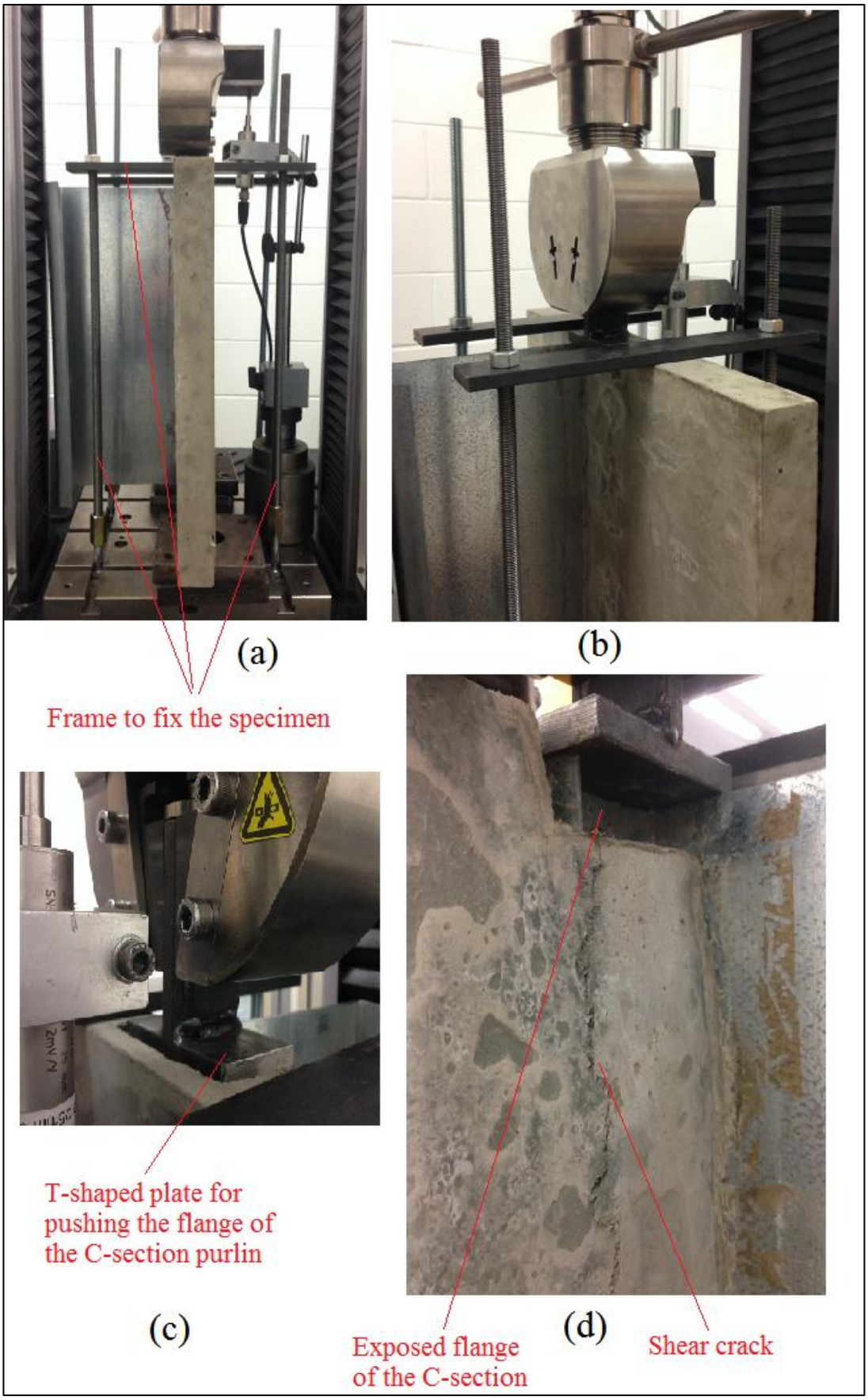

Figure 12-9: Different views of the test setup for push-out shear test

Table 12-7: Push-out shear test results

Specimen designation	Maximum shear force (kN)	Corresponding displacement (mm)	Experimental shear flow (N/mm)	Theoretical shear flow (N/mm)	Exp. / Theo. ratio
Spec 1-W/O [a]	10.1	1.91	23.5	104.4	0.22
Spec 2-W/O	9.0	2.38	20.4		0.20
Ave.-W/O [c]	9.5	2.15	21.9		0.21
Spec 1-W/ [b]	46.2	4.12	108.7		1.04
Spec 2-W/	51.3	4.00	119.9		1.15
Ave.-W/ [d]	48.8	4.06	114.3		1.09

[a] W/O denotes specimen without shear connectors.

[b] W/ denotes specimen with shear connectors.

[c] Average values of the two specimens without shear connectors.

[d] Average values of the two specimens with shear connectors.

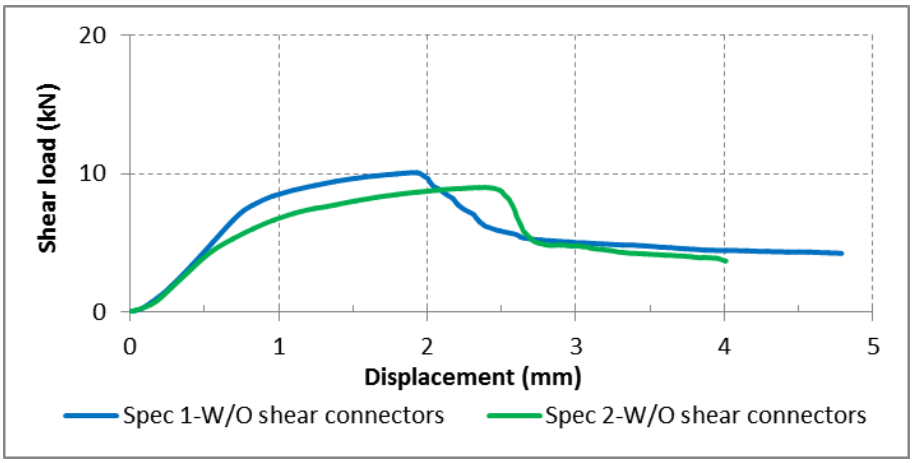

Figure 12-10: Load-displacement responses of the specimens without shear connectors

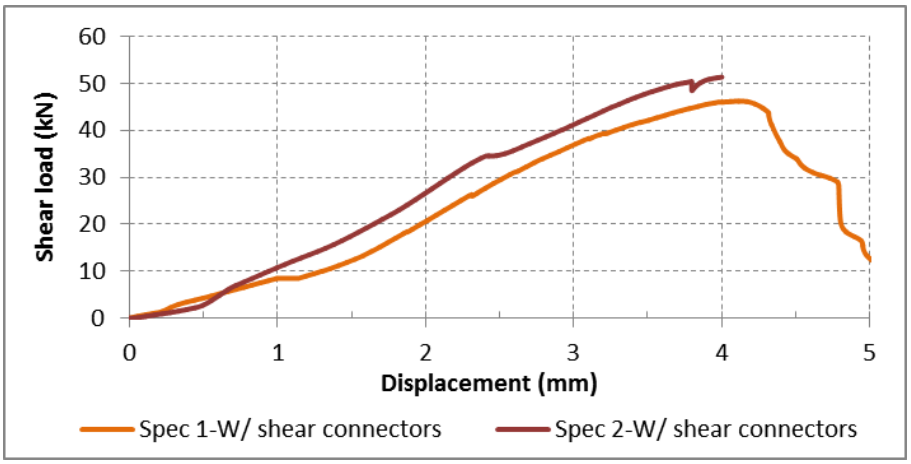

Figure 12-11: Load-displacement responses of the specimens with shear connectors

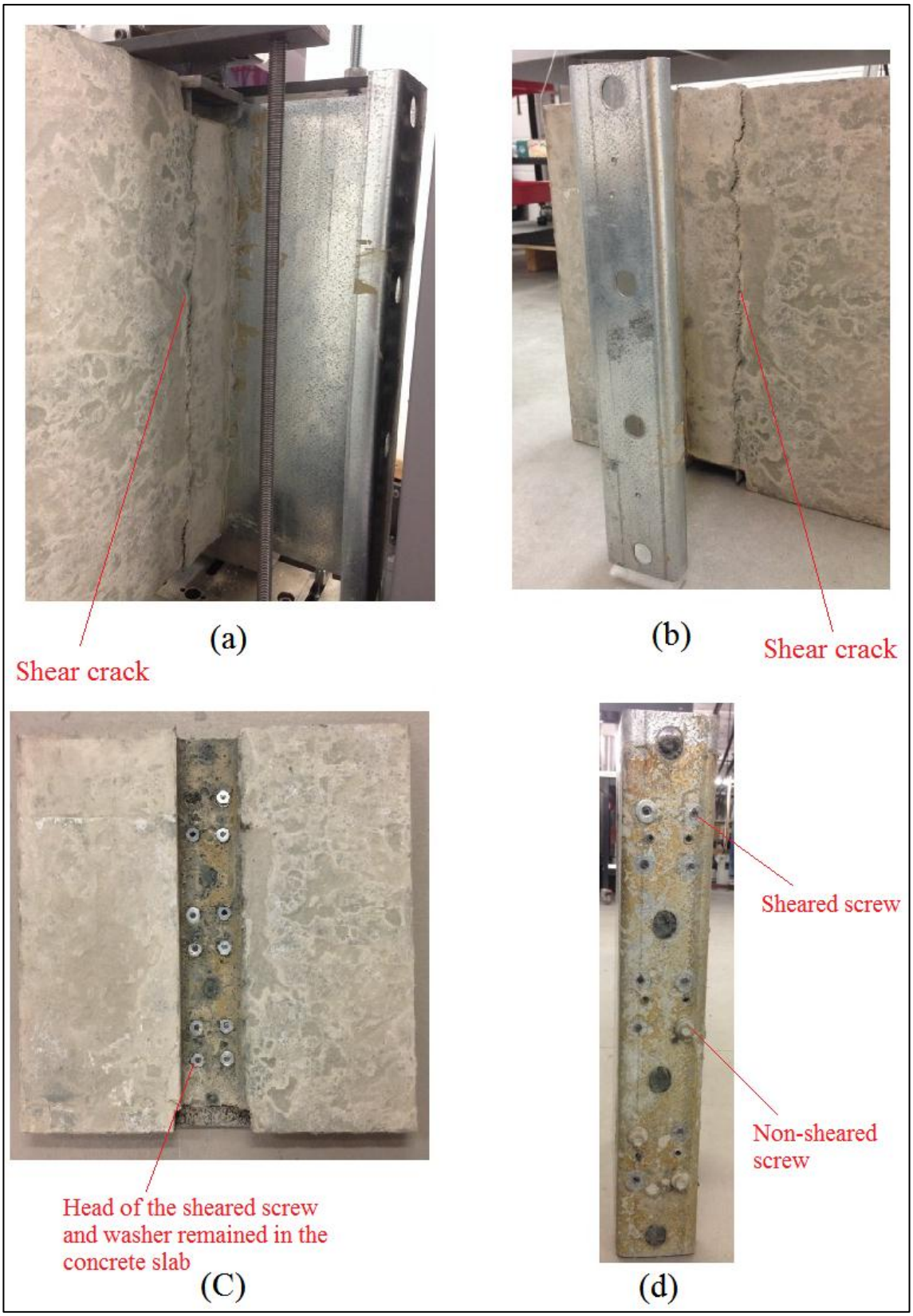

Figure 12-12: Different views of the specimen after the push-out shear test

12.4 Large Scale Experimental Tests

This section describes the experimental tests conducted on large-scale specimens of the proposed precast lightweight composite floor to evaluate its structural behavior under the flexural loading.

12.4.1 Fabrication of large-scale specimens

In this study, three large-scale floor specimens with the dimensions of 4.0 m in length and 0.9 m in width were manufactured. The test parameter was the thickness of the C-section purlin used to make the specimens. The C-section purlins with three different thickness were used in this study. Dimensions and section properties of the C-section purlins are presented in Tables 12-8 and 12-9, respectively.

Table 12-8: Dimensions of C-section purlins

C-section designation	t (mm)	D (mm)	B (mm)	L (mm)	Mass per unit length (kg/m)
C20015	1.5	203	76	15.5	4.49
C20019	1.9	203	76	19.0	5.74
C20024	2.4	203	76	21.0	7.24

Note: Refer to Figure 12-2-(a) for the notations used.

Table 12-9: Section properties of C-section purlins

C-section designation	Area (mm^2)	Second moment of area ($10^6\ mm^4$)		Section modulus ($10^3\ mm^3$)		Centroid (mm)
	A	I_x	I_y	Z_x	Z_y	$\bar{X}$
C20015	555	3.53	0.396	34.7	7.17	19.9
C20019	713	4.51	0.531	44.4	9.77	20.8
C20024	904	5.69	0.681	56.0	12.7	21.1

Figure 12-13 shows the configurations of shear connectors used for each C-section. As can be seen, the number of shear connectors used in large-scale specimens were more than that of the small-scale specimens used in push-out shear test. The decision to increase the number of shear connectors were based on the assumption that this increase would be a conservative for shear failure.

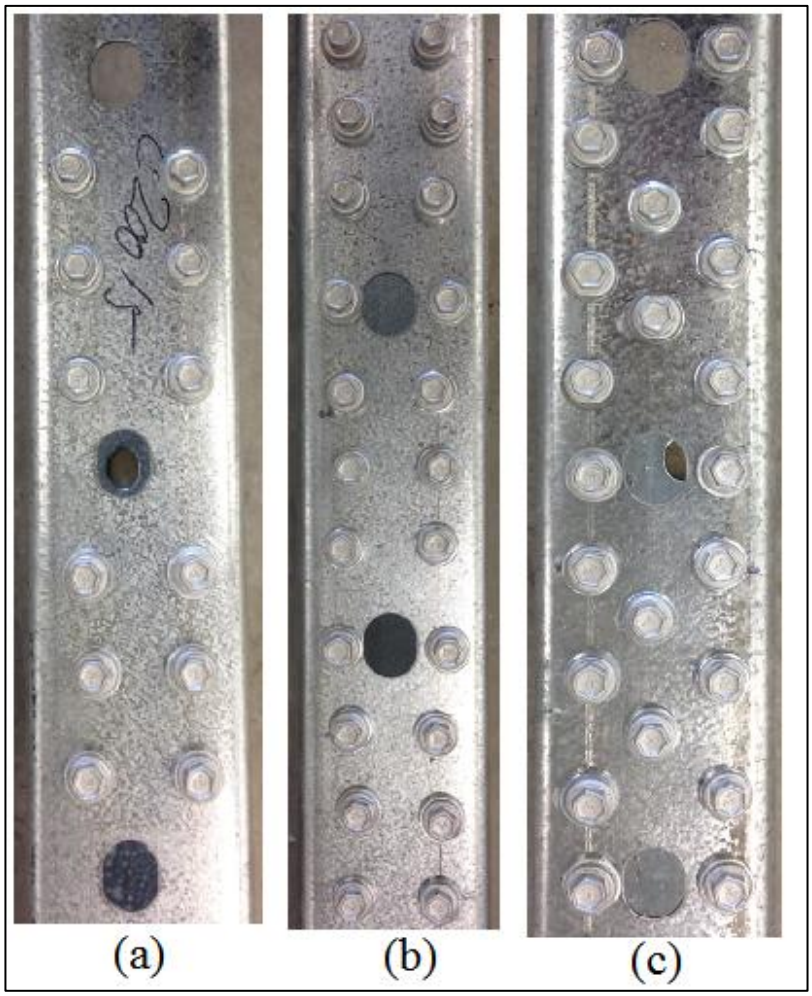

Figure 12-13: Configurations of shear connectors in (a): C20015 section, (b): C20019 section, and (c):C20014 section

For fabrication of the specimens, three wooden molds with the inner dimensions of 4000 mm in length, 900 mm in width, and 40 mm in depth were prepared. The shear connectors were installed on each of the C-sections in accordance with the configurations shown in Figure 12-13. Subsequently, the two C-sections of the same thickness were connected together via all-thread rods, as shown in Figure 12-14-(b), and then installed on the molds, in accordance with the dimensions given in Figure 12-1. As shown in Figure 12-14-(c), appropriate plastic bar chairs were used to provide enough cover under the C-sections. Oil lubricant was used to ease demolding of the specimens. Figure 12-14-(a) shows a photograph of one of the specimens ready for casting. As can be seen, the specimen was cast upside down, which will be flipped over after casting and curing. This approach

provides a smooth floor surface without having the necessity of concrete finishing, thereby provides saving both in terms of cost and time.

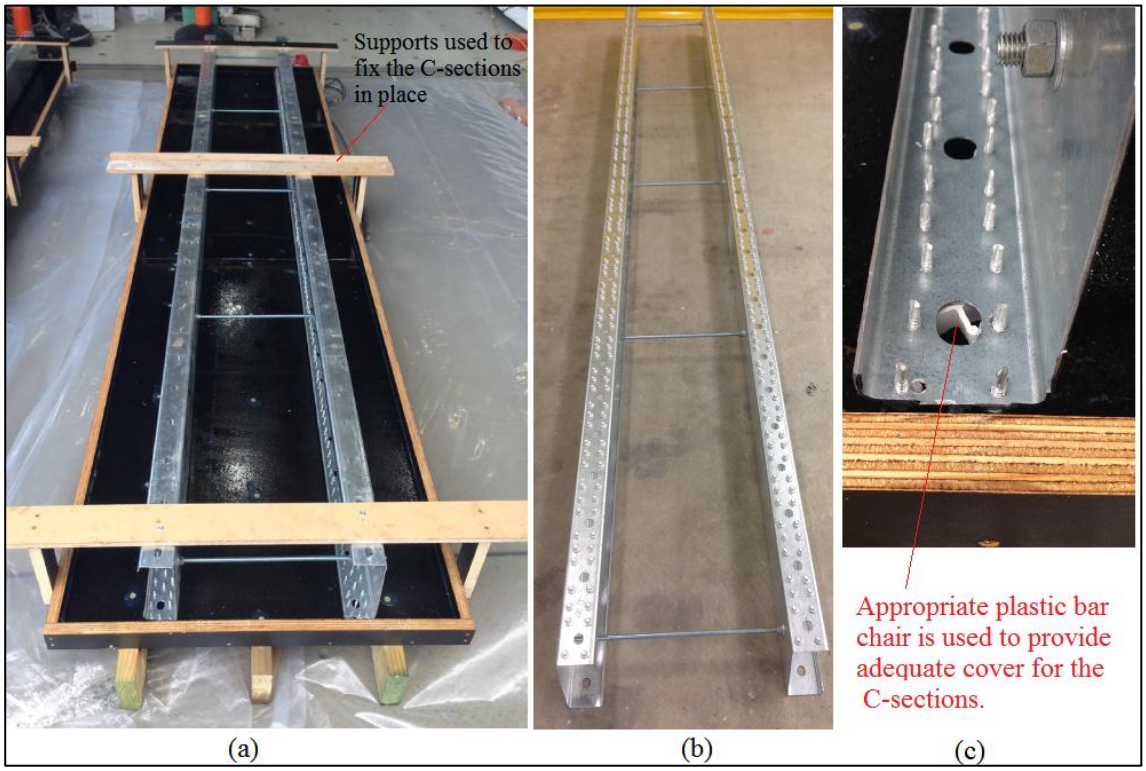

Figure 12-14: (a): Installation of the C-sections inside the mold before casting, (b): Connection of two C-sections using all-thread rods, (c): Use of appropriate plastic bar chair to provide cover for the C-sections

The materials and mix proportion of the one-part SHGC mixture used for casting the slab are the same as those of "one-part SHGC-T" mixture presented in Section 10-2 of Chapter 10. Based on the required volume of concrete, it is decided that the concrete to be supplied and mixed using a mini-truck mixer from a commercial ready-mixed plant. The following mixing procedure was adopted:

Step 1: Fly ash, slag and 80% of the needed water were added to the mini-truck mixer at the batching plant and mixed at low speed while the mixer was on the way to the casting site. (It should be noted that the distance from the batching plant to the casting site was 10 to 15 min).

Step 2: Once the truck mixer arrived at the casting site, PVA fibers were gradually added to the mixing drum and mixed for about 10 to 15 minutes at low speed. (It should be noted that a scissor lift was used to provide access to the opening of the mixing drum).

Step 3: Once the fibers were thoroughly dispersed, the solid activator and the remaining water were gradually added to the mixing drum and mixed for about 10 minutes at low speed. Subsequently, the drum speed was increased and the mixing was continued for another 5 minutes, after which the one-part SHGC mixture was ready for casting. The whole mixing procedure took about 35 to 45 minutes.

Figure 12-15 shows photographs taken from different stages of the mixing procedure. Casting was done with the help of the mini-truck mixer chute and wheelbarrow. The molds were externally vibrated moderately using electrical poker vibrators.

Figure 12-15: Different stages of the mixing procedure, (a): arrival of mini-truck mixer containing fly ash, slag and 80% of the needed water at the casting site, (b): addition of the PVA fibers gradually, (c): addition of the solid activator and remaining water gradually, (d) and (e): appearance of fresh composite ready for casting

At least nine 50 mm cubes specimens and two 100 × 200 mm cylinders were also cast to measure the compressive strength and elastic modulus of the composite. Figure 12-16 shows different views of the specimens after casting.

Figure 12-16: Different views of the large-scale specimens after casting

Heat curing approach (24 hours at 60 °C) was adopted in this study. In this regard, a curing chamber was made using heavy duty Tarpaulin as the isolation cover. A 9 kW three-phase (415V / 50 HZ) portable electric space heater was used to blow hot air inside the curing chamber. A 3 kW portable reverse cycle air conditioner was also used to circulate the hot air inside the curing chamber. A container filled with water was placed inside the curing chamber to prevent excessive moisture loss. Five thermocouples were installed in four corners and the center of the curing chamber to monitor the temperature at different locations periodically. Figure 12-17 shows the photographs taken from the curing chamber. Figure 12-18 shows one of the specimens after completion of the heat curing. The specimens were first flipped over with the help of the overhead crane and

slings, while they were still in the mold. They were then demolded and kept in the laboratory under ambient temperature until the day of testing.

Figure 12-17: Curing chamber for heat curing of the specimens

12.4.2 Test setup and testing procedure

Flexural tests were conducted to evaluate the flexural behavior of the developed lightweight composite floor. All large-scale specimens were tested in a four-point

bending test setup under displacement control with the mid-span measuring 1000 mm. The displacement rate was 0.5 mm/min. A LVDT was used to measure the displacement of the specimen at mid-span. Figure 12-19 shows the photographs taken from different views of the test setup. Figure 12-20 shows schematic drawings of the test setup. Resulting load versus mid-span deflection data were recorded and load versus mid-span deflection curves were plotted.

Figure 12-18: The large-scale specimen after completion of the heat curing period

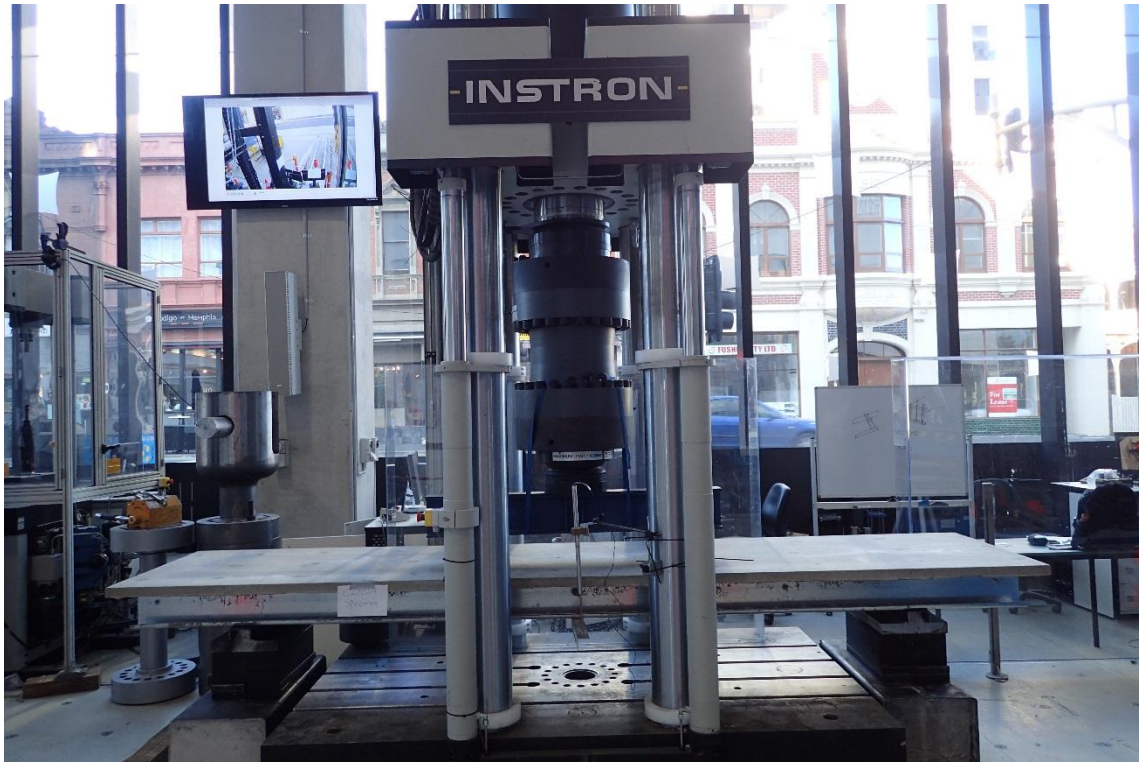

Figure 12-19: Different views of the four-point bending test setup

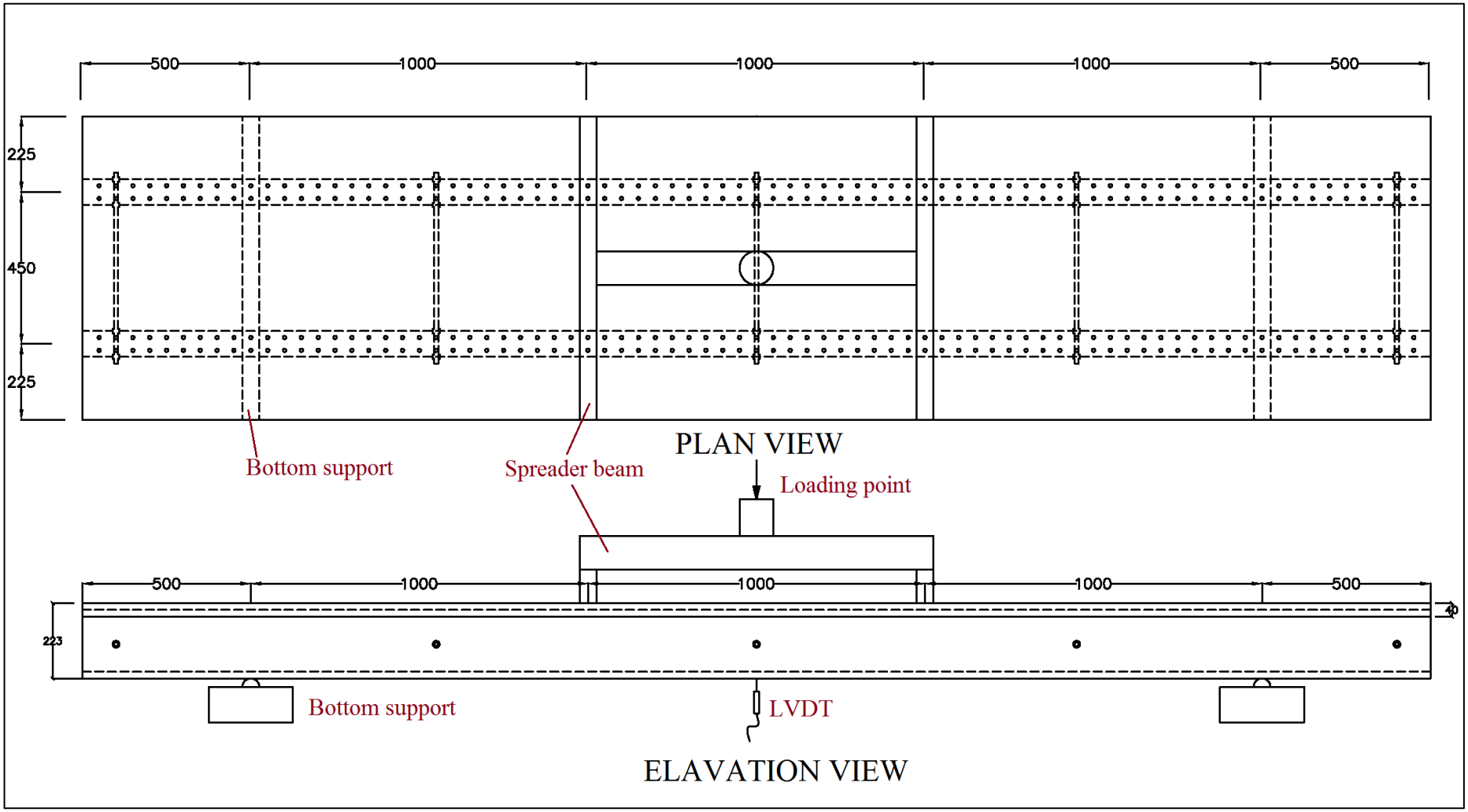

Figure 12-20: Schematic drawings of the four-point bending test setup

12.4.3 Experimental results and discussion

As can be seen in Figure 12-21, as the load was applied, the specimen gradually started to deflect along its length. As the load was increased, the top flanges of the C-sections which were in compression would tend to buckle sideways. However, movement was restricted by the bottom flanges of the C-sections, which in fact were in tension. At this stage of the test, it was observed that the web and bottom flange of the C-sections started to gradually twist and displaced laterally along the complete length of the specimen (Figure 12-22). The overall effect was to cause the middle of the C-sections to twist over as well as move sideways. This mode of buckling is referred to as lateral torsional buckling (LTB), which caused development of long cracks on the top surface of the slab along the location of the top flanges of the C-sections (Figure 12-23). As can be seen in Figure 12-23, it should be noted that in all specimens the LTB of one of the C-sections was more than the other one, which caused excessive widening of the developed cracks and eventually resulted in failure of the specimen, before reaching to the ultimate bending moment capacity of the specimen. As can be seen in Figure 12-24, it should also be noted that in all specimens when the load was removed, the C-sections returned to their original shape, indicating that the LTB of all C-sections was “elastic”. Slender members with a long unbraced length, such as the C-sections used in this study, may experience “elastic” LTB, which occurs when the member is slender enough to deflect without yielding. This type of buckling is elastic, thereby when the load is removed the member returns to its original shape.

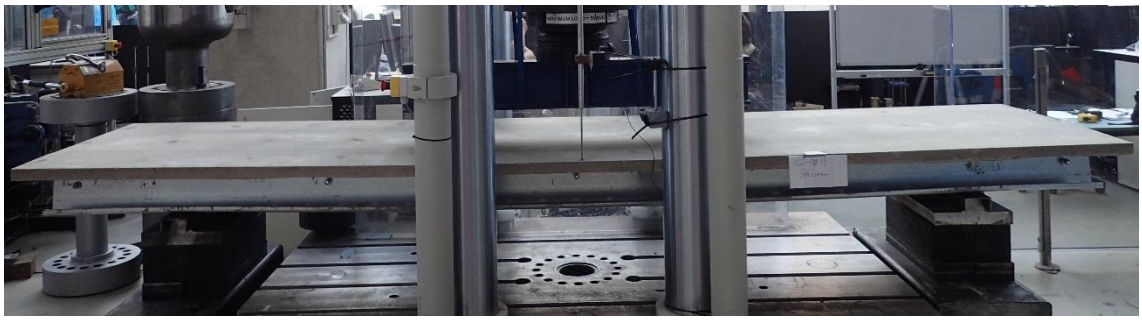

Figure 12-21: Deflection of the specimen along its length at the start of the test

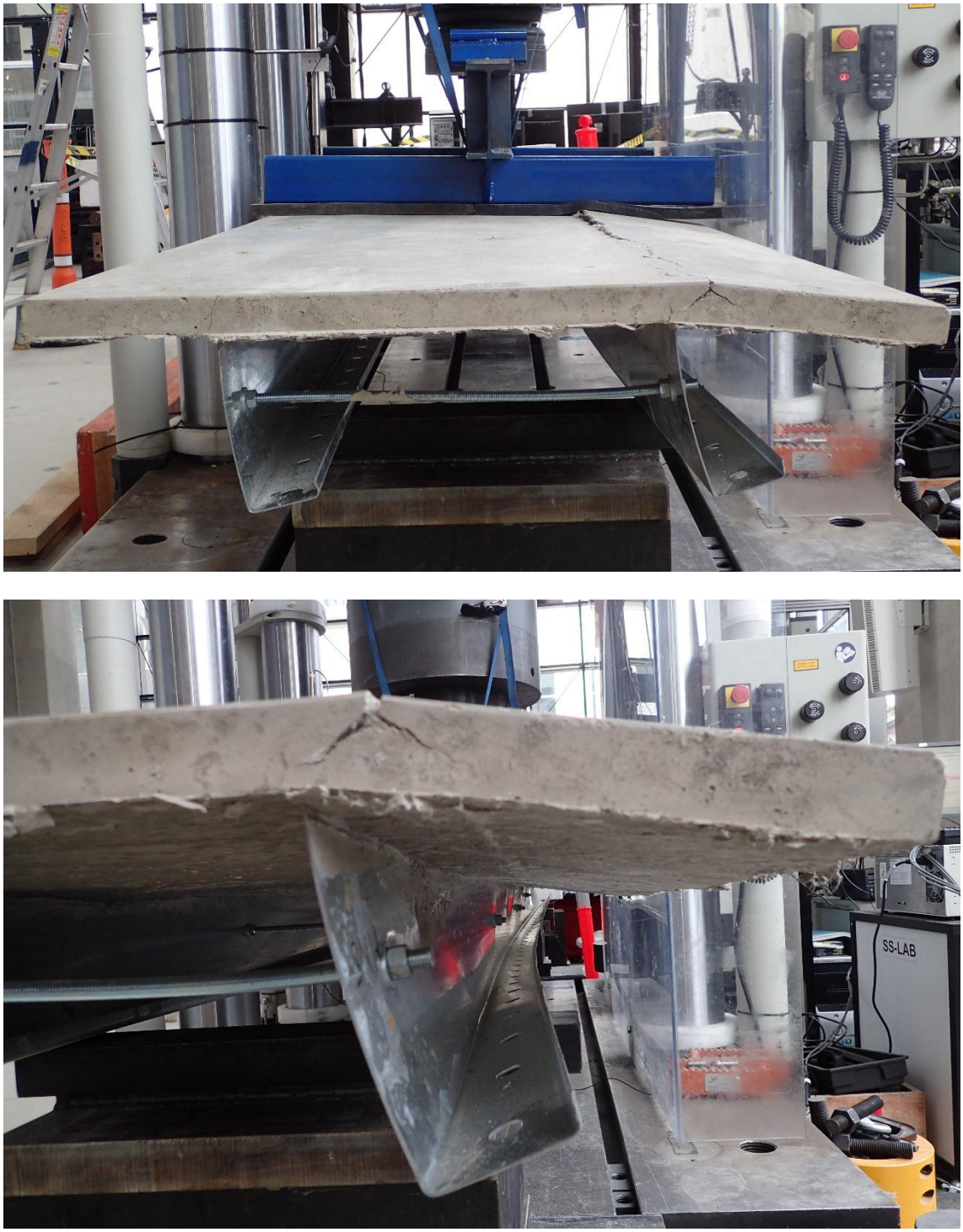

Figure 12-22: Elastic lateral torsional buckling of the C-sections

Figure 12-23: Development of long cracks on the top surface of the slab along the location of the top flange of one of the C-section

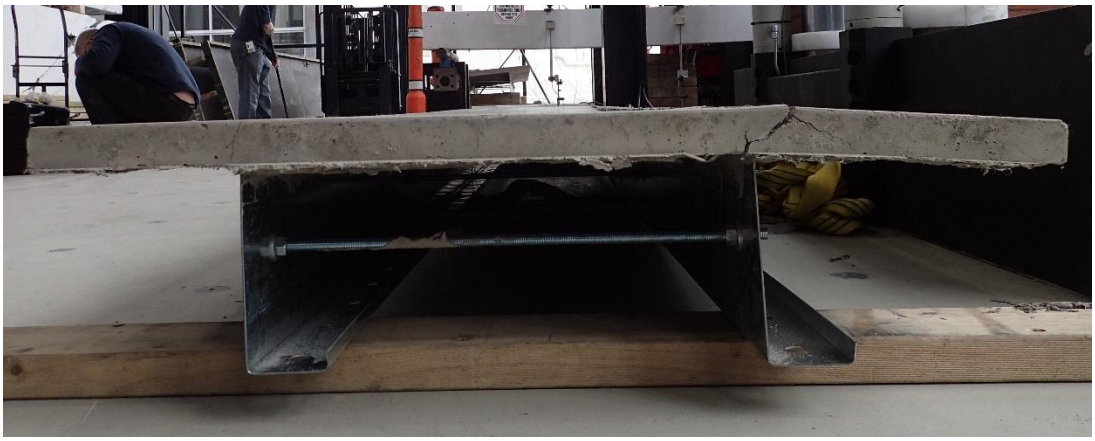

Figure 12-24: Return of C-sections to their original shape after unloading, indicating that all C-sections experienced "elastic" LTB

When a slender member is loaded in bending, LTB may occur which is characterized by the lateral and torsional displacement of the cross section along the complete length of the member (Sonck and Belis, 2016). In general, a beam can experience LTB due to buckling of its compression flange. The compression flange by itself would tend to buckle much like a column. However, the web is responsible to prevent the flange from bucking about its minor axis. But if the compression force is large enough, and there is no lateral support, then the web and flange would buckle together. On the other hand, the tension flange, which is stable, restrains the web and the compression flange, causing the beam to twist, which results in LTB.

Figure 12-22 presents the load versus mid-span deflection responses of the specimens. As can be seen, each graphs shows an initial linear relationship between the applied forced and the mid-span deflection. This corresponds to the bending of the specimen. However, when "elastic" LTB of the C-section occurred, the slop of the graph reduced rapidly. Eventually, widening of the cracks developed on the top surface of the slab along the location of the top flange of one of the C-sections caused ultimate failure of the specimen.

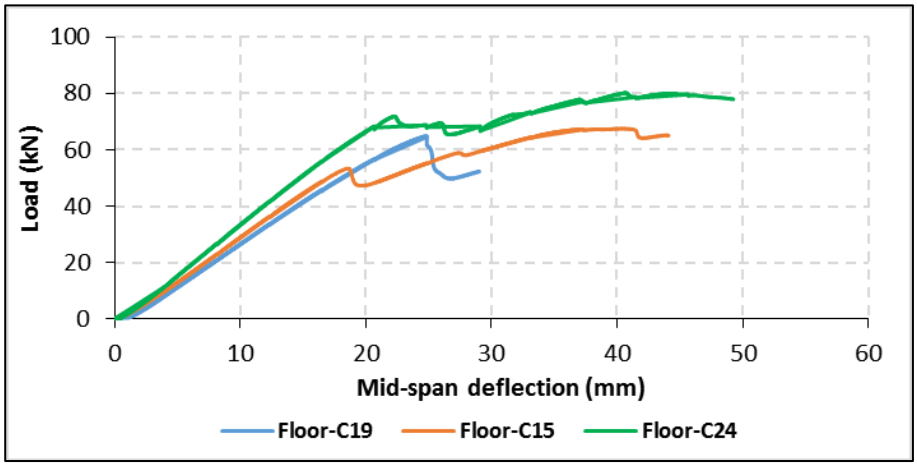

Figure 12-25: Load vs mid-span deflection responses of the large-scale specimens

The test results including the experimental failure load and the corresponding deflection, as well as, the theoretical (expected) failure load (P_{Theo}) are presented in Table 12-10. The theoretical (expected) moment capacity (M_{Theo}) and the corresponding theoretical failure load ($P_{Theo} = 2 \times M_{Theo}$) of the specimens were determined based on the similar procedure to derive ϕM_u as mentioned in Section 12.2.1, except with the following differences. First

of all, in calculation of the M_{Theo} the mean value of cube compressive strength (f_c' = 47.4 MPa) was used, instead of using the characteristic compressive strength (f_{ck}' = 36.4 MPa). In addition, in calculation of the M_{Theo} the material factor (γ_c) was equal to 1.0, instead of using γ_c = 1.3.

Table 12-10: Flexural test results

Specimen designation	Experimental failure load, P_{Exp} (kN)	Corresponding deflection (mm)	Theoretical failure load, P_{Theo} (kN)	P_{Exp} / P_{Theo}
Floor-C15[1]	67.5	40.3	94.0	0.72
Floor-C19[2]	64.8	24.8	118.1	0.55
Floor-C24[3]	80.2	40.6	147.2	0.54

[1] Composed of C20015 sections.

[2] Composed of C20019 sections.

[3] Composed of C20024 sections.

As can be seen in Table 12-10, the ratio of the experimental failure load to the theoretical failure load was on average equal to 0.60, which indicates that in all specimens the theoretical failure load was on average 40% higher than the experimental failure load. This is due to the fact that, as observed during the experimental test, the failure of all specimens was due to "elastic" LTB of the C-sections, prior to reaching to their ultimate bending moment capacity. It should be noted that in calculation of the theoretical failure load of the specimens, it was assumed that both C-sections would yield. However, as mentioned earlier and can be seen in Figure 12-23, the LTB of the C-sections was "elastic", therefore the C-sections did not yield when the specimens failed. This is the reason that the theoretical failure load of each specimen was more than the experimental failure load. It should be noted that although the experimental failure load was less than the theoretical value, the experimental failure load and its corresponding bending moment capacity were still far greater than the design load and design bending moment (as shown in Table 12.2 W^* = 5.23 kN/m and M^* = 10.5 kN.m) under ULS condition.

12.5 Conclusion

A lightweight precast composite floor as a sustainable alternative to "conventional" precast composite floor is presented in this study. The self-weight of the lightweight

composite floor was only 85 kg/m^2 which is 70% lighter than the "conventional" precast composite floor (with a self-weight of around 300 kg/m^2). The developed lightweight precast composite floor was composed of a 40 mm thick one-part SHGC slab and lightweight C-section purlins. Self-drilling metal screws were used as shear connectors to interconnect the concrete slab and the C-section purlins, thereby enabling the two components to act together as a composite structural member with much greater bending strength and stiffness. At first, the lightweight composite floor was designed based on the first principles in conjunction with Recommendations for Design and Construction of High Performance Fiber Reinforced Cement Composites with Multiple Fine Cracks (HPFRCC) (2008) and the relevant Australian standards. Push-out shear tests on small-scale specimens were conducted to evaluate the load-slip behavior and ascertain the adequacy of the proposed configuration of the self-drilling screws as the shear connectors.

In the second stage, three large-scale floor specimens with the dimensions of 4.0 m in length and 0.9 m in width were manufactured and tested in a four-point bending test setup to investigate the flexural behavior of the developed lightweight composite floor. The test parameter was the thickness of the C-section purlins used to make the floor specimens. The ratio of the experimental failure load to the theoretical failure load was on average equal to 0.60, which indicates that in all specimens the theoretical failure load was on average 40% higher than the experimental failure load. This is due to the fact that, as observed during the experimental test, the failure of all specimens was due to "elastic" lateral torsional buckling of the C-section purlins, prior to reaching to their ultimate bending moment capacity. It should be noted that although the experimental failure load was less than the theoretical value, the experimental failure load and its corresponding bending moment capacity were still far greater than the design load and design bending moment under ULS condition.

12.6 References

AS 1170.0. 2002. Structural design actions - General principles. Australia: Standards Australia.

AS 2327.1. 2003. Composite structures - Simply supported beams. Australia: Standards Australia.

AS 3566.1. 2002. Self-drilling screws for the building and construction industries - General requirements and mechanical properties. Australia: Standards Australia.

AS 3566.2. 2002. Self-drilling screws for the building and construction industries - Corrosion resistance requirements. Australia: Standards Australia.

AS 4100. 1998. Steel structures. Australia: Standards Australia.

Design Booklet DB1.1. 2001. Design of Simply-Supported Composite Beams for Strength (To Australian Standard AS 2327.1−1996). *Composite Structures Design Manual*. OneSteel Market Mills.

Recommendations for Design and Construction of High Performance Fiber Reinforced Cement Composites with Multiple Fine Cracks (HPFRCC). 2008. *Concrete Engineering Series 82*. Japan Society of Civil Engineers.

SONCK, D. & BELIS, J. 2016. Elastic lateral-torsional buckling of glass beams with continuous lateral restraints. *Glass Structures & Engineering*, 1, 173-194.

CHAPTER 13

SUMMARY, CONCLUSIONS AND RECOMMENDATIONS FOR FUTURE RESEARCH

13.1 Summary and Conclusions

This doctoral research focused on multi-scale development and investigation of a sustainable alternative to typical SHCCs. Geopolymer is used as a sustainable alternative binder to OPC to develop strain hardening composites, named strain hardening geopolymer composites (SHGCs). A series of systematic and detailed studies have been conducted to provide an in-depth knowledge on properties and performances of these geopolymer composites. The conclusions drawn from the research studies conducted in each chapter are presented in detail at the end of the respective chapter. The main conclusions reached in this doctoral thesis are summarized in this chapter.

In Chapter 3, the effect of six different commercial superplasticizers (SPs) on the workability and compressive strength of a low calcium fly ash-based geopolymer were investigated. Two different activator solutions including 8.0 M NaOH solution and a multi-compound activator composed of 8.0 M NaOH and Na_2SiO_3 solutions with Na_2SiO_3/NaOH mass ratio of 2.5 were used. The results indicated that the effect of a SP on the workability and compressive strength of fly ash-based geopolymer directly depends on the type of activator and SP. In the case of using only 8.0 M NaOH solution as the activator, the naphthalene-based SP (the second generation) was the most effective in increasing the workability of the fly ash-based geopolymer up to 136%, without having any negative effect on the compressive strength compared to the mixture with no SP. However, when the multi-compound activator was used, the modified Polycarboxylate-based SP (the latest generation) was the most effective in increasing the workability of the fly ash-based geopolymer in the range of 39−45%, at the expense of at most 29% reduction in the compressive strength compared to the mixture with no SP.

In general, it was concluded that with the current SPs technology, there is no commercial SP that exactly matches with geopolymer chemistry to be really effective in geopolymer systems similar to the OPC-based system. In addition, possible detrimental effects of the available SPs on other properties of geopolymer (apart from the compressive strength)

are still unknown. Therefore, in this doctoral research it was decided not to use any commercial admixtures (including SPs and viscosity modifying agents) in the mixture design of the SHGCs. Instead, the type and/or content of the activator, as well as the extra water in the mixture design were adjusted to control the workability and rheology of the mixture for uniform fiber dispersion.

The research works on SHGCs presented in this doctoral thesis are divided into two main parts. Part I focuses on heat cured two-part fly ash-based SHGCs, while the focus of Part II is on ambient temperature cured one-part SHGCs. Part I is comprised of five chapters (i.e. Chapters 4 to 8). The effects of four different activators on the properties of heat-cured two-part fly ash-based SHGCs were investigated in Chapter 4. It was found that the type of activator had significant effects on the matrix and composite properties of fly ash-based SHGCs. Among the activators investigated in this chapter, the use of a sodium-based activator composed of 8.0 M NaOH solution (28.6% w/w) and Na_2SiO_3 solution (71.4% w/w) with a SiO_2/Na_2O ratio of 2.0 was highly beneficial in terms of lower cost, higher compressive strength gain and matrix fracture properties, along with superior uniaxial tensile and flexural behaviors. The fly ash-based SHGC made from the sodium-based activator exhibited the highest compressive and tensile strengths, and modulus of rupture with very high tensile strain capacity and deflection capacity of 63.7 MPa, 4.7 MPa, 11.5 MPa, 4.3%, and 39.7 mm, respectively.

In Chapter 5, the effects of other matrix-related parameters such as water to geopolymer solids ratio (W/GP solids), sand size and sand content on the matrix and composite properties of the fly ash-based SHGC made from the sodium-based activator were investigated. It was found that lowering the W/GP solids (i.e. the water content) and the addition of sand enhanced the elastic modulus of the geopolymer matrix and composite in all cases. However, the excessive use of fine sand and the use of coarse sand adversely affected the strain hardening behavior of the fly ash-based SHGCs due to the increase of the matrix fracture toughness and the first-crack strength of the composite. Only the geopolymer matrices with suitable fracture toughness maintained the desirable tensile ductility of the composite. These findings are consistent with micromechanics-based design theory, which indicates that the sand size and content must be limited in the matrix to maintain tensile ductility of the composite. As a result, the fly ash-based SHGC containing appropriate amount of normal weight micro-silica sand exhibited the

compressive strength of 56.8 MPa, tensile strength of 5.0 MPa, and tensile strain capacity of 3.6%, comparable to those of typical SHCC mix 45 (M45). At the same time, the material sustainability evaluation results indicated that the developed composite provides 52% less carbon emissions and 17% less energy consumption as compared to SHCC M45. In addition, the developed composite with an average density of 1828 kg/m^3, unlike SHCC M45 (2077 kg/m^3), can be classified as lightweight concrete.

In Chapter 6, the effects of replacing the normal weight micro-silica sand with three types of lightweight aggregates on the mechanical and thermal properties of the fly ash-based SHGC developed in Chapter 5 were experimentally evaluated. The lightweight fly ash-based SHGCs developed in this chapter exhibited density of 1586−1833 kg/m^3, compressive strength of 43.4−48.2 MPa, thermal conductivity of 1.144−0.934 W/m.K, tensile strength of 3.4−4.3 MPa, and tensile strain capacity of 3.5−3.7%, depending on the type of lightweight aggregates. Replacing normal weight micro-silica sand with lightweight aggregates reduced the compressive and tensile strengths of the SHGCs by a maximum of 24% and 32%, respectively. However, the tensile ductility of the SHGCs containing lightweight aggregates was comparable to that of the SHGC containing normal weight micro-silica sand.

Among the lightweight aggregates investigated in this chapter, hollow ceramic microsphere was the most effective in reducing the density of the composite, with comparable tensile ductility and considerably (38%) lower thermal conductivity, at the expense of 18% reduction in the compressive strength compared to those of the SHGC containing normal weight micro-silica sand. The results of thermal conductivity measurements indicated that expanded recycled glass was the most effective in reducing the thermal conductivity of the composite compared to the SHGC containing normal weight micro-silica sand. It was concluded that incorporation of lightweight aggregates can effectively (up to 49%) reduce the thermal conductivity of the composite, which can potentially reduce heat exchange and total energy consumption in buildings constructed with the sustainable lightweight fly ash-based SHGCs.

In Chapter 7, a detailed microscale investigation of fly ash-based SHGCs is presented, which explains the experimentally observed macroscopic tensile performance of these geopolymer composites. The investigation involved determination of the quantitative

influences of the type of activator, W/GP solids and fiber surface oil coating on the microscale fiber-matrix interface properties using single-fiber pullout tests. The results indicated that (a) the chemical bond and slip hardening coefficient between the oil-coated poly vinyl alcohol (PVA) fiber and the geopolymer matrix were significantly lower than those of the virgin (un-coated) fiber. (b) On the other hand, the frictional bond between the oil-coated fiber and the geopolymer matrix was higher than that of the virgin fiber. The behaviors (a) and (b) are true irrespective of the type of activator and W/GP solids. However, when compares to cement-based matrix, (a) is the same, but (b) is the opposite.

It is hypothesized that the virgin PVA fiber with very high chemical bond may be weakened in the geopolymer matrix due to the presence of strong alkaline environment and may be damaged during the debonding stage when the tunnel crack propagates along the interface and branches into the virgin fiber, resulting in delamination damage of fiber. The SEM images of the typical pulled-out fiber supported this hypothesis. The delamination surface of the pulled-out virgin fiber was relatively smooth as compared to the surface of the oil-coated fiber, which explains the low interface frictional bond of the virgin PVA-SHGC system. On the contrary, for the oil-coated PVA fiber in the Na-based SHGC with low chemical bond, the pulled-out fiber tip was covered with matrix debris and its diameter was relatively un-changed as compared to the original fiber diameter. This suggests that, similar to PVA-SHCC, tunnel crack propagates along the fiber-matrix interface transition zone and does not branch into the oil-coated fiber. Fiber surface oil coating may effectively protect the PVA fibers when they are in contact with strong alkaline solution in the sodium-based geopolymer matrix.

The results also indicated that the fiber surface oil-coating does not provide much benefit when used with the potassium-based activator compared to the sodium-based activator. The chemical bond of the oil-coated fiber in the potassium-based SHGC was considerably higher than that of the sodium-based SHGCs. It was concluded that the potassium-based activator significantly enhances the chemical bond between the PVA fiber and the geopolymer matrix, similar to the effect of using virgin fiber, which may result in delamination damage of the fiber during the debonding stage. On the other hand, the frictional bond and slip hardening coefficient of the oil-coated fiber in the potassium-based SHGC were considerably lower than those of the sodium-based SHGCs, due to the relatively smooth delamination surface of the fiber.

The decrease in W/GP solids resulted in an increase in the chemical bond, but a decrease in the frictional bond of the PVA fiber with the sodium-based geopolymer matrix. However, the slip hardening coefficient was relatively stable, independent of the W/GP solids. This trend is true for both virgin and oil-coated PVA fibers. This is not the case in cement-based matrix, where the decrease in water to cement ratio (W/C) was reported to increase the frictional bond strength of the PVA fibers, but the chemical bond strength was relatively stable, independent of W/C.

Uniaxial tension test results indicated that the sodium-based SHGCs exhibited superior tensile performance to the potassium-based SHGC, in spite of the higher fracture toughness of the sodium-based SHGC matrix. This is due to the significantly higher complementary energy of the sodium-based SHGCs, resulted from their beneficial fiber-matrix interface properties. In addition, the sodium-based geopolymer matrix with lower W/GP solids enhanced the composite tensile ductility, due to the significant increase of the complementary energy of the composite, in spite of the increase of the matrix toughness. The experimentally observed macroscopic composite tensile ductility corresponded well with the two pseudo strain-hardening (PSH) performance indices of the composite calculated based on the computed crack bridging relation of the fly ash-based SHGCs. It was found that the two PSH performance indices of the sodium-based SHGCs were considerably higher than those of the potassium-based SHGC, thus providing a rational basis for the observed superior tensile performance of the sodium-based SHGCs.

The micromechanics-based modelling and optimization of fly ash-based SHGCs are presented in Chapter 8. The crack bridging $\sigma(\delta)$ relation of the developed fly ash-based SHGC was computed using the available micromechanics-based model for typical SHCCs. The computed $\sigma(\delta)$ relation of the composite was then compared with the uniaxial tension test results to verify the applicability of the model for evaluating the tensile performance of fly ash-based SHGCs. In general, the predicted peak bridging stress σ_0 and its corresponding deflection δ_0 was in good agreement with the ultimate tensile strength and the corresponding crack opening measured experimentally from the uniaxial tension tests.

The ratio of the experimental to the theoretical σ_0 was dependent on the fiber orientation assumption. In the case of 3D fiber orientation assumption, the predicted σ_0 was remarkably consistent with the ultimate tensile strength measured experimentally from the uniaxial tension tests. However, when 2D fiber orientation was assumed, the model overestimated the σ_0 by 23%. The ratio of the experimental to the theoretical δ_0 was also dependent on the fiber orientation assumption. In the case of 3D fiber orientation assumption, the model underestimated the δ_0 by about 20%. However, when 2D fiber orientation was assumed, the predicted δ_0 was well consistent with the crack opening corresponding to the experimentally measured ultimate tensile strength. These results are consistent with those reported in the literature on micromechanics-based modelling of typical SHCCs.

Subsequently in the second part of Chapter 8, a parametric study was performed using the verified model to evaluate the effects of fiber length, fiber surface oil-coating, and matrix fracture toughness on the critical volume fraction of fibers. It was demonstrated how the micromechanics-based model can effectively guide towards optimization of fly ash-based SHGCs by proper tailoring of the material constituents to achieve saturated PSH behavior with the lowest amount of fiber, and thereby the lowest cost.

In Part II of this doctoral thesis, an ambient temperature cured one-part SHGC developed to enhance the commercial viability of SHGCs is presented. Part II is comprised of four chapters (i.e. Chapters 9 to 12). In Chapter 9, a comprehensive and systematic experimental study was conducted to synthesize a suitable ambient temperature cured one-part geopolymer matrix with desirable mechanical properties, moderate setting time and adequate rheology for uniform fiber dispersion. The effects of the type and amount of the solid activator, the amount of fly ash replacement with slag and hydrated lime, the water content and the curing condition on the mechanical properties of the one-part geopolymer mixes were evaluated. The results indicated that GD Grade sodium silicate powder (with a chemical composition of 27 wt.% Na_2O, 54 wt.% SiO_2, and balance H_2O) was the most effective solid activator in the case of using a combination of fly ash and hydrated lime as the geopolymer source materials. On the other hand, in the case of using a combination of fly ash and slag, or a combination of fly ash, slag and hydrated lime as the aluminosilicate precursors, Anhydrous Grade sodium metasilicate powder (with a

chemical composition of 51 wt.% Na_2O, 46 wt.% SiO_2, and balance H_2O) was the most effective type of solid activator.

By using a small amount of GD Grade sodium silicate powder (e.g. 1.5 wt.%) in a (fly ash + lime) system, one-part geopolymer mixes with the compressive strength over 20 MPa were synthesized. Whereas, by using a relatively large amount of Anhydrous Grade sodium metasilicate powder (e.g. 8−12 wt.%) in a (fly ash + slag) or (fly ash + slag + lime) system, one-part geopolymer mixes with the compressive strength over 48 MPa were manufactured. It was also found that the 28-days compressive strength of the ambient temperature cured one-part geopolymer mixtures, regardless of the type of activator and geopolymer source materials, were comparable to that of the counterpart heat cured mixes. In summary, it was demonstrated that the ambient temperature cured one-part geopolymer is feasible by using fly ash and slag as the commonly used geopolymer source materials and a small amount of solid silicates. This significantly enhances the commercial viability and possibility of large-scale in-situ application of the geopolymer by eliminating the difficulties associated with handling large quantities of user-hostile alkaline solutions and the necessity for the heat curing.

In Chapter 10, the best performing ambient temperature cured one-part geopolymer mixture developed in Chapter 9 was used to develop the ambient temperature cured one-part SHGC. The quantitative influences of the curing condition and type of slag on the matrix, fiber-matrix interface and composite properties of the developed one-part PVA-SHGC were evaluated. The one-part PVA-SHGCs developed in this doctoral research exhibited density of 1800−1874 kg/m^3, compressive strength of 43.4−52.5 MPa, tensile strength of 4.3−4.6 MPa, and tensile strain capacity of 2.6−4.2%, depending on the curing condition and type of slag. The material sustainability evaluation results verified that the developed ambient temperature cured one-part PVA-SHGC is a promising sustainable alternative to SHCC M45, offering 76% less carbon emissions and 36% less energy consumption. In addition, the developed composite with an average density of 1849 kg/m^3, unlike SHCC M45 (2077 kg/m^3), can be classified as lightweight composite. The developed composite is expected to promote sustainability of the infrastructures through simultaneous improvements of material greenness and infrastructure durability via ultra-high ductility and tight crack width control.

The results indicated that the ambient temperature cured one-part PVA-SHGCs, regardless of the type of slag, exhibited superior uniaxial tensile performance to the corresponding heat cured composites. In addition, it was also found that the one-part PVA-SHGCs made with "typical" slag (which contains 2% gypsum), regardless of the curing condition, exhibited superior uniaxial tensile performance to the corresponding composites made with "gypsum-free" slag (which contains no gypsum). The curing condition and type of slag had significant effects on the fiber-matrix interface properties. The ambient temperature curing increased the chemical bond strength when "typical slag" was used in the one-part PVA-SHGC composition, whereas an opposite trend was observed when "gypsum-free" slag was used. It was also found that there is a positive correlation between the frictional bond strength of the one-part PVA-SHGC and the fracture toughness of the matrix. The higher the fracture toughness of the matrix, the higher the value of the frictional bond strength. It was concluded that the heat curing condition and using "gypsum-free" slag increased brittleness of the one-part SHGC matrix.

In Chapter 11, the tensile performance of a high ductile one-part SHGC reinforced by ultra-high-molecular-weight polyethylene (PE) fibers is presented. The quantitative influences of curing condition on the matrix, fiber-matrix interface and composite properties of the developed one-part PE-SHGC were evaluated, and the results were compared to those of the ambient temperature cured one-part PVA-SHGC developed in Chapter 10. The developed one-part PE-SHGCs exhibited density of 1837−1849 kg/m^3, compressive strength of 33.9−48.7 MPa, tensile strength of 3.3−4.6 MPa, and very high tensile strain capacity of 4.2−5.5%, depending on the curing condition. The results indicated that the ambient temperature curing condition increased the micro-scale fiber-matrix interface properties (frictional bond and slip hardening coefficient) of the PE fiber with the one-part SHGC matrix. The first-crack and ultimate tensile strengths of the ambient temperature cured one-part PE-SHGC were considerably higher than those of the counterpart heat cured composite. On the other hand, the tensile strain capacity of the heat cured one-part PE-SHGC was higher than that of the counterpart ambient temperature cured composite. This result is well consistent with the calculated PSH performance indices of the composites, where both PSH strength and energy indices of the heat cured

one-part PE-SHGC were relatively higher, resulting in the higher tensile ductility of the heat cured composite.

The type of fiber had significant effects on the microscale fiber-matrix interface properties, and thereby on the macroscopic tensile performance of the composite. The first-crack and ultimate tensile strengths of the ambient temperature cured one-part PVA-SHGC were significantly higher than those of the ambient temperature cured one-part PE-SHGC. However, the tensile strain capacity of the ambient temperature cured one-part PVA-SHGC was lower than that of the ambient temperature cured one-part PE-SHGC. This result is also in good agreement with the computed PSH performance indices of the composites, where both PSH strength and energy indices of the ambient temperature cured one-part PVA-SHGC were relatively lower. This is attributed to the strong chemical bond and higher frictional bond and slip hardening coefficient of the PVA fiber with the one-part SHGC matrix, along with the lower strength of the PVA fiber, which result in lower complimentary energy of the ambient temperature cured one-part PVA-SHGC.

Finally in Chapter 12, a lightweight precast composite floor as a sustainable alternative to "conventional" precast composite floor is presented. The composite floor had a similar strength to that of "conventional" precast composite floor, but was 70% lighter! The composite floor composed of a 40 mm thick one-part SHGC slab and lightweight C-section purlins was designed, constructed and tested. The motivation for this research arose from an industry challenge in the potential replacement of "conventional" precast composite floor with a sustainable lightweight precast composite floor. The challenge was to substantially reduce the weight of the composite floor, while maintaining the strength, stiffness and ductility.

Push-out shear tests on small-scale specimens were conducted to evaluate the load-slip behavior and ascertain the adequacy of the proposed configuration of the self-drilling screws as the shear connectors. Three large-scale floor specimens with the dimensions of 4.0 m in length and 0.9 m in width were manufactured and tested in a four-point bending test setup to investigate the flexural behavior of the developed composite floor. The results indicated that the failure of all specimens was due to elastic lateral torsional buckling of the C-section purlins, prior to reaching to their ultimate bending moment

capacity. However, the experimentally measured bending moment capacity was still far greater than the design bending moment under ultimate limit state condition.

In summary, the main conclusions are:

(1) SHGCs (geopolymer based composites) developed in this research exhibited either comparable or superior performances to typical SHCCs (cement based composites) in all mechanical aspects. At the same time, the developed SHGCs have significantly lower environmental footprints as compared to typical SHCCs.

(2) The ambient temperature cured one-part geopolymer is made to enhance the commercial viability of SHGCs. The developed composite as a "dry mix" uses a small amount of solid activator and eliminates the necessity for heat curing and handling hazardous liquids.

(3) A detailed microscale investigation of SHGCs involving determination of fiber-matrix interface properties using single-fiber pullout tests is presented. Dependence of the interface parameters on the type of activator, water content and fiber surface oil coating is determined, which clearly explains the experimentally observed macroscopic composite tensile ductility of SHGCs.

(4) The existing micromechanics-based model is applicable for the design of SHGCs. Overall, the model predictions are in good agreement with the experimental results. Using the model, it is demonstrated that SHGCs can be optimized by proper tailoring of the material constituents to achieve saturated strain hardening behavior with the lowest amount of fiber, and thereby the lowest cost.

(5) Lightweight SHGCs with density of less than 1833 kg/m^3 and compressive strength of more than 43.4 MPa can be made, meeting the density and compressive strength requirements for structural lightweight concrete. In addition, they have significantly lower thermal conductivity, resulting in composites that are sustainable, lighter and provide better thermal insulation than typical SHCCs.

(6) A lightweight precast composite floor composed of a 40 mm thick one-part SHGC slab and C-section purlins concept developed in this study is designed, constructed and tested. The composite floor has a similar strength to that of "conventional" precast composite floor, but is 70% lighter.

13.2 Recommendations for Future Research

Based on the outcome of the present study, the following investigations for continued development of strain hardening geopolymer composites (SHGCs), leading to its utilization in infrastructure applications, are recommended:

- Creep and shrinkage behaviors of SHGC
- Long term durability performance of SHGC
- Properties of SHGC under multiaxial loading and different strain rate effects
- Impact resistance performance of SHGC and steel reinforced SHGC (R/SHGC) structural members
- Structural performance of R/SHGC members under static and dynamic loads
- Development of numerical models to predict the responses of R/SHGC structural members
- Cost optimization of SHGC
- Full life cycle analysis of a potential infrastructure application of SHGC